
Response of Low Voltage Networks with High Photovoltaic Systems Penetration to Transmission Network Faults

Konstantinos Skaloumpakas

Supervisors:

Prof. ir. Mart van der Meijden

Dr. ir. Madeleine Gibescu

Dip.-Ing. Jens C. Boemer

M.Sc. Thesis in Sustainable Energy Technology

Faculty of Applied Sciences

Specialization in Electrical Power Engineering

Delft, January 2014

Preface-Acknowledgments

Nowadays the rapid growth of technology that surrounds renewable forms of energy is one of the main discussion topics in the energy sector. For the purpose of securing our future energy supplies, and given the realistic scenario of depletion of traditional energy sources (oil, gas and coal), renewables seem to be one of the few viable alternatives. The basis of research on renewables focuses on developing the technology in order to make exploitation of solar, wind, biomass and the rest of clean energy sources economically feasible. In this framework renewables need to achieve high efficiency and affordable costs for installation and maintenance. However, despite the technologies themselves, there is a need to integrate the new forms of energy with their individual characteristics inside the already existing power supply system. As discussed in [1] the integration of PV installations on all levels of the grid is going to introduce different characteristics in the energy production. Research is needed to specify the impact on the system operational security.

This thesis has been a very interesting journey in the field of Power systems. Throughout this journey I gained a lot of experience as a researcher by reading vast amounts of publications, performing detailed modelling of networks, understanding the details of power systems in terms of policy but also operation and behaviour. I understood the importance of planning and organization in order to maximize efficiency and output of work and most importantly I learned how to manage myself and meet the deadlines even in the expense of sleep hours. This research of course would not be the same without the help of my daily supervisor and mentor Jens C. Boemer that guided me throughout this project and freely shared his knowledge and experience with me, spending long days and nights to help and guide me. Moreover I want to thank Ass. Prof. Madeleine Gibescu for making it possible for me to be part of this project and for always keeping a close eye on me making sure I am on the right path. Furthermore Prof. Mart van der Meijden that despite his busy schedule always showed interest in my work and encouraged my endeavours. Finally I want to thank the members of the IEPG group of the EWI faculty at TU Delft for their support and also my family and friends.

Abstract

The need for fault ride-through (FRT) capability is not yet documented for the low voltage connected DG. The realization that an increase in the capacity of installed DG power in the specific voltage level can trigger disconnection, in case of transmission faults, of massive amounts of power from DG and jeopardize system stability is forming.

In order to investigate the response of low voltage distribution systems with high penetration of PVs, in case of a fault in the transmission system, a complex network model is created consisting of different voltage levels, from eHV (220 kV) to LV (400 V). This model is implemented as a benchmark system with DG capacities chosen to match the German network. Also an elaborate PV model is used to simulate different behaviours during and after fault and assist in examining the impact of different sensitivity factors on network stability. The problem is analysed through root mean square (RMS) stability simulations performed on the models of the network and the DG. The projected year that this study takes place is 2022 and the DG capacity is chosen for that year. The commercially available DigSilent PowerFactory software version 14.1 is used to carry out these simulations.

A sensitivity analysis is performed for different control modes of the PV that range from disconnection in the event of a fault to full dynamic network support during fault. Also different pre-fault states of the network are used to examine the effect of the state of the network in the results; these states vary from normal top-down power flow to full reverse power flow when PVs are at full capacity. Moreover the effect of delayed post-fault active power recovery of the LV connected DG is discussed.

The conclusions and analysis show the importance of introducing FRT criteria even for low voltage connected DG and give an insight on the behaviour of the system under the circumstances described. The differences between control modes are affecting stability of the system and the various phenomena that take place are analysed and explained. Finally corrective steps that need to be taken in order to avoid future stability problems for the network are outlined and justified and recommendations for future grid connection requirements for low voltage installed DG are given.

Table of Contents

Nomenclature	xi
List of definitions	xiii
List of abbreviations	xv
List of Figures	xvii
List of Tables	xxi
List of equations.....	xxiii
Chapter 1: Introduction	- 1 -
1.1 Background.....	- 1 -
1.2 Problem Definition	- 2 -
1.3 Objective and Research Questions.....	- 3 -
1.4 Research Approach	- 3 -
1.5 Outline of the Thesis.....	- 5 -
Chapter 2: Literature Survey.....	- 7 -
2.1 Power System Stability	- 7 -
2.2 Grid Codes and Fault Ride-Through Requirements - Status Quo.....	- 9 -
2.3 Impact of Fault Ride-Through and Additional Reactive Current Injection During Fault on Line and Generation Protection	- 12 -
2.4 Photovoltaic Systems – Current Settings and Operational Performance	- 16 -
2.4.1 Equation of a PV array	- 16 -
2.4.2 Modelling of a PV system.....	- 17 -
2.5 Types of Faults	- 19 -
2.6 Conclusions	- 19 -
Chapter 3: Test System and Distributed Generation Modelling.....	- 21 -
3.1 Introduction	- 21 -
3.2 Structure of the Test System	- 21 -

3.3	System levels.....	- 22 -
3.3.1	IEEE 39-Bus, 10-Machines new England network	- 22 -
3.3.2	Typical German sub-transmission 110 kV ring network.....	- 23 -
3.3.3	CIGRÉ medium voltage benchmark network	- 24 -
3.3.4	CIGRÉ low voltage benchmark system.....	- 26 -
3.3.4.1	Simplifications.....	- 26 -
3.3.4.2	Kron transformation (for overhead lines, cables).....	- 27 -
3.4	Distributed Generation Modelling.....	- 28 -
3.4.1	Photovoltaic power Park module (PVPPM).....	- 28 -
3.4.1.1	Existing model (DC side, DC/AC inverter control).....	- 28 -
3.4.1.2	Network fault control modes and extensions	- 30 -
3.4.2	Wind turbine generators.....	- 40 -
3.5	Load Modelling	- 41 -
3.6	Conclusions	- 42 -
Chapter 4: Case study and Sensitivity Analysis		- 43 -
4.1	Introduction	- 43 -
4.2	System Conditions.....	- 43 -
4.2.1	General overview of the system	- 43 -
4.2.2	Scenarios for installed PV capacity.....	- 44 -
4.3	Sensitivity Factors.....	- 46 -
4.3.1	Load/ Generation profile.....	- 46 -
4.3.1.1	Base case unidirectional power flow	- 47 -
4.3.1.2	Partial (MV and HV) reverse power flow	- 48 -
4.3.1.3	Complete (LV to HV) reverse power flow	- 49 -
4.3.2	Network fault control mode settings	- 50 -
4.3.3	Overview of sensitivity cases.....	- 50 -
4.4	Presentation and Analysis of Results.....	- 51 -
4.4.1	Base Case with no-LVRT	- 51 -
4.4.1.1	Presentation of results.....	- 51 -
4.4.1.2	Analysis of results	- 54 -
4.4.2	Comparison between no-LVRT/ZPM/aRCI/aRACI for the base case	- 57 -
4.4.2.1	Presentation of results.....	- 57 -
4.4.2.2	Analysis of results	- 59 -
4.4.3	Comparison between no-LVRT/ZPM/aRCI/aRACI in the case of full reverse power flow	- 62 -
4.4.3.1	Presentation of results.....	- 62 -
4.4.3.2	Analysis of results	- 64 -
4.4.4	Effect of pre-fault starting point	- 67 -

4.4.4.1	Presentation of results.....	- 67 -
4.4.4.2	Analysis of results	- 68 -
4.4.5	Effect of delayed active power recovery (dAPR)	- 69 -
4.4.5.1	Presentation of results.....	- 69 -
4.4.5.2	Analysis of results	- 72 -
4.5	Conclusions	- 73 -
Chapter 5: Conclusions and Future Research		- 75 -
5.1	Introduction	- 75 -
5.2	Conclusions	- 75 -
5.2.1	Voltage dip-depth sensitivity in LV networks with high penetration of PV...-	75 -
5.2.2	Impact of reverse power flow	- 77 -
5.2.3	Recommendations for network fault control modes	- 77 -
5.2.4	Relevance of delayed active power recovery after fault.....	- 78 -
5.2.5	Considerations on the applicability of the results to the German network..-	79 -
5.3	Recommendations for Future Research	- 81 -
References.....		- 83 -
Appendix A	IEEE 39-Bus, 10-Machine New England Test System	- 89 -
Appendix B	Typical German Sub-Transmission 110 kV Ring System	- 91 -
Appendix C	CIGRÉ Medium Voltage Benchmark System.....	- 92 -
Appendix D	CIGRÉ Low Voltage Benchmark System	- 93 -
Appendix E	Transformer Tap Changers Positions.....	- 96 -
Appendix F	Results.....	- 97 -
Appendix G	PowerFactory Lessons Learned	- 142 -

Nomenclature

Symbols

V	voltage
I	current
N	number of photovoltaic panels
R	electrical resistance
DB	dead band
K	proportional gain
T	time constant
P, Q	active and reactive power
ϕ	phase angle in [rad]
Scaler	function used to scale variables
Θ	angle for current injection
X	state of a system variable
\dot{x}	state Derivative
$f(x)$	function of the state
<i>Post-fault</i>	logical function that is equal to 1 when the system is in the post-fault state
a, b	load parameter used in polynomial and exponential load modelling
e_{aP}, e_{aQ}	load parameters used in exponential load modelling
s	Laplace operator
<i>fault</i>	logical function that is equal to 1 when the system is in the fault state

Subscripts

pv	photovoltaic
s	connected in series
p	connected in parallel
d	saturation
ph	photo-generated
T	junction thermal
0	initial value
o	output signals
g	grid quantity
V	voltage
d, q	components of space vector in rotating reference frame
a, b	components of space vector in stationary reference frame
ref	reference value
max	maximum value used for protection relays or controller limitations
min	minimum value used for protection relays or controller limitations

dc	direct current
AC	alternating current
aRCI	case of additional reactive current injection
pre-fault	pre-fault values
I	current
I	input signals
<i>aR&ACI</i>	case of additional reactive and active current injection
<i>tracker</i>	function of the tracker used in delayed active power recovery
<i>slow</i>	used in gains to define a slow tracker
<i>fault</i>	used in gains to define a fast tracker
Filter	function for filter
<i>ZIP</i>	polynomial static load model
<i>exp</i>	exponential static load model
P,Q	active and reactive power
dyn	dynamic load
r	rated power

Superscripts

<	arbitrary coordinate system
< Ug	Reference frame aligned to positive sequence grid voltage at terminals

List of definitions

Short-term interruption

Short (for less than 2 seconds) disconnection of a wind turbine generator from the grid - via a circuit breaker or power electronics of the machine's stator - until the fault has been cleared followed by fast restoration of pre-fault power output; used to be relevant for WTG design of specific manufacturers [2].

Short-circuit ratio

The ratio of the transmission system's three-phase short-circuit MVA, divided by the rated MW of the variable generation plant [3].

Active sign convention

Also mentioned as generation convention or producer-oriented, because positive power refers to production of power. Positive current exits the higher voltage (+) of an element.

Reverse power flow

The phenomenon of producing power in a lower voltage level and transporting this power to a higher voltage level through the network.

Voltage dip-depth

The difference of the voltage value at a specific element (busbar, connection point, etc.) immediately after a fault occurred and the lower boundary of the admissible voltage band at that element.

Maximum power point tracking

Search algorithms implemented in photovoltaic (PV) power park modules, which allow optimal power tracking for different weather conditions and also can consider effects like shading of PV panels.

Fault ride-through

Voltage control in the event of fault in the high and extra-high voltage network that results in voltage dip in the medium and low voltage network aiming at avoiding unintentional disconnection of large power in-feed. That means that generating facilities must be able in technical terms:

- not to disconnect from the network in the event of network faults [4], [5].

Low voltage ride-through

The ability of the power generating module to ride-through events of under-voltages at PCC for defined time periods.

Dynamic network support

Voltage control in the event of faults in the high and extra-high voltage network that result in voltage dips in the medium and low voltage network aiming at avoiding unintentional disconnection of large power in-feed. That means that generating facilities must be able in technical terms:

- not to disconnect from the network in the event of network faults,
- to support the network voltage during a network fault by feeding a reactive current into the network,
- not to extract from the medium voltage network after fault clearance more inductive reactive power than prior to the occurrence of the fault [4], [5].

Dead band

Dead band is the range through which an input can be varied without initiating an observable response. Dead band is usually expressed in percent of span. The dead band is used in aRCI control to determine the insensitivity of the control towards voltage changes. [Own definition]

List of abbreviations

DG	distributed generation
RPF	reverse power flow
FRT	fault ride-through
OLTC	On-load tap changer
rms	root mean square
HVdc	high voltage direct current
DSO	distribution system operator
LVRT	low voltage ride-through
WPP	wind power park
PEC	power electronic converter
ENTSO-E	European network of transmission system operators for electricity
VDE FNN	Forum network technology / network operation
TSO	transmission system operator
STI	short-term interruption
WTG	wind turbine generator
MPPT	maximum power point tracker
PLL	phase locked loop
PV	photovoltaic
emt	electromagnetic transient
CT	clearing time
PVPPM	photovoltaic power park module
eHV	extra-high voltage
HV	high voltage
MV	medium voltage
LV	low voltage
SC	short circuit
VSC	voltage source converter
PCC	point of common coupling
ZPM	zero power mode
aRCI	additional reactive current injection
aRACI	additional reactive and active current injection
non-LVRT	not low voltage ride through able
DFAG	doubly fed asynchronous generator
FCG	full converter generator
dAPR	delayed active power recovery after fault

List of Figures

Figure 1.1: Horizontally operated power system	- 2 -
Figure 1.2: Reverse power flow in substation in a Germany	- 2 -
Figure 1.3: Installed PV power in Germany (1998-2012)	- 4 -
Figure 1.4: Projected progress in installed PV power in the German grid (2013-2017)	- 5 -
Figure 2.1: Power system operating states	- 7 -
Figure 2.2: Power system stability classification	- 8 -
Figure 2.3: FRT requirements for type II generators in the German MV network	- 10 -
Figure 2.4: FRT requirements for type II generators in the German HV network	- 11 -
Figure 2.5: DG connected to the grid-importance of impedance in aRCI	- 13 -
Figure 2.6: Reactive current support during fault	- 14 -
Figure 2.7: False tripping	- 15 -
Figure 2.8: Blinding of protection	- 15 -
Figure 2.9: PV array current-voltage curve with power output	- 17 -
Figure 2.10: PV inverter system	- 18 -
Figure 3.1: Structure of the Test System	- 21 -
Figure 3.2: IEEE 39-bus, 10-machine New England test system	- 23 -
Figure 3.3: 110 kV Sub-transmission ring	- 24 -
Figure 3.4: Cigré MV Network	- 25 -
Figure 3.5: Cigré LV benchmark network	- 26 -
Figure 3.6: PVPPM components	- 28 -
Figure 3.7: PVPPM system set up	- 29 -

Figure 3.8: Power factor relative to active power output _____	- 30 -
Figure 3.9: Typical voltage rms value plot divided into time periods of the network fault	- 30 -
Figure 3.10: State Diagram of PVPPM control _____	- 31 -
Figure 3.11: No-LVRT requirement for type A generators, power generating modules with a connection point below 110 kV and maximum Capacity of 0.8 kW or less [13] by Forum network technology / network operation (VDE) _____	- 32 -
Figure 3.12: D-axis and q-axis currents of a PV Power Plant set for No-LVRT during fault	- 32 -
Figure 3.13: D-axis and q-axis currents of a PV Power Plant set for ZPM during fault ____	- 33 -
Figure 3.14: D-axis and q-axis currents of a PVPPM set for aRCI during fault _____	- 35 -
Figure 3.15: Inverter d-axis and q-axis current diagrams for presenting scaling scheme _	- 36 -
Figure 3.16: D- axis and q-axis currents of a PVPPM set for aR&ACI during fault _____	- 37 -
Figure 3.17: D-axis and q-axis current in aRACI with delayed active power recovery ____	- 38 -
Figure 3.18: German grid step response _____	- 40 -
Figure 4.1: Installed load and DG generation in the 2022 Scenario for the HV/MV/LV networks _____	- 46 -
Figure 4.2: Load and DG generation for HV/MV/LV networks for Base case power flow _	- 47 -
Figure 4.3: Unidirectional power flow from eHV to LV network at Base Case _____	- 48 -
Figure 4.4: Load and DG generation for HV/MV/LV networks for HV and MV reverse power flow _____	- 48 -
Figure 4.5: Split reverse power flow from MV and HV to eHV network _____	- 49 -
Figure 4.6: Load and DG generation for HV/MV/LV networks for LV to eHV reverse power flow _____	- 49 -
Figure 4.7: Full reverse power flow from LV to eHV network _____	- 49 -
Figure 4.8: Voltage in p.u. at all busbars of the eHV network (different colours represent different busbars) _____	- 52 -

- Figure 4.9: Voltages in p.u. at busbar R1 of the low voltage networks connected to busbar 1 of the MV networks with R/X ratio 4.4 (different colours indicate different MV networks) _____ - 53 -
- Figure 4.10: Voltages in p.u. at busbar R15 of the low voltage networks connected to busbar 1 of the MV networks with R/X ratio 0.43 (different colours indicate different MV networks) _____ - 54 -
- Figure 4.11: Active Power exchange over one of the 38 parallel 500 kVA MV/LV transformers connected to busbar 1 of the MV network in p.u. (different colours indicate different MV networks, base value 500 kVA) _____ - 55 -
- Figure 4.12: Active power output of all 38 parallel LV connected PVPPMs connected to busbar R1 of the LV network connected to MV busbar 1, in p.u. with an aggregated base value of 4 560 kVA _____ - 55 -
- Figure 4.13: Reactive Power exchange over one of the 38 parallel 500 kVA MV/LV transformers connected in busbar 1 of the MV network in p.u. (different colours indicate different MV networks, base value 500 kVA) _____ - 56 -
- Figure 4.14: Voltages in p.u. at busbar R1 of the low voltage networks connected at busbar 1 of the MV networks with R/X ratio 4.4 for four different control modes ____ - 58 -
- Figure 4.15: Voltages in p.u. at busbar R15 of the low voltage networks connected at busbar 1 of the MV network with R/X ratio 0.43 for four different control modes __ - 59 -
- Figure 4.16: Active Power exchange over one of the 38 parallel 500 kVA MV/LV transformers connected in busbar 1 of the MV network for all MV networks in p.u. for all control cases (base value 500 kVA) _____ - 60 -
- Figure 4.17: Reactive Power exchange over one of the 38 parallel 500 KVA MV/LV transformers connected in busbar 1 of the MV network for all MV networks in p.u. for all control cases (base value 500 kVA) _____ - 61 -
- Figure 4.18: Voltages in p.u. at busbar R1 of the low voltage networks connected at busbar 1 of the MV networks with R/X ratio 4.4 for four different control modes in fRPF _____ - 63 -
- Figure 4.19: Voltage in p.u. at busbar R1 of the low voltage network connected at busbar 10 of the MV networks with R/X ratio 4.4 for four different control modes in fRPF _____ - 63 -
- Figure 4.20: Voltages in p.u. at busbar R15 of the low voltage networks connected at busbar 1 of the MV networks with R/X ratio 0.43 for four different control modes in fRPF _____ - 64 -

Figure 4.21: Active Power exchange over one of the 38 parallel 500 kVA MV/LV transformers connected in busbar 1 of the MV network in p.u. for all control cases in fRPF (base value 500 kVA) _____ - 65 -

Figure 4.22: Reactive Power exchange over one of the 38 parallel 500 kVA MV/LV transformers connected in busbar 1 of the MV network in p.u. for all control cases in fRPF (base value 500 kVA) _____ - 66 -

Figure 4.23: Voltages in p.u. at busbar R1 of the low voltage networks connected at busbar 1 of the MV networks with R/X ratio 4.4 during ZPM for all load cases _____ - 67 -

Figure 4.24: Voltages in p.u. at node R15 of the low voltage networks connected at busbar 1 of the MV networks with R/X ratio 0.43 during ZPM for all load cases _____ - 68 -

Figure 4.25: Voltage in p.u. at busbar R1 of the low voltage network connected to busbar 10 of the MV network for ZPM with and without delayed active power recovery _____ - 70 -

Figure 4.26: Voltage in p.u. at busbar R15 of the low voltage network connected to busbar 10 of the MV network for ZPM with and without delayed active power recovery _____ - 70 -

Figure 4.27: Voltage in p.u. at busbar R1 of the low voltage network connected to busbar 10 of the MV network for ZPM with and without delayed active power recovery in fRPF _____ - 71 -

Figure 4.28: Voltage in p.u. at busbar R15 of the low voltage network connected to busbar 10 of the MV network for ZPM with and without delayed active power recovery in fRPF _____ - 72 -

List of Tables

<i>Table 2.1: Timing for tripping of generation protection.....</i>	<i>- 18 -</i>
<i>Table 3.1: eHV important data overview</i>	<i>- 23 -</i>
<i>Table 3.2: HV Wind Power Parks Ratings</i>	<i>- 23 -</i>
<i>Table 3.3: MV Wind Power Parks and Photovoltaic Power Plants Ratings</i>	<i>- 25 -</i>
<i>Table 3.4: LV Photovoltaic Power Plants Rating.....</i>	<i>- 26 -</i>
<i>Table 3.5: Scaling factors for lines, loads, transformers and PVPPM ratings per MV network node for all types of LV networks.</i>	<i>- 27 -</i>
<i>Table 3.6: Exponential Load Parameters.....</i>	<i>- 42 -</i>
<i>Table 4.1: Details of fault event.....</i>	<i>- 43 -</i>
<i>Table 4.2: Details of transformers tap changing strategy.....</i>	<i>- 44 -</i>
<i>Table 4.3: MV connected DG installed powers and connection points for the 2012 scenario</i>	<i>- 45 -</i>
<i>Table 4.4: Installed power of LV connected PVPPMs with their corresponding connection point for the 2012 scenario</i>	<i>- 45 -</i>
<i>Table 4.5: Installed Load and Production in the eHV network</i>	<i>- 46 -</i>
<i>Table 4.6: Multipliers for installed load and PVPPMs power output for setting up of load cases</i>	<i>- 47 -</i>
<i>Table 4.7: Connection points of PVPPMs in the network and angle of aRACI chosen for each point.....</i>	<i>- 50 -</i>
<i>Table 4.8: The study cases formed by varying the sensitivity factors of load cases and PVPPM's control modes.....</i>	<i>- 50 -</i>
<i>Table A.1: Line parameters for the eHV network</i>	<i>- 89 -</i>
<i>Table A.2: Load parameters of eHV network</i>	<i>- 90 -</i>

<i>Table A.3: Apparent power and power factor for load flow initialization of eHV synchronous generators for normal power flow scenario, also d and q axis reactance in p.u.</i>	- 90 -
<i>Table B.1: Parameters of line type of the HV network</i>	- 91 -
<i>Table B.2: Length and type of the HV networks lines</i>	- 91 -
<i>Table B.3: Parameters of eHV to HV transformers</i>	- 91 -
<i>Table C.1: Line parameters of MV network</i>	- 92 -
<i>Table C.2: HV/MV transformer parameters</i>	- 92 -
<i>Table C.3: Load parameters of MV network</i>	- 92 -
<i>Table D.1: Line parameters of LV residential network</i>	- 93 -
<i>Table D.2: Conductor parameters for overhead lines of the LV network</i>	- 93 -
<i>Table D.3: Conductor parameters for underground cables of the LV network</i>	- 93 -
<i>Table D.4: Line parameters of LV commercial network</i>	- 94 -
<i>Table D.5: Line parameters of LV industrial network</i>	- 94 -
<i>Table D.6: Phase Impedance matrix after Kron reduction of all three phase lines in the LV network</i>	- 95 -
<i>Table D.7: MV to LV transformer parameters</i>	- 95 -
<i>Table D.8: Load parameters of all LV loads</i>	- 95 -
<i>Table E.1: Tap changer positions of transformers per load case</i>	- 96 -
<i>Table F.1: Schematic representation of voltage results</i>	- 98 -
<i>Table F.2: Schematic representation of transformers power exchange results</i>	- 98 -
<i>Table F.3: Schematic representation of DG and SG power output results</i>	- 99 -
<i>Table G.1: Passive sign convention</i>	- 145 -
<i>Table G.2: Active sign convention</i>	- 145 -

List of equations

$$I = n_p \cdot I_{ph} - n_p \cdot I_0 \cdot \left(\exp\left(\frac{V_{pv} - R_s I_{pv}}{n_s \cdot V_T}\right) - 1 \right) \quad - 16 -$$

$$I_{g,d_e}^{<Ug} = K \cdot \left(1 + \frac{1}{T}\right) \cdot (U_{dc,ref} - U_{dc}) \quad - 29 -$$

$$Q_{ref} = \sqrt{P^2 \cdot \left(\frac{1}{\cos^2 \varphi} - 1\right)} \quad - 29 -$$

$$I_{q_{aRCI}} = \begin{cases} I_{q_{pre-fault}} + K_{Iq} \cdot \frac{|dV_{AC}|}{dV_{AC}} \cdot (|dV_{AC}| - db), & I_{q_{aRCI}} \leq I_{max} \\ I_{max}, & I_{q_{aRCI}} > I_{max} \end{cases} \quad - 34 -$$

$$I_{d_{aRCI}} = \begin{cases} I_{d_{pre-fault}}, & I_{max} \geq \sqrt{I_{d_{pre-fault}}^2 + I_{q_{aRCI}}^2} \\ \sqrt{I_{max}^2 - I_{q_{aRCI}}^2}, & I_{max} < \sqrt{I_{d_{pre-fault}}^2 + I_{q_{aRCI}}^2} \end{cases} \quad - 34 -$$

$$I_{q_{aR\&ACI}} = \left\{ I_{q_{pre-fault}} + \left[K_{Iq} \cdot \frac{|dV_{AC}|}{dV_{AC}} \cdot (|dV_{AC}| - db) \right] \cdot \sin \theta \right\} \cdot Scaler \quad - 35 -$$

$$I_{d_{aR\&ACI}} = \left\{ I_{d_{pre-fault}} + \left[K_{Id} \cdot \frac{|dV_{AC}|}{dV_{AC}} \cdot (|dV_{AC}| - db) \right] \cdot \cos \theta \right\} \cdot Scaler \quad - 35 -$$

$$Scaler_{aR\&ACI} = \begin{cases} 1, & I_{max} \geq \sqrt{I_{d_{aR\&ACI}}^2 + I_{q_{aR\&ACI}}^2} \\ I_{max} / \sqrt{I_{d_{aR\&ACI}}^2 + I_{q_{aR\&ACI}}^2}, & I_{max} < \sqrt{I_{d_{aR\&ACI}}^2 + I_{q_{aR\&ACI}}^2} \end{cases} \quad - 36 -$$

$$\dot{x}_{tracker} = \begin{cases} f(x) = \begin{cases} 0.2, & I_{d_i} < I_{d_{pre-fault}} \\ (I_{d_i} - x_{tracker}) \cdot K_{slow}, & I_{d_i} > I_{d_{pre-fault}} \end{cases}, & Post - fault = 1 \\ (I_{d_i} - x_{tracker}) \cdot K_{fast}, & Post - fault \neq 1 \end{cases} \quad - 37 -$$

$$I_{d_o} = \begin{cases} x_{tracker}, & Post - fault = 1 \\ I_{d_i}, & Post - fault \neq 1 \end{cases} \quad - 37 -$$

$$\dot{x}_{filter} = \frac{K \cdot (I_{d_i} - x_{filter})}{T} \quad - 40 -$$

$$I_{d_o} = \begin{cases} I_{d_i}, & fault \neq 1 \\ x_{filter}, & fault = 1 \end{cases} \quad - 40 -$$

$$P_{ZIP} = P_0 \cdot \left[a_p \cdot \left(\frac{V}{V_0}\right)^2 + b_p \cdot \left(\frac{V}{V_0}\right) + (1 - a_p - b_p) \right] \quad - 41 -$$

$$Q_{ZIP} = Q_0 \cdot \left[a_Q \cdot \left(\frac{V}{V_0}\right)^2 + b_Q \cdot \left(\frac{V}{V_0}\right) + (1 - a_Q - b_Q) \right] \quad - 42 -$$

$$P_{exp} = P_0 \cdot \left[a_p \cdot \left(\frac{V}{V_0} \right)^{e_{-aP}} \right] \text{-----} - 42 -$$

$$Q_{exp} = Q_0 \cdot \left[a_Q \cdot \left(\frac{V}{V_0} \right)^{e_{-aQ}} \right] \text{-----} - 42 -$$

$$P_{dyn} = \left(dV_c \cdot \frac{K_{p_v} + s \cdot T_{p_v}}{1 + s \cdot T_{dyn}} + 1 \right) \cdot \%_{dyn} \cdot P_r \text{-----} - 42 -$$

$$Q_{dyn} = \left(dV_{ac} \cdot \frac{K_{q_v} + s \cdot T_{q_v}}{1 + s \cdot T_{dyn}} + 1 \right) \cdot \%_{dyn} \cdot Q_r \text{-----} - 42 -$$

Chapter 1 : Introduction

1.1 Background

Traditionally the power system transports power from the power generating facilities to consumers, both industrial and residential. It is common practice to classify the transmission network into the following subsystems: transmission system, sub-transmission system, distribution system [6]. The transmission system interconnects all major generation and main load centres in the system. It forms the backbone of the integrated power system and is operated at the highest voltage levels (typically in Europe, 150 kV and above). Power is transmitted to transmission substations where the voltages are stepped down to the sub-transmission level (typically in Europe, 110 kV). The sub-transmission system is the intermediate system that transfers power from the transmission to the distribution system and feeds large industrial customers. Finally the distribution system is the last stage of energy transfer and delivers power to the individual customers. Voltages in primary distribution feeders range from 4 kV to 34.5 kV and deliver power to small industrial customers whilst the secondary feeders supply residential and commercial customers at 240 V [6].

This type of hierarchical power system structure can be defined as a vertically operated power system as described in [7]. This working principle, however, has been changing and will further change in the future. Local distributed generation (DG) sources are introduced in the network, mainly due to the integration of renewable sources. In general, DG can be defined as electric power generation within distribution networks or on the customer side of the network [8]. The power rating of these sources has large variation and many of them are connected on the sub-transmission and distribution networks; even some at the secondary feeders of the distribution network, i.e. photovoltaic (PV) on roofs.

A direct effect of the implementation of DG in the distribution grid is that electrical power is generated closer to the load which will affect the local power flow and as the penetration level of DG increases; the total amount of generated electric power can exceed the total connected load. This phenomenon will eventually lead to exporting electrical power to neighbouring distribution grids and will convert the power system into a horizontally operated one [7], as it can be seen in Figure 1.1 . The phenomenon of producing power in a lower voltage level and transporting this power to a higher voltage level through the network is called reverse power flow (RPF) and in countries with regionally high penetration of renewables, such as Germany, it is already in effect. In Figure 1.2 RPF is seen at a substation of the German distribution network.

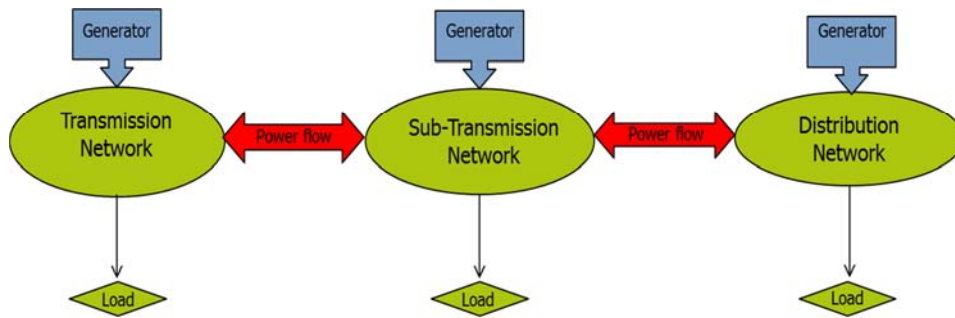


Figure 1.1: Horizontally operated power system [own representation based on 7]

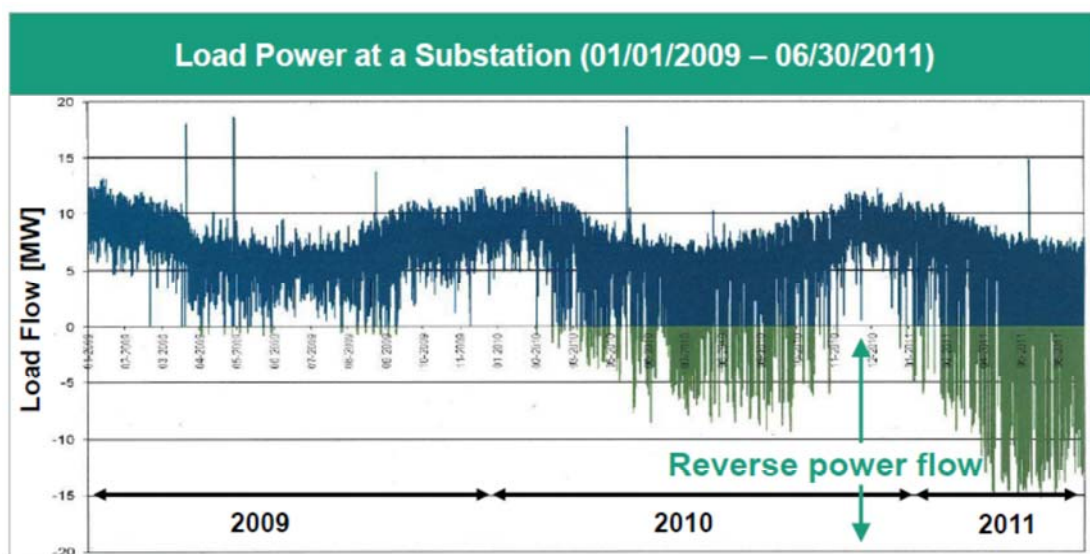


Figure 1.2: Reverse power flow in substation in a Germany [9]

1.2 Problem Definition

This transition from a vertically to a horizontally operated power system holds many potential challenges for the security and stability of energy transfer. An important challenge is the behaviour of the protective system in case of a fault, and also the load and generation balance in case of massive disconnection of DG. In general the behaviour of such a system must be thoroughly investigated under all possible circumstances to ensure proper operation.

An interesting case is a severe fault, i.e. system fault, loss of generation or circuit contingency, in the transmission level at a very high in-feed of DG power into the grid. The behaviour of the system for a serious disturbance during reverse power flow (RPF) is of special interest. The scenario mentioned above will result in a voltage dip that will propagate to the distribution system and might trigger the disconnection of connected DG in different voltage levels depending on their fault ride through (FRT) capabilities and therefore pose a threat to system stability. Network codes (sets of rules that apply to one or more parts of

the energy sector and provide for agreements by relevant network operators on various technical requirements [12]) for DG generators varies for different voltage levels and the FRT requirements are already applied for the high and medium voltage levels but not for the low voltage connected DGs [10–12].

The need for FRT capability is not yet documented for the low voltage distribution system but a lot of discussions already refer to the possibility of including FRT capabilities even for type A generators, that is power generating modules with a connection point below 110 kV and maximum capacity of 0.8 kW or less [13]. The realization that an increase in the capacity of installed DG power in the specific voltage level can trigger disconnection, in case of transmission faults, of massive amounts of power from DG and jeopardize system stability is forming.

Numerous organizations are starting to consider FRT important for lower voltage levels and smaller generators, amongst them the VDE Association for Electrical, Electronic and Information Technologies e.V, the European Network of Transmission System Operators for electricity (ENTSO-e) and the European Committee for Electro-technical Standardization (CENELEC) [14–18].

1.3 Objective and Research Questions

The objective of this thesis is to investigate the response of low voltage distribution systems with high penetration of PV in case of a fault in the transmission system and define a FRT voltage curve appropriate to low voltage connected PV.

The research questions are:

- If current requirements are applied will the system stay within reasonable stability boundaries? Or will it be lead to instability?
- If so, what are the necessary measures that the TSOs and/or DSOs need to take in order to avoid this possibility? Is FRT capability important and relevant for the low voltage distribution system?
- What are the critical power flow situations that would lead LV connected DG to disconnect in case of transmission and sub-transmission faults?
- What is the sensitivity of the voltage, during fault, in low-voltage networks with large amounts of generation from LV connected DG installations w.r.t. network topology and behaviour of the PV installation?
- Which amendments to interconnection standards (grid codes) of DG in low-voltage networks are recommended?

1.4 Research Approach

The problem will be analysed through root mean square (RMS) stability simulations performed on appropriate models of the network and the DG. The projected year that this study takes place will be 2022 and the DG capacity will be chosen for that year. The model

will be implemented as a benchmark system with DG capacities chosen to match the German network. The commercially available DIgSilent PowerFactory software version 14.1 will be used to carry out these simulations. Furthermore a sensitivity analysis will be performed w.r.t. load, generation and behaviour of PV to transmission system faults. Selected simulation results will be presented in graphs and analysed. These results will provide the basis for implications on grid connection requirements for low voltage connected DG's and finally recommendations for future grid connection requirements for low voltage installed DG will be given.

A good candidate for a case study is a network that has, regionally, a high penetration of DG. In our case the German network, which has been pioneered in renewable integration and has a major amount of photovoltaic installed power in the low voltage distribution network will be considered. The following graphs (Figure 1.3, Figure 1.4) are indicative of the development of installed PV power over the last decade and the foreseen development based on a linear projection. Numerous reasons have led the increase of solar PV plants capacity over the last 15 years. Most significant reasons are cost reduction of PV modules, market incentives for electricity production, social awareness about global warming etc.

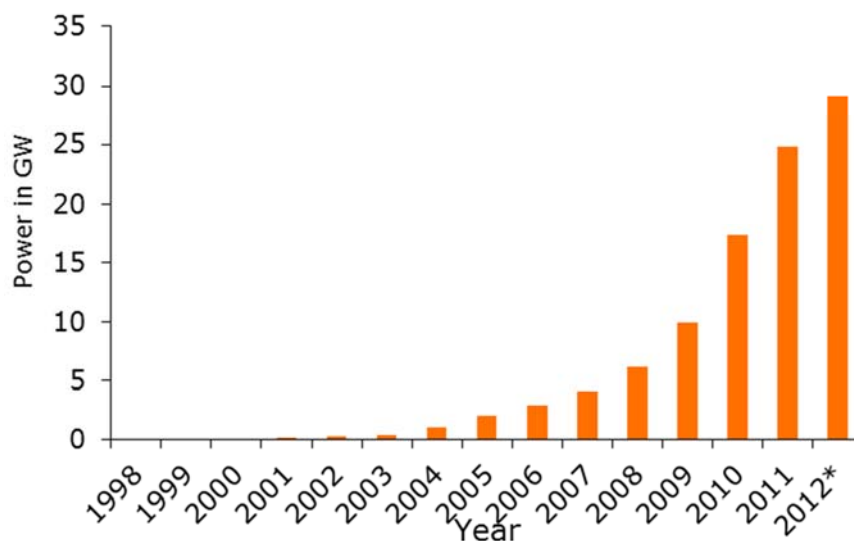


Figure 1.3: Installed PV power in Germany (1998-2012) [19]

From these graphs it is clear that PV deployment has been massive in the German network: The installed photovoltaic capacity in Germany on the 31st of January 2013 was 32,663 Mwp according to [20]. Moreover by the end of 2010, approximately 80% of cumulative installed photovoltaic (PV) capacity, roughly 14 GW, was connected to the low voltage distribution level, as reported by [21]. The high penetration of PV in the German network justifies the choice of this network for this study.

The conclusions that will be drawn from this research will not only be restricted to the specific network but to all networks that share similar characteristics and have a high amount of installed DG power. The choice of benchmark networks used ensures that all other network characteristics will be similar to most of the European networks.

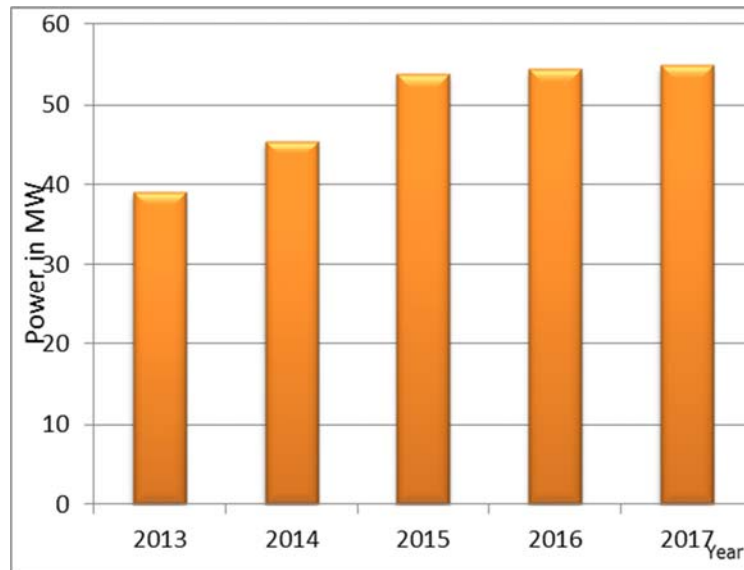


Figure 1.4: Projected progress in installed PV power in the German grid (2013-2017) [22]

1.5 Outline of the Thesis

Chapter 1 gives an introduction to the study topic. In this chapter the background for the research topic is explained, and the objective and research questions of the thesis are stated.

In Chapter 2 the literature survey is presented. The important, for this study, power system stability issues are explained, and an analytical research on current grid codes is presented. The impact of FRT criteria on line and generation protection is discussed as well as the current state of photovoltaic system inverters.

In Chapter 3 the test system used for this study is presented. The modelling approach of different networks for different voltage levels is explained. The analytical model of the PVPPM is presented along with all the additions for FRT capability. Finally the WPP model and the modelling of the loads are described.

In Chapter 4 the case study and the simulation results are presented. The scenarios for the installed DG capacity of the system are presented. The choice of sensitivity factors that formulate the different study cases is justified and the sensitivity factors are explained. The presentation and analysis of results for different study cases follows.

Finally, in Chapter 5 the conclusions drawn from the results are discussed. Also recommendations for further research are proposed. The general findings of the research are presented first and then the implications for German grid codes and the German network are presented. The recommendations for future work close this chapter.

Chapter 2 : Literature Survey

2.1 Power System Stability

Power systems stability is the ability of an electric power system, for a given initial operating condition, to regain a state of operating equilibrium after being subjected to a physical disturbance, with most system variables bounded so that practically the entire system remains intact [23].

In order to understand in depth the term power system stability, it is important to have an overview of the operating states of a power system as seen in Figure 2.10.



Figure 2.1: Power system operating states [6]

The five operational states of the power system are: normal, alert, emergency, in extremis, and restorative. In the normal state, all system variables are within the normal range and the system is able to withstand a contingency with no overloading of equipment. The alert state is the same as the normal state but a possible contingency can cause problems in the network. If a sufficiently severe disturbance occurs when the system is in the alert state then the emergency state is entered, where voltages at many buses are low and/or equipment loadings exceed short-term emergency ratings. Then emergency control actions take place: fault clearing, excitation control, generation tripping, generation run-back, HVDC modulation, and load curtailment. If the above measures are ineffective, the system is in extremis; the result is cascading outages and possibly a shut-down of a major portion of the system.

Control actions, such as load shedding and controlled system separation, are aimed at saving as much of the system as possible from a widespread blackout. Finally the restorative state is reached when actions aim at connecting all the system and restoring the problems [6]. The state we are interested in is the emergency state and how to define correctly FRT criteria in order to avoid moving into the in extremis state.

Therefore for our modelling, fault clearing time and fast control actions are relevant to describe the situation during and immediately after a fault. We propose classifying the stability studied in this thesis as large disturbance voltage stability for the transient fault

response of the system. We are interested in checking whether bus voltages are kept within limits in order to avoid major loss of DG generation due to under voltage protection during a fault. The study period is short term and can reach up to tens of second if the post-fault system is included. This classification is shown in Figure 2.2, where the relation between a short term study period and large disturbance voltage stability is shown.

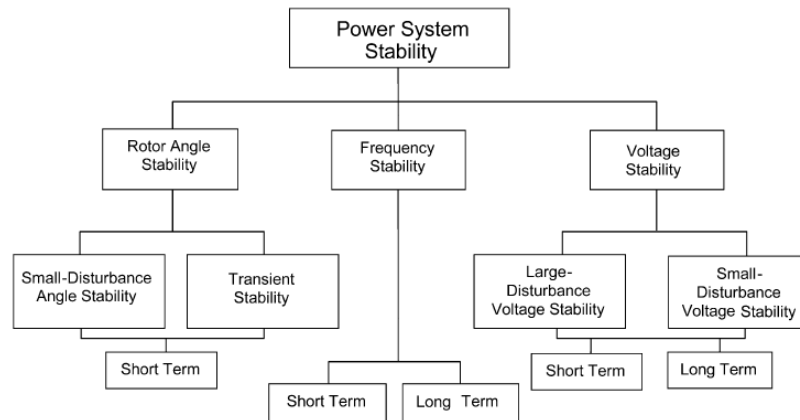


Figure 2.2: Power system stability classification [23]

Most definitions for voltage stability refer to longer time frames and incorporate the response of OLTCs (On-Load Tap Changers) and generator field-current limiters [6]. However transient stability refers to the short transient period but deals mainly with rotor angle stability and not voltage profiles. “Solid-state inverters do not behave like rotating generators. Solid-state inverters have no inertia in their output and can respond immediately to changes in the ac power system.” [24]. Based on this claim we can say that the lack of inertia of an inverter may be the reason why we cannot easily classify our stability issue. However the classification of stability that is based on [6, 23] in our study is large disturbance voltage stability.

On the other hand DGs ability to solve network problems has been debated for distribution networks. Unfortunately, the distribution system operator (DSO) has no control or influence on DG location and size below a certain limit. Nevertheless, DG placement impacts critically the operation of the distribution network. Inappropriate DG placement may increase system losses and network capital and operating costs. On the contrary, optimal DG placement can improve network performance in terms of voltage profile, reduce flows and system losses, and improve power quality and reliability of supply [25].

There are more benefits that DGs can offer in terms of power system stability. If power electronic converter (PEC) coupled DG’s are disconnected from the network during fault, then maximum rotor acceleration is restricted and thus transient stability is benefited. On the other hand large penetration levels of DG result in imbalance of load and production during fault if the same practice is followed, resulting in poor frequency and voltage stability. However, keeping the DG connected can help damp out oscillations faster post-fault due to the immediate reaction of the PEC that is not bound by its inertia, which can supply reactive

power during fault and contribute to the fault current. In contrast to electrical machines the short circuit current of a PEC is limited by its protection and exceeds the nominal current only slightly [26]. All these results are presented in [27].

To mitigate the effect of DG on power system stability grid operators have defined fault ride-through criteria for DG (see section 2.2). These criteria are already in effect for power plants connected to higher voltage levels but now also become operational for DG connected to distribution grids. Fault ride-through criteria define for what voltage dips with specific duration the DG have to stay connected to the grid. Depending on the size of the DG-unit the fault ride-through criteria can also require additional grid support, such as voltage and frequency support, during and after a disturbance.

2.2 Grid Codes and Fault Ride-Through Requirements - Status Quo

An important feature of grid connected power generating facilities is the Fault Ride-Through (FRT) or Low Voltage Ride-Through (LVRT) capability, defined in [1] specifically for PVs as the: "PV inverters' capability of remaining connected to the grid in the event of grid failures, of not supplying any active power during a grid fault, and of delivering active power directly after clearing the fault, thus stabilizing the grid". Secondly there is the capability of injecting an additional reactive current into the grid in case of grid fault, with the purpose to provide voltage support during fault conditions.

Some German grid codes (GC) have already specific requests for inverter coupled DG's. These requirements have arisen from the large penetration of PV technology in the German grid. The way DG was regarded by TSO'S in the past was as a passive component; thus not allowed to take any type of action during fault. However more contemporary grid codes change this view and introduce FRT criteria for PV plants connected to the MV (since 2009) [5] sub-transmission network and transmission network (since 2007) [28]. Within these codes solar plants need to be able to sustain certain amount of voltage dips for specific time frames without disconnecting from the grid. The basic type of requirement is provided as a voltage versus time graph at the grid connection point for a generating facility depicting the behaviour of a system within certain areas of the limiting voltage curves, an example can be seen in Figure 2.3 [28]. An alternative approach is presented at [3] where a different type of curve for voltage profiles that defines FRT requirements is presented. The cumulative severity-duration type of specification is more closely associated with the actual stresses on equipment and the actual behaviour of many protective relays [3].

Besides meeting the specifications for FRT curves during the fault period there is a requirement for solar plants to provide additional reactive current injection in order to aid in maintaining the voltage profile of the network. Maintaining the voltage profile of the network by limiting the dip-depth is desirable during a fault because it prevents disconnection of old generation plants (e.g. wind farms) that are not able to ride through a fault and in general limits the severity of the fault as seen by all power generating facilities.

In the German GC for medium voltage networks, entering into force on April 1st, 2011, PV plants have to be capable to participate in complete dynamic network support during

grid faults [29]. Complete dynamic network supports is defined as voltage control in the event of faults in the high and extra-high voltage network that result in voltage dips in the medium and low voltage networks aiming at avoiding unintentional disconnection of large feed-in power, and thus network collapse. That means that generating facilities must be able in technical terms:

- Not to disconnect from the network in the event of network faults
- To support the network voltage during a network fault by feeding a reactive current into the network,
- Not to extract from the medium voltage network after fault clearance more inductive reactive power than prior to the occurrence of the fault [10], [5].

The voltage profiles in the following figures refer to a type II generating unit [28], defined as all generator units that are not synchronous generators directly connected to the network.

In Figure 2.3 the MV voltage FRT requirements are shown in novel graphs based on the technical guideline for generating plants connected to the medium-voltage network by the German Association of Energy and Water Industries (BDEW) [5]. The requirements specify that voltage dips with values above the red dashed line must not lead to instability or to disconnection of the generator from the network. In the area between the two red lines generating units should pass through the fault without disconnecting from the network. Furthermore, in consultation with the network operator, a short-term interruption (STI) from the network is allowed if the generating plant can be resynchronized within 2 seconds, at the latest, after disconnecting. The STI term was originally used for a wind turbine generator (WTG) of specific manufacturers where the generator concept used a crow-bar at the stator [2]. After resynchronization, the active power must be increased with a gradient of at least 10 % of the nominal capacity per second. Below borderline 2, a short-term disconnection of the generator may be carried out with longer reconnection times and lower gradients of the active power in comparison with the previous case. Below the blue line no requirements for FRT apply.

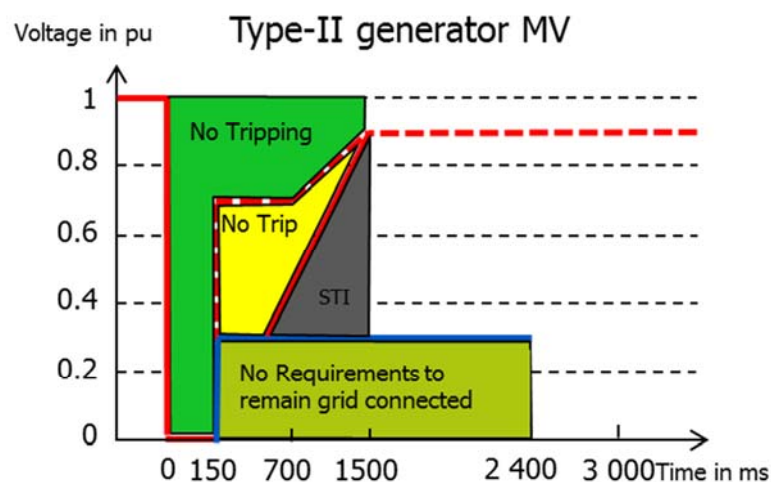


Figure 2.3: FRT requirements for type II generators in the German MV network

In Figure 2.4 the respective HV FRT requirements are shown based on [28]. The green, yellow and grey areas correspond to the same requirements presented for the MV network. The area between 1.5 and 2.4 seconds corresponds to stepwise tripping of the faulted generators within the plant. The main difference, however, is the lack of the blue line and, therefore, the HV FRT requirements are slightly stricter than the MV FRT requirements.

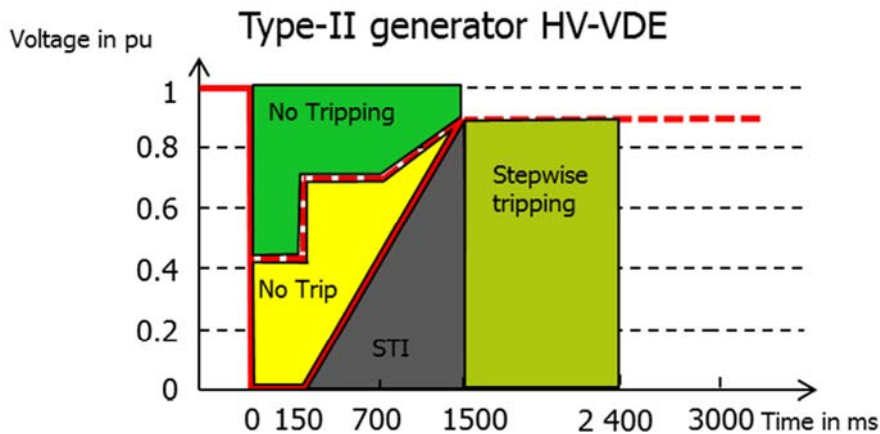


Figure 2.4: FRT requirements for type II generators in the German HV network

Therefore in the MV and HV networks FRT criteria are already in effect for DG. However that does not hold true for the LV distribution network. In the LV network DG units are required to intentionally disconnect from the grid during a dip. The two most relevant and important standards are the IEEE-Std. 1547 that was created in 2003, and the VDE-AR-N 4105-Std. from 2011. Both of these standards require a mandatory disconnection of LV connected DG during fault. The disconnection is based on the OR logic, by monitoring all phases separately, if one phase is below the voltage threshold set from the protection device then the module disconnects [10, 11].

The fundamental drivers for these standards were many. An important concern was the possible interference of the DG units with the protection schemes of the network. Another reason is the sensitivity to over-currents and over-voltages by the power electronic converters (PECs) coupling the DG units to the network [26]. Furthermore these standards were created at a time when high penetration of DG was not envisioned. Therefore as observed in [30] the mandatory disconnection requirement negatively impacts bulk system reliability in a high DG penetration scenario-where excessive loss of generation might result in system instability. Moreover certain categories of DG, e.g. PV, can use the reactive power capability that the power electronics converter (PEC) provides to ensure minimum deviation in their voltage profile at the point of common coupling (PCC),- point in the public network closest to the customer system to which further customer systems are connected or can be connected [10],- however based on IEEE-1547 standards DG may not change their reactive power output in direct response to the magnitude of the voltage [31].

At this point it is good to observe that these standards are merely guidelines that need to be revised and reconsidered continuously to be kept up to date. The hypothesis that in networks with a large DG penetration level the disconnection of all DG units can cause

serious problems as it may result in a large power generation deficit and in stability problems is worthy of investigation. In addition a draft of the ENTSO-E Network Code “Requirements for All Generators” included a requirement even for type A units, which are generating units with 0.8 KW rating or more connected in 110 KV or lower voltage level, not to trip in vast numbers simultaneously in response to a single fault at the highest voltage level [13]. Even though this opinion of the ENTSO-E did not become part of the final Network Code, it reveals the need for a deeper insight. Furthermore in [15] ENTSO-E welcomes the intention of CENELEC to introduce a FRT requirement for generators connected at medium and low voltages ($>16A/\text{phase}$), which would also extend to include type A generators. Furthermore CENELEC states that the industry is ready for this requirement as many technologies have this capability already. Finally new requirements of FRT for PV systems connected to a single phase on the -200V- low voltage distribution feeder were recently investigated and proposed to cope with expected future large penetration. This analysis occurred as part of Japanese research governmental program contracted with the NEDO, Japan’s largest public R&D management organization [32].

2.3 Impact of Fault Ride-Through and Additional Reactive Current Injection During Fault on Line and Generation Protection

When defining new requirements for network connected devices it is very important to take into account the impact these measures will have on the device itself and the whole network. This section focuses on the latter. Important parts of the network are the protection devices and schemes used to ensure proper function of the network during faults. In order to understand the impact of these criteria on the protection system of the network a better understanding of how protection devices work is needed.

On the distribution level simple protective schemes are used and their operation focuses on the detection of a fault current significantly larger than the nominal current of the grid components [7]. The protection relays used for such a task are the over-current relays. To operate this relay only the current has to be measured. When the current exceeds the set limit, it triggers a trip signal that is sent to the circuit breaker disconnecting the faulted line. However, different relay characteristics based on the principle of operation can be developed by varying pick-up current and time response of the device. Two important features of the protective system are selectivity and sensitivity. Meaning that the protective system must be sensitive enough to faults but also disconnect the least part of the network needed to clear a fault without interfering with the healthy part of the network. For that reason, most protective systems overcurrent relays have to be coordinated with other protection devices [7].

It is not in the focus of this Thesis to go into lengths analysing the protection mechanisms but rather to provide a fundamental insight of the principle of operation in order to assist in the understanding of the interference of the FRT and reactive current injection of the DG units on protection. However the most important protection schemes are explained:

- Re-closure fuse coordination

Based on over-current relays that are commonly used on overhead lines where brief interruption and quick reconnection is desirable due to non-permanent faults, e.g. lightning.

- Differential protection

Two current quantities are measured on either side of a protected element. If the currents are not equal then the element is disconnected, examples of elements for the use of this protection device are transformers and bus bars. A drawback of this protection mechanism is the need for a communication channel to compare the current quantities. When the distances between the current transformers are large, as it would hold for transmission lines, this can lead to high costs.

- Distance protection

A protection device is used which makes use of the linear relation between U and I. Voltage and current are measured in order to calculate impedance. A change in the ratio indicates a physical alteration in the existing circuit and thus it is de-energized [7].

For readers that wish to learn more on protection, chapter 3.4 from [7] has a description of a protective system for simple radial and meshed grids indicative of European grids.

The added requirement that is already incorporated into the MV and HV grid codes of Germany is the additional reactive current injection (aRCI) from DG generators during a fault. The fundamental concept behind this requirement is that due to the high X/R ratio of the transmission and distribution networks, reactive current raises the voltage level of the network. As seen in [33] the higher the X/R ratio the reactive current contributes more to raising the network voltage. The concept can be easily demonstrated through a simply radial network representation as shown in Figure 2.5.

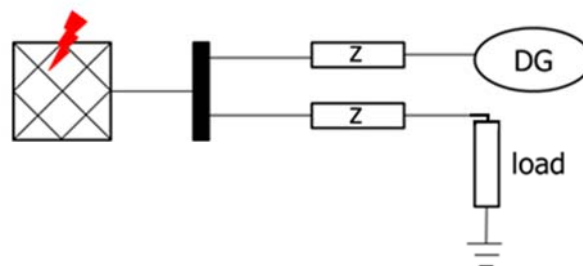


Figure 2.5: DG connected to the grid-impedance of impedance in aRCI

Assume that during the pre-fault period active power is pushed into the transmission system by the aggregated DG and in order to limit the voltage rise DG is consuming reactive power. During a fault inside the transmission network the voltage of the bus bar is lowered significantly by the propagation of the voltage dip to the distribution system. In order to

raise the voltage a reactive current component additional to the pre-fault value is provided by the DG and, therefore, the total reactive current consumed at the bus bar is decreased and can even become negative, i.e. reactive power is fed into the network. Therefore the reactive current that is passing through the reactance of the lines is raising the voltage levels at bus-bars between the fault and the PCC. The requirements for aRCI are shown in Figure 2.6.

According to this requirement DG generators have to supply at least 1.0 p.u. reactive current when the voltage falls below 50 %. A dead band of 10 % is introduced to avoid undesirable control actions [34] and to prevent conflicts with power factor control during steady state.

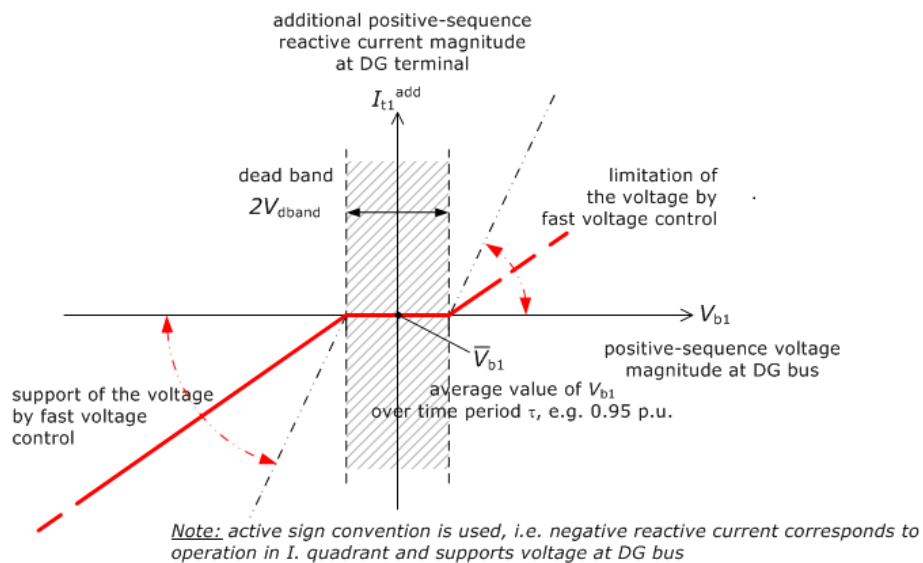


Figure 2.6: Reactive current support during fault [34]

After explaining the principles of protection and introducing aRCI we have all the tools to understand the reason FRT requirements can disrupt the current protection mechanisms. Integration of DG not only alters the power flow but will also change the fault currents in the distribution grid. These changing fault currents can affect proper operation of the current protective system. The three main issues we can identify are false tripping, blinding of protection and reverse fault currents.

For these reasons the standard practice, up to a few years back, taken by grid operators was to demand immediate disconnection of the DG-units in case of a fault or short-circuit. Immediate disconnection of DG-units restore the distribution grid to a grid with only one source of supply and the protective system can function as it was implemented to do so during the design stage of the distribution grid [7]. The under-voltage protection of the DG would disconnect them from the network, however due to the large penetration level of DG this practice is not applicable any more for the HV and MV networks. False tripping can occur in case of a faulted feeder when DG connected to this or adjacent feeders can contribute to the fault current and as a result, the protective system of the respective feeder would unnecessary disconnect healthy feeders. The schematic representation of Figure 2.7 can assist in understanding this phenomenon. The DG located on the adjacent feeder of the

faulted one feeds current to the fault location. This current can exceed the pickup current of the DG feeder protection and disconnect the healthy (DG) feeder.

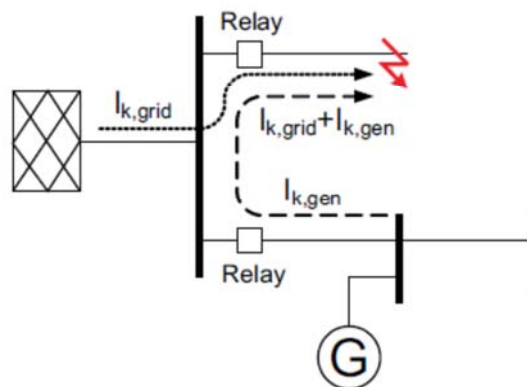


Figure 2.7: False tripping [7]

Blinding of protection can also occur in some situations as it is seen in Figure 2.8. The fault occurs in location 1, and due to the fault current provided by the DG the grid contribution to the fault current can stay undetected by the overcurrent relay in the beginning of the feeder thus failing to disconnect the faulted feeder from the rest of the network.

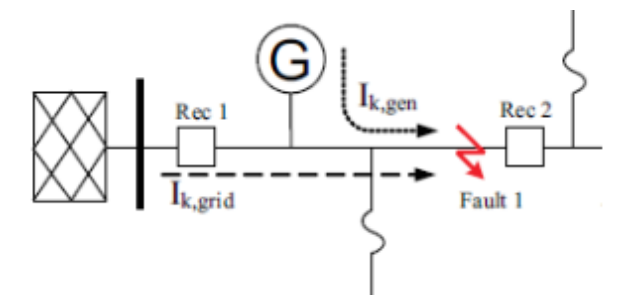


Figure 2.8: Blinding of protection [7]

The previous issues while valid are out of the scope of this thesis as they are referring to faults on the distribution level, while we are considering faults on the transmission level. However there are a lot of proposed solutions to overcome these issues and interested readers can find these solutions in [7, 24]. Morren [33] even disagrees with the statement that DG can prevent the proper operation of the feeder protection and proves that converter based DG can limit their current during a fault and, hence, minimize the influence on the network protection. The issue that is relevant for this Thesis is the reverse power flow during fault that can disrupt the protective system.

In radial distribution grids normally there is only one source of supply and application of overcurrent relays as protection devices are prevalent. However, selective protection with overcurrent relays of distribution grids with a meshed structure, or when bi-directional fault currents occur can cause undesired disconnection of circuits. To provide proper protection of these grid structures and cope with bi-directional fault currents a directional element has

to be added to the overcurrent relay. This directional element determines the direction of the power flow in the associated distribution feeder. The power flow direction is determined with a reference signal which is often a voltage.

These relays will issue a trip signal to the circuit breaker when both the direction setting and the current pick-up value are met. So these relays are set in the same manner as simple overcurrent relays but also a specific direction is chosen. By using two relay set ups, each for different direction, for each line the protective system can be adapted to handle bi-directional currents while ensuring sensitivity and selectivity. This adaptation is adequate to ensure that transmission faults with FRT criteria for DG on the LV distribution system will not disrupt the protective mechanisms of the network [7].

2.4 Photovoltaic Systems – Current Settings and Operational Performance

2.4.1 Equation of a PV array

The energy captured from a PV array is proportional to the irradiance and depends upon the location of the operating point of the solar panels. The formula that describes the relationship between current and voltage in a PV array is given (Equation 2-1).

$$I = n_p \cdot I_{ph} - n_p \cdot I_d \cdot \left(\exp \left(\frac{V_{pv} - R_s \cdot I_{pv}}{n_s \cdot V_T} \right) - 1 \right) \quad \text{Equation 2-1 [35]}$$

With V_{pv} : PV array output voltage

I_{pv} : PV array output current

n_s : Number of panels in series

n_p : Number of panels in parallel

I_d : Dark saturation current

R_s : Cell series resistance

I_{ph} : Photo-generated current

V_T : Junction thermal voltage

In Figure 2.9 a graphic representation of this formula for a given temperature and irradiance is depicted. The operating point in this curve can be shifted and the power production is changed accordingly.

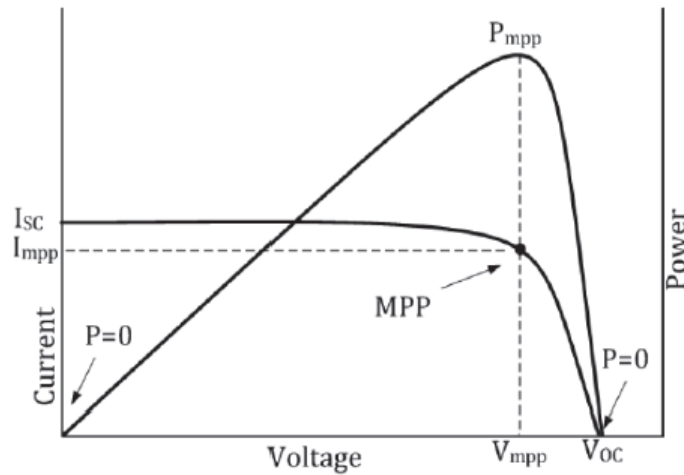


Figure 2.9: PV array current-voltage curve with power output [35]

2.4.2 Modelling of a PV system

For maximization of produced power the usual practice is to use an algorithm that shifts the operating point of the curve of Figure 2.9. The algorithm is called maximum power point tracking (MPPT) and it is applied on the DC/DC converter that connects the output of the PV panels to the DC/AC inverter that is used for grid connection. This set-up is called a two stage PV systems, which is a PV system with a DC/DC converter and a DC/AC inverter. In one stage PV systems (only inverter) this function is performed by the DC/AC inverter. This algorithm is modulating the frequency of the switching elements inside the DC/DC converter to regulate the DC link voltage.

The phase locked loop (PLL) algorithm that is implemented on the DC/AC inverter is of great importance to the PV grid connection. This is because it must guarantee the synchronization of the inverter voltage vector with the grid voltage vector, through the detection of its phase angle. The grid voltages are the input into the algorithm and they are transformed into synchronous reference frame by means of the abc / dq transformation module. The phase locking is realized by controlling the d-voltage component to be zero. U_d is compared with its reference value and with a PI regulator the value of grid frequency is calculated. After the integration of the grid frequency, the voltage angle is obtained. Nowadays, the PLL technique is the state-of-the-art method to extract the phase angle of the grid voltages [1].

A representation of the state-of-the-art PV inverter system can be seen in Figure 2.10. It uses both PLL and MPPT algorithms. Concerning LVRT capability, we must consider that the main reasons for inverter disconnection during voltage dips are excessive DC voltage, overcurrent due to low voltage (in constant P operation), and loss of synchronism [1]. In particular, overcurrent occurs because the DC link voltage control is generally designed to keep the DC voltage equal to the reference (MPP). In this way, the active power is always constant resulting in distorted current when the voltage is unbalanced. However modern inverters are capable of enforcing FRT without encountering problems.

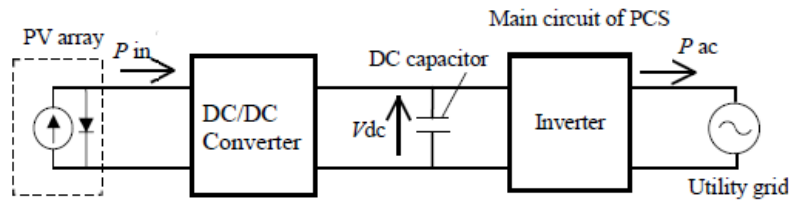


Figure 2.10: PV inverter system[32]

In our modelling of the PV inverter we are going to use a DigSILENT PowerFactory model developed by Samadi [36]. In the paper by Samadi the model is validated in comparison with a PSCAD model to ensure that the results from an average modelling program such as PowerFactory do not have any significant difference with an EMT model. The PLL algorithm and the MPPT are included, as well as active and reactive power control. More details for the model will be discussed later on.

In general the protection mechanisms that disconnect the DG in low voltage distribution networks are under and over voltage (and also frequency) protection. It is within the scope of the modelling to represent the protection mechanisms that disconnect the PV plant from the network, also known as generation protection. The timings according to the VDE-AR-N 4105 standard for low voltage connected generators are presented in Table 2.1.

Voltage/Frequency at PCC	Maximum Trip Time	Circuit Breaker Time
$V < 0,8 \times V_n$	$< 0,1 \text{ s}$	$0,1 \text{ s}$
$V > 1,1 \times V_n$	$< 0,1 \text{ s}$	$0,1 \text{ s}$
$F < 47,5 \text{ Hz}$	$< 0,1 \text{ s}$	$0,1 \text{ s}$
$F > 51,5 \text{ Hz}$	$< 0,1 \text{ s}$	$0,1 \text{ s}$

Table 2.1: Timing for tripping of generation protection [10]

When we apply the standards used nowadays, the protection is set to disconnect DG from the network in the event of a fault based on Table 2.1 values. But when FRT criteria are developed these values have to be adapted to ensure that the protection devices do not disconnect the DG from the network before a set time.

Furthermore the existence of a DC/DC converter will not be modelled because, although it is part of the DG interface with the network, its dynamic response is so fast that it can be ignored without a problem. Typical response times are in the order of 5 ms as known from discussions with SMA and TU Braunschweig [37].

Finally it is worth noticing that in [32], results have shown that post-fault there are some inverters that disconnect due to under voltage of the DC link. As explained in [32], this phenomenon occurs at voltage recovery due to rapid ac voltage rise at PCC resulting in a DC under-voltage. However the discussions with SMA and TU Braunschweig revealed that for the European PV market portfolio such behaviour is not relevant.

2.5 Types of Faults

The faults we are considering in this thesis are transmission system faults. These faults occur at the HV network and the related voltage dip may propagate throughout the sub-transmission and distribution network. A voltage dip propagation results in an under voltage in the bus bars of the low voltage connected DG, whose behaviour we wish to investigate under fault. The clearance time (CT) of the fault in the HV network is very small. Values between 90 and 120 *ms* are common [7], however to ensure a proper safety margin and based on the existing FRT curves a value of 150 *ms* for CT is chosen in the simulations.

The types of faults that we will consider are only symmetric three phase faults which are the most severe ones from the network perspective. These types of faults are also easier to study given that we have a three phase PV system model. Also the propagation of the voltage through different transformers does not affect the voltage profile in these types of faults.

2.6 Conclusions

In this chapter the literature survey was presented. The nature of the investigation in terms of network stability was explained, also the current grid code standards were analysed as well as the current state of PV inverters technology. The importance of protection scheme choice was analysed and the possibility of interference with DG behaviour in case of a fault. Finally the reasoning for the choice of type of fault study is presented.

Chapter 3 : Test System and Distributed Generation Modelling

3.1 Introduction

In this chapter the modelling approach of the study is explained and a detailed review of all components of the test system is included. Initially, the structure of the test system comprising of different voltage levels is presented. This setup allows for a systemic approach and analysis of photovoltaic power park modules (PVPPM) contribution to system performance and stability. The second essential component is a realistic model of a PVPPM with adequate control functionalities able to perform different levels of dynamic voltage support. This model will aid in understanding and evaluating the impact of low voltage connected, inverter-coupled, generators contribution to system stability during transmission faults. The wind power plant (WPP) used is also described as well as load and line modelling.

3.2 Structure of the Test System

The structure of the test system is presented in Figure 3.1. The different voltage levels are marked from the extra-high voltage (eHV) network (blue) to the low voltage (LV) network (green).

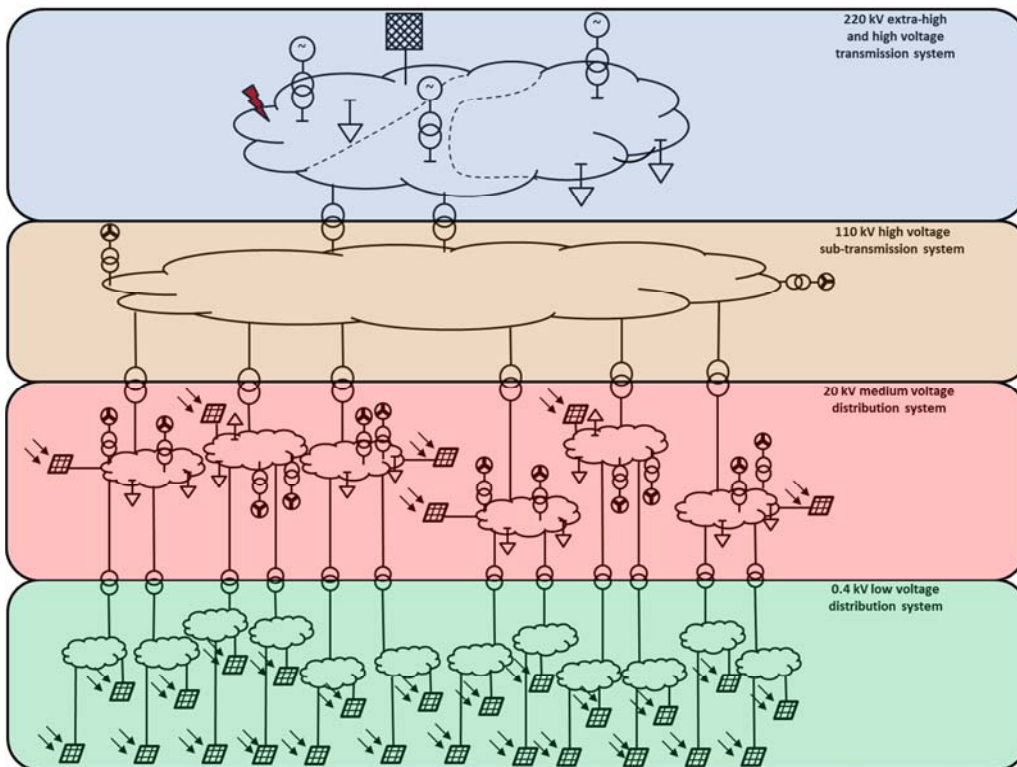


Figure 3.1: Structure of the Test System

The eHV network (220 kV) has one connection point (two transformers) to a HV transmission ring (110 kV). This transmission ring connects to six identical MV networks.

Each one of them connects to two LV networks. This structure represents a complex multilevel system approach to resemble an actual power system.

Each voltage level encompasses various types of elements including synchronous generators, loads and distributed generation (DG). Loads are present in all voltage levels whereas synchronous generators are only placed on the eHV network. WPPs are placed in the High Voltage (HV) and Medium Voltage (MV) networks and PVPPM's in the MV and LV networks. Existing Cigré benchmark networks are used to create this system and will be presented in paragraph 3.2. In general the test system is used to create a combination of networks (lines, loads, transformers) with synchronous and/or distributed generation.

The aim is to investigate how the low voltage connected PVPPM controls will affect system stability following a network fault in the transmission system. The added value of using such a complicated network is the expectation to be able to recognise more realistic interactions that are present in an actual network rather than focus on the fundamental relationships between different components.

3.3 System levels

3.3.1 IEEE 39-Bus, 10-Machines new England network

The eHV network chosen for this study is a DigSILENT PowerFactory model of the 39-bus 10-machines New England network validated by IEEE, for stability controlled performance [38]. The single line diagram of the network is shown in Figure 3.2.

The network has 10 generators connected in different busbars (BB) via step up transformers. The nominal frequency was 60 Hz. Voltage level of the received network was originally 345 kV but was changed into 220 kV and 50 Hz in order to resemble the German transmission system. The voltage at the generation buses is 22 kV. The connection point with the under laying integrated HV, MV, LV network is placed at BB 8 (blue arrows) via two 150 MVA transformers.

The connection point for the HV network was chosen after short circuit power (SC) calculations. The SC capacity of a busbar is the product of the magnitude of the pre-fault voltage and fault current. It is a measure of the strength of the system at that connection point and, therefore, of the ability to retain its voltage under system faults; on the other hand, the busbar with the lowest SC capacity will be the one affected the most by the response of the distribution system. In order to consider the worst case, the weakest BB is chosen. The most important parameters of the network are presented in Table 3.1, more details can be found in Appendix A.

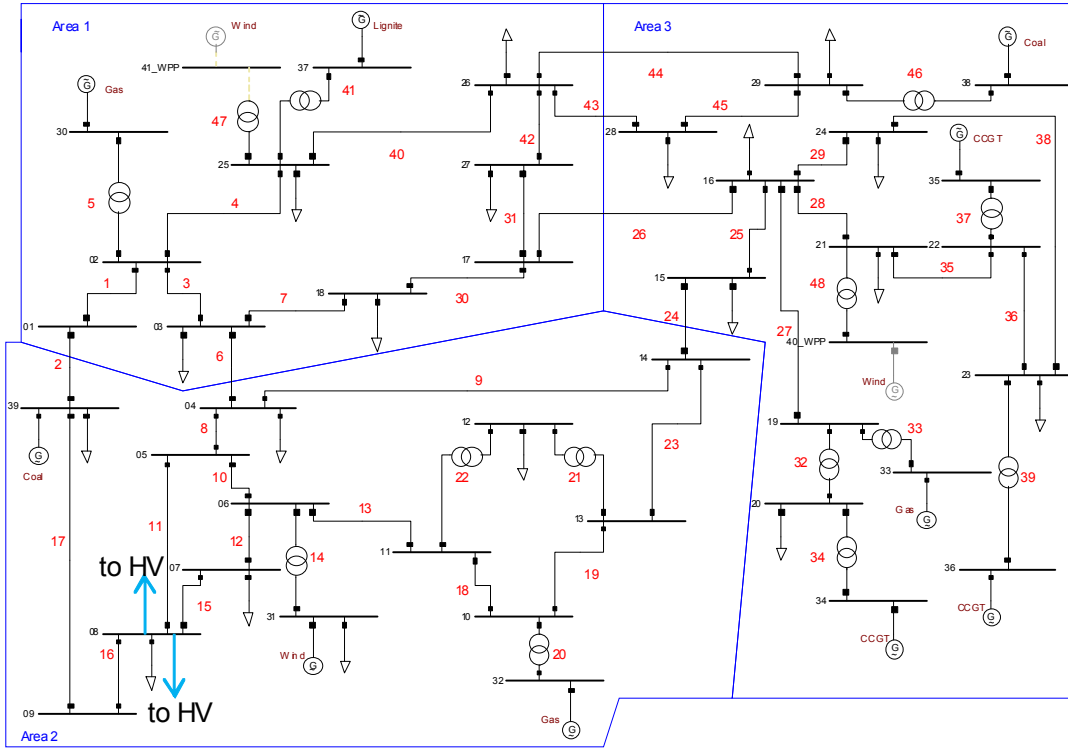


Figure 3.2: IEEE 39-bus, 10-machine New England test system [39]

Total MVA Generation	Total MW Load	Average Load power factor	Short circuit power at BB 8
5 960 MVA (excluding slack generator)	6 097 MW	0.915 inductive	6 000 MVA

Table 3.1: eHV important data overview

3.3.2 Typical German sub-transmission 110 kV ring network

The HV network, Figure 3.3, is a 110 kV sub-transmission ring implemented according to [40]. It represents a typical sub-transmission level of the German network consisting of six buses. Every bus connects to a different MV network through two transformers with 25 MVA of capacity each. Buses three and five are connected to the eHV network via the three-winding transformers. Buses two and six have a WPP connected each, the ratings of which are given in Table 3.2. The analytical data for this network can be seen in Appendix B.

Bus	WPP Rating
3	50 MW
5	50 MW

Table 3.2: HV Wind Power Parks Ratings

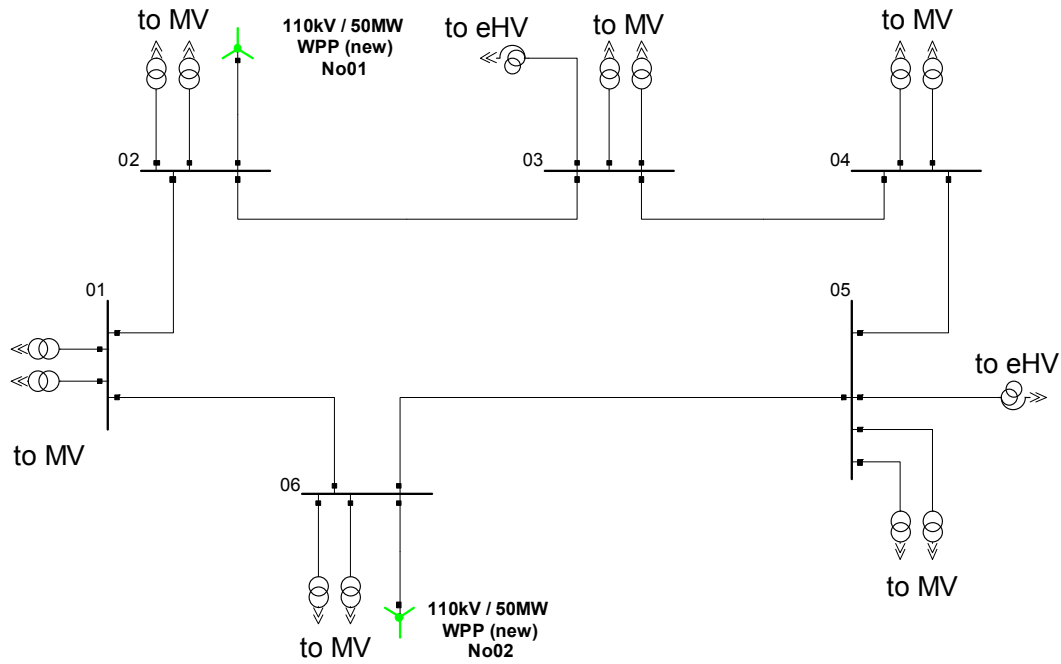


Figure 3.3: 110 kV Sub-transmission ring [40]

3.3.3 CIGRÉ medium voltage benchmark network

The MV network used in this study was chosen after an extensive comparison of different systems presented in literature [41–47]. The Cigré medium voltage (MV) distribution benchmark network is derived from a physical MV network in southern Germany, which supplies a small town and the surrounding rural area. Due to the focus of this thesis on the German situation and the previous use of this system in DG integration studies the Cigré MV benchmark was chosen, Figure 3.4, as presented in [47].

The network consists of 14 nodes with a rated voltage level of 20 kV. It is connected to the HV network through two 110/20 kV transformers of 25 MVA capacity. Each of the six MV network „clones” used in this study connect to a different busbar of the HV network. The line modelling along with the load modelling and values of installed capacity were implemented based on the [47]. The details can be found in Appendix C.

In each of the MV networks one wind power plant is connected at busbars 8 and 9 respectively and two photovoltaic power plants are connected on each of busbars 6 and 12. The ratings and connection points are shown in Table 3.3. The choice for the installed power of the DG followed a statistical analysis of data from the German situation [48].

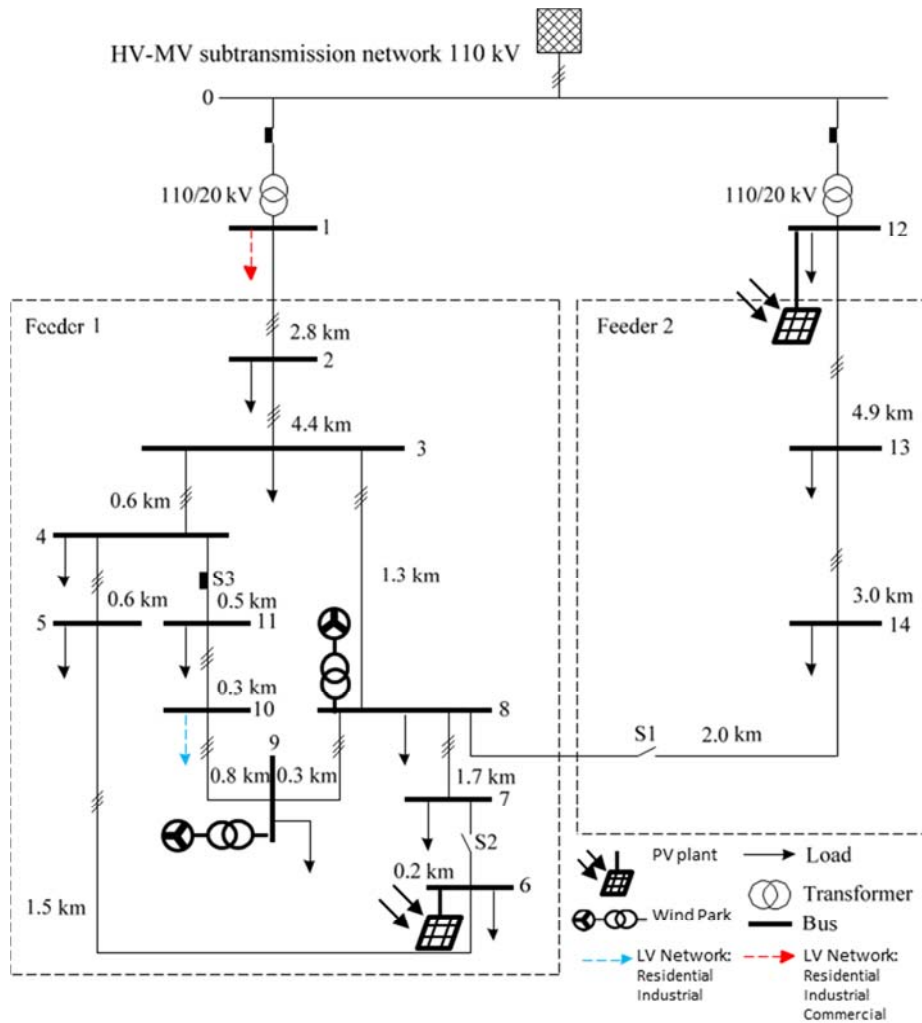


Figure 3.4: Cigré MV Network [47]

Bus	WPP Rating
8	10 MW
9	6 MW

Bus	PVPPM Rating
6	120 KW
12	3700 KW

Table 3.3: MV Wind Power Parks and Photovoltaic Power Plants Ratings

Some of the MV loads need to be replaced by LV networks in order to be able to include low voltage connected PVPPM and loads. The choice of loads to be replaced needs to ensure validity for the results without over-complicating the structure of the system. BB's 1 and 10 of the MV networks are connected to a LV network each, creating one connection point close to the transformer and one deep in the MV voltage network. This strategy allows mitigation of the risk of bias in the results, while ensuring a reasonable level of complexity for the network topology. The connection was done by replacing the loads on the specific BBs with the LV systems. Scaling took place, as it will be explained in section 3.3.4, in order to maintain the power profile of the MV network as described in [47]. Details for the modelling of the network can also be found in the Appendix C.

3.3.4 CIGRÉ low voltage benchmark system

3.3.4.1 Simplifications

The Cigré low voltage (LV) benchmark network is used in this study, Figure 3.5. The network consists of three radial feeders representing the residential loads, the industrial and the commercial ones. On the residential feeder, at junction nodes R1 and R15, one PVPPM is included. The size of the PVPPMs was based on statistical data of the German network and the values are presented in Table 3.4. The network is modelled based on the [47].

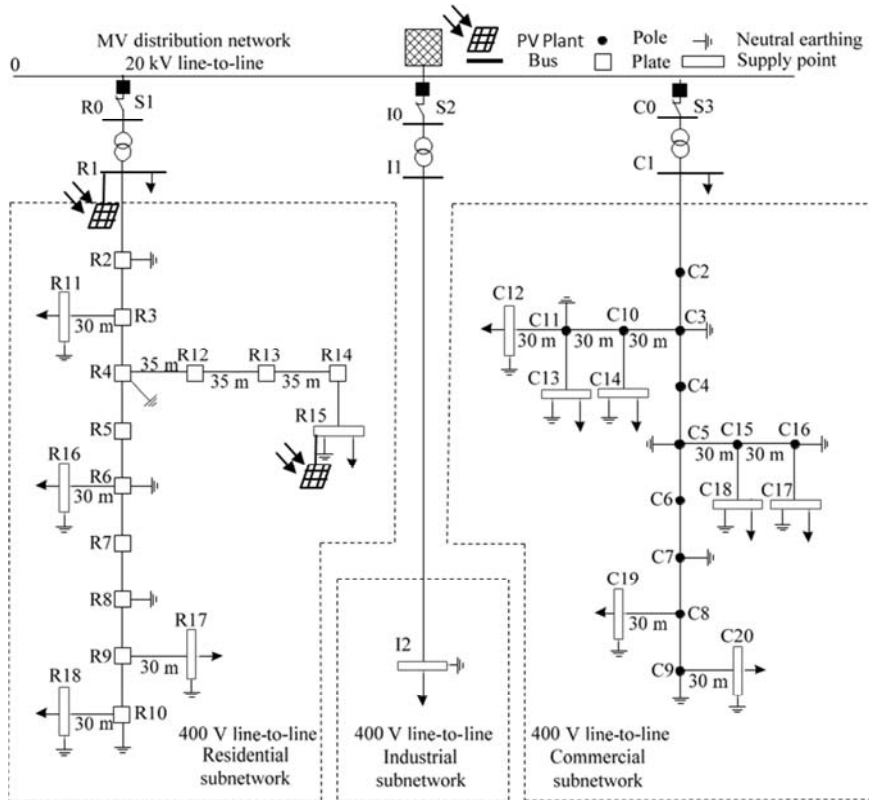


Figure 3.5: Cigré LV benchmark network [47]

The LV network is „cloned” twelve times and it is connected to busbars 1 and 10 of every one of the six MV network as mentioned in the previous paragraph. In order to keep the MV load constant the residential part of the low voltage network needs to match the residential load on the MV busbar and the same holds for the industrial/commercial part of the network.

Bus	PVPPM Rating
R1	10 kW
R15	5 kW

Table 3.4: LV Photovoltaic Power Plants Rating

This procedure leads to the following results: „clones” of the low voltage network connected to busbar 1 of every MV network include a scaling of the residential feeder by 38 times and of the commercial/industrial feeder by 15 times. The scaling procedure includes

the rating of the transformer, the installed load and the line current capacity. Also in the residential part of the network the output power of the PVPPM's is scaled accordingly. For the „clones” of the LV network connected to busbar 10 no scaling is necessary but the commercial feeder is removed in order to match the industrial MV load. The details of the network modelling can be found in the Appendix D along with the scaling manual for the PVPPM model [49], Appendix G.

LV	PVPPM	MV Node 01	MV Node 10
Residential	X*	38	1
Industrial	-	15	1
Commercial	-	15	-

Table 3.5: Scaling factors for lines, loads, transformers and PVPPM ratings per MV network node for all types of LV networks.

*X marks the type of LV network that includes PVPPM, in this case only residential.

3.3.4.2 Kron transformation (for overhead lines, cables)

The line modelling for the low voltage system was done in a detailed fashion. Two different types of lines are used based on the type of LV network. The commercial network consists of overhead lines and the residential and industrial network of underground cables. The modelling for each type is presented below, the parameters and values can be found in Appendix D.

Overhead Lines

For modelling power lines a number of modelling approaches are available in the commercial modelling software used (DigSILENT PowerFactory v14.1). The most suitable for overhead lines is the so-called Typtow and Typcon elements [50]. The Typtow element allows the user to define the zero sequence and positive sequence reactance and resistance of the line as well as the number of line circuits that are included in the overhead transmission system. It does not give the option of including a neutral wire whilst the Cigré LV benchmark network data is given with a neutral wire configuration and is a 4-wire network. To solve this issue the Kron reduced impedance matrices were used, that take into account the neutral contribution on the phase impedance. Inside the Typtow element a conductor type must be defined, the Typcon element. The electrical parameters needed for defining this element were available from the Cigré report, all except the dc resistance of the wire at 20° Celsius. These values were acquired from the IEC 60287 [51]. An overview of the electrical parameters used can be found in Appendix D.

Underground cables

For the modelling of underground cables another element type was used. The TypLne element is used which allows the modelling of the neutral wire and therefore the parameters given in the primitive admittance matrix were used [47]. The capacitance of the cables was not considered due to the small lengths of the cables, as instructed in the benchmark report [47].

3.4 Distributed Generation Modelling

3.4.1 Photovoltaic power Park module (PVPPM)

3.4.1.1 Existing model (DC side, DC/AC inverter control)

As stated in section 2.4, the model used to represent the PVPPM originates from a publication of Samadi [36]. This PVPPM, as presented in the single line diagram of Figure 3.6, consists of the dc current source representing the PV array, the dc-link capacitor and the voltages source converter (VSC). It is a three phase single-stage PVPPM connected through a transformer to the distribution grid.

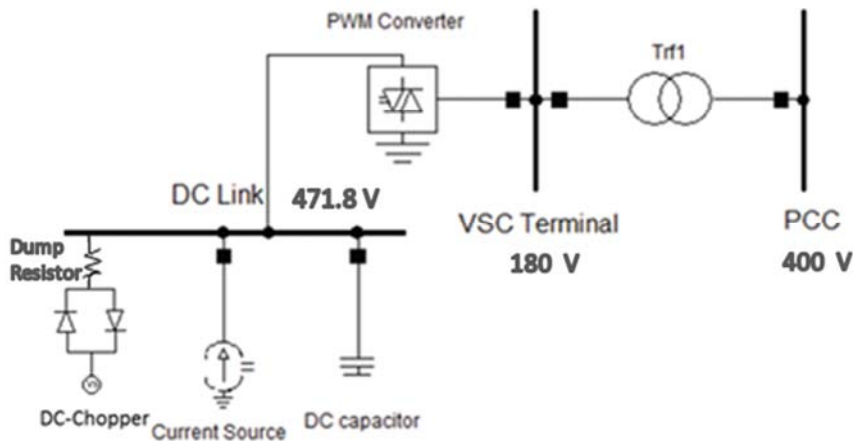


Figure 3.6: PVPPM components [36]

The setup of the model is presented in Figure 3.7. The PV array seen consists of solar cells which are, combined in series and in parallel to form PV modules, which in turn are interfaced to form solar panels that are also connected to form the PV array. Finally the end product, the PV array, has adequate voltage and power for grid connection.

The description of the operation of the model follows: The dc output power of the PV array is fed to the dc link, where a parallel connected capacitor is used to stabilize the voltage. The voltage source converter (VSC) inverts the current and voltage waveforms to connect to the ac side. The VSC terminals are connected to the point of common coupling (PCC) via the interface reactor, and a step-up transformer. The transformer serves two purposes: it provides an isolated ground for the PVPPM and it raises the voltage level to match the voltage of the ac network. The shunt capacitor on the ac side in combination with the inductance of the transformer and interface reactor forms a filter that absorbs any undesired current harmonics. The PLL algorithm is used to synchronize the control system with the grid frequency by a transformation from the a/b/c-reference frame to a d/q-frame reference.

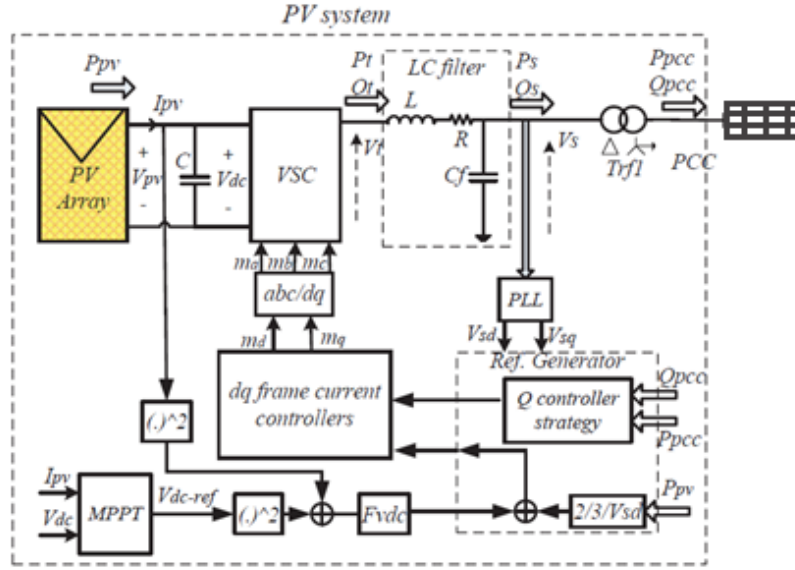


Figure 3.7: PVPPM system set up [36]

The model is equipped with a variety of control functionalities. The ones relevant for this study will be explained in this chapter. The d-axis and q-axis are decoupled through the PLL and therefore active (d) and reactive power (q) control are as well.

The active power control strategy is done through controlling the dc link voltage. The reference set-point is calculated through the PV equation (Equation 2-1) and then is perturbed by the maximum power point tracker (MPPT) to find the PV operation point with maximum efficiency, the knee of the V-I curve of the PV. The error signal between the set-point and the actual value is fed to a PI controller that calculates the d-axis current. The equation can be seen below.

$$I_{g,d_{ref}}^{<U_g} = K \cdot \left(1 + \frac{1}{T \cdot s}\right) \cdot (U_{dc_{ref}} - U_{dc}) \quad \text{Equation 3-1[36]}$$

In this study the dynamic power factor scheme is used for steady-state reactive power control, as proposed by German grid connection requirements [10]. The calculated reactive power reference set-point is compared with the reactive power output and the deviation signal is fed to a PI controller that calculates the q-axis current of the VSC. The reactive power set-point calculation is done based on the power factor. By measuring the active power output and applying the characteristic presented in Figure 3.8 the target power factor is calculated. By applying Equation 3-2 the reactive power set-point is calculated. Therefore when the PVPPM is exporting maximum active power then it is also consuming reactive power in order to lower the voltage at the PCC.

$$Q_{ref} = \sqrt{P^2 \cdot \left(\frac{1}{\cos^2 \varphi} - 1\right)} \quad \text{Equation 3-2}$$

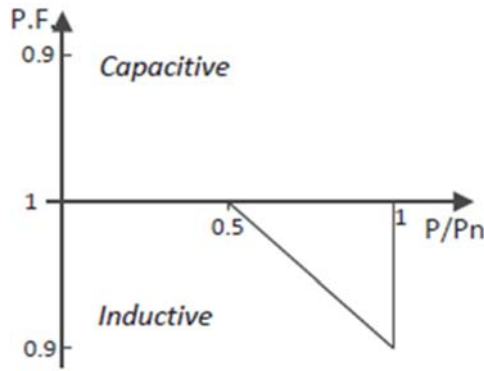


Figure 3.8: Power factor relative to active power output [36]

3.4.1.2 Network fault control modes and extensions

This section describes extensions of the PVPPM model necessary for a realistic representation of voltage ride-through (LVRT) behavior. The stability simulations performed in the present study are based on rms (average value), positive-sequence models because the focus lies on the power system behaviour rather than specific issues of PV systems or converter designs, therefore some simplifications will also be included.

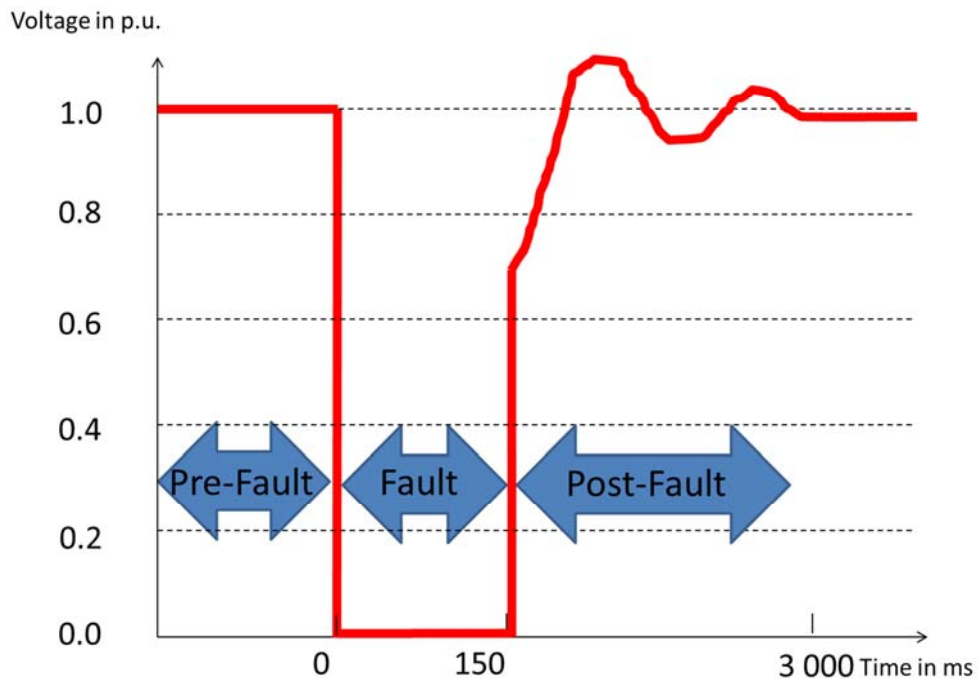


Figure 3.9: Typical voltage rms value plot divided into time periods of the network fault

The network fault response of PVPPMs can be differentiated into three time periods as defined in Figure 3.9. The pre-fault period spans from the start of the simulation until the occurrence of the fault. In this time period the pre-existing pre-fault controller is used and all system variables are in steady state. The fault period starts with the fault occurrence and ends with the fault clearance; it is characterized by heavy transients. In this time frame four different control modes are added to the PVPPM as explained below. The post-fault period follows the fault period and depending on the choice of control mode can either use the pre-

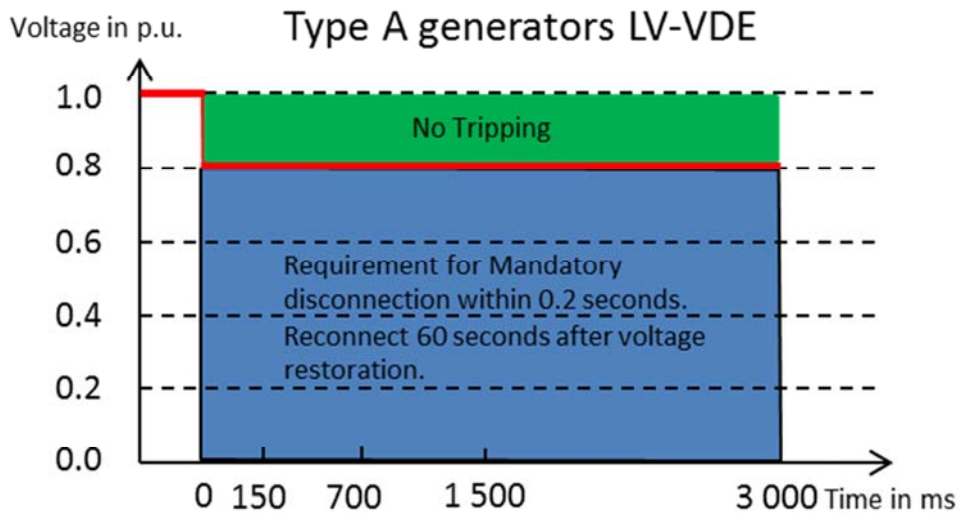


Figure 3.11: No-LVRT requirement for type A generators, power generating modules with a connection point below 110 kV and maximum Capacity of 0.8 kW or less [13] by Forum network technology / network operation (VDE) [10]

The control setting chosen for modelling the undervoltage protection sets the voltage boundary at the PCC at 0.8 p.u. resulting in termination of active and reactive power exchange with the network for 60 seconds, should the voltage drop below this boundary. The time delay for the protection relay response is 0.1 s. This value is chosen as to fulfill the requirement of disconnection within 0.2 s without being borderline compliant. Figure 3.12 demonstrates this operation for type A generators, which are power generating modules with a connection point below 110 kV and maximum Capacity of 0.8 kW or less [13].

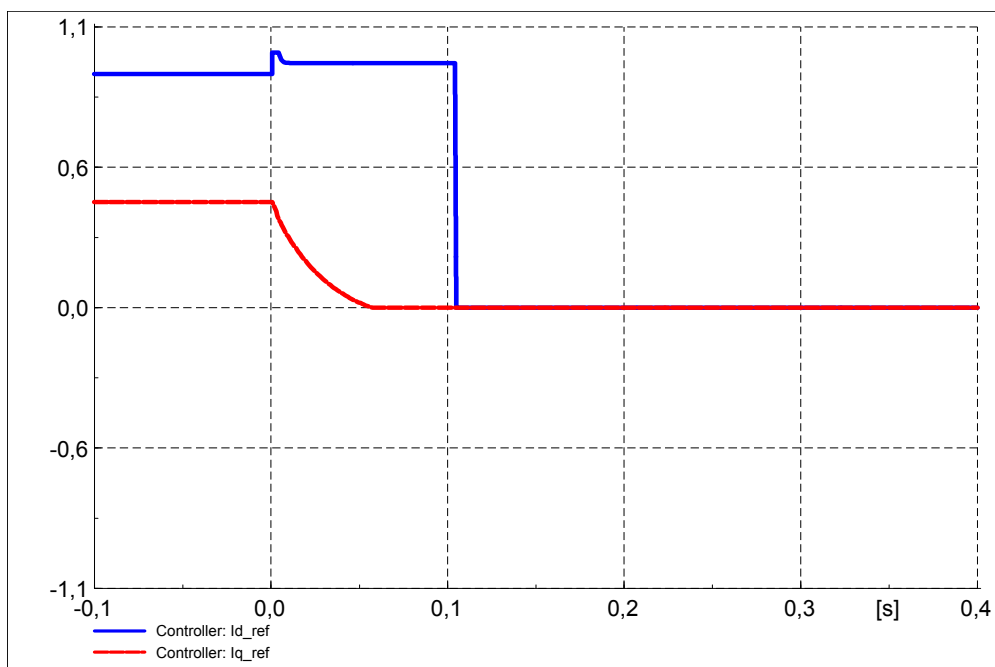


Figure 3.12: D-axis and q-axis currents of a PV Power Plant set for No-LVRT during fault
Source: own simulation

The d-axis and q-axis currents of a PVPPM are depicted during a fault. The fault occurs at $t = 0$ s and within 0.1 s the PVPPM ceases power exchange with the network. The rise in active current during the first 100 ms of the fault is due to the response of the pre-fault controller trying to balance the ac/dc power imbalance at the terminals of the inverter caused by the voltage drop at the ac side. The corresponding drop in reactive current is also the response of the pre-fault controller applying the dynamic power factor control strategy.

Zero power mode

The zero power mode (ZPM) is a fault ride-through (FRT) mode during which the power generating module does not in-feed any power (active or reactive) into the network. This control mode is desired by many distribution system operators (DSO) to avoid conflicts of DG with network protection [5]. Therefore when the voltage drops below 0.9 p.u. at the PCC then the VSC of the PVPPM stops any power exchange with the network while staying connected. The difference with the status quo is that by staying connected with the network the PLL synchronization algorithm is applied continuously and as soon as the voltage is restored, the active power of the PVPPM recovers instantaneously and therefore is not disturbing the active power balance post-fault by staying disconnected.

In that way the ZPM is providing service to the network post-fault by reconnecting faster and taking part in the restoration of the power balance. This control strategy is implemented during the fault by blocking the inverter switches and directing the power production from the PVPPM to the dc chopper. By doing so, the power is dissipated over the series 'dump' resistance of the chopper. It can, therefore, be concluded that this control mode is implemented mainly during fault but the service to the grid is manifested during the post-fault behaviour of the system.

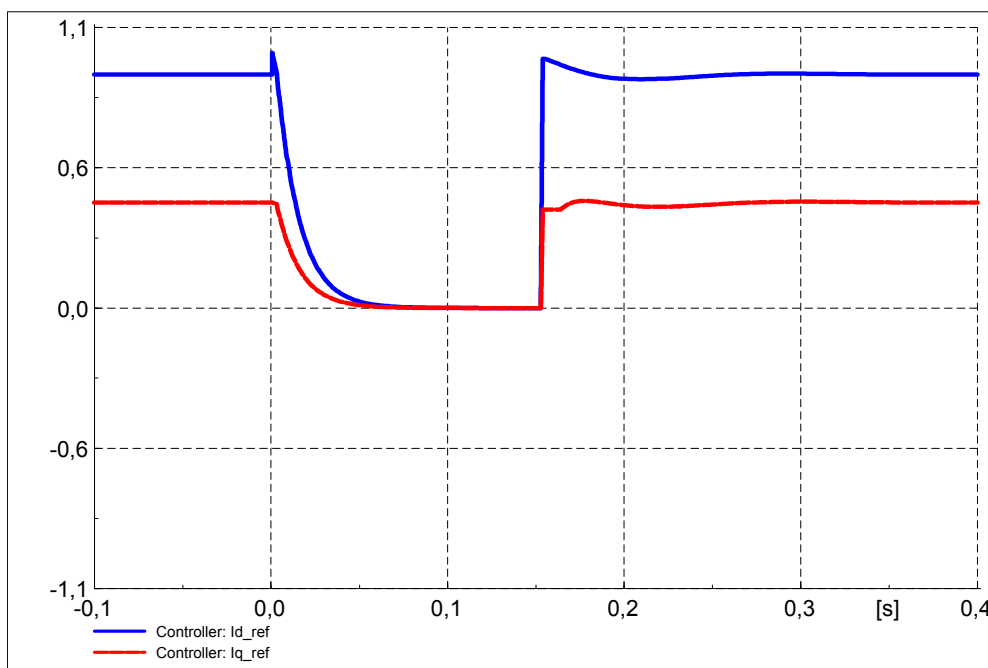


Figure 3.13: D-axis and q-axis currents of a PV Power Plant set for ZPM during fault

In Figure 3.13 the d-axis and q-axis currents of the PVPPM's inverter are shown. The fault occurs at $t=0$ s and the controller is driving the power exchange/currents to zero. After fault clearance, 150 ms later, the pre-fault controller is coupled with the network and the currents return to the pre-fault set-points. No delay is implemented in the recovery of active power in order not to interact with the pre-fault controller. The voltage, not shown, is recovering immediately and enables the fast response of the controller. The difference between the No-LVRT and ZPM is evident by comparing Figure 3.12 and Figure 3.13. The zero power exchange is achieved in less time as the controller is faster than the protection relay. Also the ripples seen at fault restoration are due to the voltage oscillation post-fault that triggers the action of the steady state controller.

Additional reactive current injection (aRCI)

Another requirement for applying dynamic network support during fault, as defined by the German grid connection requirements [5], is the additional injection of current during fault to assist in raising the voltage at the PCC. Usually this additional current depends on the type of network the DG is connected to. Therefore when medium voltage or high voltage networks are considered the current is purely reactive as the networks X/R ratio is high and the strongest impact in raising the voltage can be achieved by injecting an additional reactive current component.

Prior to the fault the inverter of the PVPPM is injecting active and reactive power into the grid which corresponds to the active and reactive current. The vector sum of those currents forms the total current injected into the grid. During fault it is desirable to maintain the pre-fault operating point and inject an additional reactive current component.

As soon as the fault is detected, the inputs to the pre-fault controller are frozen to the pre-fault values. Then an additional proportional controller is added to the output of the PI q-axis current controller. The additional controller uses the deviation of the ac voltage to raise the q-axis current. The equations for the reactive and active current are shown in Equation 3-3 and Equation 3-4, respectively. The gain parameter K_{Iq} is adjustable. The total current is then passed through a limiter to ensure that the current capacity of the inverter is not exceeded. For the limiter a value of 1.1 p.u. is used for the sum of the currents. In case the set-points are exceeding the capacity then the d-axis current is scaled down in order to remain within the inverter capacity. The scaling function of the limiter can be seen in Equation 3-4. dV_{AC} is the deviation of the voltage from the nominal value in p.u. where db is the deadband around the voltage deviation.

$$I_{q_{aRCI}} = \begin{cases} I_{q_{pre-fault}} + K_{Iq} \cdot \frac{|dV_{AC}|}{dV_{AC}} \cdot (|dV_{AC}| - db), & I_{q_{aRCI}} \leq I_{max} \\ I_{max}, & I_{q_{aRCI}} > I_{max} \end{cases} \quad \text{Equation 3-3}$$

$$I_{d_{aRCI}} = \begin{cases} I_{d_{pre-fault}}, & I_{max} \geq \sqrt{I_{d_{pre-fault}}^2 + I_{q_{aRCI}}^2} \\ \sqrt{I_{max}^2 - I_{q_{aRCI}}^2}, & I_{max} < \sqrt{I_{d_{pre-fault}}^2 + I_{q_{aRCI}}^2} \end{cases} \quad \text{Equation 3-4}$$

After fault clearance the state of the controller is unchanged until the voltage recovers to 0.9 p.u. at the PCC. After that point the additional controller is disabled and the pre-fault controller takes over. A small adjustment follows, before the pre-fault controller returns to the point of operation prior to the fault. Figure 3.14 depicts the process described.

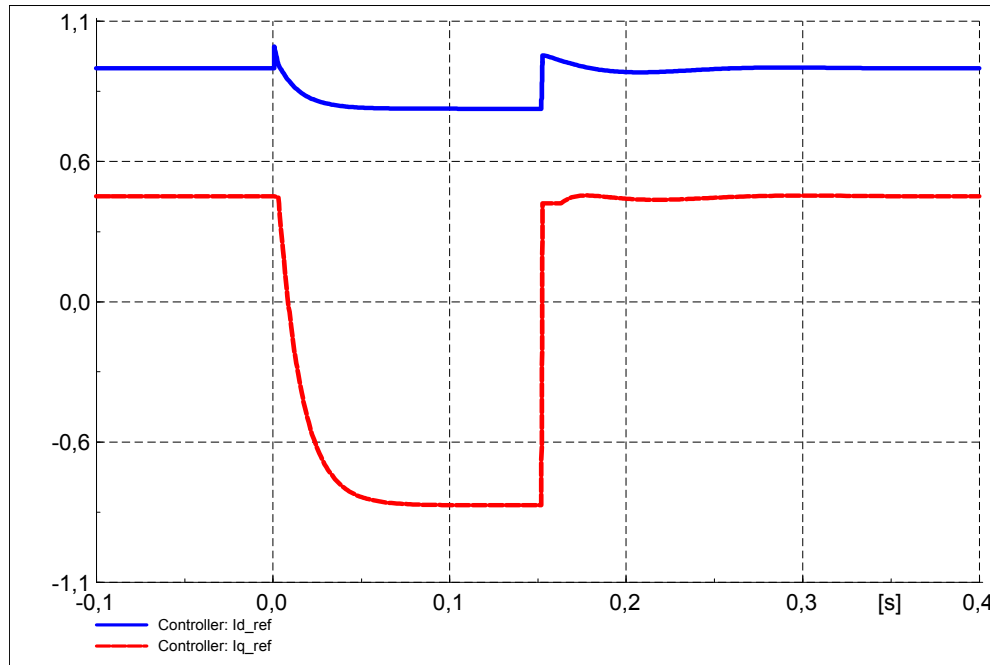


Figure 3.14: D-axis and q-axis currents of a PVPPM set for aRCI during fault

Mixed additional reactive & active current injection

The final control functionality implemented for the fault period is the mixed aR&ACI. This control option is similar to the aRCI, while the additional component of the current also has an active part. The reason for this addition stems from the X/R ratio of the low voltage network that can be lower than one unlike the MV or HV guide. This translates into active current having a dominant impact on the voltage support. The additional current is injected at an adjustable angle between active and reactive current.

The pre-fault controller values of the d-axis and q-axis currents are frozen as described in 3.4.1.2. During fault a proportional controller is added for both active and reactive current. The reactive and active current equations are Equation 3-5 and Equation 3-6, respectively. The addition in both equations is the cosine and sinus terms, which take care of the angle of injection if the same K factor is used ($K_{Iq} = K_{Id}$).

$$I_{q_{aR\&ACI}} = \left\{ I_{q_{pre-fault}} + \left[K_{Iq} \cdot \frac{|dV_{AC}|}{dV_{AC}} \cdot (|dV_{AC}| - db) \right] \cdot \sin \theta \right\} \cdot Scaler \quad \text{Equation 3-5}$$

$$I_{d_{aR\&ACI}} = \left\{ I_{d_{pre-fault}} + \left[K_{Id} \cdot \frac{|dV_{AC}|}{dV_{AC}} \cdot (|dV_{AC}| - db) \right] \cdot \cos \theta \right\} \cdot Scaler \quad \text{Equation 3-6}$$

$$Scaler_{aR\&ACI} = \begin{cases} 1, & I_{max} \geq \sqrt{I_{d_{aR\&ACI}}^2 + I_{q_{aR\&ACI}}^2} \\ I_{max} / \sqrt{I_{d_{aR\&ACI}}^2 + I_{q_{aR\&ACI}}^2}, & I_{max} < \sqrt{I_{d_{aR\&ACI}}^2 + I_{q_{aR\&ACI}}^2} \end{cases} \quad \text{Equation 3-7}$$

The equation for the scaling can be seen in Equation 3-7. The graphical explanation for the scaling procedure is presented in Figure 3.15.

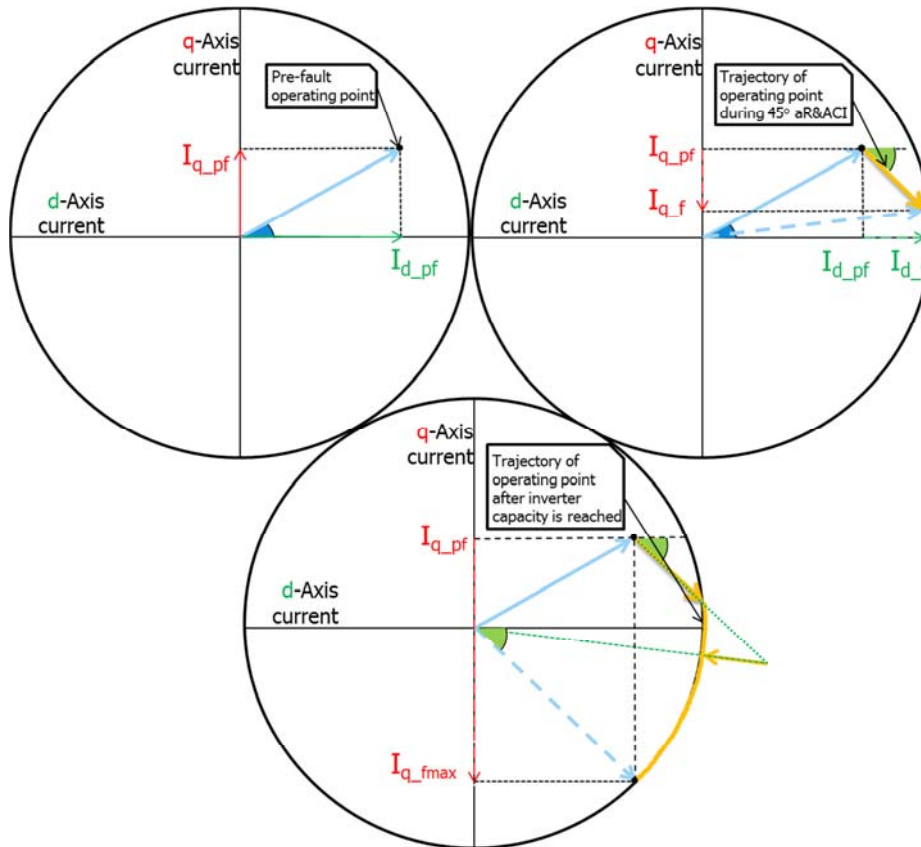


Figure 3.15: Inverter d-axis and q-axis current diagrams for presenting scaling scheme

The initial set-point for both active and reactive current is marked in the graph with the blue arrow, from that starting point there is an additional directional current component added to the total current that stems from the fault proportional controllers (orange arrow). If the total current of the inverter exceeds the inverter’s capacity, scaling is taking place. The magnitude of the total current is intercepted with the corresponding straight line from the origin of the two axes. Moving on that line the set-point is shifted until it is inside the capability limit of the inverter. With this scaling technique the current set-point is shifted during the fault period until the angle between the y axis and the straight line connecting the origin and the current set-point can reach the maximum of the additional current injecting angle, whilst staying within the capability limits of the inverter.

The same procedure can be seen in Figure 3.16 for the same angle (45°) as presented in Figure 3.15. The fault occurs at $t= 0$ s and is cleared 150 ms later. The voltage drop at the PCC determines if the maximum angle will be reached. In this case the current is not

exceeding the limit of the inverter (1.1 p.u.) and therefore the final angle differs from the injection angle.

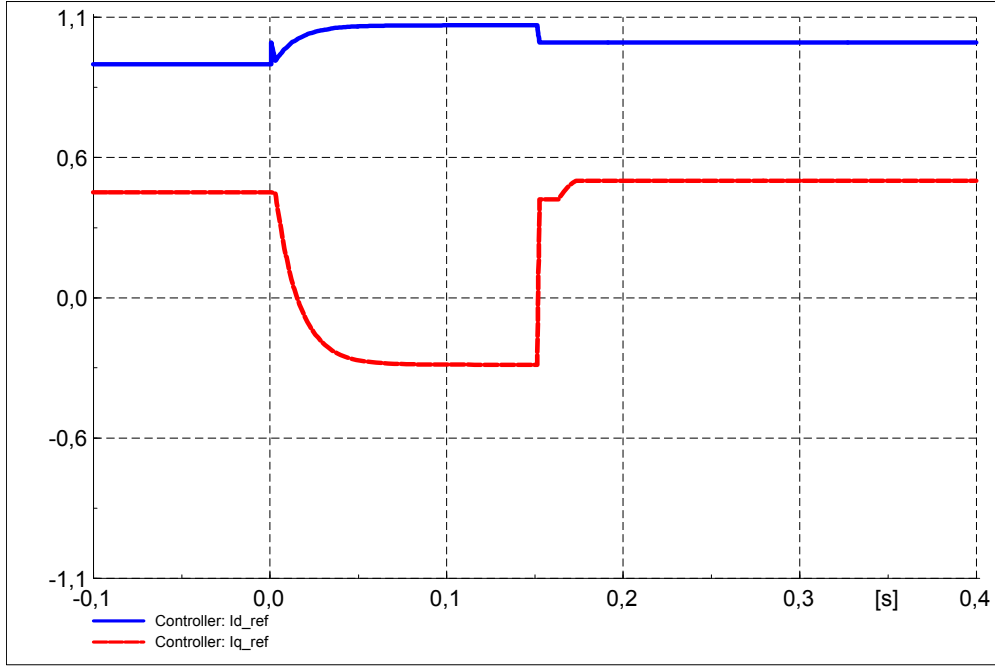


Figure 3.16: D-axis and q-axis currents of a PVPPM set for aR&ACI during fault

Delayed post-fault active power recovery

The final control strategy added to the model is the post-fault active power recovery. The restoration of the active power post-fault value at the end of the fault-period to the pre-fault active power set-point is achieved through a ramp with a specific inclination. The German grid connection requirements ask for a restoration of active power to the pre fault state with a 20% increase of active power every second until the pre fault active power is reached [28]. This control strategy is implemented with a filter function. The response of the controller is almost immediate in providing the pre-fault set-point. This response is filtered through the tracker by a first order filter function with the required time delay to achieve the ramp features required. The ramp is activated post-fault and deactivated when the pre-fault active power is reached. The tracker equations can be seen below (Equation 3-8, Equation 3-9).

$$\dot{x}_{tracker} = \begin{cases} f(x) = \begin{cases} 0.2, & I_{d,i} < I_{d,pre-fault} \\ (I_{d,i} - x_{tracker}) \cdot K_{slow}, & I_{d,i} > I_{d,pre-fault} \end{cases}, & Post - fault = 1 \\ (I_{d,i} - x_{tracker}) \cdot K_{fast}, & Post - fault \neq 1 \end{cases} \quad \text{Equation 3-8}$$

$$I_{d,o} = \begin{cases} x_{tracker}, & Post - fault = 1 \\ I_{d,i}, & Post - fault \neq 1 \end{cases} \quad \text{Equation 3-9}$$

The format that the equations are presented is the state space, and the final output comes from Equation 3-9. The condition *Post - fault* is a boolean term which, if true, indicates that the system is within the post-fault period. This condition is true for 5 seconds

after the fault in order to ensure that the d-axis current will be restored to the pre-fault value even if we are in the worst case (5 seconds needed for 0-1 pu, with 20 % raise per second). The value 0.2 is chosen as the specified rate of increase. The K values for the fast and slow trackers are 10^4 and 10^3 respectively. The results are shown in Figure 3.17 as implemented by the PVPPM modelled. The fault is cleared at 2.15 s and then the delay in active power restoration affects the reactive power as well as it is a function of active power (Equation 3-2).

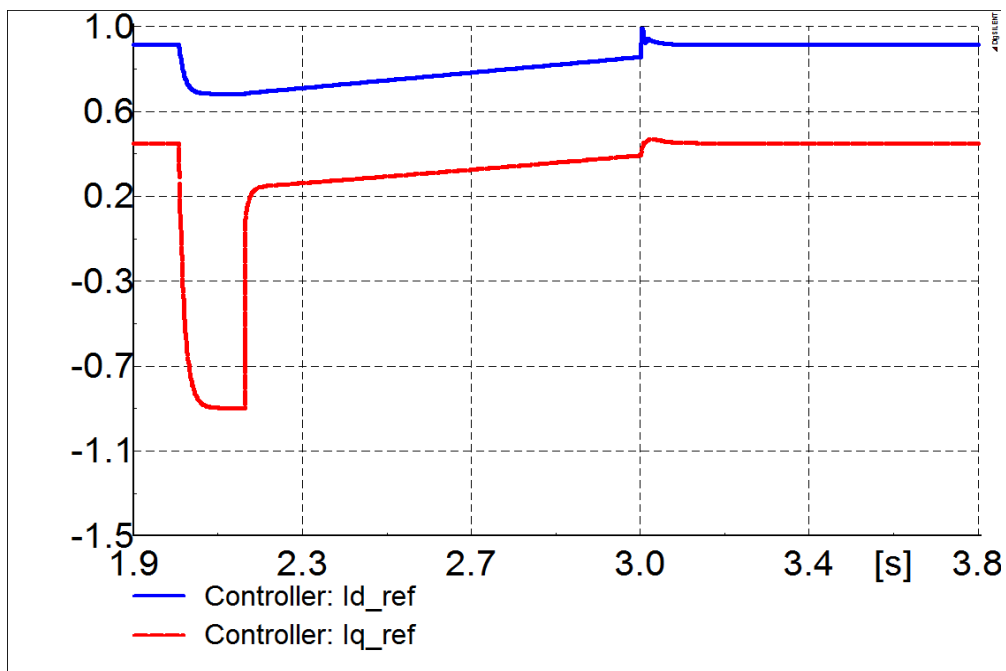


Figure 3.17: D-axis and q-axis current in aRACI with delayed active power recovery

DC-Chopper

[32] reports undesired disconnection of PVPPMs during or after network faults triggered by the internal dc circuit protection, even if the PVPPMs were supposed to perform LVRT, as follows. The dc link voltage initially rises during a fault on the ac side of the PVPPM due to the active power imbalance between the ac and dc side of the voltage source converter. The controller responds by increasing the ac current and thereby tries to restore the active power balance. However, the current limits of the inverter may be reached before an active power balance can be restored and that ultimately leads to a further increase of the dc voltage. This behaviour is reversed in the post-fault period. The ac voltage is recovered almost instantly at fault clearance without giving the controller sufficient time to reduce the ac side current to its pre-fault level. The result is an active power imbalance between the ac and dc side of the inverter. Since the active power flow through the grid side converter is larger than the one from the dc source, the dc capacitor is discharged, i.e. the dc voltage decreases. In certain cases the dc voltage may drop below the minimum allowed value and that would trigger the internal dc circuit protection to disconnect the PVPPM from the network.

Discussions between TU Delft with Laudahn (TU Braunschweig) indicated that such issues are unlikely to occur for PVPPM inverters sold on the German market [37]. Proprietary control strategies of the grid side converter and/or dc-dc converter would take care of levelling the dc voltage within the allowable voltage band and prevent disconnection of PVPPMs during or after network faults due to the internal dc circuit protection.

The active power is controlled by adjusting the dc link voltage and the reactive power is calculated via the dynamic power factor approach, as described in section 3.4.1.1. Thus it is obvious that the dc link voltage is an important parameter for controlling the PV behaviour. The importance of the dc voltage is further stressed by the constraints imposed by the protection of the PVPPM. If the dc voltage exceeds certain limits the protection relay will disconnect the PVPPM from the grid. Therefore in order to be able to safely apply any control scheme during fault we must ensure that the dc link voltage will stay within certain limits.

Given the power system focus of the present study and the lack of information regarding different proprietary control strategies for PVPPMs, simplifications in the modelling of the PVPPMs are required and justified. Originating from the detailed representation of both the dc and ac sides of a PVPPM [36] and aiming at a stable operation during and after network faults while disregarding any specific and potentially proprietary control strategies, an active dc chopper in the dc circuit is assumed during LVRT operation and for a certain time after voltage recovery. The chopper comprises of two anti-parallel diodes connected to the dc bus and in series to a voltage source behind an impedance (see Figure 3.6). For steady-state operation no chopper is assumed. The chopper keeps the dc voltage at the pre-fault value during the fault. For an adjustable time after fault clearance it is assumed to continue operation which further prevents undesired dc voltage fluctuations post-fault.

Reactive current time performance

Another addition to the PVPPM model is the compliance with the reactive current time performance as required by German grid codes and presented in Figure 3.18. The step response defined by German grid codes is the marginally accepted behaviour of a generator performing a control induced change in its current/power set-point. Therefore every PVPPM that has to connect to the German grid must prove that the step response to a change of the current set-point can be performed within the margins specified in Figure 3.18. In detail, 90 % of the final set-point value must be achieved within 30 ms (rise time) and the final signal must be settled between 90 % and 120 % of the final value within 60 ms (settling time) [52].

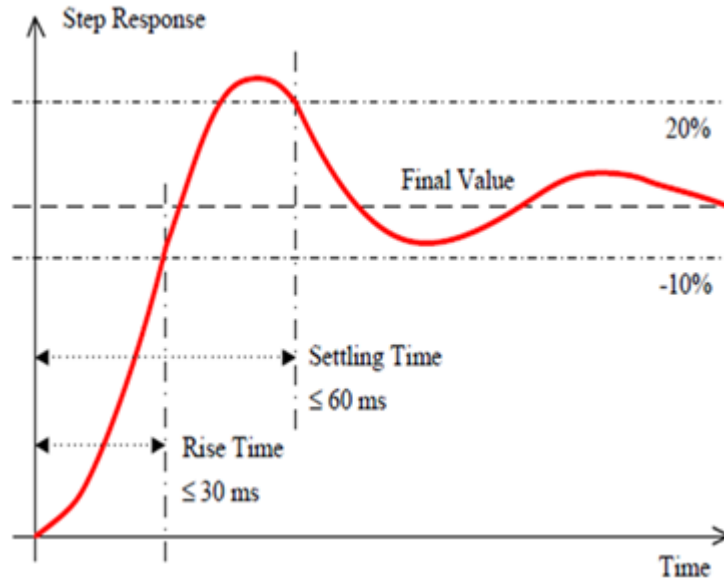


Figure 3.18: German grid step response [52]

The PVPPM model was already complying with these requirements. However it is unrealistic to consider that all the installed PVPPM's have a very fast response as they were installed in the past and therefore it could be that they do not comply to these requirements. In order to ensure that the model is realistic and it considers the worst case rather than the best a filter was implemented so that the step response requirement is met marginally. For the implementation of the filter a first order function was used as it is shown in Equation 3-10 and Equation 3-11. The parameter tuning was done with a heuristic approach in order to achieve the delays of 30 ms and 60 ms for each set-point percentage. The variable *fault* is a boolean which is true only during the fault period. The diagrams presented for all the control modes include this filter.

$$\dot{x}_{filter} = \frac{K \cdot (I_{d_i} - x_{filter})}{T} \quad \text{Equation 3-10}$$

$$I_{d_o} = \begin{cases} I_{d_i}, & \text{fault} \neq 1 \\ x_{filter}, & \text{fault} = 1 \end{cases} \quad \text{Equation 3-11}$$

3.4.2 Wind turbine generators

The WPPs models used in this study originate from [40]. The models for WPPs used consist of:

- Doubly-fed asynchronous generators (DFAG), and
- Full-converter generators (FCG).

The WPP connected in each of the six MV networks consist of both type of generators. The 10 MW WPP consists of a 6 MW aggregated FCG generator and a 4 MW aggregated DFAG generator. The smaller 6 MW WPP consists of a 4 MW aggregated FCG generator and a 2 MW aggregated DFAG generator.

All WPPs are able to ride through faults and inject reactive current to the network in the event of a fault. The type of fault control applied to these WPPs is the additional reactive current injection (aRCI) control mode similar to the PVPPMs. The gain is set at 2 and this behaviour is in compliance with current grid codes for MV and HV connected DG [5],[28]. The modelling details of the WPPs will not be discussed as they are not in the focus of this thesis but rather support the realistic representation of the German network. However details in the mode of operation of these models can be found in [53] for the DFAG model and in [54] for the FCG model as they are both based on the corresponding PowerFactory templates.

3.5 Load Modelling

Through an extensive literature survey on load modelling, it became clear that the model structure of the load and the identification of the load parameters is an important factor in stability studies [55], [56–62]. Different load model structures may make stability study results totally different [55].

A load can be modelled as either static, dynamic or aggregated. A static load model describes the relation of the active and reactive power at any time with the voltage and/or frequency at the same instant of time [56]. A static load can have either a polynomial (ZIP) or exponential form. On the other hand, a dynamic load model expresses this relation as a function of the voltage and/or frequency time history, including normally the present moment [56]. Dynamic load models can be represented by induction motor models or input-output models that are based on differential equations [55]. The aggregated load combines both modelling types by a percentage split between dynamic and static load.

PowerFactory provides a variety of options to model loads. For the static load model both polynomial and exponential load modelling is possible. Also the model can be part dynamic and part static where the dynamic part can be based on linear or non-linear second order differential equations. Finally there is always the option to use an induction motor in order to represent dynamic load [62]. However the parameter identification for load modelling is a difficult and time consuming procedure that stems from statistical analysis of historical data combined with optimization algorithms for curve fitting. The choice of parameters for this study is done based on the work of [55, 63] and [64]. The frequency dependent part of the load is ignored.

For the static part of the load the polynomial (ZIP) approach is presented first. In this approach the load can be classified into constant power, constant current and constant impedance load, depending on the power relation to the voltage [56]. As it can be seen in Equation 3-12 and Equation 3-13 for constant impedance load, the power dependence on voltage is quadratic, for a constant current it is linear, and for a constant power, the power is independent of changes in voltage.

$$P_{ZIP} = P_0 \cdot \left[a_P \cdot \left(\frac{V}{V_0} \right)^2 + b_P \cdot \left(\frac{V}{V_0} \right) + (1 - a_P - b_P) \right] \quad \text{Equation 3-12}$$

$$Q_{ZIP} = Q_0 \cdot \left[a_Q \cdot \left(\frac{V}{V_0} \right)^2 + b_Q \cdot \left(\frac{V}{V_0} \right) + (1 - a_Q - b_Q) \right] \quad \text{Equation 3-13}$$

For the exponential approach Equation 3-14 and Equation 3-15 give the active and reactive power dependency of the load on voltage as found in [65]. For this thesis the exponential approach was chosen as parameters for exponentially modelled loads for different voltage levels and type of networks were easier to be found.

$$P_{exp} = P_0 \cdot \left[a_P \cdot \left(\frac{V}{V_0} \right)^{e_{aP}} \right] \quad \text{Equation 3-14}$$

$$Q_{exp} = Q_0 \cdot \left[a_Q \cdot \left(\frac{V}{V_0} \right)^{e_{aQ}} \right] \quad \text{Equation 3-15}$$

The values for load parameter chosen for each type of network are presented in Table 3.6. The eHV static load parameters presented are taken from [64] and for the rest of the loads from [63].

Exponential Load Parameters	eHV loads	MV Loads		LV Loads		
		Suburban	Rural	Residential	Industrial	Commercial
a_P	1.0	1.0	1.0	1.0	1.0	1.0
e_{aP}	1.0	1.7	1.4	1.7	0.8	4
a_Q	1.0	1.0	1.0	1.0	1.0	1.0
e_{aQ}	3.2	4.7	5.5	4.7	4.5	5.5

Table 3.6: Exponential Load Parameters

For the dynamic part of the load the non-linear differential equation model of DigSILENT PowerFactory is available (Equation 3-16, Equation 3-17) [62]. As it can be seen the voltage deviation from 1 p.u. plays a role in the installed power which is time dependent. However in this study no consideration of dynamic load will take place as it would further complicate the study and parameters for time constants are difficult to find.

$$P_{dyn} = \left(dV_{ac} \cdot \frac{K_{p-v} + s \cdot T_{p-v}}{1 + s \cdot T_{dyn}} + 1 \right) \cdot \%_{dyn} \cdot P_r \quad \text{Equation 3-16}$$

$$Q_{dyn} = \left(dV_{ac} \cdot \frac{K_{qv} + s \cdot T_{qv}}{1 + s \cdot T_{dyn}} + 1 \right) \cdot \%_{dyn} \cdot Q_r \quad \text{Equation 3-17}$$

3.6 Conclusions

Concluding the modelling chapter, an overview of the study network structure was given and every voltage level was explained in more detail. The components included in the study network were identified and the modelling procedure was described. The PVPPM model was presented in detail along with all the control functionalities that were included for the purpose of the simulations to be performed in Chapter 4. The WPP models were briefly mentioned as well as load modelling and choices made.

Chapter 4 : Case study and Sensitivity Analysis

4.1 Introduction

In this chapter the structure of the case studies is explained in detail. The principles of operation of the study system are defined and a general outlook of the study is given. Moreover the choice of sensitivity factors that formulate the case studies is explained and justified and finally selected results are presented and analysed. The results presented are the most important as a selection had to be made due to the volume of cases analysed.

4.2 System Conditions

4.2.1 General overview of the system

The test system described in Chapter 3 is used to simulate transmission system faults and investigate the system performance under different conditions. The parameters that are not varied under different case studies are presented in this section.

The location of the fault is placed at the middle of line 9 of the eHV network (see Figure 3.2). The choice of the fault location is made in order to ensure that the fault is close to the busbar that connects the eHV network with the sub-transmission and distribution system also due to the low short-circuit ratio of that location to ensure a severe voltage drop. The fault duration is chosen to be 150 ms in accordance with the findings of the literature survey presented in section 2.5. The fault occurs at 0 s and is cleared 150 ms later. The type of fault that will be analysed is a three-phase fault with no fault impedance. This type of fault is chosen in order to investigate the most severe case that would bring the system closer to instability. The details of the fault location and duration are presented in Table 4.1.

Fault Location	Middle of line 9 of eHV network
Fault duration	150 ms (0-150 ms)
Fault Impedance	0 Ohm
Distance from busbar 8	2.5 km

Table 4.1: Details of fault event

Furthermore due to the use of different load and generation profiles for the starting point of the simulation, the positions of the transformer tap-changers need to be defined. In order to ensure a proper initial voltage for all busbars of the network in all load and generation cases the following strategy was devised.

The eHV/HV transformers are equipped with automatic tap-changing and regulate the secondary-side busbar, in this case the busbar of the HV network they are connected to, at a target voltage of 1.0 p.u. The HV/MV transformers use remote voltage control, and regulate busbar number 10 of the MV network (see Figure 3.4), at a target voltage of 1.0 p.u. Finally the MV/LV transformers are not equipped with automatic tap changers but have manual tap changers. Therefore for the starting point of the simulation the residential LV network

transformers fix their tap changers in order to ensure a remote target voltage of 1.0 p.u. in terminal R15 of the LV network (see Figure 3.5). The transformers of the LV industrial and commercial networks regulate the LV connected busbar with a target voltage at 1.0 p.u. All transformers equipped with automatic tap changers have a time constant of 20 s for changing their taps as a response to a change of voltage at their respective control node. The scheme for transformer tap changers can be seen in Table 4.2.

Transformers Settings	eHV/HV	HV/MV suburban	HV/MV rural	MV/LV residential	MV/LV commercial & industrial
Target node	HV 03/05	MV 10	MV 12	R15	C1/I1
Target voltage	1 p.u.	1 p.u.	1 p.u.	1 p.u.	1 p.u.
Time constant	20 s	20 sec	20 sec	-	-
Number of taps	+/-16	+/-16	+/-16	+/- 2	+/- 2
Voltage per tap	0.625%	0.625%	0.625%	2.5%	2.5%

Table 4.2: Details of transformers tap changing strategy

With regard to the behaviour of DG installations and in order to respect the already defined German grid codes, the MV connected PVPPMs and the respective HV and MV connected WPPs are equipped with FRT capability and additional reactive current injection during fault. In this way a more realistic approach equivalent to today's behaviour of the German system is modelled. Also in the LV network part, the old PVPPMs installations are not able to perform FRT and disconnect in the event of a fault to model the already existing PVPPMs that are connected up to 2012 and are not able to ride through a fault.

PVPPMs connected to the LV network after 2012 and up to 2022 are given the option of FRT and current injection during a fault. Those are the PVPPMs that will change their respective control in the control mode variations that will be explained in section 4.3.2.

Finally in the event of a transmission system fault the shortage of active and reactive power of the network is covered by generator 2 of the eHV network which is modelled as a slack generator (see Figure 3.2).

4.2.2 Scenarios for installed PV capacity

This study is performed as a possible scenario for the year 2022. Therefore the system is modelled for the year 2022 but 2012 DG installations are also considered. In the year 2012 the system already includes the DG connected today that are compliant with current grid codes. In the year 2022 an additional projected installed capacity of PVPPMs is added in the LV and MV networks. The details for the network at each year are explained below.

In the 2012 German scenario the total installed capacity of PVPPMs per MV network was 7 640 kW. As it can be seen in Table 3.3 the sizes of PV installations for the rural and suburban part of the MV network are 120 kW and 3 700 kW respectively. So in order to match the capacities with the total size of the installed PVPPMs, two of each size of PVPPMs where connected in their respective network. For simplification of the study an aggregate model of 240 kW was created for the suburban part of the MV network and an aggregate model of 7 400 kW for the rural part of the MV network. The connection points of the two

PVPPMs are busbar 6 for the suburban part of the MV network and busbar 12 for the rural part. These PVPPMs are able to ride through a fault and provide reactive current with a gain factor of 2 as demanded by German grid codes [5]. For the MV and HV connected WPPs the ratings and connection points are kept the same as described in Table 3.2 and Table 3.3. The same FRT and reactive current injection controls are included for the WPPs as well.

MV busbar	PVPPMs 2012	MV busbar	WPPs 2012
06 suburban	240 kW	09 suburban	6 000 kW
12 rural	7 400 kW	08 suburban	10 000 kW
Total (6 MV Networks)	45 840 kW	Total (6 MV Networks)	96 000 kW

Table 4.3: MV connected DG installed powers and connection points for the 2012 scenario.

For the LV connected PVPPMs the total installed capacity per LV network was 180 kW. In 2012 the sizes of the LV connected PVPPMs can be seen in Table 3.4. In order to match the capacities with the size of installed PVPPMs, 12 installations of 10 kW and 12 installations of 5 kW are chosen per LV network. The aggregating procedure outcome is a PVPPM of 120 kW of installed power connected in busbar R1 of the LV network and a PVPPM of 60 kW installed power connected in node R15 of the LV network (see Figure 3.5).

The LV network connected to MV busbar 10 has this installed capacity of PVPPMs, however the aggregate LV network connected to busbar 1 of the MV network is additionally scaled by a factor of 38 for the residential part of the network. Therefore the PVPPM's connected at that LV network are also scaled by that factor delivering an aggregate PVPPM of 4 560 kW installed power connected at busbar R1 and an aggregate PVPPM of 2 280 kW installed power in node R15 of the LV network connected in MV busbar 1. The final DG connected installations for the 2012 scenario can be seen in Table 4.4.

LV node/busbar	MV busbar of LV network	PVPPM size	# aggregated PV	# aggregate LV networks	PVPPM installed power
R1	01	10 kW	12	38	4560 kW
R15	01	5 kW	12	38	2 280 kW
R1	10	10 kW	12	1	120 kW
R15	10	5 kW	12	1	60 kW
Total (12 LV networks)	-	-	-	-	42120 kW

Table 4.4: Installed power of LV connected PVPPMs with their corresponding connection point for the 2012 scenario

Furthermore LV connected PVPPMs for the 2012 scenario abides by current German grid codes [10] that ask for mandatory disconnection in the event of a fault. The disconnection time is chosen to be 100 ms after the occurrence of the fault in order to represent the worst case.

In the 2022 scenario the installed synchronous generation, WPPs and load are kept the same as in 2012. The installed capacity of PVPPMs in the MV and LV networks is doubled in comparison to the 2012 scenario presented in Table 4.4. So all busbars and nodes of the

network that were connected to a PVPPM of a certain rating in the 2012 scenario, are in the 2022 scenario connected to two PVPPMs of the same rating. The newly installed PVPPMs are able to perform different control strategies whilst the ones connected in 2012 cannot ride through fault. Doubling the installed PV capacity in both the MV and LV network over 10 years is a realistic assumption as it can be seen in the literature survey chapter for the projected growth of PVPPMs installed capacity in Germany.

In Figure 4.1 the installed load and DG production can be seen for all the MV and LV networks in the 2022 scenario. Due to having an aggregated and a single LV network connected to different busbars of the MV network their installed loads and productions are presented separately. The load and production of the eHV and HV networks are shown in Table 4.5. The HV network has no load.

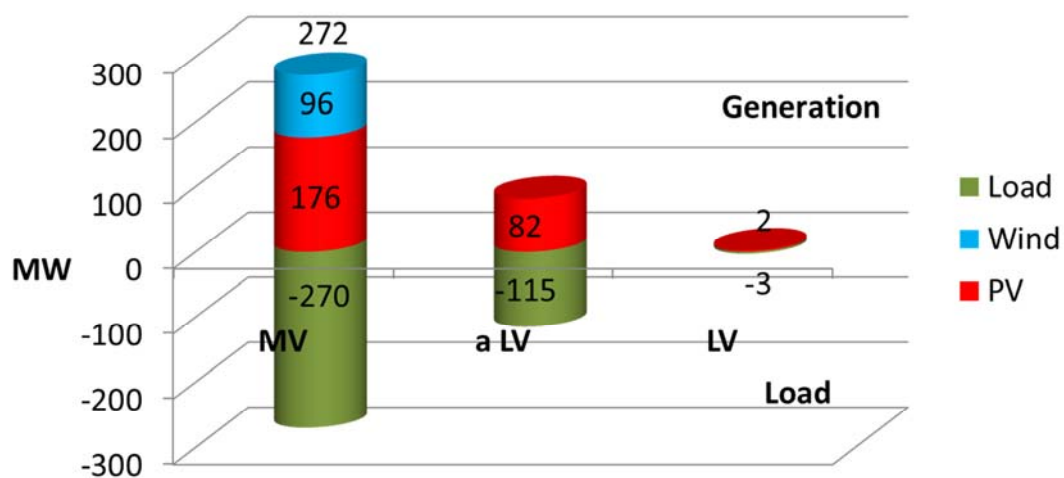


Figure 4.1: Installed load and DG generation in the 2022 Scenario for the HV/MV/LV networks

eHV Load	eHV Production (without slack machine)	HV Production (Wind Power Parks)
6 097 MW	5960 MW	100 MW

Table 4.5: Installed Load and Production in the eHV network

4.3 Sensitivity Factors

4.3.1 Load/ Generation profile

The first sensitivity factor presented is the load and generation profile. Namely as explained before the system has a fixed installed generation and load power. However in different periods of time only a part of the load is actually connected to the network due to the time varying needs of consumers. Also renewable based DG power output is dependent on solar irradiation for PVPPMs and wind speed for WPPs. Therefore only a part of the installed power of DG is actually fed to the network at different times. Synchronous generation also takes into account the needs of the network in terms of active and reactive power and produces the rest of the power needed.

The aim is to define three pre-fault operating points for the network, based on load consumption and PVPPMs production. The load can be either at 1 p.u. when in the high load case or at 0.5 p.u. at the low load case as seen in Table 4.6. Similarly the irradiation is at the corresponding value to produce 1 p.u. active power output from the PVPPMs in the high generation case and is halved so that PVPPMs produce 0.5 p.u. active power in the low generation case (Table 4.6). WPP production is considered the same for all cases and is fixed at 1 p.u. for all WPPs. The three pre-fault operating points of the network are created by varying the load and generation cases. Each of them creates a different power flow as it will be explained in the next three sections.

Load Case	Multiplier on peak load	PVPPM Case	Multiplier on generation
High Load	1	High Generation	1
Low Load	0.5	Low Generation	0.5

Table 4.6: Multipliers for installed load and PVPPMs power output for setting up of load cases

4.3.1.1 Base case unidirectional power flow

By using a factor of 1 for installed load (high load) and 0.5 for installed PVPPMs power output (low generation) the load and distributed generation profile seen in Figure 4.2 is realised. As it can be seen the DG in the MV and LV networks are not able to cover the load demand within their respective voltage levels and the 100 MW of power that the HV network can provide also does not cover the total load demand. Hence the power remaining will be provided by the eHV network. This load/generation profile will therefore create a vertical power flow inside the study network stemming from the eHV network down to all LV networks. So in this case the system's pre-fault condition will be a unidirectional power flow as seen in Figure 4.3.

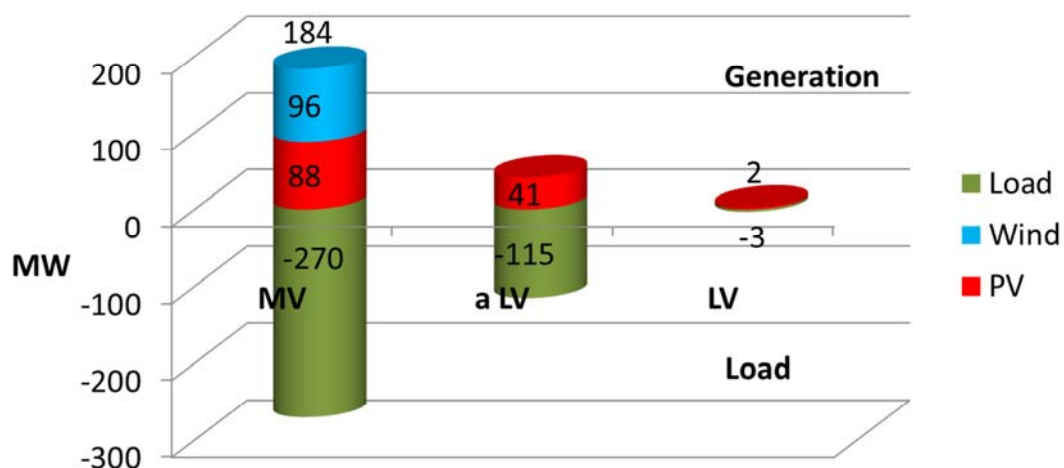


Figure 4.2: Load and DG generation for HV/MV/LV networks for Base case power flow

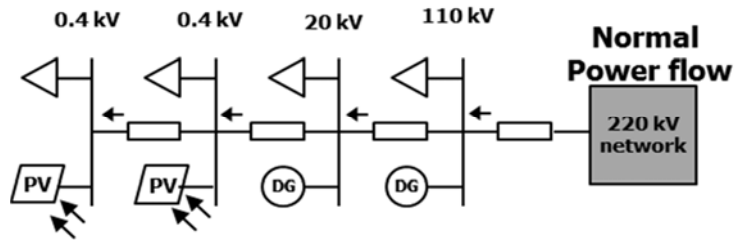


Figure 4.3: Unidirectional power flow from eHV to LV network at Base Case

4.3.1.2 Partial (MV and HV) reverse power flow

By using a factor of 0.5 p.u. for peak load (low load) and 0.5 for installed PVPPMs power output (low generation) the load and distributed generation profile seen in Figure 4.4 is realised.

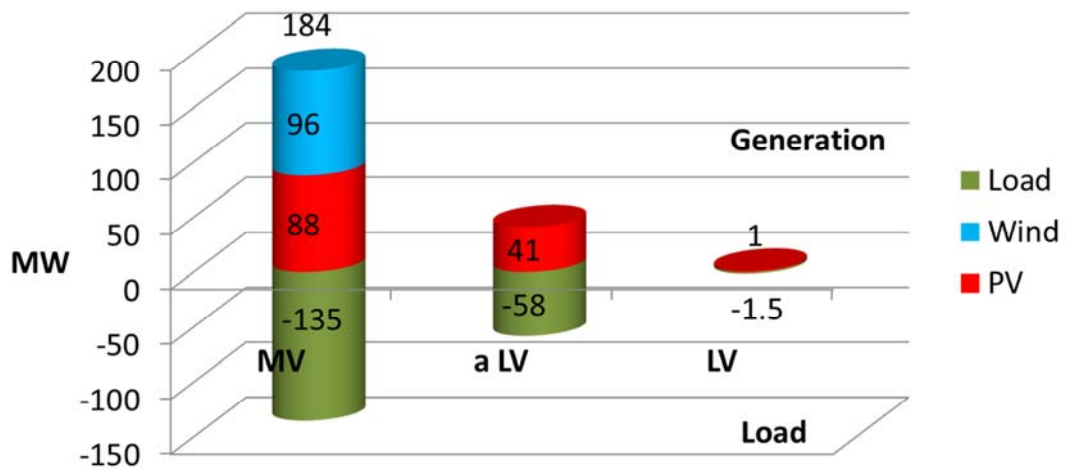


Figure 4.4: Load and DG generation for HV/MV/LV networks for HV and MV reverse power flow

As it can be seen the DG in the LV networks are not able to cover the load demand within their respective voltage levels, contrary to the MV networks that even have a surplus of power. The 49 MW of excess power in the MV networks are enough to cover the almost 18 MW of shortage in the LV networks and export power towards the HV level. The HV network having no installed load will export active power towards the eHV network. This load/generation profile will therefore create a split reverse power flow inside the study network, resulting in reverse power flow from the MV and HV voltage levels as seen in Figure 4.5.

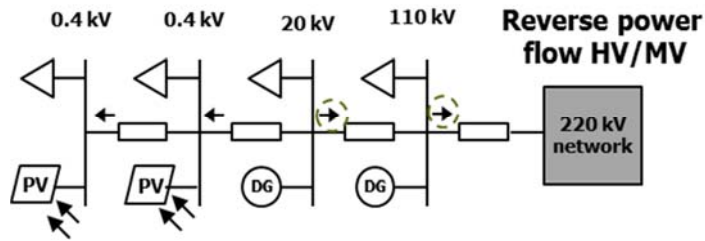


Figure 4.5: Split reverse power flow from MV and HV to eHV network

4.3.1.3 Complete (LV to HV) reverse power flow

By using a factor of 0.5 p.u. for peak load (low load) and 1 p.u. for installed PVPPMs power output (high generation) the load and distributed generation profile seen in Figure 4.6 is realised. As it can be seen the DG in the LV and MV networks are able to cover the load demand within their respective voltage levels and export the excess of active power to the HV network. The HV network having no installed load will export active power towards the eHV network. This load/generation profile will therefore create a full reverse power flow inside the study network, resulting in a reverse power flow from the LV, MV and HV networks towards the eHV network, as seen in Figure 4.7.

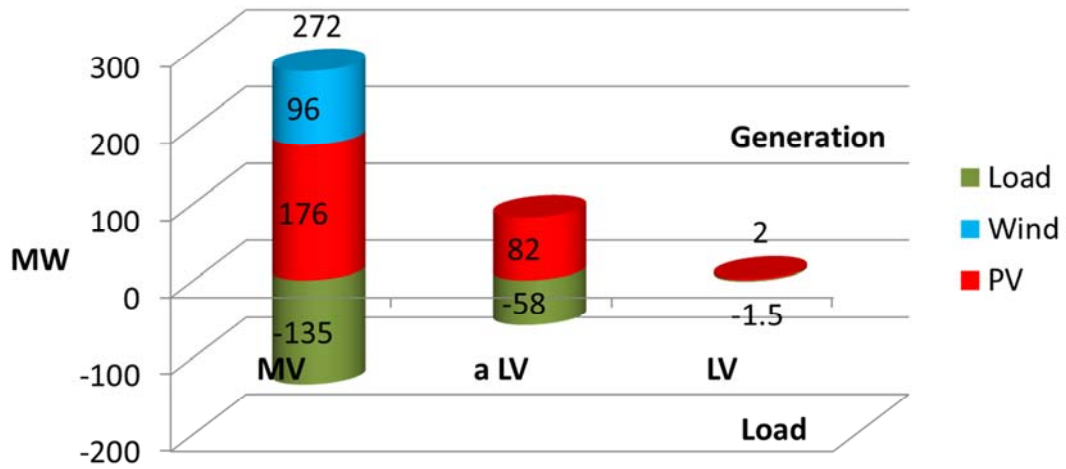


Figure 4.6: Load and DG generation for HV/MV/LV networks for LV to eHV reverse power flow

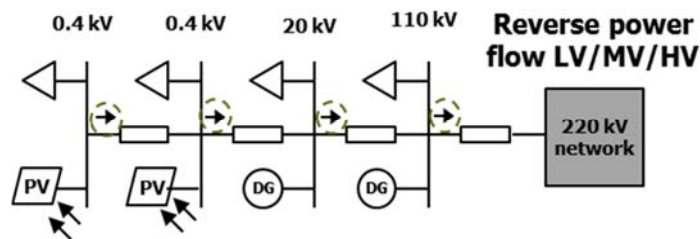


Figure 4.7: Full reverse power flow from LV to eHV network

4.3.2 Network fault control mode settings

The PVPPM’s network fault control settings that are explained in section 3.4.1.2 are applicable only to the low voltage connected PVPPMs installed after 2012. The sensitivity towards the behaviour of PVPPMs during and after the fault is applied by changing the control strategy followed by the aforementioned PVPPMs between no-LVRT (no Low Voltage Ride Through), ZPM (Zero Power Mode), aRCI (additional Reactive Current Injection) and aRACI (additional Reactive and Active Current Injection).

Also the option of delayed post-fault active power recovery can be implemented in any of the three control modes except for the no-LVRT. In total this allows for seven different control modes that will aid in understanding the sensitivity of the voltage in the LV network based on the behaviour of the PVPPMs during and shortly after fault and the benefit of applying dynamic voltage support at the LV level through the LV connected DG.

For the case of aRACI the choice of angle for injecting the mixture of active and reactive current during the fault is based on the network impedance angle seen from the PCC (point of common coupling) of each LV connected PVPPM. The possible four different locations of the connection point of PVPPMs in the low voltage network are shown in Table 4.7 with their respective angle for performing aRACI.

MV busbar/ LV busbar of connected PVPPM	aRACI angle
01/R1	77 °
01/R15	26 °
10/R1	73 °
10/R15	15 °

Table 4.7: Connection points of PVPPMs in the network and angle of aRACI chosen for each point

4.3.3 Overview of sensitivity cases

Control Modes Load Cases	Control Modes						
	No LVRT	ZPM	aRCI	aRACI	ZPM with APR	aRCI with APR	aRACI with APR
Base Case	X	X	X	X	X	X	X
Split Reverse Power flow	X	X	X	X	X	X	X
Reverse Power flow	X	X	X	X	X	X	X

Table 4.8: The study cases formed by varying the sensitivity factors of load cases and PVPPM's control modes

The final overview of sensitivities that stems from the variation of the pre-fault network set-point (load case) and the variation of the control strategy followed by PVPPMs connected in the LV network after 2012 forms the final 21 study cases (Table 4.8).

Due to the high number of study cases only one load case will be presented fully and then comparative graphs will be shown between different control modes and power flow scenarios. The results for the study cases not presented here are included in the Appendix F. Also for the cases with delayed post-fault active power recovery only an overview of the effect of this control strategy will be presented through selected graphs.

4.4 Presentation and Analysis of Results

Four cases will be presented in this section. The structure of presenting and analysing the results is kept the same throughout the cases. The voltages at different busbars of the low voltage network are presented and then with the aid of supporting graphs the analysis of the voltage pattern takes place. Firstly the no-LVRT control scenario for the base case, normal load flow, will be presented as it shows the projected state of the network if German grid codes stay unchanged until 2022. Following this case the comparative results for all control scenarios, besides the ones' with dAPR, in the base case will be presented to demonstrate the effect of different control modes on the voltage profile. The third case is going to be a comparative case between all control modes for the LV to eHV reverse power flow scenario. Finally the effect of delayed active power recovery will be presented.

4.4.1 Base Case with no-LVRT

In the base case the simulation starts from a pre-fault state of top-down power flow from the eHV to the LV network. This case represents the most commonly experienced power flow state of the network nowadays. The parameters that usually ensure a vertical power flow are a high load demand and a low active power in-feed from DG connected to the distribution network.

4.4.1.1 Presentation of results

In this scenario a three phase fault is triggered at 0 s in line 9 of the eHV network and 150 ms later the fault is cleared. HV and MV connected DG abide with the current grid code requirements (GCR) and inject reactive current during the fault to support the voltage. LV connected PVPPMs abide with the LV GCR and disconnect from the network 100 ms after the fault is detected via the voltage drop at the PCC. Also in this case MV and LV connected PVPPMs are producing at half of rated active power output due to the assumed irradiation at the time of the fault. During this period of 100 ms the pre-fault controller of the PVPPMs is operational.

In Figure 4.8 the voltage profiles of all busbars of the eHV network are seen. The fault causes different voltage dips at different locations in the eHV network depending on the distance from the fault and the short-circuit ratio of each location. As it can be seen the range of voltage drop varies from 0.1 p.u. to almost 0.8 p.u.

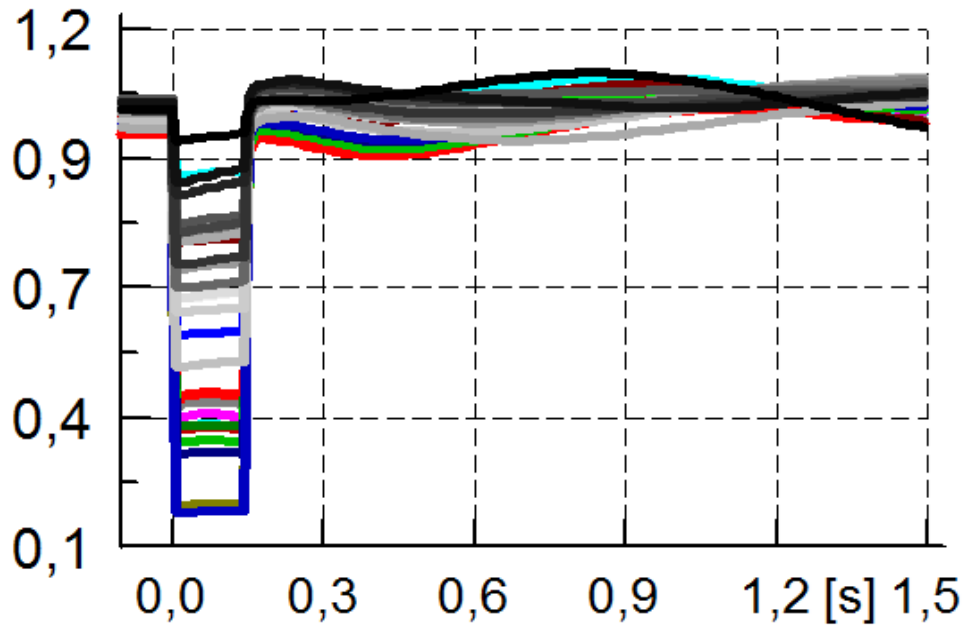


Figure 4.8: Voltage in p.u. at all busbars of the eHV network (different colours represent different busbars)

The fault at busbar 8 of the eHV network, where the distribution system is connected, is the red line of the graph and the voltage dip at that point reaches down to 0.4 p.u. Due to the reactive current injection during fault there is a rise in the voltage in that period but it is not significant. Then the disconnection of the PVPPMs at 100 ms causes a slight voltage decrease, and at 150 ms the fault is cleared and the voltage is restored at a slightly lower steady state value than the pre-fault.

The oscillation of the voltage is caused by the oscillation in the in-feed of active and reactive power by the synchronous generators of the eHV network. This behaviour is typical of SG after faults.

For the LV connected PVPPMs there are four different positions in which they can connect. Every one of the six MV networks of the test system is connected to 2 LV networks; one at busbar 1 and the other at busbar 10 of the MV network (see Figure 3.4). Each of the two LV networks has two connection points for PVPPMs, one at busbar R1 and one at node R15 of the LV network. Due to the similarity in the behaviour of the two different LV networks only the voltage profile of the LV networks connected to busbar 1 of the MV networks will be presented. The rest can be found in Appendix F.

Firstly, in Figure 4.9, the voltage profile of busbar R1 of the LV network connected to MV busbar 1 is depicted for all MV networks in different colours.

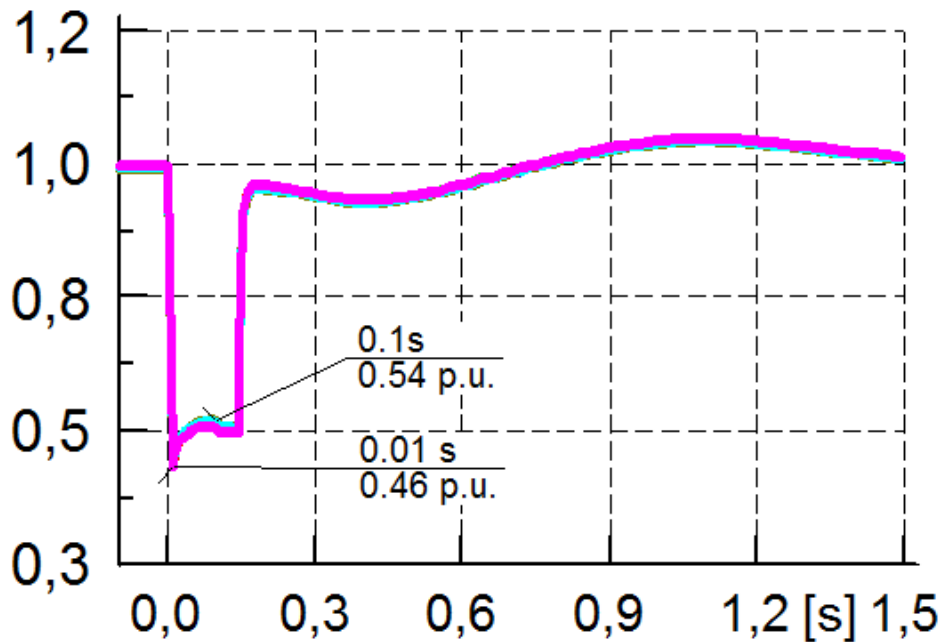


Figure 4.9: Voltages in p.u. at busbar R1 of the low voltage networks connected to busbar 1 of the MV networks with R/X ratio 4.4 (different colours indicate different MV networks)

As seen the starting point of the voltage is at 1 p.u. in all networks. At the occurrence of the fault the voltage drops to 0.46 p.u. and then for the first 100 ms of the fault period it is being raised to 0.54 p.u. At 100 ms a second voltage plateau is depicted lowering the voltage marginally above 0.5 p.u. It should be noted that the voltage traces are very similar among the 6 MV networks.

Finally at 150 ms the fault is cleared and the voltage rises close to the pre-fault value. However, even though the swing of the voltage that is seen post-fault complicates the graph, the steady state voltage post-fault will be slightly lower than the pre-fault starting point. The total loss of active power per aggregate LV network is in the order of 7 MW or approximately 35 % of their peak load (see Table 4.4).

In Figure 4.10 the voltage profile of node R15 of the same MV-connected LV network as the previous graph is shown. The same pattern of behaviour as in Figure 4.9 is depicted. The pre-fault voltage is almost at 1 p.u. and at fault occurrence the voltage drops to 0.48 p.u. The voltage is then raised during the first 100 ms of the fault to the value of 0.56 p.u. In addition, at 100 ms a voltage plateau at 0.48 p.u. is noticed. At 150 ms the fault is cleared and the voltage is raised slightly above 0.9 p.u. Then the voltage oscillates due to the oscillation of the synchronous generators of the eHV network.

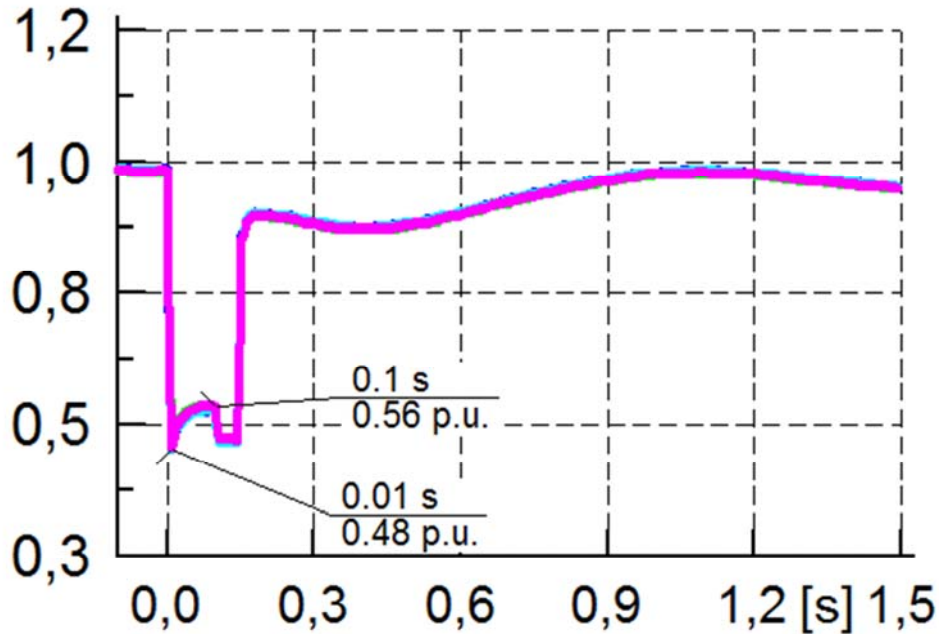


Figure 4.10: Voltages in p.u. at busbar R15 of the low voltage networks connected to busbar 1 of the MV networks with R/X ratio 0.43 (different colours indicate different MV networks)

4.4.1.2 Analysis of results

Firstly in Figure 4.9, the starting point of the voltage is at 1 p.u. due to the remote control option of the MV/HV transformers. As explained before the MV/HV transformers of the MV suburban network target busbar 10 of the MV network. Since the highest load of the MV suburban network is located at busbar 1 the power flow inside the MV network is directed to bus bar 1 and the corresponding voltage drop lowers the voltage at that busbar and consequently at the LV network that is connected to that specific busbar. In the same figure the voltage rise seen during the fault is an outcome of the reactive current injection performed by the MV and HV connected DGs. Even though there is no reactive current injection inside the LV network the voltage is raised as the voltage of the corresponding MV busbar is raised.

At 100 ms the voltage dip seen is an outcome of the disconnection of PVPPMs in the LV network. The active power that the PVPPMs were injecting into the network during the first 100 ms of the fault is now lost. This power is provided from the MV network and creates a larger voltage drop over the impedance of the MV lines and the MV to LV transformer in order to supply the load.

This phenomenon is also noticeable in Figure 4.11 where the active power exchange over the MV/LV transformer can be seen for this LV network. At 100 ms a raise in the active power in-feed from the MV to LV network is seen as a response to the loss of the PVPPMs active power production. The blue line indicates the areas of normal power flow and reverse power flow.

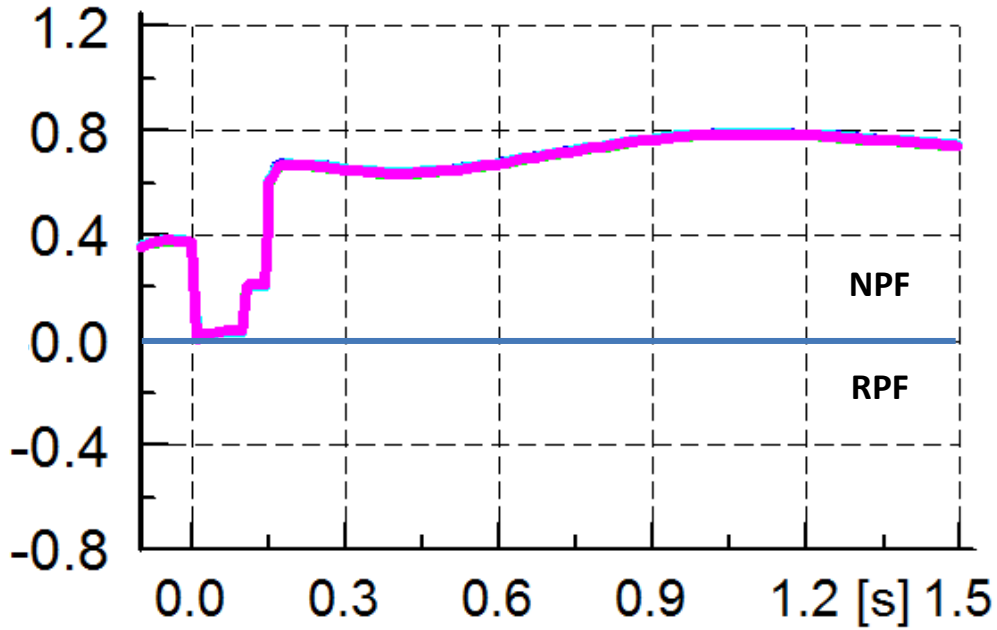


Figure 4.11: Active Power exchange over one of the 38 parallel 500 kVA MV/LV transformers connected to busbar 1 of the MV network in p.u. (different colours indicate different MV networks, base value 500 kVA)

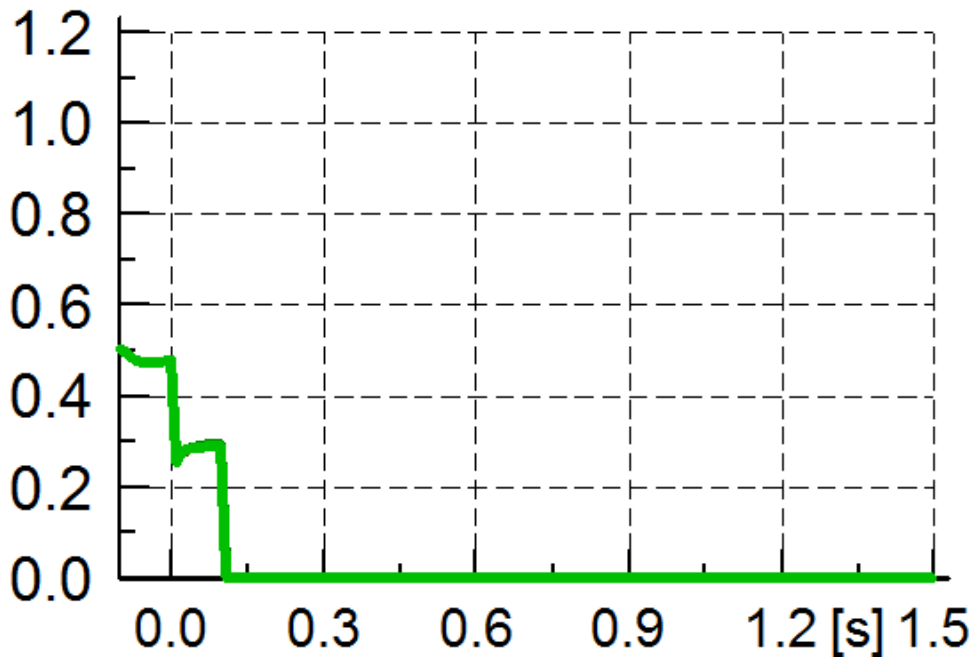


Figure 4.12: Active power output of all 38 parallel LV connected PVPPMs connected to busbar R1 of the LV network connected to MV busbar 1, in p.u. with an aggregated base value of 4 560 kVA

Finally the decrease in the post-fault voltage as compared with the pre-fault value is also explained by Figure 4.11. In this figure the post-fault active power received from the MV network is raised, from 0.4 p.u. to about 0.8 p.u., to cover the deficit of active power inside the LV network caused by the PVPPMs disconnection. This rise in active power received from the MV network results in a slightly higher voltage drop over the transformer, lowering the voltage at busbar R1 and in a significantly higher voltage drop over the LV cables resulting in a lower voltage at node R15.

In Figure 4.10 the voltage profile of node R15 of the examined LV network shows differences as compared to Figure 4.9 of busbar R1. The main difference is that the voltage drop at the occurrence of the fault is slightly smaller, due to the longer distance from the fault location as node R15 is situated deeper in the LV network. Also the voltage at node R15 is raised higher as compared to busbar R1 during the first 100 ms of the fault due to the active current injection performed by the PVPPM of the LV network, which keeps a certain amount of active power in-feed during the first 100 ms of the fault (Figure 4.12) prior to disconnecting.

Furthermore the disconnection of the PVPPMs causes a larger voltage dip and a lower post-fault voltage as compared to Figure 4.9. The reason for both these behaviours is the fact that the PVPPM is connected deeper into the LV network and experiences the combined loss of active power in-feed from the PVPPM connected higher in the LV network at R1 and its own loss. Also this power needs to be provided by the MV network causing an even higher voltage drop than before due to the low X/R ratio of the lines inside the LV network. This state is prolonged post-fault as PVPPMs stay disconnected and therefore the voltage remains at a lower value as compared to the pre-fault one.

Figure 4.13 shows the reactive power exchange over the MV/LV transformer connected at busbar 1 of the MV network in p.u. The rating of the transformer is 500 kVA and the positive sign is attributed to a power flow from the MV to the LV level. As seen the pre-fault and post-fault states are the same as no PVPPM was consuming or producing any reactive power pre-fault. During fault, the voltage drop lowers the reactive power consumption of the voltage-dependent loads and the reactive power losses over the lines. In general the reactive power exchange did not have any important influence in this load case.

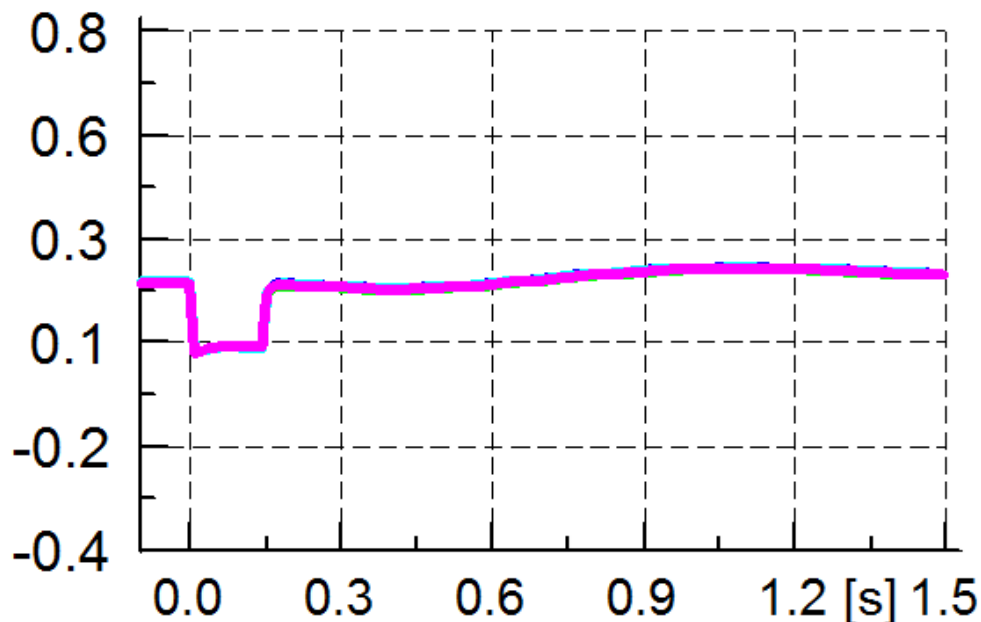


Figure 4.13: Reactive Power exchange over one of the 38 parallel 500 kVA MV/LV transformers connected in busbar 1 of the MV network in p.u. (different colours indicate different MV networks, base value 500 kVA)

Finally it is worth noticing that the fault created a voltage drop down to 0.4 p.u. in the eHV busbar 8, however the LV network inside the distribution system connected to busbar 8 experienced a voltage drop to 0.5 p.u. and in the case of the LV networks connected to busbar 10 of the MV network to 0.6 p.u. (as this is located even further from the fault location). This shows the high retained voltage in the LV networks during a transmission system fault.

Also this fault created a loss in photovoltaic power in-feed of 42 MW (see Figure 4.2) which corresponds to 35 % of the peak load of all LV networks. If every busbar of the eHV network had an identical distribution system attached to it the same fault would potentially cause a loss of 1 600 MW of photovoltaic active power!

4.4.2 Comparison between no-LVRT/ZPM/aRCI/aRACI for the base case

4.4.2.1 Presentation of results

After presenting the no-LVRT base case and performing an analysis of the results, a comparison between the four basic control modes for this load case is presented. In this comparison only the voltage profiles of the LV network connected to busbar 1 of the MV network are presented as they are similar to the other LV network.

In Figure 4.14 the voltage profile at busbar R1 of the LV network connected to MV busbar 1, for all different control modes is shown. The different control cases are depicted with different colours as explained in the graph. In the left side of the graph the fault period is enlarged for facilitating the analysis of the results.

The starting voltage for all control cases is 0.97 p.u., at 0 s the fault occurs and drives the voltage down to approximately 0.46 p.u. for all cases. However it is notable that in the ZPM (green line) case the voltage drops even lower (0.44 p.u.). During the first 100 ms of the fault the voltage rises in all cases but with a different slope. The rise is greater in the case of aRCI (blue line) followed closely by aRACI (black line), both of these cases achieve a voltage of almost 0.58p.u. The ZPM exhibits the lowest rise in voltage as well as the no-LVRT (red line) which manage to raise the voltage to only 0.54 p.u. whereas the other control modes rise to 0.58 p.u. At 100 ms a second voltage plateau is seen for all cases. Post-fault the voltage stays at lower level with respect to the pre-fault value in all cases and even lower in the no-LVRT case.

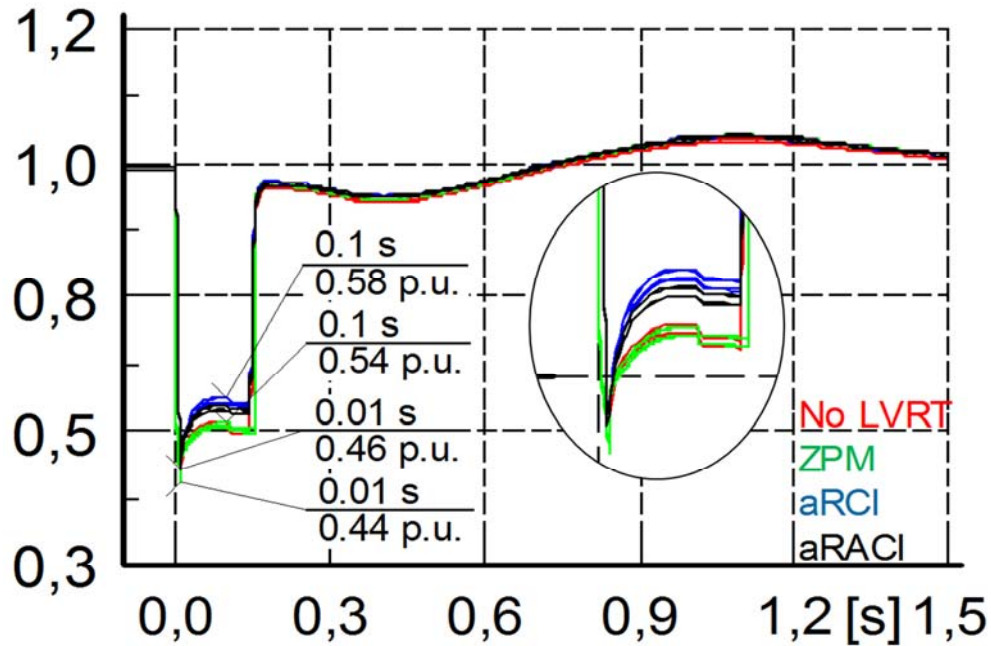


Figure 4.14: Voltages in p.u. at busbar R1 of the low voltage networks connected at busbar 1 of the MV networks with R/X ratio 4.4 for four different control modes

In Figure 4.15 the voltage at node R15 of the low voltage network connected to busbar 1 of the MV network is presented. Again the same pattern is seen, with the voltage starting point slightly lower than in Figure 4.14. The voltage drop at fault occurrence reaches 0.48 p.u., and in the case of ZPM (green line), 0.46 p.u. In the first 100 ms of the fault the rise in voltage is steeper for the aRACI reaching almost 0.6 p.u. while, aRCI (blue line) also has a steep slope, followed by no-LVRT (red line) at 0.56 p.u. and the least rise in voltage is exhibited by ZPM where the voltage is 0.53 p.u. At 100 ms the voltage exhibits a plateau in all cases but as seen in the graph the ZPM and no-LVRT drop below 0.5 p.u. whereas aRCI and aRACI stay higher.

Post-fault the voltage is lower in all cases compared to the pre-fault, however the no-LVRT case has a significantly lower voltage than the rest of the cases. The ZPM case keeps the same voltage as no-LVRT until 0.7 s and then the voltage rises to match up with the other controlled cases. It is important to notice that during the first 550ms after fault clearance the voltage in ZPM and no-LVRT stays below 0.9 p.u.

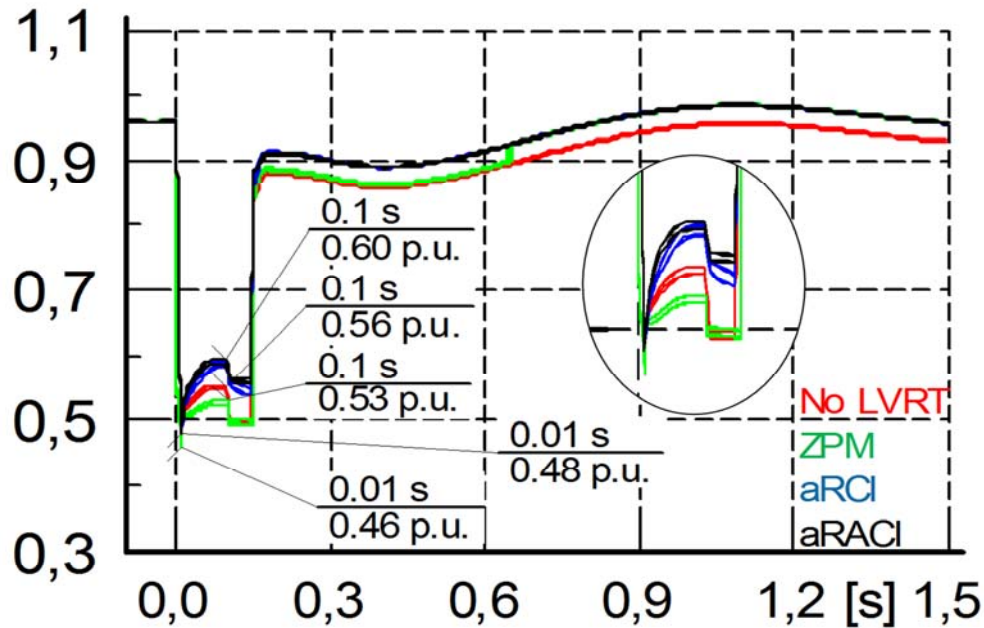


Figure 4.15: Voltages in p.u. at busbar R15 of the low voltage networks connected at busbar 1 of the MV network with R/X ratio 0.43 for four different control modes

4.4.2.2 Analysis of results

As seen in Figure 4.14 for the ZPM (green line) the voltage drop is lower at the occurrence of the fault (0.44 p.u.) with regard to the other control modes (0.46 p.u.). Also the voltage during the fault is marginally lower for the ZPM case (0.54 p.u.) relative to the no-LVRT (red line) and significantly lower if compared with the aRCI (black line) and aRACI (blue line), 0.58 p.u. This behaviour of the ZPM control case can be explained from Figure 4.16 and Figure 4.17.

In Figure 4.16 the active power exchange over the MV/LV 500 kVA transformer can be seen for all control cases. As seen in this graph at the occurrence of the fault the ZPM curve (green line) stays higher than the rest except for the aRCI curve (blue line). This means that for the first 100 ms the PVPPMs of the LV network stop any active power exchange with the network and therefore this power is now provided by the MV network creating a larger voltage drop over the transformers and lines, thus lowering the voltage even further. In the case of no-LVRT (red line) the PVPPMs produce some active power for the first period of the fault and therefore less power is required from the MV network, making the voltage drop smaller. In this figure the aRACI case (black line) is injecting active current at the same level as the no-LVRT case whilst aRCI (green line) far less as the limiters are enabled after 50 ms due to reactive current injection priority during fault.

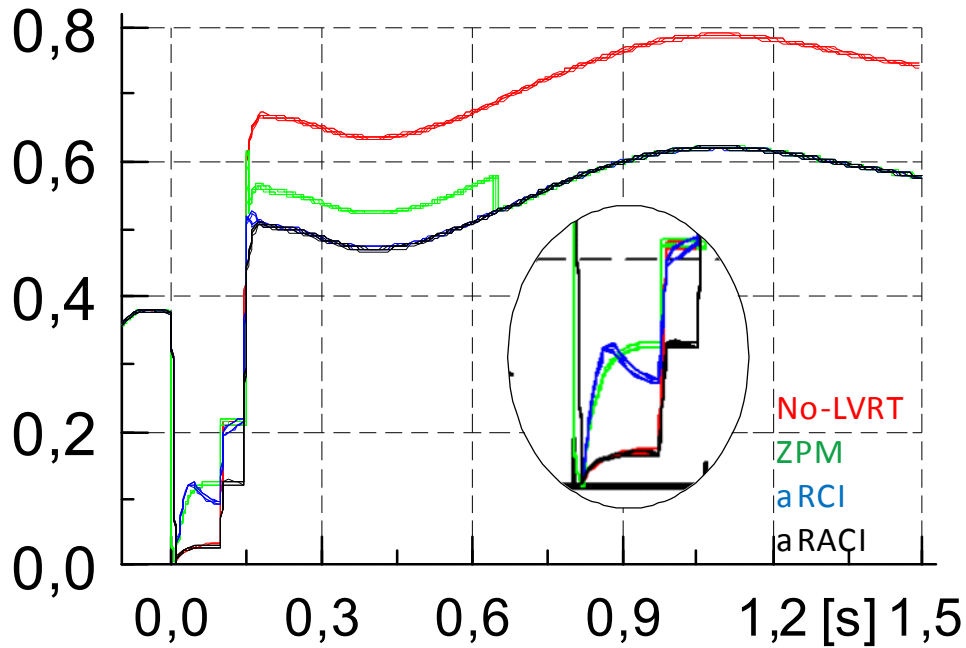


Figure 4.16: Active Power exchange over one of the 38 parallel 500 kVA MV/LV transformers connected in busbar 1 of the MV network for all MV networks in p.u. for all control cases (base value 500 kVA)

At the disconnection of the PVPPMs at 100 ms ZPM and no-LVRT are at the exact same level as in both case at that time no PVPPMs are producing any active power in the LV network. For the aRCI also active power production is low but there is some, as half of the PVPPMs are still connected. Finally the aRACI produces the most active power of all control modes during fault.

The pattern seen in Figure 4.16 would lead to a higher voltage during fault for the no-LVRT and aRACI, however, the voltage profile of Figure 4.14 is measured close to the MV/LV distribution transformer and the X/R ratio of the network at that point is higher than 1 due to the reactive nature of the lines of the MV network. Therefore reactive power exchange over the transformer will influence the voltage profile stronger than active power.

In Figure 4.17 the reactive power exchange over the MV/LV 500 kVA transformer is depicted for all control modes. Pre-fault the LV network is consuming reactive power, which due to the voltage drop at the occurrence of the fault is lowered significantly.

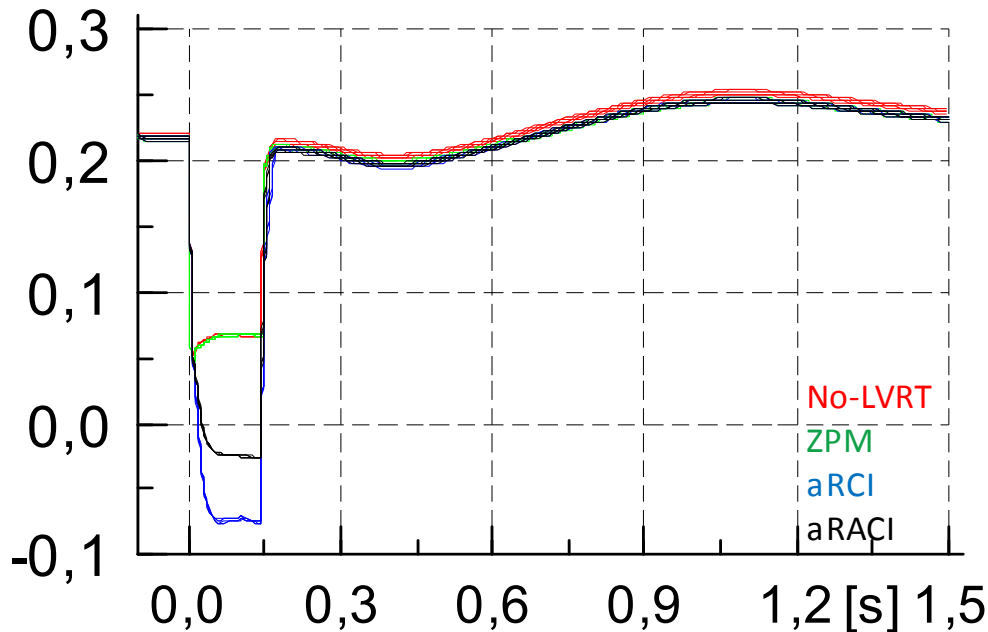


Figure 4.17: Reactive Power exchange over one of the 38 parallel 500 KVA MV/LV transformers connected in busbar 1 of the MV network for all MV networks in p.u. for all control cases (base value 500 kVA)

For the aRCI and aRACI it is lowered further and eventually reversed due to the 2022 connected PVPPMs which inject reactive current to support the voltage.

The disconnection of the PVPPMs at 100 ms lowers the voltage of the network which in turn slightly decreases the consumption of reactive power of the LV network. In total the active power and reactive power graphs of the transformers show that during the fault only aRCI and aRACI inject reactive power to the network while aRACI and no-LVRT inject active power until they disconnect. The outcome of this procedure is a higher voltage during fault for the control modes that inject reactive power and only slight differences for the active power injection proving the role of the high X/R ratio at busbar R1 of the low voltage network.

Finally for the post-fault time frame in Figure 4.14 all control modes have a lower post-fault voltage due to the active power loss of the disconnected PVPPMs and in the case of no-LVRT the voltage is slightly lower due to double the loss of active power as in this case all LV connected PVPPMs disconnect from the network. However the difference is not very significant as active power lost is replaced by the MV network and for busbar R1 the losses are not very large due to the short distance from production and high X/R ratio of the network at that busbar.

The results differ for Figure 4.15, as the post-fault voltage is lower in all cases and furthermore the no-LVRT case has a voltage lower by 0.05 p.u. relative to the other cases, stressing the importance of the loss of active power on the voltage, deep inside the LV network that have a longer distance from production and a low X/R ratio.

In the ZPM case the post-fault voltage stays also at the levels of the no-LVRT up until 0.7 s when it rises to the level of the other control modes. The reason for this behaviour is

that the voltage threshold for deactivating ZPM (0.9 p.u.) is not reached at fault clearance. Hence the ZPM is applied also post-fault and therefore until 0.63 s when the voltage reaches 0.9 p.u. PVPPMs are not exchanging any active or reactive power with the network similarly to the behaviour of no-LVRT. The outcome of this behaviour is also seen in Figure 4.16, where the active power drawn by the MV network is higher post-fault for the ZPM but lower than no-LVRT as only the PVPPMs connected to node R15 (where the voltage recovers slower) are applying the control mode post-fault. By contrast, the PVPPMs connected at busbar R1 are already producing the pre-fault power at fault clearance as the voltage threshold is met at that busbar.

ZPM has the lowest voltage during the first 100 ms of the fault as it injects no active power, no-LVRT is second worse as it injects only active and no reactive power and aRACI raises the voltage by 0.1 p.u., which is significant during the fault as it injects both active and reactive power with the same angle as the network impedance in node R15.

The conclusions of this analysis are that the no-LVRT causes under-voltages post-fault in the low voltage network which are more severe deeper inside the network where the X/R ratio is smaller. About one third of the peak load is lost in generation which seems unacceptable from a system perspective.

This behaviour is corrected by all other control modes due to fast post-fault reconnection of the PVPPMs. While ZPM allows for fast reconnection of PVPPM post-fault in principle this reconnection might be delayed due to delayed voltage recovery. This would be unacceptable for a power system with low inertia.

Finally aRCI and aRACI are by far the superior control modes for raising the voltage during fault, as seen in all figures, and have a similar effect to the voltage close to the transformer, but deeper inside the network aRACI shows better results. Disregarding detrimental effects on network protection, they are the preferred control modes.

4.4.3 Comparison between no-LVRT/ZPM/aRCI/aRACI in the case of full reverse power flow

4.4.3.1 Presentation of results

After presenting the comparison between control modes for the base case, the corresponding comparative results for all control modes in full reverse power flow (fRPF) of the network will be presented.

In Figure 4.18 the voltage at busbar R1 of the LV network connected to MV busbar 1 is shown for all control scenarios. The voltage starts at 0.97 p.u. As it is depicted the voltage drops down to 0.41 p.u. at the moment of fault occurrence for all control modes except for ZPM where it drops to 0.38 p.u. During the first 100 ms of the fault there is a steep voltage rise that leads the voltage to 0.56 p.u. in aRCI and 0.52 p.u. in the no-LVRT case. The differences between cases are small but as it can be seen in the enlarged part of the figure, the strongest influence on the voltage during the first 100 ms of the fault is applied by aRCI, followed by aRACI, ZPM and finally last is no-LVRT. After the first 100 ms of the fault, the

disconnection of the LV connected PVPPMs is triggered resulting in a voltage rise for all control modes, a rather unintuitive behaviour based on the results of the normal power flow. In this 50 ms time frame voltage support between control modes follows the same order as for the first 100 ms of the fault. At fault clearance the voltage rises to a higher value than the pre-fault for all cases. The most significant difference between pre-fault and post-fault voltage is noticed in the no-LVRT case. The rest of the cases have similar post-fault voltages.

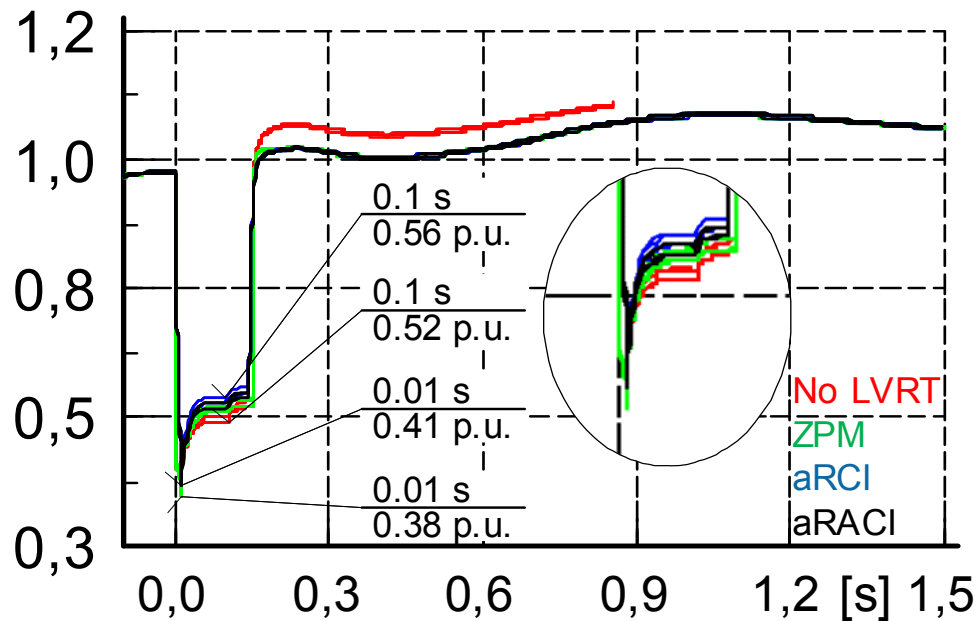


Figure 4.18: Voltages in p.u. at busbar R1 of the low voltage networks connected at busbar 1 of the MV networks with R/X ratio 4.4 for four different control modes in FRPF

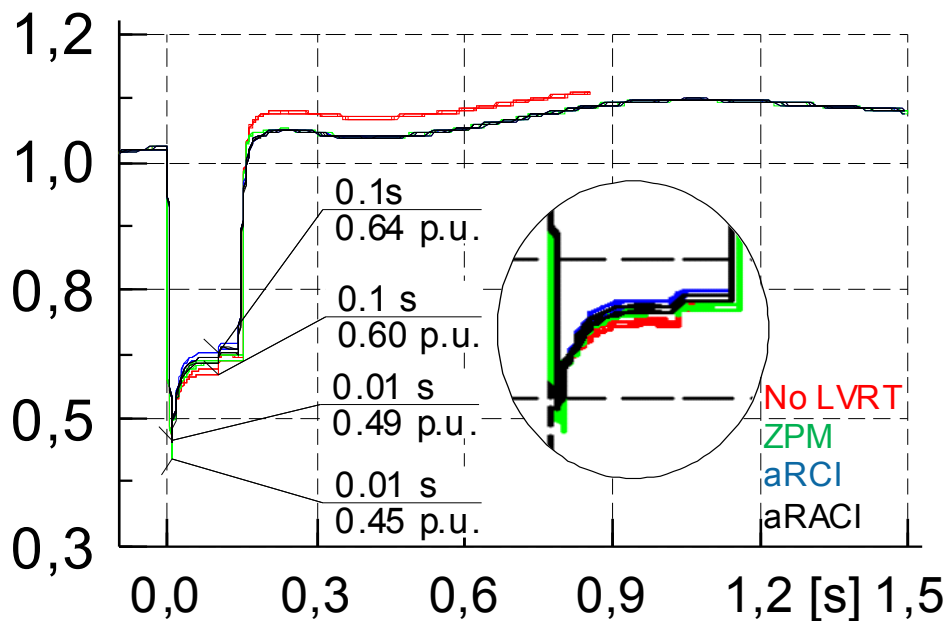


Figure 4.19: Voltage in p.u. at busbar R1 of the low voltage network connected at busbar 10 of the MV networks with R/X ratio 4.4 for four different control modes in FRPF

In Figure 4.19 the voltage of busbar R1 of the corresponding LV network connected in busbar 10 of the MV network is shown. As seen the behaviour is similar to the previous graph with the only difference of a higher retained voltage during the fault due to the location of this busbar deeper into the MV network and further from the fault. However this results in higher post-fault voltages values that in the no-LVRT case reach the overvoltage limit of 1.1 p.u. Then disconnection of loads and production is triggered and the simulation at that point could not converge anymore as the system was led to instability.

In Figure 4.20 the voltage profile at busbar R15 of the LV network connected to busbar 1 of the MV network is presented. A difference in the behaviour of the voltage curves relative to Figure 4.18 is noticed. The voltage drop is not as deep as in Figure 4.18, and the voltage rise during the fault is significantly higher leading the voltage to a value of 0.64 p.u. in the aRACI case.

Also the difference between the control cases in raising the voltage during the fault is more pronounced. Moreover in the ZPM case the voltage increases less than the other cases (0.57 p.u.) and in the aRACI the most, contrary to the voltage profile of busbar R1. Furthermore the disconnection of PVPPMs at 100 ms causes a voltage drop instead of an increase, and post-fault the voltage returns to the pre-fault operating point. The no-LVRT case depicts a slightly lower voltage post-fault in comparison with the other cases but the difference is not as pronounced as in Figure 4.18.

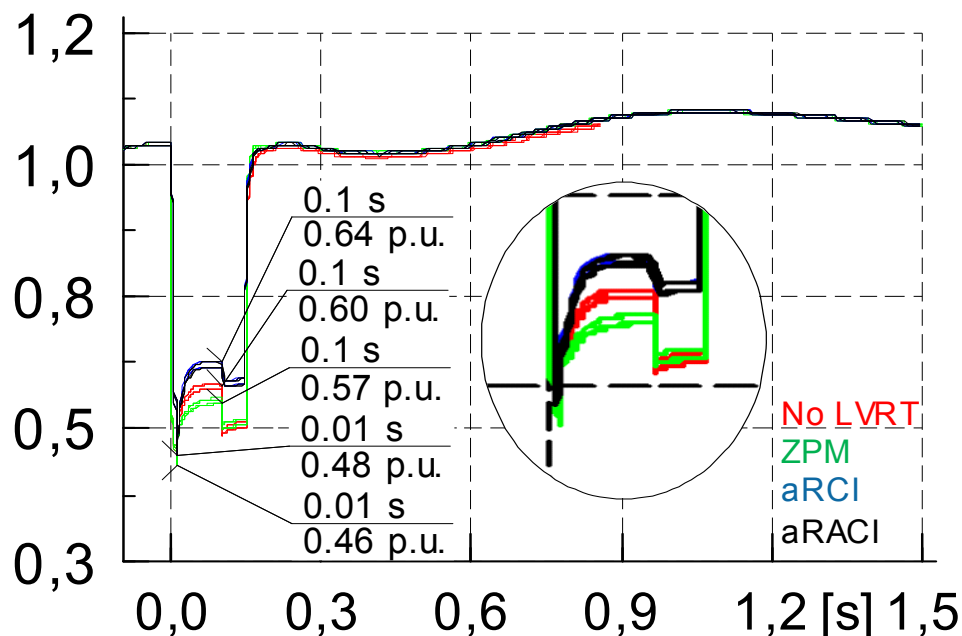


Figure 4.20: Voltages in p.u. at busbar R15 of the low voltage networks connected at busbar 1 of the MV networks with R/X ratio 0.43 for four different control modes in fRPF

4.4.3.2 Analysis of results

The results presented in the previous section will be analysed in this section with the aid of Figure 4.21 and Figure 4.22 that depict the active and reactive power exchange over the MV/LV transformer for all control cases. It is important to notice for the analysis that due to

PVPPMs producing active power at 1 p.u., in order for the network to enter reverse power flow, they also consume reactive power pre-fault due to their dynamic power factor control as explained in section 3.4.1. This behaviour is apparent also from Figure 4.22 where the pre-fault point has a very high reactive power consumption if compared with the base case (Figure 4.13). The behaviours will be analysed first for the fault period and then for the post-fault.

For the fault period ZPM exhibits the lowest voltage dip at the moment of fault occurrence both in Figure 4.18 and Figure 4.20. That behaviour can be explained as the 2022 PVPPMs that perform the ZPM control strategy at the occurrence of the fault drive the active power production to zero faster than in the no-LVRT case as deduced from Figure 4.21. The loss of active power production that needs to be replaced from active power from the MV network causes a larger voltage drop due to the losses over the larger impedance that stands between production and load. Also ZPM shows the lowest voltage for the first 100 ms of the fault in Figure 4.20, but only the second lowest after no-LVRT in Figure 4.18. This behaviour is the combined effect of ZPM providing the least active current injection during fault (Figure 4.21) and the second largest reactive power consumption (Figure 4.22). Due to the high X/R ratio of the LV network at busbar R1 reactive power consumption is a more crucial factor in lowering the voltage than the rise caused by active current injection and therefore the no-LVRT that consumes the higher reactive power during the fault has the lowest voltage profile. At node R15 of the LV network the X/R ratio is below 1 and hence active power is more influential to the voltage. Hence, ZPM which injects less active power than other control modes during the first 100 ms of the fault has the lowest voltage (Figure 4.21).

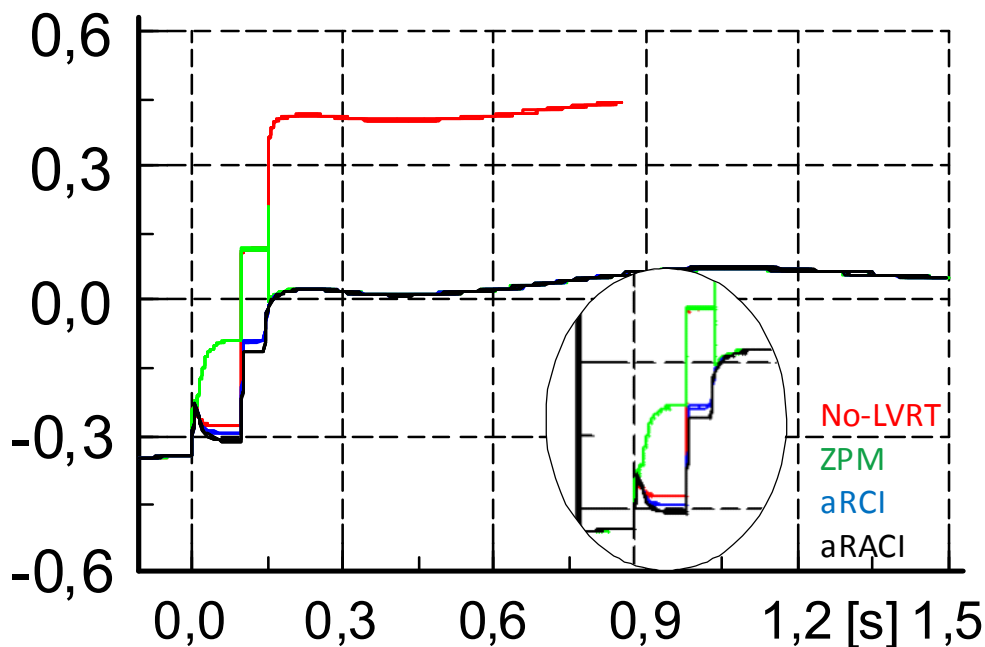


Figure 4.21: Active Power exchange over one of the 38 parallel 500 kVA MV/LV transformers connected in busbar 1 of the MV network in p.u. for all control cases in fRPF (base value 500 kVA)

For the first 100 ms of the fault period the aRCI strategy, which injects the highest reactive current and the second highest active current shows the best performance at busbar R1 of the LV network (Figure 4.18) that has a high X/R ratio. At busbar R15 of the LV network (Figure 4.20) that has a low X/R ratio aRACI exhibits the higher voltage rise as it injects the most active current and the second highest reactive current.

Disconnection of the PVPPMs at 100 ms results in a significant loss of active power (Figure 4.21) that leads the network into normal power flow in the cases of no-LVRT and ZPM. However, the disconnection of the PVPPMs and the loss of reactive power consumption performed by them, lead to an excess of reactive power that is now exported to the MV network (Figure 4.22). Besides the loss of consumption of reactive power there is also some production of reactive power due to the capacitive nature of the lines. That is why we see export of reactive power to the MV level even in ZPM (green line) where the PVPPMs do not produce any reactive power.

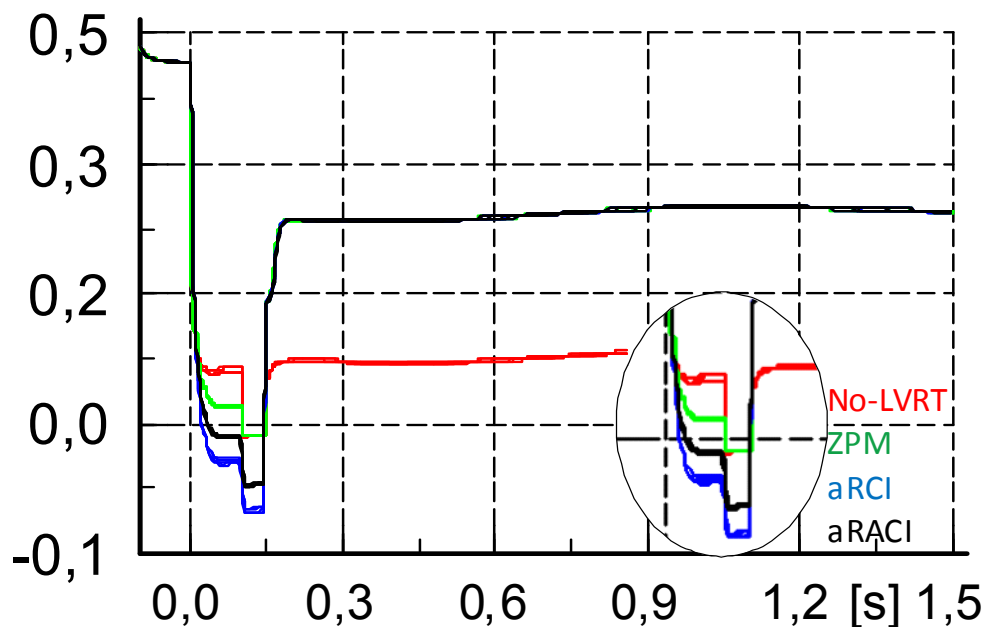


Figure 4.22: Reactive Power exchange over one of the 38 parallel 500 kVA MV/LV transformers connected in busbar 1 of the MV network in p.u. for all control cases in fRPF (base value 500 kVA)

The combined effect of these two phenomena that have opposing effects: the loss of active power leads to a voltage drop and the excess of reactive power to a voltage increase affects in a different way busbars R1 and R15 of the LV network. The difference in X/R ratio leads the voltage at busbar R1 to rise (Figure 4.18), due to the higher influence of reactive power, and the voltage at node R15 to drop, due to the higher influence of active power (Figure 4.20).

For the post-fault period the voltage behaviour is again affected differently by active and reactive power. Post-fault reconnection of the PVPPMs in all control modes except for the no-LVRT results in less active power consumption from the LV network, and creates a slightly higher voltage post-fault at node R15 (Figure 4.20). However, the reconnection of PVPPMs creates a higher reactive power consumption for all control modes except the no-LVRT that

result, in a lower post-fault voltage for those modes at busbar R1 (Figure 4.18) . In general there is an increase in the post-fault voltage mostly at busbar R1 due to the 2012 PVPPMs that disconnected and lowered the post-fault reactive power consumption as compared to the pre-fault one.

Therefore the interaction between dynamic power factor control and obligatory disconnection during fault can lead to over-voltages. Also the pre-fault voltage drop compensation by transformer tap-changers can raise the post-fault voltage value due to the different voltage profile of the network post-fault.

4.4.4 Effect of pre-fault starting point

4.4.4.1 Presentation of results

The voltage drop during the fault is also affected by the pre-fault starting point of the network. In order to present this effect the ZPM control case was chosen for all three different power flows as seen in Figure 4.23.

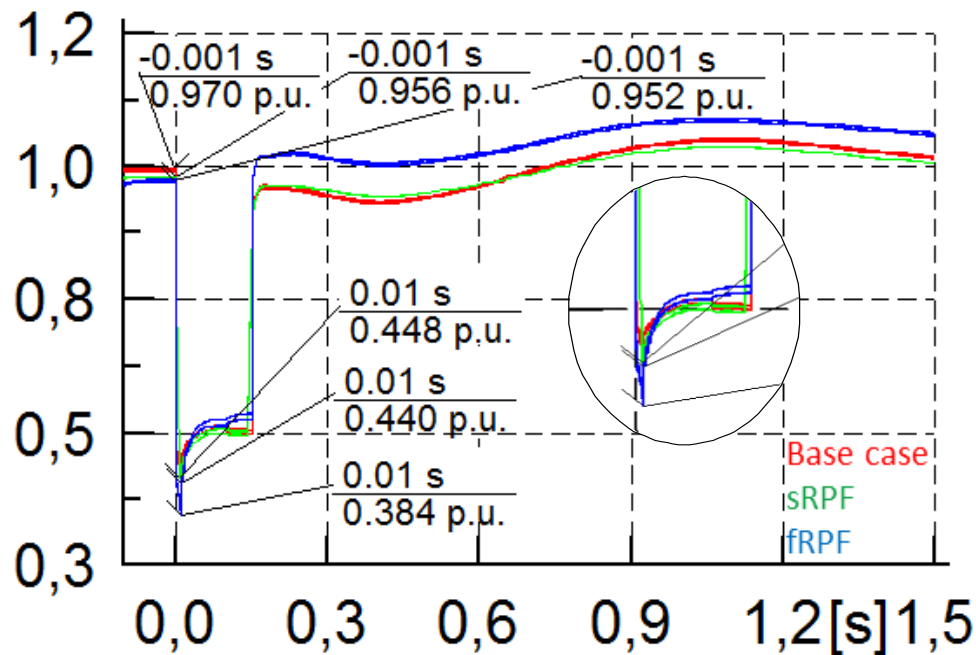


Figure 4.23: Voltages in p.u. at busbar R1 of the low voltage networks connected at busbar 1 of the MV networks with R/X ratio 4.4 during ZPM for all load cases

In this figure the voltage at busbar R1 of the LV network connected to MV busbar 1 is shown. The voltage at the occurrence of the fault is different for all load cases as well as the depth of the dip. The second plateau appears as a voltage decrease for the base case (red line) and the sRPF (green line) and as a voltage increase for the fRPF (blue line). Post-fault the voltage stays lower than the pre-fault for the base case and sRPF but in the fRPF it stays significantly higher.

In Figure 4.24 the voltage at node R15 of the LV network connected to MV busbar 1 is shown for all load cases. In this figure the pre-fault voltage is different for all load cases as well but not the same way as in Figure 4.23. During the fault the voltage support is more

intense in the fRPF case and post-fault the voltage stays at different levels in all load case. At 0.66 s in the base case there is a vertical rise in the voltage.

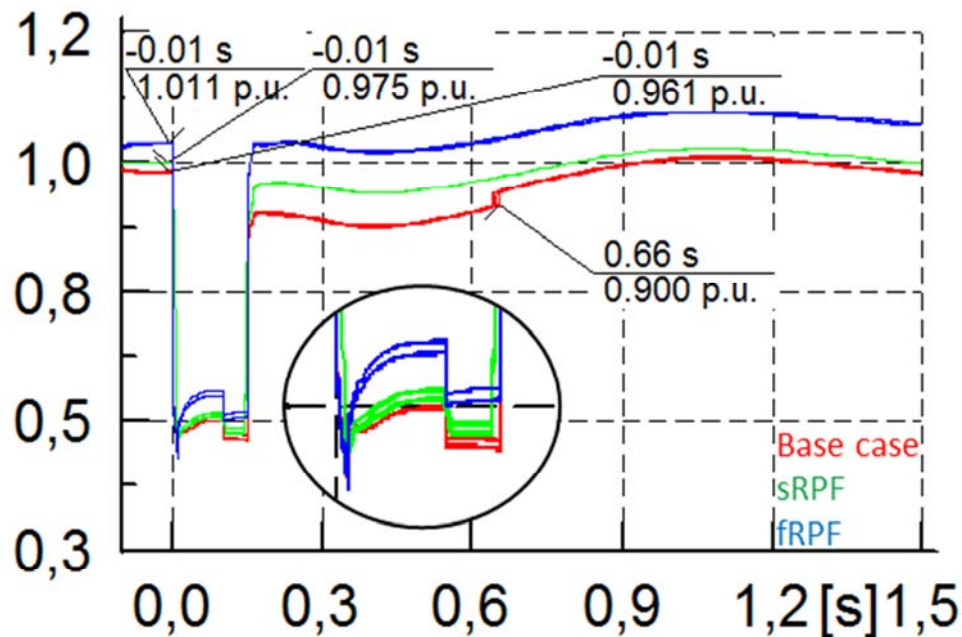


Figure 4.24: Voltages in p.u. at node R15 of the low voltage networks connected at busbar 1 of the MV networks with R/X ratio 0.43 during ZPM for all load cases

4.4.4.2 Analysis of results

In order to analyse the results between different load cases, the effect of the tap-changers must be removed. By subtracting from the pre-fault voltage of every load case the voltage at the fault the absolute voltage dip can be compared in order to see in which case the voltage drop was the worse at busbar R1 (Figure 4.23). In the fRPF the absolute voltage drop was 0.568 p.u, in the sRPF it was 0.516 p.u. and in the base case it was 0.522 p.u.

So the worst voltage drop was experienced at fRPF where at the instance of the fault the reactive power exchange over the transformer dropped by 0.4 p.u. (Figure 4.22). In the base case where the voltage drop was smaller the reactive power exchange over the transformer dropped by 0.18 p.u. (Figure 4.17) and in the sRPF by less than 0.1 p.u. (Appendix F). As the short circuit voltage of the MV/LV transformer is 4.1%, the voltage drop is proportional to the voltage drop caused over the transformer impedance due to the reactive and active power loss at the instance of the fault. Therefore this graph aids in understanding the reasoning for the differences in voltage drop between different load cases. The behaviour post-fault is already explained by previous cases.

In Figure 4.24 the important things to note are that pre-fault the higher voltage (1.011 p.u.) is seen for the fRPF, second higher for sRPF (0.975 p.u.) and the lowest for the base case (0.961 p.u.). This is happening due to the difference in power flow direction between cases. In the fRPF and sRPF the power flows from node R15 to busbar R1 and that is why the

voltage is higher in these cases in the R15 node. For the base case the flow is from busbar R1 to node R15.

The second important finding of this graph is that in the base case at 0.66 s the impact of ZPM delayed switchover from fault to normal operating control mode on the voltage can be seen. Due to the lower voltage of that case and the fact that in ZPM during fault there is no support on the voltage, at fault clearance, the voltage fails to ascend higher than 0.9 p.u. The threshold for returning to normal operating condition is not met and the PVs stay in fault mode having no active or reactive power exchange with the network. Therefore with no active power boosting the voltage in the post-fault period stays low until at 0.66 s the threshold is met and the PVs return to the normal operating state. Then the voltage is raised significantly due to the active power in-feed of the PVs.

4.4.5 Effect of delayed active power recovery (dAPR)

In order to demonstrate the effect of delayed active power recovery (dAPR) on the voltage profile of the LV network two cases will be compared with the corresponding cases including dAPR. The choice of cases aims to showcase the extent of the influence of dAPR. For this reason results will be presented for the ZPM case in comparison with ZPM with dAPR for the base case and the LV to HV reverse power flow. Then the results from those two cases will be analysed.

4.4.5.1 Presentation of results

Base Case

In Figure 4.25 the voltage profile of busbar R1 of the LV network connected to busbar 10 of the MV network is presented for the case with ZPM and the case with ZPM and delayed active power recovery (dAPR) during a normal power flow. The choice of ZPM as the control mode for presenting the effect of dAPR, is based on dAPR addition showing the most difference in results as active power drop during fault is the greatest between the three other control modes.

As explained in section 3.4.1.2, the dAPR is applied post-fault and, therefore, the effect of enabling the dAPR can only be seen post-fault. As seen in Figure 4.25 the voltage profile shows minor differences between the case with dAPR (green line) which stays slightly lower at fault restoration from the case without dAPR (red line).

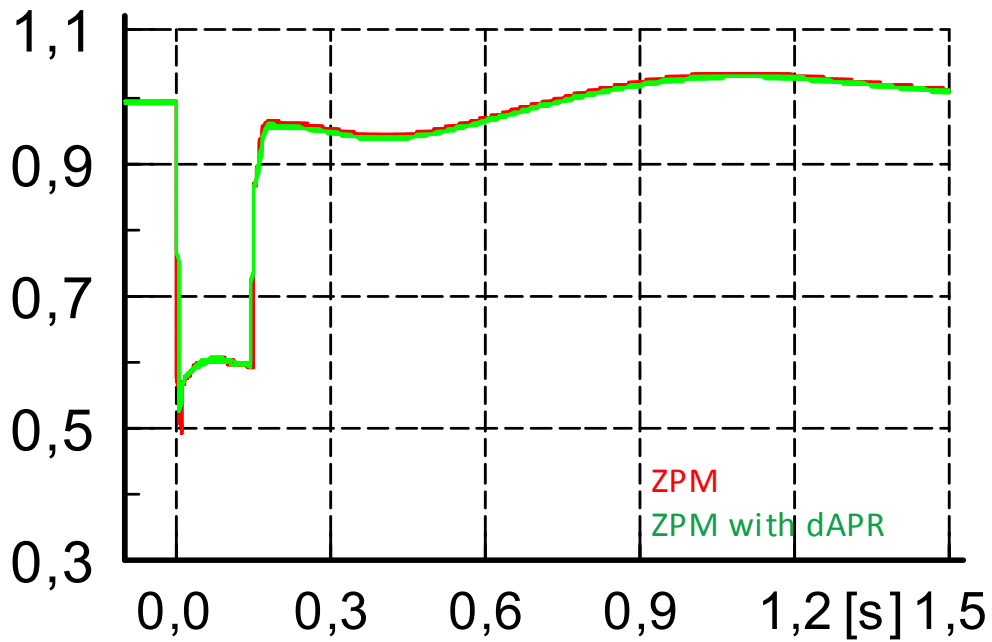


Figure 4.25: Voltage in p.u. at busbar R1 of the low voltage network connected to busbar 10 of the MV network for ZPM with and without delayed active power recovery

The case is different in Figure 4.26 where the voltage profile at node R15 inside the same LV network is shown for both cases. Here the difference in the post-fault voltage is close to 0.05 p.u. and the effect of delaying the return to active power lowers the voltage post-fault enough to keep the fault state of the PVPPMs until 0.6 s when the voltage rises above the threshold of 0.9 p.u.

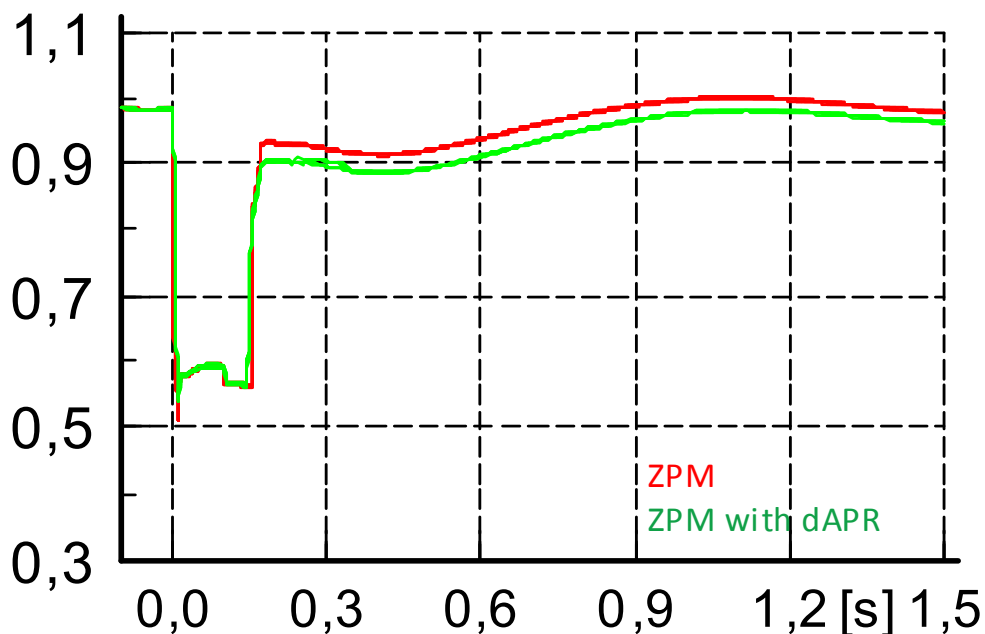


Figure 4.26: Voltage in p.u. at busbar R15 of the low voltage network connected to busbar 10 of the MV network for ZPM with and without delayed active power recovery

LV to HV RPF

The same control case, ZPM, is chosen to present the performance of dAPR in the case of full reverse power flow (fRPF) from the LV network to the eHV network. In Figure 4.27 the voltage at busbar R1 of the LV connected to busbar 10 of the MV network is presented, for ZPM (red line) and ZPM with dAPR (green line). The rise of the voltage in this load flow scenario, post-fault, is higher in the case with dAPR. More importantly, whilst in the case of ZPM the voltage stays lower and avoids reaching the high voltage threshold of 1.1 p.u., in the case with dAPR the threshold is met and further disconnections are triggered forcing the simulation to stop.

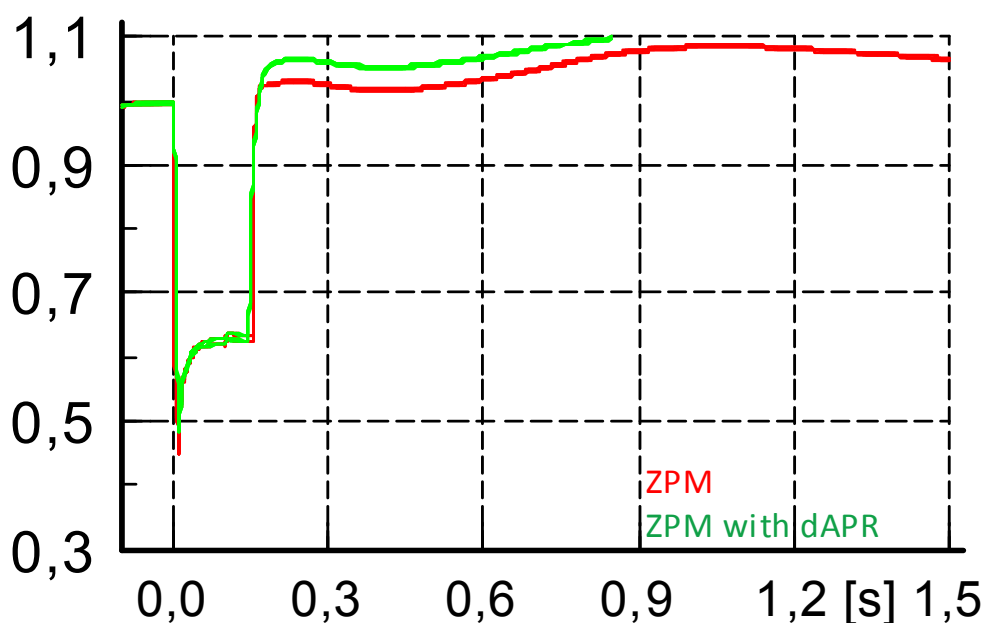


Figure 4.27: Voltage in p.u. at busbar R1 of the low voltage network connected to busbar 10 of the MV network for ZPM with and without delayed active power recovery in fRPF

In Figure 4.28 the voltage profile at busbar R15 inside the LV network connected to busbar 10 of the MV network for reverse power flow for both control scenarios is presented. After fault restoration at 150 ms the voltage in the ZPM (red line) case has a higher value than in the case with dAPR (green line), but the difference is marginal and much less than in Figure 4.27. Also here the simulation for ZPM with dAPR ends before 0.9 s.

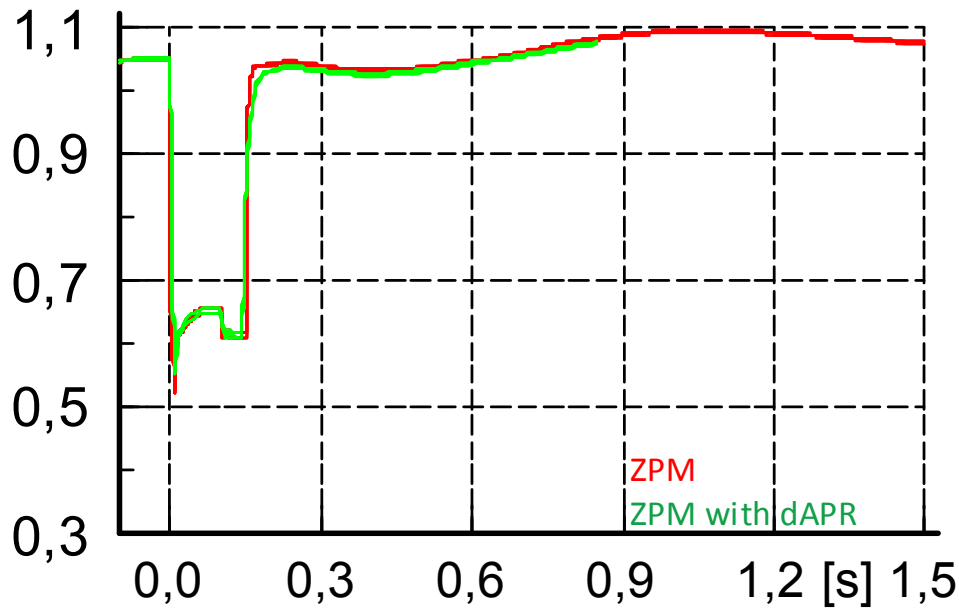


Figure 4.28: Voltage in p.u. at busbar R15 of the low voltage network connected to busbar 10 of the MV network for ZPM with and without delayed active power recovery in fRPF

4.4.5.2 Analysis of results

Base Case

In Figure 4.25 and Figure 4.26 the lower voltage of the case with dAPR is due to the delayed active power recovery post-fault. Only part of the active power of the 2022 connected PVPPMs is injected in the case with dAPR and therefore the rest of the active power provided by the MV network causes a larger voltage drop over the transformers and lines.

This effect is less intense in busbar R1, due to the small distance from the MV network and the high X/R ratio at that point of the network that minimizes the effect of active power on the voltage. However it is more apparent in node R15 (Figure 4.26) due to the longer distance of this node from the MV network and the low X/R ratio inside the LV network that increases the influence of active power on the voltage. Thus the addition of dAPR creates a significant difference in the voltage post-fault that increases the severity of the fault.

It is concluded that in the base case (normal power flow) dAPR creates under-voltages post-fault that worsen the state of the network stability.

LV to HV RPF

In Figure 4.27 and Figure 4.28 the results for the influence of dAPR on fRPF are much different than in the base case. This behaviour can be explained by the state of the PVPPMs in the full reverse power flow case. In this case the PVPPMs, pre-fault, are producing active power at 1 p.u. and therefore consume reactive power in order to keep a power factor of 0.9 inductive as described in section 3.4.1.1. In the ZPM, active power production during fault drops to zero and so does reactive power consumption. Hence post-fault if active

power recovery is delayed so is reactive power consumption. This behaviour creates a deficit of active power post-fault and an excess of reactive power, since PVPPMs don't consume reactive power as pre-fault. The combined effect of these two components raises the voltage in busbar R1 due to the low X/R ratio which favours the effect of reactive power over active on the voltage. This eventually creates post-fault over-voltages that lead the system to further disconnections of production and load.

In Figure 4.28, the effect is reversed as at node R15 the X/R ratio is below 1, and therefore the active power deficit has a stronger influence on the voltage than the excess of reactive power. The previously described conditions apply as well but the end result is different, as the voltage in the case with dAPR is lower than the case with instantaneous active power recovery due to the delay of active power in-feed by the 2022 PVPPMs lowering the voltage. However due to the excess of reactive power at the network this effect is milder and the voltage drop is barely noticeable.

It is concluded that in the FRPF case the effect of APR is creating over-voltages higher in the LV network while connection points deep in the LV network slightly reduces the over-voltages created.

4.5 Conclusions

In this chapter the main simulation results of this thesis were presented, for a number of specific system conditions and control modes. First the test system was presented, with an argumentation for the choice of DG capacity that reflect the level of PV penetration for Germany in 2022. A thorough description of the sensitivity factors that helped build the study cases was given. Finally the results for the most important cases were presented and analysed in depth. The conclusions of this analysis will be presented in the next chapter.

Chapter 5 : Conclusions and Future Research

5.1 Introduction

In this chapter the conclusions of this thesis will be presented. The general recommendations, based on the findings of the study, regarding the sensitivity of the voltage dip-depth in LV networks with high penetration of DG will be presented. Also, the impact of reverse power flow will be discussed with a focus on the consequences for the post-fault period. Furthermore, the recommendations for different control modes will be mentioned, as well as the relevance of delayed post-fault active power recovery. The correlation between the results and the German network will be analysed and finally, recommendations for future research will be proposed.

5.2 Conclusions

5.2.1 Voltage dip-depth sensitivity in LV networks with high penetration of PV

The results presented in this study depend, to a certain extent, on the particular network topology and are only applicable for the chosen DG penetration levels. Only balanced transmission system faults were studied, as they are the most severe type of faults. The main conclusions for the voltage sensitivity in LV networks with high penetration of PVs during transmission system faults, will be presented in bullet points and analysed below.

- Retained voltage at the LV network is higher as compared to other voltage levels during fault. Higher power in-feed during fault from LV connected DG is therefore possible.

As seen from the results, the retained voltage in the LV network, during a fault, stays 0.1 to 0.2 p.u. higher as compared to the eHV busbar connected to the distribution network (BB 8). Therefore, current in-feed during the fault results in higher power, due to the higher retained voltage at the LV network. Of course, the dip in voltage also controls the amount of current that the DG injects. Hence, the total contribution can be the same above a certain voltage in both locations.

- The depth of the voltage dip is sensitive to loss of production of both active and reactive power at the instance of the fault.

At the first ms after the occurrence of the fault the amount of active and reactive power lost instantaneously has an impact on the voltage drop, as seen especially in the case of ZPM. In this case, the loss of active and reactive power is maximized due to the propriety control strategy resulting in the lowest voltage drop during the fault. Therefore, a good approach would be to try and keep the loss of active and reactive power at fault occurrence as low as possible to minimize the voltage drop.

- Voltage support from LV connected DG, during fault, can increase the voltage significantly.

As seen from the results, the cases with aRCI or aRACI provide strong support to the voltage during fault. Also, in these cases the voltage profile of the network is higher as compared to the cases where all LV connected PV disconnect by 0.1 p.u or more. This finding also proves the importance of providing reactive and active current support to the network in case of a fault.

- Active current injection during fault has a more profound effect than reactive current injection in supporting the voltage, deep inside the LV network.

The aRACI control strategy used showed improved voltage support as compared to the aRCI strategy when applied deep inside the LV network. The reason for the high influence of active power on the voltage is due to the low X/R ratio of the LV network. Therefore, it is safe to assume that this type of support is relevant for the DG connected deep inside the LV network and should be preferred over the aRCI.

- Reactive current injection, during fault, performs better in supporting the voltage closer to the MV/LV transformer of the LV network.

The aRCI control strategy proposed, achieved the best voltage support as compared to the rest of the strategies when applied close to the transformer of the LV network. The reason for the high influence of reactive power on the voltage is due to the high X/R ratio of the LV network close to the MV/LV transformer. Therefore, this type of support is effective for the DGs connected close to the MV/LV transformer.

- During normal power flow or MV to HV reverse power flow, disconnection of PVs in the event of a transmission system fault create a significant voltage drop, during the fault, throughout the network.

The loss of active power during normal power flow or partial reverse power flow from MV to HV level, creates a voltage dip which is more intense inside the LV network than in other busbars of the system. This voltage dip is created as an imminent result of the loss of DG active power at the disconnection moment of DG. The active power lost from LV connected DG is now provided by the higher voltage level resulting in a lower voltage, due to an increased voltage drop over the lines and transformers of the network. This effect is stronger inside the LV network, as the distance is longer and the lines have a higher resistance resulting in a larger voltage drop. The second voltage plateau should be considered in a possible FRT curve to specify if the voltage dip is deeper at the occurrence of the fault or at the disconnection of the DG. Of course, this will depend on the amount of LV connected DG.

- Disconnection of PVs in the event of a transmission system fault creates a significant voltage drop, during the fault, inside the LV network. However, close to the MV/LV transformer and in the rest of the network, during LV to HV full reverse power flow, the disconnection of PVs results in the voltage being raised.

The disconnection of PVs in the case of full reverse power flow creates a deficit of active power and an excess of reactive power, as LV connected PVs were consuming reactive power pre-fault. The final outcome is a voltage rise at the points of the network with a high X/R ratio and a voltage dip at the points of the network with a low X/R ratio.

- Impact of X/R ratio of the LV network is influential when performing voltage support.

As seen from the results, the impedance angle of the network at the DG connection points plays an important role in the influence of reactive and active power on the voltage. Therefore, it should be taken into account when performing voltage support.

- Post-fault reconnection of the PVs benefits the voltage profile significantly in all cases.

Post-fault under-voltages in the base case and in MV to HV reverse power flow are lower if current practices are followed and PVs do not reconnect immediately to the network. In the LV to HV reverse power flow, post-fault over-voltages are higher if current practices are followed and PVs don't reconnect immediately to the network.

5.2.2 Impact of reverse power flow

In the case of reverse power flow the results were very different than in the other load flow cases, for all control modes. The results from reverse power flow are also linked with the PVs producing maximum active power and therefore, consuming reactive power during the pre-fault period. The results for the fRPF would change if the PVs' steady state dynamic power factor control was different.

The joined effect of loss of active power and loss of reactive power consumption is the main trigger for the difference in results. The voltage support during fault boosts the voltage higher in the reverse power flow case. Post-fault the voltage stays significantly higher than pre-fault due to the excess of reactive power in the network, caused by the PV disconnection.

The impact of reverse power flow is, in essence, the impact of the PVPPM pre-fault reactive power consumption that creates post-fault over-voltages and alters the behaviour of the network during the fault.

Also, another factor that plays a role in the post-fault behaviour of the voltage is the effect of the tap-changers of the transformers. Pre-fault tap-changers are set to compensate for the voltage drop over the lines, but due to the different load flow state of the system post-fault their settings are further boosting the over-voltage of the network.

5.2.3 Recommendations for network fault control modes

The network fault control modes used in this study were compared with the current standards for disconnection of the low voltage connected DGs. Their performance varied, but in general showed improvement regarding voltage support and system voltage stability. In the event of a system fault, the application of current standards would lead to a loss of

42-84 MW of active power in-feed, representing 35-70 % of LV peak load. These values would be halved by applying any of the control modes presented.

Specifically, the first control mode used, ZPM, as compared with the no-LVRT, decreased the voltage further at the occurrence of the fault and during the fault supported the voltage slightly less in the base case and MV to HV reverse power flow. On the positive side, it supported the voltage more during LV to HV reverse power flow close to the MV/LV transformer, and post-fault kept the voltage closer to the pre-fault value. It is an improvement with respect to the no-LVRT mode only regarding the post-fault behaviour of the system voltage. During fault it performs worse than the no-LVRT mode in supporting the voltage, with few exceptions. Also, it can lead to delayed voltage recovery, as seen in the results for node R15, deep inside the LV network in the base case.

The second mode used, aRCI, as compared with the no-LVRT, helps in supporting the voltage profile during fault in all cases. The voltage support during fault was always 0.05 p.u. or more, higher than the no-LVRT mode and 0.07 p.u. higher than in ZPM. The influence of aRCI on the voltage was stronger closer to the MV/LV transformer due to the higher X/R ratio of the network. This fault mode also improved the voltage post-fault in all load flow scenarios better than the no-LVRT mode. In total the aRCI control strategy would be beneficial for the network in the event of a transmission system fault, if it was applied to the DG's connected closer to the MV/LV transformer in the low voltage network.

Finally, the aRACI strategy showed improved voltage support during the fault with values similar to the aRCI case. In the case of low voltage connected DG, deep inside the LV network the performance was even better than aRCI as the X/R ratio of the network, at that point, was below 1 and active current injection was more influential to the voltage than reactive current. Post-fault, as in all control cases, the voltage was benefited by the reconnection to the network of the 2022 connected PVPPMs. This control mode would be very beneficial to the network, if applied to the DG connected deeper inside the LV network. However, the possibility of interference with network protection should be investigated, even though the literature survey done in this thesis suggests that it is not an issue.

5.2.4 Relevance of delayed, post-fault, active power recovery

The addition of delayed active power recovery post-fault (dAPR) was investigated for the post-fault behaviour of the voltage in all control cases. Due to the nature of aRCI and aRACI that kept the same, if not higher, active current in-feed to the network during fault, the application of dAPR was rarely activated, in those control cases. This behaviour can be explained through the condition for performing dAPR: active current in-feed of DG at fault restoration must be lower than the pre-fault one.

In the case of ZPM however this requirement was met and the behaviour of dAPR was analysed. As seen from the results of section 4.4.5, dAPR is mostly inhibiting, post-fault, restoration of the voltage. In the base case and MV to HV reverse power flow, the general post-fault under-voltage is worsened with the addition of dAPR. DAPR lowers the active power in-feed of DG at fault restoration and, consequently, increases the power extracted

from the MV network and the voltage drop it induces. This behaviour can lead to PVPPMs staying in fault mode longer than without dAPR.

In the LV to MV full reverse power flow, the post-fault over-voltage is typically raised even more with the addition of dAPR, as the PVs delay their reactive power consumption post-fault and therefore, the excess of reactive power is higher and raises the voltage more.

As a general conclusion, the effect of dAPR in the low voltage network in terms of voltage stability is negative in all cases as it leads to post-fault under-voltages or over-voltages. From a voltage stability point of view it should not be included in future LV connected DG.

5.2.5 Considerations on the applicability of the results to the German network

The modelling structure of the test system used in this study was based on the German network and the behaviour of installed DG was modelled based on the grid codes of Germany. However some aspects of the modelling are not 100 % representative of typical German distribution networks. The major difference between this study and the German network is that installed load data were taken from the Cigré benchmark reports rather than from statistical data of the German network. The reason was the unavailability of German load data during the modelling phase. However, most benchmark reports used are based on existing German networks and consequently, certain resemblance for the load data is expected.

Therefore, it is not safe to assume that this network describes in detail the behaviour of the German network, but rather that it gives the outline of its response to a network fault. Another point of difference is that no dynamic load was considered in this study, only static load.

Nevertheless some general conclusions can be drawn for the German network based on this study:

- German grid codes amendment point: Steady state reactive power consumption of PVPPMs combined with disconnection at fault leads to post-fault over voltages in reverse power flow.

The LV grid codes of Germany stipulate that during steady state operation of the network, installed PVPPMs of the LV network are obliged to consume reactive power at full active power output in order to maintain a power factor of 0.9 inductive in case of installations larger than 13.8 KVA and 0.95 in case of installations smaller than 13.8 KVA [10]. This requirement is based on avoiding over-voltages at the PCC of PVPPMs, due to high active power in-feed. Furthermore in the same publication by VDE-FNN low voltage connected PVPPMs are required to disconnect from the network in the event of a network fault that, would lower the voltage at the PCC below 0.8 p.u. [10].

The combination of these two requirements, as seen from the results of this study, creates post-fault over-voltages in the network as the reactive power consumption from

PVPPMs is not applied post-fault, due to the disconnection. Consequently, the excess of reactive power in the network creates over-voltages up to 1.1 p.u. that lead to unstable post-fault behavior and may disconnect further load and production from the grid. This behavior is an outcome of the combined effect of these grid codes that hinder the network response in the event of a fault during reverse power flow and degrade the stability of the system.

As seen in the results chapter, when the requirement for reactive power consumption is withdrawn, post-fault behavior of the network is benefited and system stability is favored. Therefore, it is recommended that the relevant grid codes should be revised within a reasonable time-frame in order to ensure that this behavior is avoided. The final outcome of this procedure will depend on more factors than voltage stability and it will need further research and understanding of the benefits and pitfalls that a proposed solution will introduce. However, it is a finding of this study that the current grid codes hinder system stability under specific circumstances and that this issue should be investigated and resolved.

- Retained voltage at LV network nodes is high during fault and that allows for support.

As already explained in the general conclusions, the retained voltage in the LV network during a fault is high and that makes the LV network a strategic location for current injection during the fault in order to support the voltage. This is an added benefit of using voltage support in the LV network.

- Post-fault reconnection benefits the voltage significantly.

Post-fault reconnection of the DG has a positive effect in the voltage in all load cases. In normal power flow or MV to HV reverse power flow the under-voltage seen post-fault is significantly raised in case of reconnection of DG. In the case of LV to HV reverse power flow the general overvoltage seen post-fault is lowered in case of DG, post-fault, reconnection due to DGs resuming reactive power consumption. So regardless of the fault control mode followed, post-fault reconnection has a positive effect on the voltage stability of the network and should be considered for setting future grid code requirements.

- FRT criteria for LV networks are relevant and may need to be adjusted depending on DG location.

The general result of applying FRT control modes is a significant voltage support during fault and post-fault. The feasibility of such an addition should be investigated further, but the benefit for the voltage profile of the network is significant and therefore, makes FRT requirements relevant. Specifically, the aRCI strategy shows the best results for voltage support for DG connected near the MV/LV transformer and aRACI for DG connected deeper inside the LV network.

5.3 Recommendations for Future Research

For future research there are a number of topics that seem interesting for continuing the work done on this thesis:

- Use of this network as a validation model for aggregated network structures.

The network structure created in this study is elaborate and rather complicated in the attempt made to resemble an actual network with different voltage levels. Of course creating such a structure is time consuming and also delays simulations and makes the system harder to work with. A good way of taking advantage of this work is the creation of an equivalent aggregate distribution system that can prove easier to work with and validate the results of this system with the detailed system presented in this study. This would also overcome the limitation of the present model that has only one distribution grid connected at eHV busbar 8.

- Include load data from German network and a percentage of dynamic load.

An addition to this study that would make results even more relevant for the German network is introducing load data for installed loads that stem from statistical analysis of the German network. Also the use of dynamic load for a percentage of the installed load would ensure higher accuracy of the results and would also make the network more realistic.

- Perform sensitivity on fault location.

The number of sensitivity factors is numerous for this study. An interesting choice would be to vary the fault location in order to study the importance of voltage support from LV connected generators during faults that are very severe or very mild to the distribution system connected on a specific busbar of the eHV network.

- Perform sensitivity on SC power of transmission system.

Short circuit power of the transmission system is very important in assessing the contribution of the LV network to the fault. A sensitivity analysis should be performed with different unit commitment at eHV level depending on the power flow case.

- Use of additional distribution systems.

Another interesting addition is the use of more distribution grid structures like the one used in this study connected to different eHV busbars so that the total contribution in the voltage profile can be examined. This would also make the system more realistic because in reality almost all busbars have distribution networks connected to them. This option can be combined with the use of aggregated distribution networks in order to speed-up the simulation process.

- Further work on DG models.

The modelling of DG in this study was very detailed but some simplifications needed to be made like the introduction of the chopper on the dc side of the PV inverter. There is

always space for improvement in the modelling of DG in order to ensure more detailed behaviour that could give insight to the interactions between the network and DG.

- Impact on distribution network protection.

Finally an issue with the contribution of LV connected DG during a fault is the response of protection mechanisms of the DG itself and of the network. As seen in the literature survey this issue is mostly seen in case of faults within the respective LV or MV distribution network but it is worthwhile to investigate interference of DG FRT with network protection.

- Investigate behaviour for other type of faults.

Phase-to-phase-faults, two-phase-to-earth-faults and phase-to-earth-faults require considering the effect of transformers on the type of fault. Based on [66] transformers can be classified in three main categories regarding voltage dip propagation.

- Transformers that do not affect the voltage dip. This holds for (YnYn) transformer. Both windings are star configured and grounded.
- Transformers that remove the zero-sequence voltage, such as a star-star (Yy) (one or more star points are not grounded), delta-delta (Dd) or delta-zigzag (Dz) winding configuration.
- Transformers that swap line and phase voltages. In this category star-delta(Yd), delta-star (Dy), or a star-zigzag (Yz) winding configuration transformers are included.

For example of different voltage dips propagating through a (Yd) transformer see [67].

Based on the specific transformation by Yd transformers, the effect of a two-phase-to-earth-fault would be the most severe for the voltage dip as the voltage drops below the lower boundary (0.8 p.u.) for normal operation in all three phases. Next follows the phase-to-earth-faults with only two phases below the limit and finally the phase-to-phase-faults where only one phase voltage is below the normal operating limit. Depending on the type of transformers used additional faults will be prioritized based on severity.

References

- [1] *Grid integration aspects of large solar PV installations: LVRT capability and reactive power/voltage support requirements. 2011 IEEE Trondheim PowerTech*, Trondheim, 19 - 23 June, 2011.
- [2] E.ON Netz GmbH, “Grid Connection Regulations for High and Extra High Voltage”, Apr. 2006.
- [3] NERC, “Special Reliability Assessment: Interconnection Requirements for Variable Generation”, NERC, Mar. 2012.
- [4] *Technische Bedingungen für den Anschluss und Betrieb von Kundenanlagen an das Hochspannungsnetz (TAB Hochspannung)*, E VDE-AR-N 4120, 2012.
- [5] BDEW, “Technical Guideline Generating Plants Connected to the Medium-Voltage Network. Guideline for generating plants’ connection to and parallel operation with the medium-voltage network”, BDEW Bundesverband der Energie- und Wasserwirtschaft e. V. (German association of energy and water industries), Jun. 2008.
- [6] P. Kundur, *Power system stability and control*: New York: McGraw-Hill, Inc, 1994.
- [7] E. J. Coster, “Distribution grid operation including distributed generation: Impact on grid protection and the consequences of fault ride-through behaviour”, TU Eindhoven, 2010.
- [8] Thomas Ackermann, Göran Andersson, and Lennart Söder, “Distributed generation: a definition”, *Electric Power Systems Research*, vol. 57, no. 3, pp. 195–204, 2001.
- [9] Frank Marten, Jan von Appen, and Martin Braun, “German perspectives on future energy system challenges by photovoltaic: How much PV can be integrated? - Smart PV Grid Integration”, Fraunhofer Institute for Wind Energy and Energy SystemTechnology, Mar. 2013.
- [10] *Generators in the low voltage distribution network. Application guide for generating plants’ connection to and parallel operation with the low-voltage network*, VDE-AR-N 4105, 2011.
- [11] *1547 IEEE Standard for Interconnecting Distributed Resources with Electric Power Systems*, 2003.
- [12] entso-e, *ENTSO-E Network Code for Requirements for Grid Connection applicable to all Generators*. Available: <https://www.entsoe.eu/resources/network-codes/requirements-for-generators/> (2012, Aug. 18).
- [13] *ENTSO-E Requirements in the Context of Present Practices*. Available: <https://www.entsoe.eu/resources/network-codes/requirements-for-generators/> (2012, Aug. 18).

- [14] FNN, *VDE/FNN-Roadmap identifiziert weiteren Entwicklungsbedarf zum Umbau der Netze: Press release*. Berlin, 2012.
- [15] entso-e, *Briefing Note to all interested parties on the status of the Network Code on "Requirements for Generators"* (2013, Apr. 02).
- [16] *Requirements for the connection of micro-generators in parallel with public low-voltage distribution networks*, prEN 50438: 2012-08, 2010.
- [17] *Requirements for the connection of generators above 16 A per phase - Part 1: Connection to the LV distribution system*, CLC/FprTS 50549-1:2011, 2012.
- [18] *IEEE SA - P1547.8 - Recommended Practice for Establishing Methods and Procedures that Provide Supplemental Support for Implementation Strategies for Expanded Use of IEEE Standard 1547*. Available: <http://standards.ieee.org/develop/project/1547.8.html> (2013, Apr. 02).
- [19] Ecofys, "Facilitation of Renewables. Work Package 3 Final Report", in *All Island TSO Facilitation of Renewables Studies*: EirGrid, 2010.
- [20] Bundesnetzagentur Photovoltaikanlagen, *Datenmeldungen sowie EEG-Vergütungssätze*. Available: http://www.bundesnetzagentur.de/cln_1931/DE/Sachgebiete/ElektrizitaetGas/ErneuerbareEnergienGesetz/VerguetungssaetzePVAnlagen/VerguetungssaetzePhotovoltaik_node.html#doc149586bodyText3 (2013, Mar. 04).
- [21] J. C. Boemer, K. Burges, P. Zolotarev, J. Lehner, P. Wajant, M. Fürst, R. Brohm, and T. Kumm, "Overview of German Grid Issues and Retrofit of German Photovoltaic Power Plants for the Prevention of Frequency Stability Problems in Abnormal System Conditions of the ENTSO-E Region Continental Europe", in *Proc. 1st International Workshop on Integration of Solar Power into Power*, Aarhus, Denmark, 2011.
- [22] "EEG-Trend for pv installed power in Germany 2013-2017," http://www.eeg-kwk.net/de/file/Zusammenfassung_Mifri_Einspeisung_2013_-_2017.pdf.
- [23] P. Kundur, J. Paserba, V. Ajjarapu, G. Andersson, A. Bose, C. Canizares, N. Hatziargyriou, D. Hill, A. Stankovic, C. Taylor, T. van Cutsem, and V. Vittal, "Definition and Classification of Power System Stability," *Power Systems, IEEE Transactions, Definition and classification of power system stability IEEE/CIGRE joint task force on stability terms and definitions*, vol. 19, no. 3, pp. 1387–1401, 2004.
- [24] M. Baran and I. El Markabi, "Adaptive over current protection for distribution feeders with distributed generators," in *Power Systems Conference and Exposition, 2004. IEEE PES*, pp. 715–719, 2004.
- [25] P. S. Georgilakis and N. D. Hatziargyriou, "Optimal Distributed Generation Placement in Power Distribution Networks: Models, Methods, and Future Research", *Power Systems, IEEE Transactions on*, vol. PP, no. 99, pp. 1–9, <http://ieeexplore.ieee.org/stamp/stamp.jsp?arnumber=6418071>, 2013.

- [26] J. Morren and S. de Haan, "Impact of distributed generation units with power electronic converters on distribution network protection," in *Developments in Power System Protection, 2008. DPSP 2008. IET 9th International Conference on*, pp. 664–669, 2008.
- [27] J. G. Slootweg and W. L. Kling, "Impacts of distributed generation on power system transient stability: Power Engineering Society Summer Meeting, 2002 IEEE", *Power Engineering Society Summer Meeting, 2002 IEEE*, vol. 2, pp. 862–867 vol.2, 2002.
- [28] VDN, "TransmissionCode 2007. Network and System Rules of the German Transmission System Operators", Verband der Netzbetreiber - VDN – e.V. beim VDEW (German Association of Network Operators, since beginning of 2008 part of BDEW), Aug. 2007.
- [29] BDEW, "Ergänzung zur Technischen Richtlinie Erzeugungsanlagen am Mittelspannungsnetz. Richtlinie für Anschluss und Parallelbetrieb von Erzeugungsanlagen am Mittelspannungsnetz", BDEW Bundesverband der Energie- und Wasserwirtschaft e. V, Feb. 2011.
- [30] R. Walling, "DER Impacts on Bulk Grid Dynamic Performance A Retrospective View of a Prescient Thought Exercise", *Inverter Based Generation Interconnection Requirements PJM, April 11, 2012*, <http://mydocs.epri.com/docs/publicmeetingmaterials/4-17-2012/05B-DER-Impacts-on-Bulk-Grid-Dynamic-Performance-Reigh-Walling.pdf>.
- [31] E. Camm, M. Edds, C. Murray, W. Peter, and P. Valverde, "Current Renewable Energy Generator Technical Interconnection Requirements", in *2012 IEEE PES General Meeting, 22-26 July 2011, San Diego, USA 2012 IEEE PES General Meeting*, San Diego, USA, 2012.
- [32] H. Kobayashi, "Fault Ride Through Requirements and Measures of Distributed PV Systems in Japan", in *2012 IEEE PES General Meeting, 22-26 July 2011, San Diego, USA 2012 IEEE PES General Meeting*, San Diego, USA, 2012.
- [33] Johan Morren, "Grid support by power electronic converters of Distributed Generation units", Dissertation, Delft University of Technology, Delft, 2006.
- [34] I. Erlich and H. Brakelmann, "Integration of Wind Power into the German High Voltage Transmission Grid," in *Power Engineering Society General Meeting, 2007. IEEE*, pp. 1–8, 2007.
- [35] Bauer P, "System aspects of solar photovoltaic power generators," Lecture script, Delft University of Technology, May 2012.
- [36] A. Samadi, R. Eriksson, Della Jose, F. Mahmood, M. Ghandhari, and L. Söder, "Comparison of a Three-Phase Single-Stage PV System in PSCAD and PowerFactory", in *Conference Proceedings 11th International Workshop on Large-Scale Integration of Wind Power into Power Systems as well as on Transmission Networks for Offshore Wind Power Farms*, Lisbon, Portugal, 2012.
- [37] TU Braunschweig, "PV plant configurations", Jan. 2013.

- [38] D. Molina, "Progress report on the development and validation of DigSILENT PowerFactory model of the 39-Bus benchmark system for stability controls: Addressed to IEEE Task Force on Benchmark Systems for Stability Controls", Sep. 2012.
- [39] Evangelos Galinas, "Sensitivity Analysis for Expansion of Transmission Systems with High Amounts of Renewables", Master Thesis, TU Delft, Delft, 2013.
- [40] J. C. Boemer, A. van der Meer, B. G. Rawn, R. L. Hendriks, A. R. Ciupuliga, M. Gibescu, W. L. Kling, and J. A. Ferreira, "Fault Ride-through Requirements for Onshore Wind Power Plants in Europe: the Needs of the Power System", in *2011 IEEE PES General Meeting, 24-28 July 2011, Detroit, USA*, 2011 IEEE PES General Meeting, Detroit, USA, 2011.
- [41] A. Yazdani, A. R. Di Fazio, H. Ghoddami, M. Russo, M. Kazerani, J. Jatskevich, K. Strunz, S. Leva, and J. A. Martinez, "Modeling Guidelines and a Benchmark for Power System Simulation Studies of Three-Phase Single-Stage Photovoltaic Systems", *IEEE Transactions on Power Delivery*, vol. 26, no. 2, pp. 1247–1264, 2011.
- [42] R. F. Arritt and R. C. Dugan, SR, "The IEEE 8500-node test feeder", in *Transmission and Distribution Conference and Exposition, 2010 IEEE PES*, pp. 1–6, 2010.
- [43] F. K. O. W. P. B. Falk Schaller, "Modellierung realitätsnaher zukünftiger Referenznetze im Verteilnetzsektor zur Überprüfung der Elektroenergiequalität", in *Internationaler ETG-Kongress 2011 (ETG-FB 130): Umsetzungskonzepte nachhaltiger Energiesysteme - Erzeugung, Netze, Verbrauch, Vorträge Fachtagungen 1 bis 5*, Internationaler ETG-Kongress, Würzburg, 2011.
- [44] K. Rudion, A. Orths, Z. Styczynski, and K. Strunz, "Design of benchmark of medium voltage distribution network for investigation of DG integration", in *Power Engineering Society General Meeting, 2006. IEEE*, pp. 6 pp, 2006.
- [45] B. Buchholz, C. Schwaegerl, T. Stephanblome, H. Frey, N. Lewald, and Z. Styczynski, "Advanced Planning And Operation Of Dispersed Generation Ensuring Power Quality, Security And Efficiency In Distribution Systems," *CIGRE 2004 Session, Paris, France*, 2004.
- [46] K. Strunz, "Developing benchmark models for studying the integration of distributed energy resources," in *Power Engineering Society General Meeting, 2006. IEEE*, pp. 2 pp, 2006.
- [47] CIGRE Task Force C6.04.02, "Benchmark Systems for Network Integration of Renewable and Distributed Energy Resources: Technical Brochure (excerpts for European HV, MV, and LV benchmark systems) ", May. 2013.
- [48] 50Hertz Transmission GmbH, Amprion GmbH, TenneT TSO GmbH, and TransnetBW GmbH, "Netzentwicklungsplan Strom 2012 (Network Development Plan Electricity 2012): 2. überarbeiteter Entwurf der Übertragungsnetzbetreiber (2nd revised draft of the transmission system operators) ", May. 2012.
- [49] K. Skaloumpakas, "Scaling the PV Template", Dec. 2013.

- [50] DigSILENT GmbH, *DigSILENT PowerFactory: TechRef Overhead Lines Models*: DigSILENT GmbH, 2009.
- [51] Ludvig Lindström, "Evaluating impact on ampacity according to IEC-60287 regarding thermally unfavourable placement of power cables: Masters' Degree Project", KTH, Stockholm, Sweden, 2011.
- [52] German Government, "Verordnung zu Systemdienstleistungen durch Windenergieanlagen (Systemdienstleistungsverordnung – SDLWindV) (Ordinance for Ancillary Services of Wind Power Plants (Ancillary Services Ordinance - SDLWindV) ", *Federal Law Gazette*, vol. I, no. 39, pp. 1734-1746, <http://www.erneuerbare-energien.de/inhalt/43342>, 2009.
- [53] DigSILENT GmbH, "DFIG Template: Manual", Gomaringen, May. 2011.
- [54] DigSILENT GmbH, "Fully Rated WTG Template: Manual", Gomaringen, May. 2011.
- [55] Hua Bai Student Member IEEE, Pei Zhang Senior Member IEEE, and Venkataramana Ajarapu Fellow IEEE, "A Novel Parameter Identification Approach via Hybrid Learning for Aggregate Load Modeling,"
- [56] Inés Romero Navarro, "Dynamic Power System Load Estimation of Parameters from Operational Data", PhD, Lund University, 2005.
- [57] KP Schneider, JC Fuller, FK Tuffner, and R Singh, "Evaluation of Conservation Voltage Reduction (CVR) on a National Level", Jul. 2010.
- [58] Ke-Yao, "Modeling power system load using intelligent methods", Master Thesis, KANSAS STATE UNIVERSITY, Manhattan, Kansas, 2011.
- [59] E. Kermendey, N. Villalobos, and M. Schmiege, "The Impact of Load Behavior on Voltage Stability, an Application Case in ENELVEN / VENEZUELA", 2009.
- [60] S. M. I. H. Guo, M. I. K. Rudion, M. I. H. Abildgaard, and a. Z. A. S. S. M. I. P. Komarnicki, "Parameter Estimation of Dynamic Load Model Using Field Measurement Data Performed by OLTC Operation", 2008.
- [61] A. Maitra Member IEEE, A. Gaikwad Member IEEE, and P. Zhang Member IEEE, "Using System Disturbance Measurement Data to Develop Improved Load Models", 2008.
- [62] DigSILENT GmbH, *DigSILENT PowerFactory: General Load Model*: DigSILENT GmbH, 2008.
- [63] Von Gunter Buse, Richard Bopp, and Harald Junkermann Kassel, "Das Verhalten der Netzleistung bei veränderlicher Netzspannung", *Elektrizitätswirtschaft*, 1983.
- [64] Von Gernot, "Die Spannungsabhängigkeit von Drehstromlasten", *Elektrizitätswirtschaft*, 1969.
- [65] DigSILENT GmbH, "General Load Model", 2008.
- [66] M. H. J. Bollen, *Understanding Power Quality Problems*: Wiley-IEEE Press, 2000.

- [67] M. Aung and J. Milanovic, "The Influence of Transformer Winding Connections on the Propagation of Voltage Sags", *IEEE Transactions on Power Delivery*, vol. 21, no. 1, pp. 262–269, <http://ieeexplore.ieee.org/ielx5/61/33198/01564208.pdf?tp=&arnumber=1564208&isnumber=33198>, 2006.

Appendix A IEEE 39-Bus, 10-Machine New England Test System

In this appendix the details of modelling the eHV network based on [38] are presented.

Lines	Positive sequence resistance (Ohm/km)	Positive sequence reactance (Ohm/km)
TL 01-02	1.852	21.742
TL 01-39	0.529	13.225
TL 02-03	0.688	7.988
TL 02-25	3.703	4.549
TL 03-04	0.688	11.268
TL 03-18	0.582	7.036
TL 04-05	0.423	6.771
TL 04-14	0.423	6.824
TL 05-06	0.106	1.375
TL 05-08	0.423	5.925
TL 06-07	0.318	4.867
TL 06-11	0.370	4.338
TL 07-08	0.212	2.433
TL 08-09	1.217	19.203
TL 09-39	0.529	13.225
TL 10-11	0.212	2.275
TL 10-13	0.212	2.275
TL 13-14	0.476	5.343
TL 14-15	0.952	11.479
TL 15-16	0.476	4.973
TL 16-17	0.370	4.708
TL 16-19	0.846	10.316
TL 16-21	0.423	7.142
TL 16-24	0.159	3.121
TL 17-18	0.370	4.338
TL 17-27	0.688	9.152
TL 21-22	0.423	7.406
TL 22-23	0.317	5.078
TL 23-24	1.164	18.515
TL 25-26	1.693	17.087
TL 26-27	0.740	7.776
TL 26-28	2.275	25.075
TL 26-29	3.015	33.063
TL 28-29	0.740	7.988

Table A.1: Line parameters for the eHV network

Busbar of Load	Active power (MW)	Reactive Power (MVar)
L03	322	2.4
L04	500	184
L07	233.8	84
L08	522	176
L12	7.5	88
L15	320	153
L16	329	32.3
L18	158	30
L20	628	103
L21	274	115
L23	247.5	84.6
L24	308.6	-92.2
L25	224	47.2
L26	139	17
L27	281	75.5
L28	206	27.6
L29	283.5	26.9
L31	9.2	4.6
L39	1104	250

Table A.2: Load parameters of eHV network

Generator	Apparent Power (MVA)	Power Factor (ind)	Xd (p.u)	Xq (p.u.)
G01	1013.24	0.99	0.020	0.019
G02	658.13	0.92	0.295	0.282
G03	694.16	0.94	0.250	0.237
G04	644.21	0.98	0.262	0.258
G05	536.03	0.95	0.670	0.620
G06	692.28	0.94	0.254	0.241
G07	572.45	0.98	0.295	0.292
G08	540.38	1.00	0.290	0.280
G09	831.81	1.00	0.211	0.205
G10	300.30	0.83	0.100	0.069

Table A.3: Apparent power and power factor for load flow initialization of eHV synchronous generators for normal power flow scenario, also d and q axis reactance in p.u.

Appendix B Typical German Sub-Transmission 110 kV Ring System

In this appendix the details of modelling the HV network based on [40] are presented.

Line type	Positive sequence resistance (Ohm/km)	Positive sequence reactance (Ohm/km)
110kV 150 MVA OHL	0.020449	0.086273

Table B.1: Parameters of line type of the HV network

Line	Busbars	Length (km)	Type
HV-L01	01-02	20	110kV 150 MVA OHL
HV-L02	02-03	20	110kV 150 MVA OHL
HV-L03	03-04	20	110kV 150 MVA OHL
HV-L04	04-05	30	110kV 150 MVA OHL
HV-L05	05-06	20	110kV 150 MVA OHL
HV-L06	06-01	20	110kV 150 MVA OHL

Table B.2: Length and type of the HV networks lines

Transformers	Busbars	Rated Power	Voltage levels	Vector Group	SC voltage
Trafo-1	eHV-08 HV-03	150 MVA	220/110/20 kV	Yd0/Yd0/DD11	10%/10%/10%
Trafo-2	eHV-08 HV-05	150 MVA	220/110/20 kV	Yd0/Yd0/DD11	10%/10%/10%

Table B.3: Parameters of eHV to HV transformers

Appendix C CIGRÉ Medium Voltage Benchmark System

In this appendix the details of modelling the MV network based on [47] are presented.

Line segment	Node from-to	Conductor ID	R'_{ph}	X'_{ph}	B'_{ph}	R'_{θ}	X'_{θ}	B'_{θ}	l	Installation
			[Ω /km]	[Ω /km]	[μ S/km]	[Ω /km]	[Ω /km]	[μ S/km]		
1	1-2	2	0.501	0.716	47.493	0.817	1.598	47.493	2.82	Underground
2	2-3	2	0.501	0.716	47.493	0.817	1.598	47.493	4.42	Underground
3	3-4	2	0.501	0.716	47.493	0.817	1.598	47.493	0.61	Underground
4	4-5	2	0.501	0.716	47.493	0.817	1.598	47.493	0.56	Underground
5	5-6	2	0.501	0.716	47.493	0.817	1.598	47.493	1.54	Underground
6	6-7	2	0.501	0.716	47.493	0.817	1.598	47.493	0.24	Underground
7	7-8	2	0.501	0.716	47.493	0.817	1.598	47.493	1.67	Underground
8	8-9	2	0.501	0.716	47.493	0.817	1.598	47.493	0.32	Underground
9	9-10	2	0.501	0.716	47.493	0.817	1.598	47.493	0.77	Underground
10	10-11	2	0.501	0.716	47.493	0.817	1.598	47.493	0.33	Underground
11	11-4	2	0.501	0.716	47.493	0.817	1.598	47.493	0.49	Underground
12	3-8	2	0.501	0.716	47.493	0.817	1.598	47.493	1.30	Underground
13	12-13	1	0.510	0.366	1.280	0.658	1.611	1.280	4.89	Overhead
14	13-14	1	0.510	0.366	1.280	0.658	1.611	1.280	2.99	Overhead
15	14-8	1	0.510	0.366	1.280	0.658	1.611	1.280	2.00	Overhead

Table C.1: Line parameters of MV network

Transformers	Node to	Connection	V_1	V_2	Z_{tr}	S_{rated}
			[kV]	[kV]	[Ω]	[MVA]
HV/MV Sub-urban	MV-01	3-ph Dyn1	110	20	0.016+j1.92	25
HV/MV Rural	MV-12	3-ph Dyn1	110	20	0.016+j1.92	25

Table C.2: HV/MV transformer parameters

Node	Apparent Power, S [kVA]		Power Factor, pf	
	Residential	Commercial/Industrial	Residential	Commercial/Industrial
1	15 300	5 100	0.98	0.95
2	---	---	---	---
3	285	265	0.97	0.85
4	445	---	0.97	---
5	750	---	0.97	---
6	565	---	0.97	---
7	---	90	---	0.85
8	605	---	0.97	---
9	---	675	---	0.85
10	490	80	0.97	0.85
11	340	---	0.97	---
12	15300	5 280	0.98	0.95
13	---	40	---	0.85
14	215	390	0.97	0.85

Table C.3: Load parameters of MV network

Appendix D CIGRÉ Low Voltage Benchmark System

In this appendix the details of modelling the LV network based on [47] are presented.

Line segment	Node from-to	Conductor ID	l	Installation
			[m]	
1	R1-R2	UG1	35	UG 3-ph
2	R2-R3	UG1	35	UG 3-ph
3	R3-R4	UG1	35	UG 3-ph
4	R4-R5	UG1	35	UG 3-ph
5	R5-R6	UG1	35	UG 3-ph
6	R6-R7	UG1	35	UG 3-ph
7	R7-R8	UG1	35	UG 3-ph
8	R8-R9	UG1	35	UG 3-ph
9	R9-R10	UG1	35	UG 3-ph
10	R3-R11	UG3	30	UG 3-ph
11	R4-R12	UG3	35	UG 3-ph
12	R12-R13	UG3	35	UG 3-ph
13	R13-R14	UG3	35	UG 3-ph
14	R14-R15	UG3	30	UG 3-ph
15	R6-R16	UG3	30	UG 3-ph
16	R9-R17	UG3	30	UG 3-ph
17	R10-R18	UG3	30	UG 3-ph

Table D.1: Line parameters of LV residential network

Conductor ID	Type	Size	Number of strands	d_c	R'_{ac} at 50 °C	GMR	a	b
		[mm ²]		[cm]	[Ω/km]	[cm]	[m]	[m]
OH1	Al	70	19	1.05	0.491	0.398	8	0.3
OH2	Al	25	7	0.63	1.320	0.228	8	0.3
OH3	Al	16	7	0.51	2.016	0.185	8	0.3

Table D.2: Conductor parameters for overhead lines of the LV network

Conductor ID	Type	Size	Number of strands	d_c	R'_{ac} at 90 °C / 70 °C	GMR	a
		[mm ²]		[cm]	[Ω/km]	[cm]	[m]
UG1	NA2XY	240	1	1.75	0.162	0.634	0.9
UG2	NA2XY	150	1	1.38	0.265	0.501	0.9
UG3	NA2XY	50	1	0.80	0.822	0.289	0.9

Table D.3: Conductor parameters for underground cables of the LV network

Line segment	Node from-to	Conductor ID	l	Installation
			[m]	
1	C1-C2	OH1	30	OH 3-ph
2	C2-C3	OH1	30	OH 3-ph
3	C3-C4	OH1	30	OH 3-ph
4	C4-C5	OH1	30	OH 3-ph
5	C5-C6	OH1	30	OH 3-ph
6	C6-C7	OH1	30	OH 3-ph
7	C7-C8	OH1	30	OH 3-ph
8	C8-C9	OH1	30	OH 3-ph
9	C3-C10	OH2	30	OH 3-ph
10	C10-C11	OH2	30	OH 3-ph
11	C11-C12	OH3	30	OH 3-ph
12	C11-C13	OH3	30	OH 3-ph
13	C10-C14	OH3	30	OH 3-ph
14	C5-C15	OH2	30	OH 3-ph
15	C15-C16	OH2	30	OH 3-ph
16	C15-C17	OH3	30	OH 3-ph
17	C16-C18	OH3	30	OH 3-ph
18	C8-C19	OH3	30	OH 3-ph
19	C9-C20	OH3	30	OH 3-ph

Table D.4: Line parameters of LV commercial network

Line segment	Node from-to	Conductor ID	l	Installation
			[m]	
1	I1-I2	UG2	200	UG 3-ph

Table D.5: Line parameters of LV industrial network

Conductor ID/Installation		Phase Impedance matrix after Kron reduction [Ω/km]		
		A	B	C
UG1 / 3-ph	A	$0.287 + j0.167$	$0.121 + j0.110$	$0.125 + j0.070$
	B	$0.121 + j0.110$	$0.279 + j0.203$	$0.121 + j0.110$
	C	$0.125 + j0.070$	$0.121 + j0.110$	$0.287 + j0.167$
UG2 / 3-ph	A	$0.455 + j0.204$	$0.185 + j0.146$	$0.190 + j0.107$
	B	$0.185 + j0.146$	$0.444 + j0.238$	$0.185 + j0.146$
	C	$0.190 + j0.107$	$0.185 + j0.146$	$0.455 + j0.204$
UG3 / 3-ph	A	$1.152 + j0.458$	$0.321 + j0.390$	$0.330 + j0.359$
	B	$0.321 + j0.390$	$1.134 + j0.477$	$0.321 + j0.390$
	C	$0.330 + j0.359$	$0.321 + j0.390$	$1.152 + j0.458$
OH1 / 3-ph	A	$0.616 + j0.588$	$0.131 + j0.306$	$0.141 + j0.245$
	B	$0.131 + j0.306$	$0.628 + j0.566$	$0.147 + j0.276$
	C	$0.141 + j0.245$	$0.147 + j0.276$	$0.650 + j0.527$
OH2 / 3-ph	A	$1.457 + j0.728$	$0.143 + j0.417$	$0.152 + j0.367$
	B	$0.143 + j0.417$	$1.469 + j0.720$	$0.159 + j0.405$
	C	$0.152 + j0.367$	$0.159 + j0.405$	$1.490 + j0.704$
OH3 / 3-ph	A	$2.137 + j0.776$	$0.125 + j0.453$	$0.133 + j0.406$
	B	$0.125 + j0.453$	$2.146 + j0.771$	$0.138 + j0.447$
	C	$0.133 + j0.406$	$0.138 + j0.447$	$2.163 + j0.762$

Table D.6: Phase Impedance matrix after Kron reduction of all three phase lines in the LV network

Transformers	Node from-to	Connection	V1	V2	Z tr	S rated
			[kV]	[kV]	[Ω]	[kVA]
Residential	R0-R1	3-ph Dyn1	20	0.4	$0.032 + j0.0128$	500
Industrial	I0-I1	3-ph Dyn1	20	0.4	$0.0107 + j0.0427$	150
Commercial	C0-C1	3-ph Dyn1	20	0.4	$0.0053 + j0.0213$	300

Table D.7: MV to LV transformer parameters

Node	Apparent Power, S [kVA]	Power Factor, pf
R1	200	0.95
R11	15	0.95
R15	52	0.95
R16	55	0.95
R17	35	0.95
R18	47	0.95
I2	100	0.85
C1	120	0.90
C12	20	0.90
C13	20	0.90
C14	25	0.90
C17	25	0.90
C18	8	0.90
C19	16	0.90
C20	8	0.90

Table D.8: Load parameters of all LV loads

Appendix E Transformer Tap Changers Positions

The tap changer positions of the HV to MV and MV to LV transformers are shown in the table below for all load cases.

Transformers	Tap changer positions			Additional voltage per tap
	Normal Power Flow	MV to eHV reverse power flow	LV to eHV reverse power flow	
110/20 kV sub-urban	-2	-9	-2/-1	0.625 %
110/20 kV rural	7	4	11	0.625 %
MV/LV (MV 01)	-2	-2	-2	2.5%
MV/LV (MV 10)	0	0	0	2.5%

Table E.1: Tap changer positions of transformers per load case

Appendix F Results

The results for all cases are presented in the following on double pages. The structure of the plots is described in the following two pages. The same structure is used for all cases.

- The voltage at the various busbars (in p.u.):

all eHV busbars	all HV busbars	MV busbar 01	LV busbar R1 (connected to MV busbar 01)
-	MV busbar 08	MV busbar 06	LV busbar R1 (connected to MV busbar 10)
-	MV busbar 09	MV busbar 10	LV node R15 (connected to MV busbar 01)
-	-	MV busbar 12	LV node R15 (connected to MV busbar 10)

Table F.1: Schematic representation of voltage results

MV busbars 08 and 09 are interesting because the WPP of the MV network are connected there. Also MV busbars 01, 10 are important because LV networks are connected on those busbars. MV busbars 06, 12 are the connection points of PVs in the MV network. Finally all the LV nodes and busbars are connection points of PVs.

- The power exchange over the transformers graphs:

Active power over all eHV transformers in p.u. with a base value of 100 MVA.	Active power over eHV/HV transformers in p.u. with a base value of 150 MVA.	Active power over HV/MV sub-urban transformers in p.u. with a base value of 25 MVA.	Active power over MV/LV transformers connected in MV busbar 01 in p.u. with a base value of 19 MVA.
Reactive power over all eHV transformers in p.u. with a base value of 100 MVA.	Reactive power over eHV/HV transformers in p.u. with a base value of 150 MVA.	Reactive power over HV/MV sub-urban transformers in p.u. with a base value of 25 MVA.	Reactive power over MV/LV transformers connected in MV busbar 01 in p.u. with a base value of 19 MVA.
[unused]	[unused]	Active power over HV/MV rural transformers in p.u. with a base value of 25 MVA.	Active power over MV/LV transformers connected in MV busbar 10 in p.u. with a base value of 0.5 MVA.
[unused]	[unused]	Reactive power over HV/MV rural transformers in p.u. with a base value of 25 MVA.	Reactive power over MV/LV transformers connected in MV busbar 10 in p.u. with a base value of 0.5 MVA.

Table F.2: Schematic representation of transformers power exchange results

- The power output of the SG and DG graphs:

Active power of all eHV generators in MVA.	Active power of all MV PV connected in MV busbar 06 in p.u. with base power of 240 kVA.	Active power of all LV PV connected in LV busbar R1 (Connected to MV busbar 01) in p.u. with base power of 4 560 kVA.	Active power of all LV PV connected in LV busbar R1 (Connected to MV busbar 10) in p.u. with base power of 120 kVA.
Reactive power of all eHV generators in MVA.	Reactive power of all MV PV connected in MV busbar 06 in p.u. with base power of 240 kVA.	Reactive power of all LV PV connected in LV busbar R1 (Connected to MV busbar 01) in p.u. with base power of 4 560 kVA.	Reactive power of all LV PV connected in LV busbar R1 (Connected to MV busbar 10) in p.u. with base power of 120 kVA.
Active power of all HV and MV WPP in p.u. with rated base power for each WPP.	Active power of all MV PV connected in MV busbar 12 in p.u. with base power of 7 400 kVA.	Active power of all LV PV connected in LV node R15 (Connected to MV busbar 01) in p.u. with base power of 2 280 kVA.	Active power of all LV PV connected in LV node R15 (Connected to MV busbar 10) in p.u. with base power of 60 kVA.
Reactive power of all HV and MV WPP in p.u. with rated base power for each WPP.	Reactive power of all MV PV connected in MV busbar 12 in p.u. with base power of 7 400 kVA.	Reactive power of all LV PV connected in LV node R15 (Connected to MV busbar 01) in p.u. with base power of 2 280 kVA.	Reactive power of all LV PV connected in LV node R15 (Connected to MV busbar 10) in p.u. with base power of 60 kVA.

Table F.3: Schematic representation of DG and SG power output results

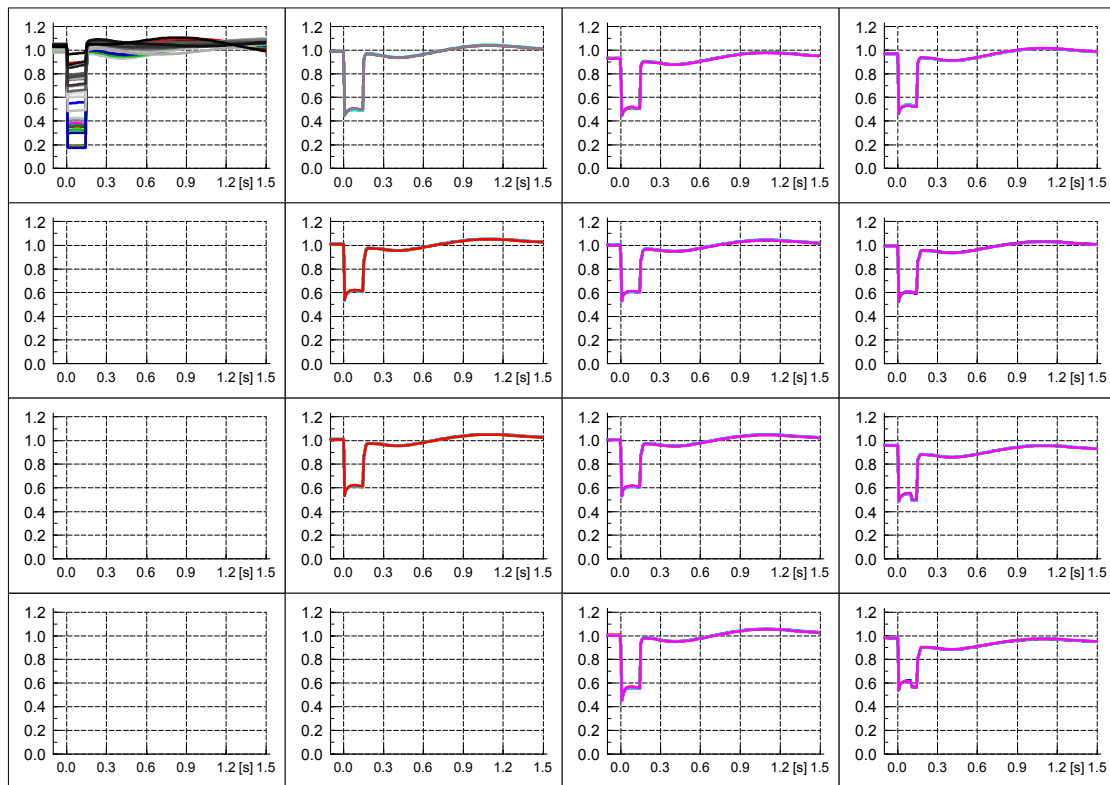
- The direct and quadrature axis currents of PV systems:

[unused]	Direct axis current of all MV PV connected in MV busbar 06 of all MV networks in p.u.	Direct axis current of all LV PV connected in LV busbar R1 of LV networks connected at MV busbar 01 in p.u.	Direct axis current of all LV PV connected in LV busbar R1 of LV networks connected at MV busbar 10 in p.u.
[unused]	Quadrature axis current of all MV PV connected in MV busbar 06 of all MV networks in p.u.	Quadrature axis current of all LV PV connected in LV busbar R1 of LV networks connected at MV busbar 01 in p.u.	Quadrature axis current of all LV PV connected in LV busbar R1 of LV networks connected at MV busbar 10 in p.u.
[unused]	Direct axis current of all MV PV connected in MV busbar 12 of all MV networks in p.u.	Direct axis current of all LV PV connected in LV node R15 of LV networks connected at MV busbar 01 in p.u.	Direct axis current of all LV PV connected in LV node R15 of LV networks connected at MV busbar 10 in p.u.
[unused]	Quadrature axis current of all MV PV connected in MV busbar 12 of all MV networks in p.u.	Quadrature axis current of all LV PV connected in LV node R15 of LV networks connected at MV busbar 01 in p.u.	Quadrature axis current of all LV PV connected in LV node R15 of LV networks connected at MV busbar 10 in p.u.

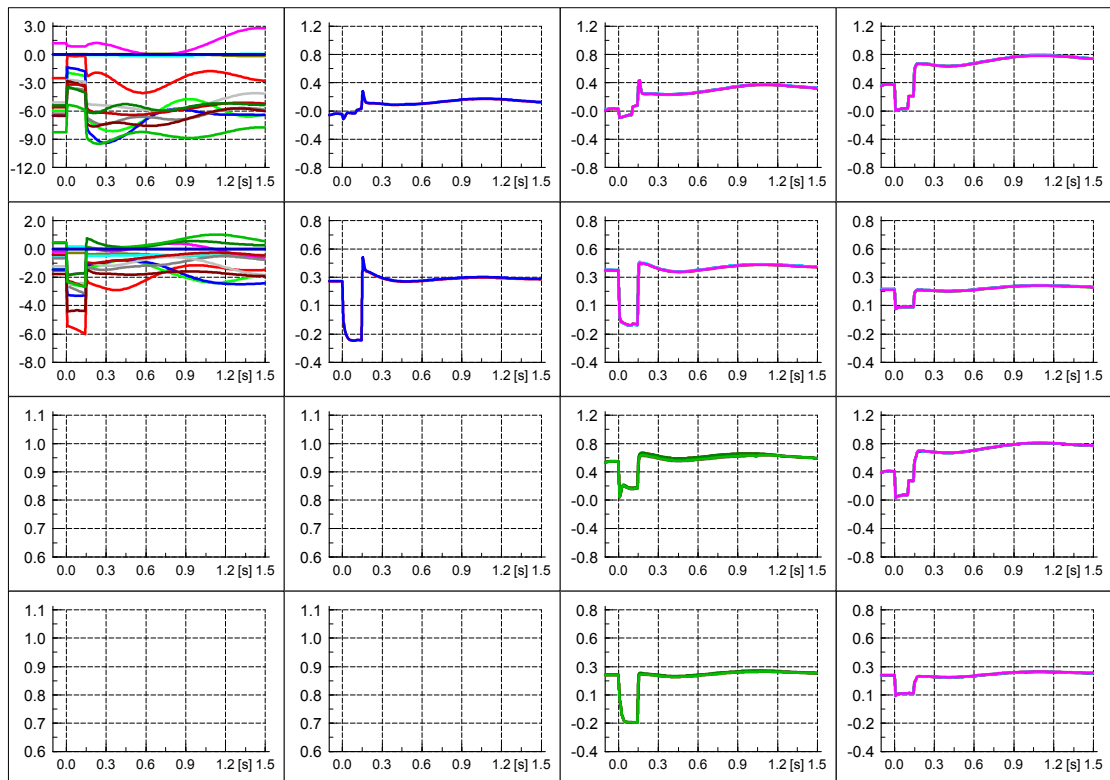
Table F.4: Schematic representation of DG and SG power output results

Base case No-LVRT

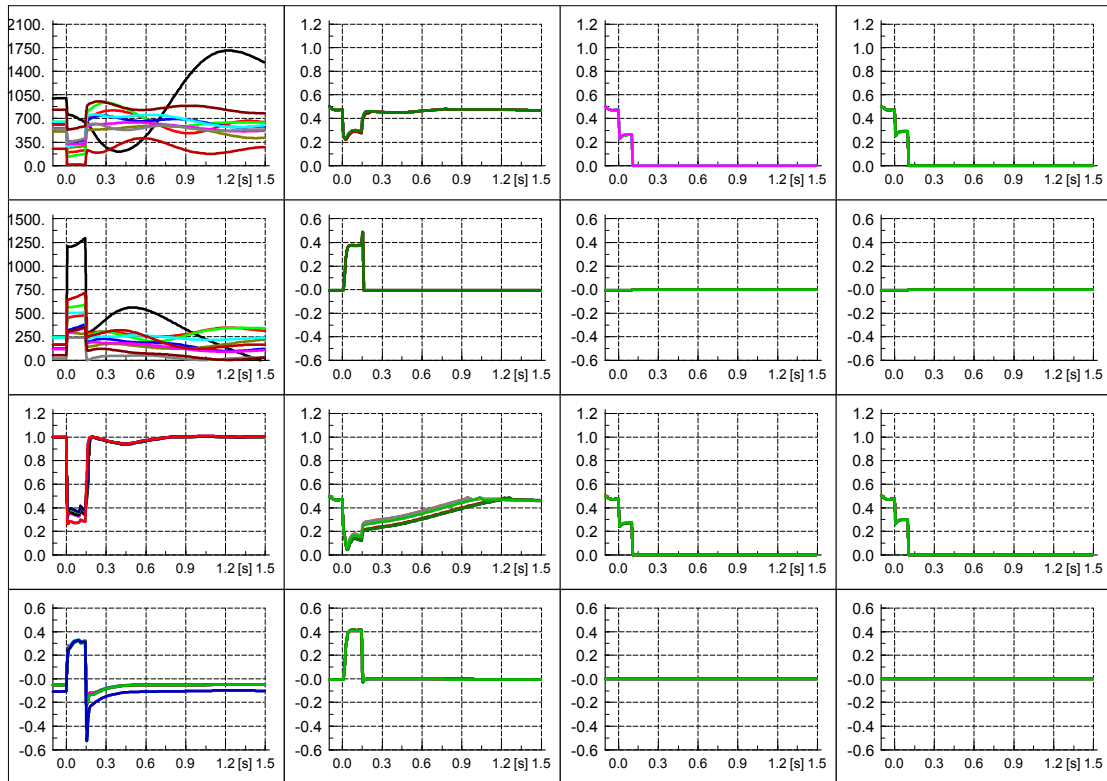
- Voltages



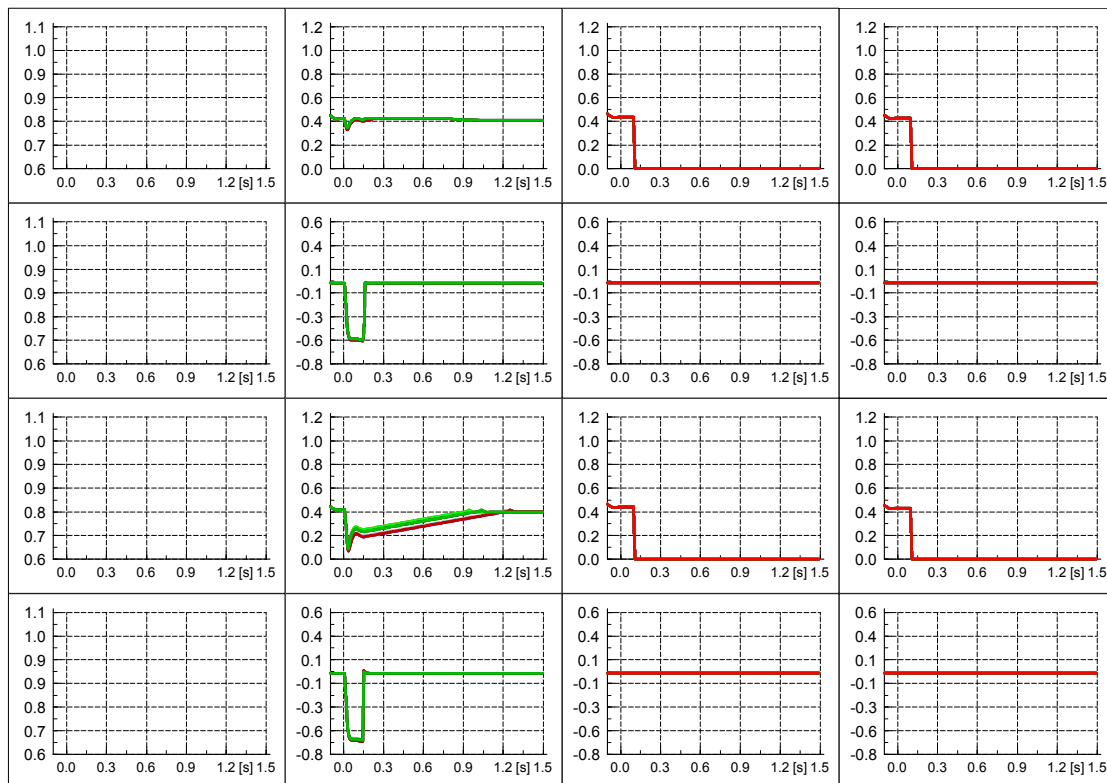
- Power exchange over the transformers



- Power production of DG and SG

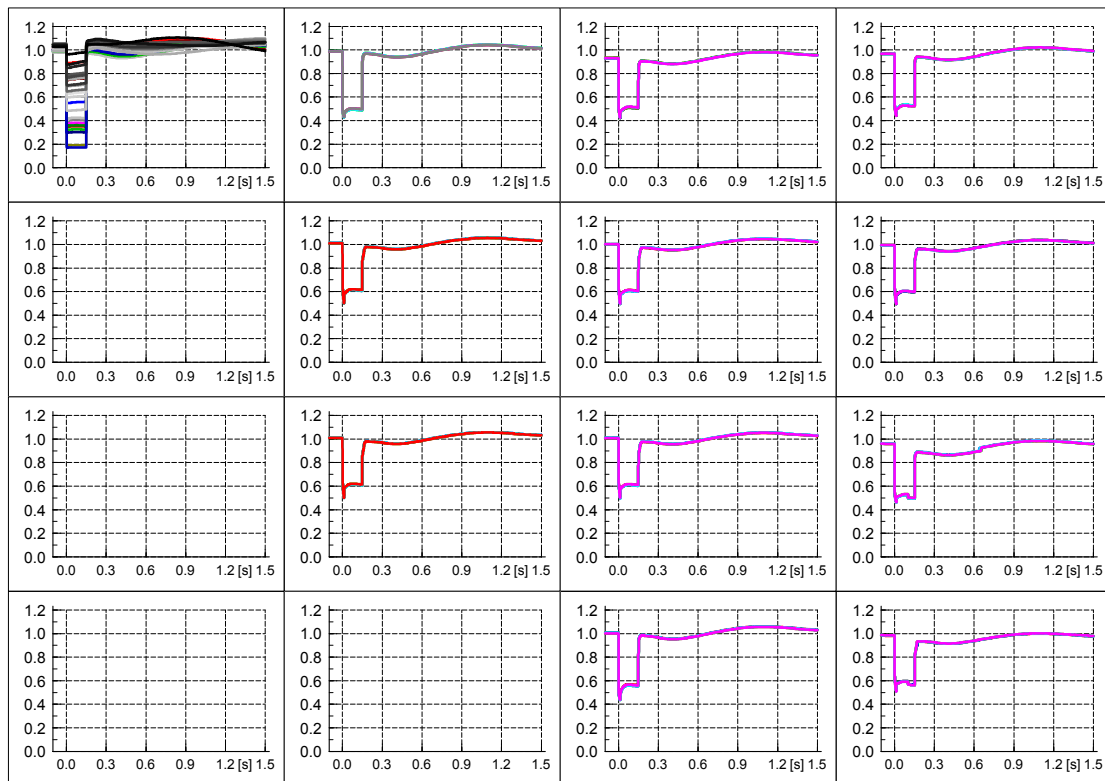


- Direct and quadrature axis currents of PV systems

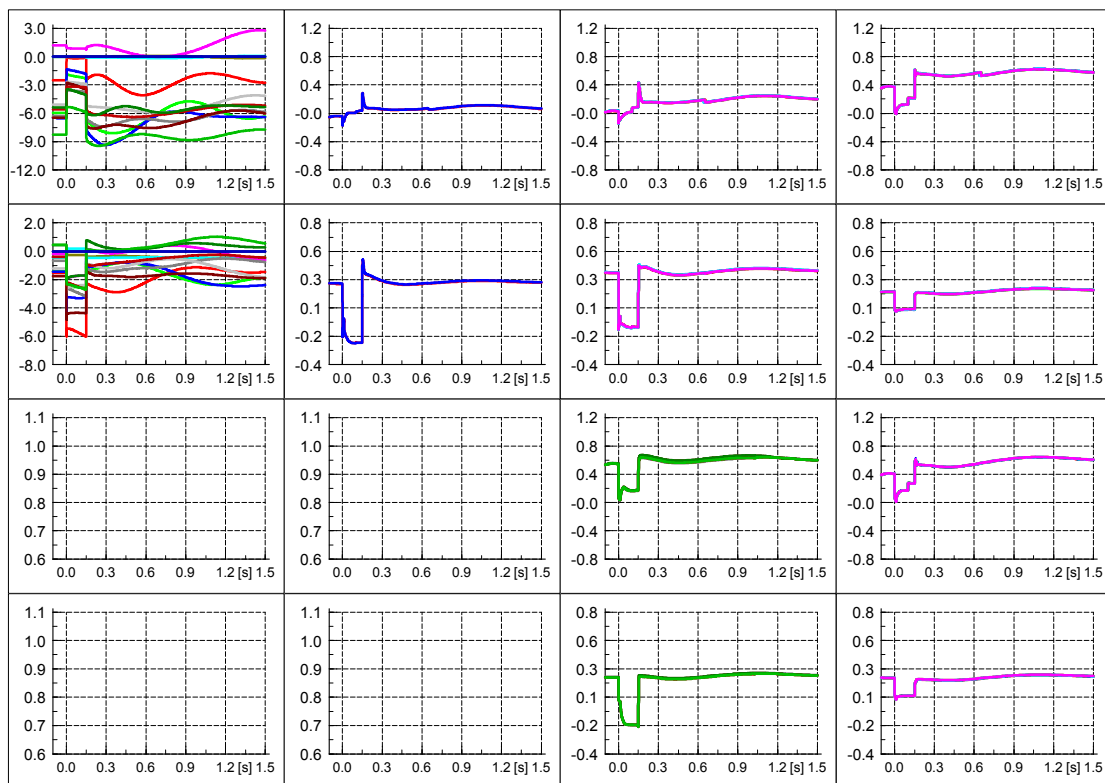


Base case ZPM

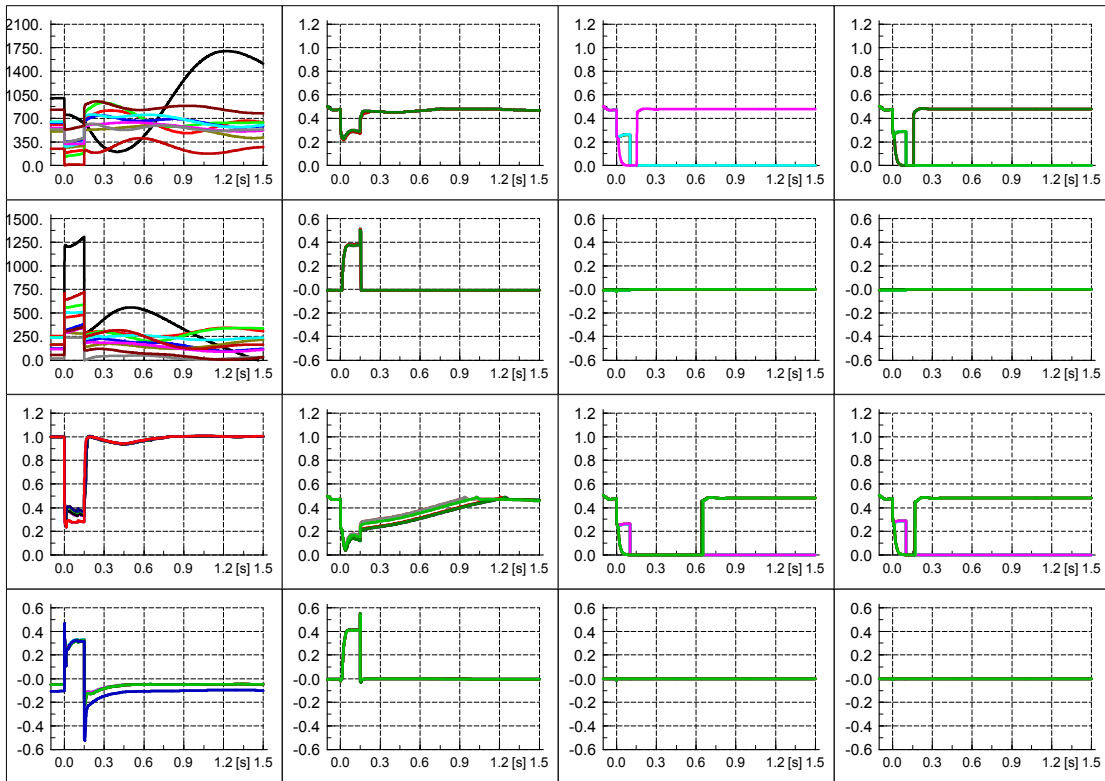
- Voltages



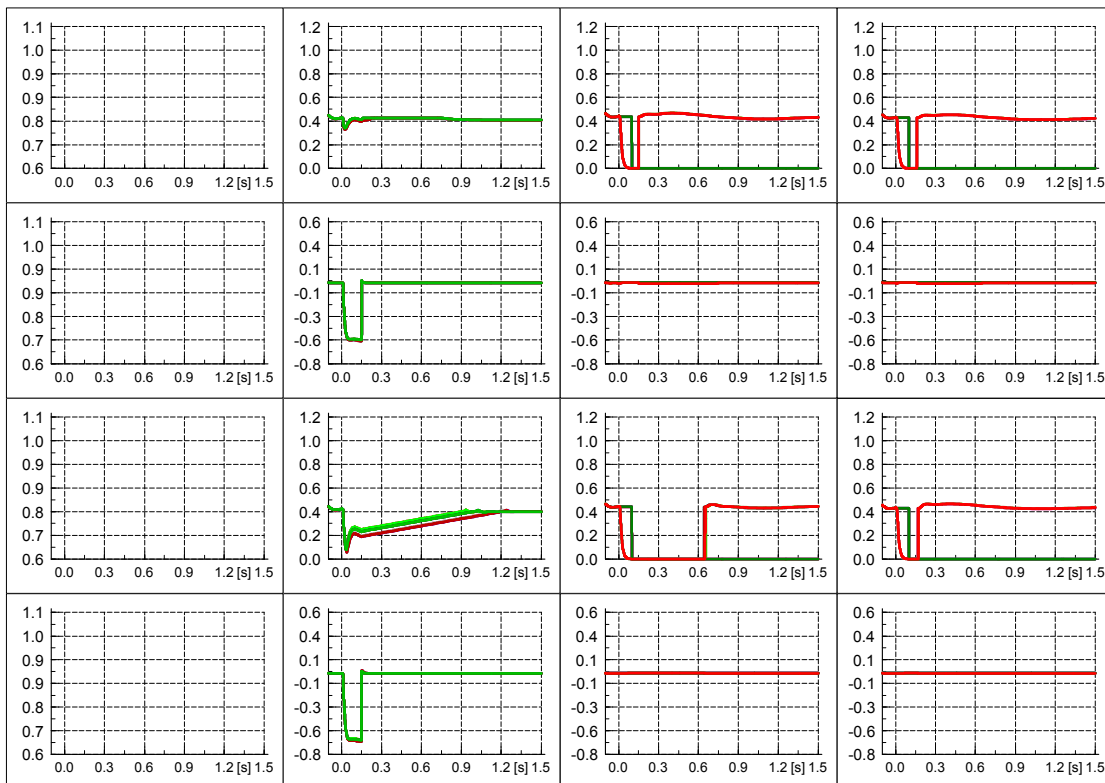
- Power exchange over the transformers



- Power production of DG and SG

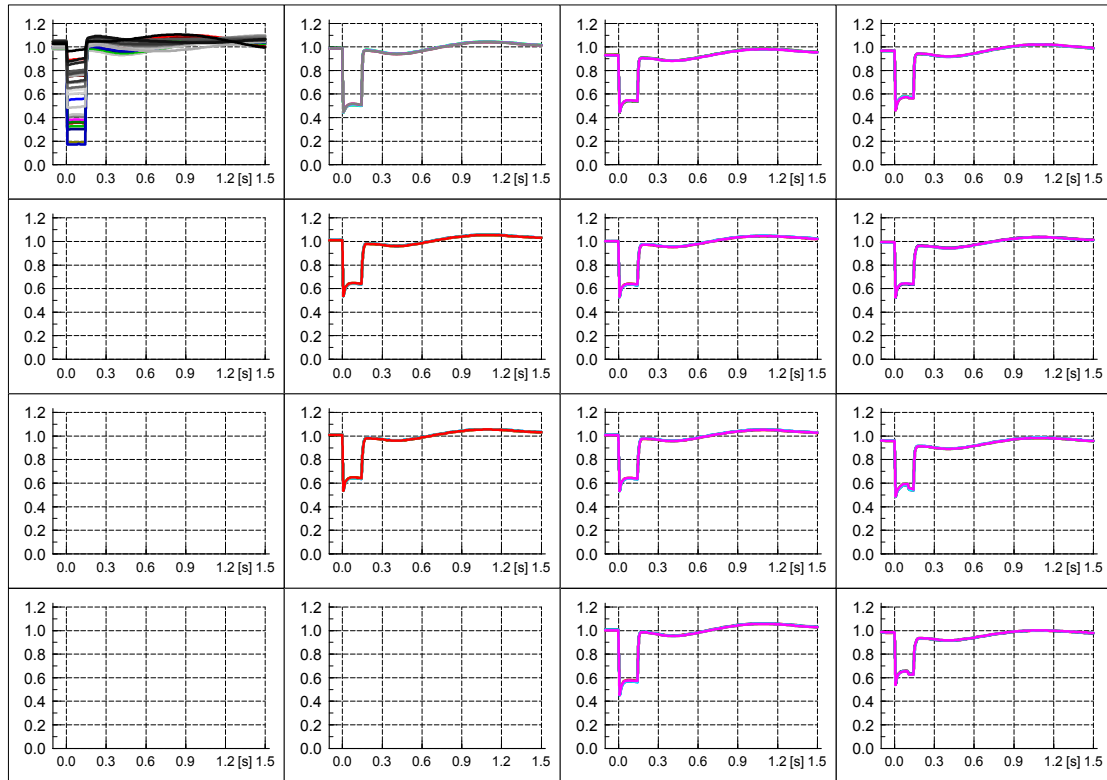


- Direct and quadrature axis currents of PV systems

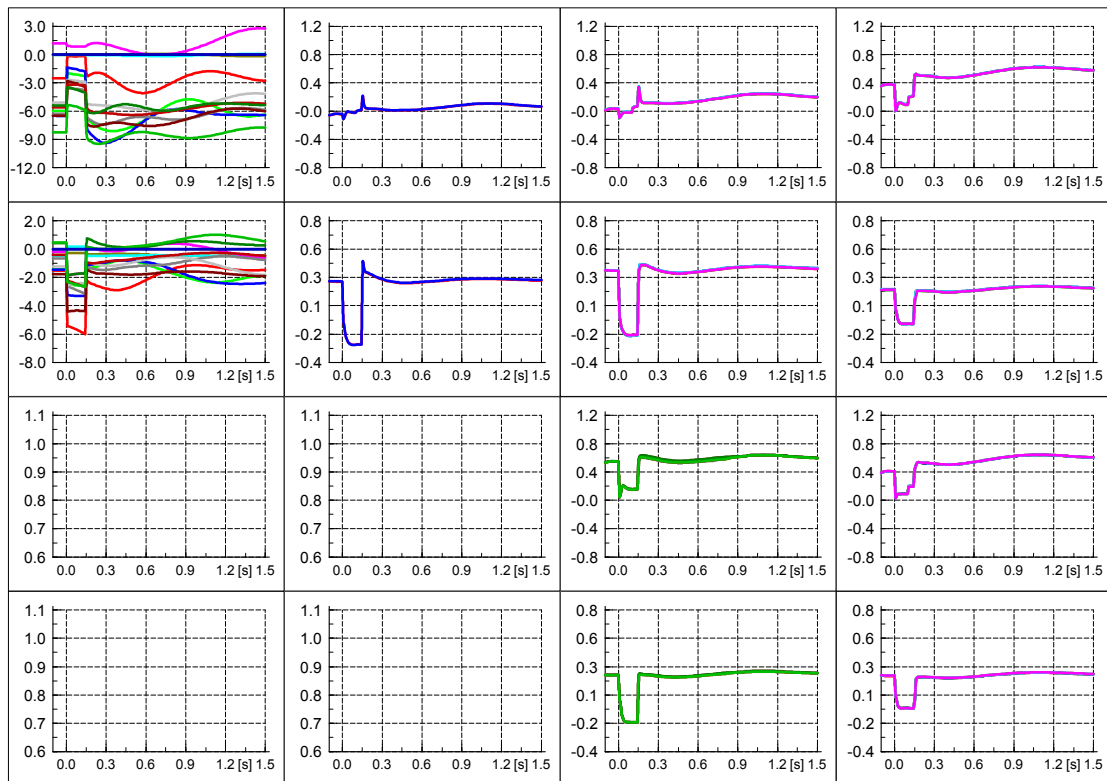


Base case aRCI

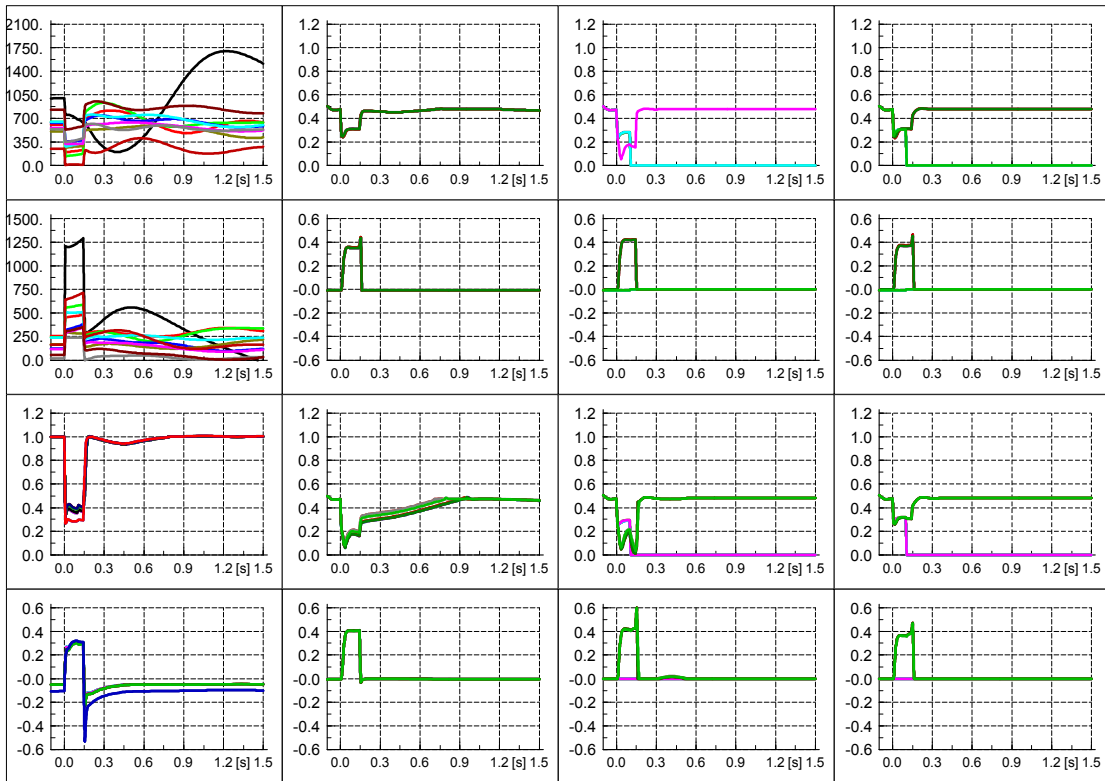
- Voltages



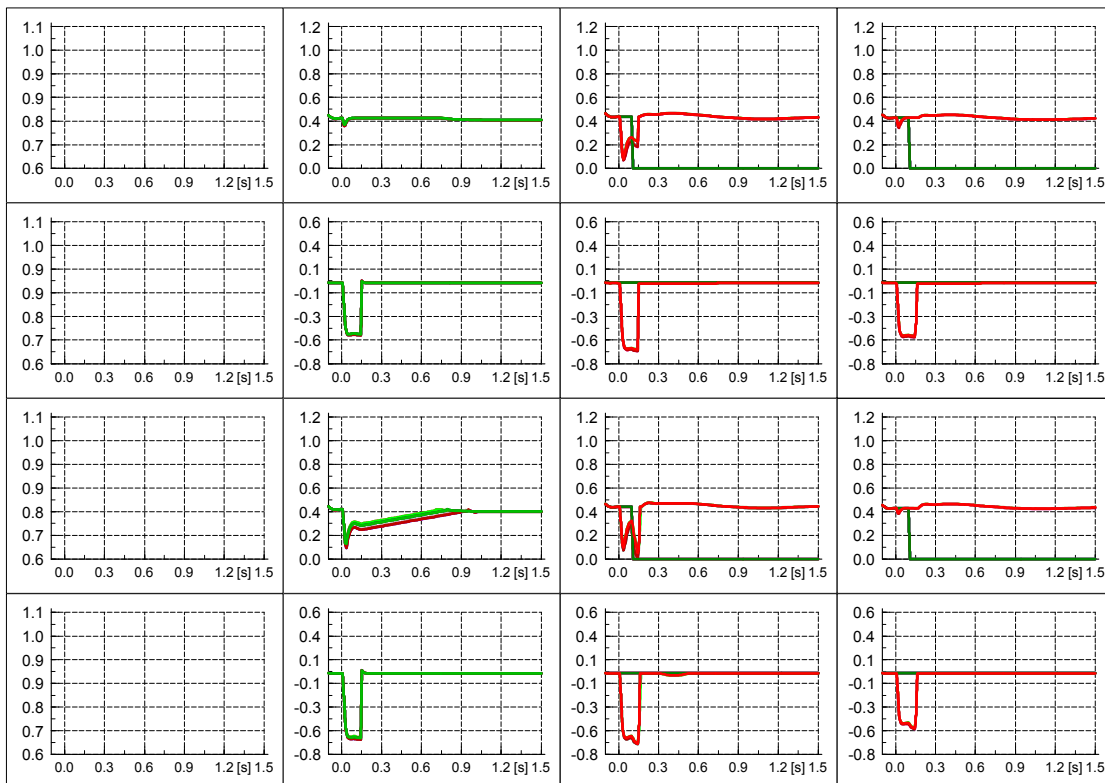
- Power exchange over the transformers



- Power production of DG and SG

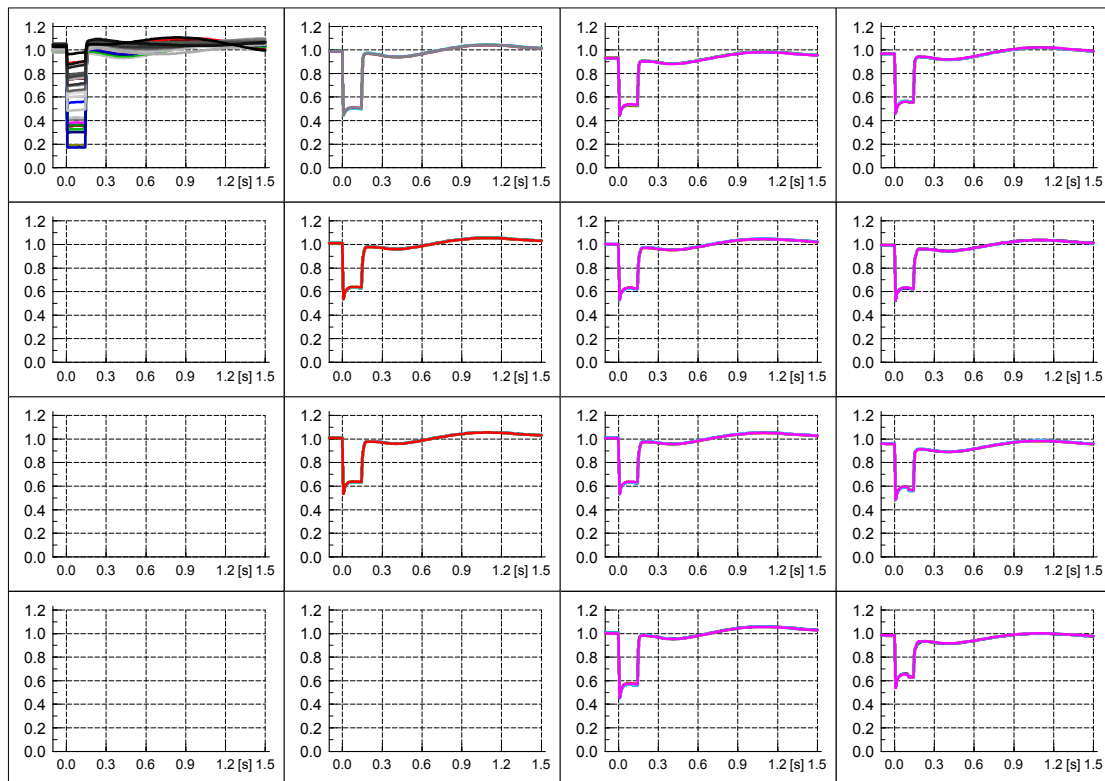


- Direct and quadrature axis currents of PV systems

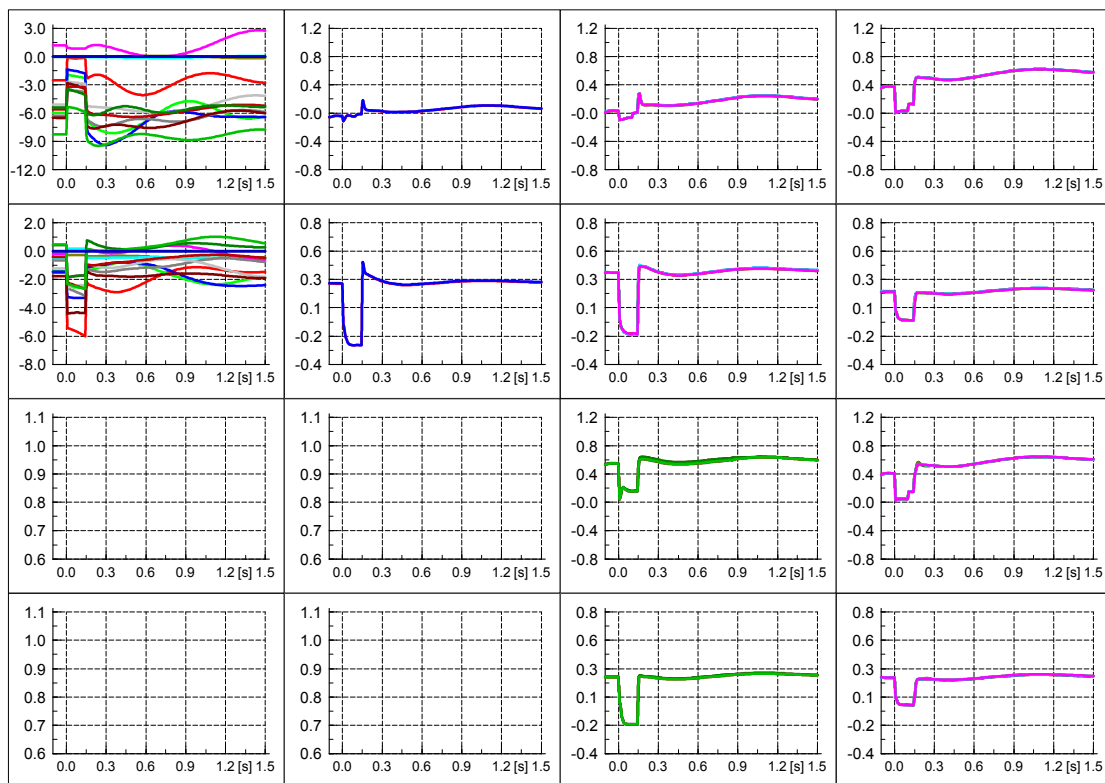


Base case aRACI

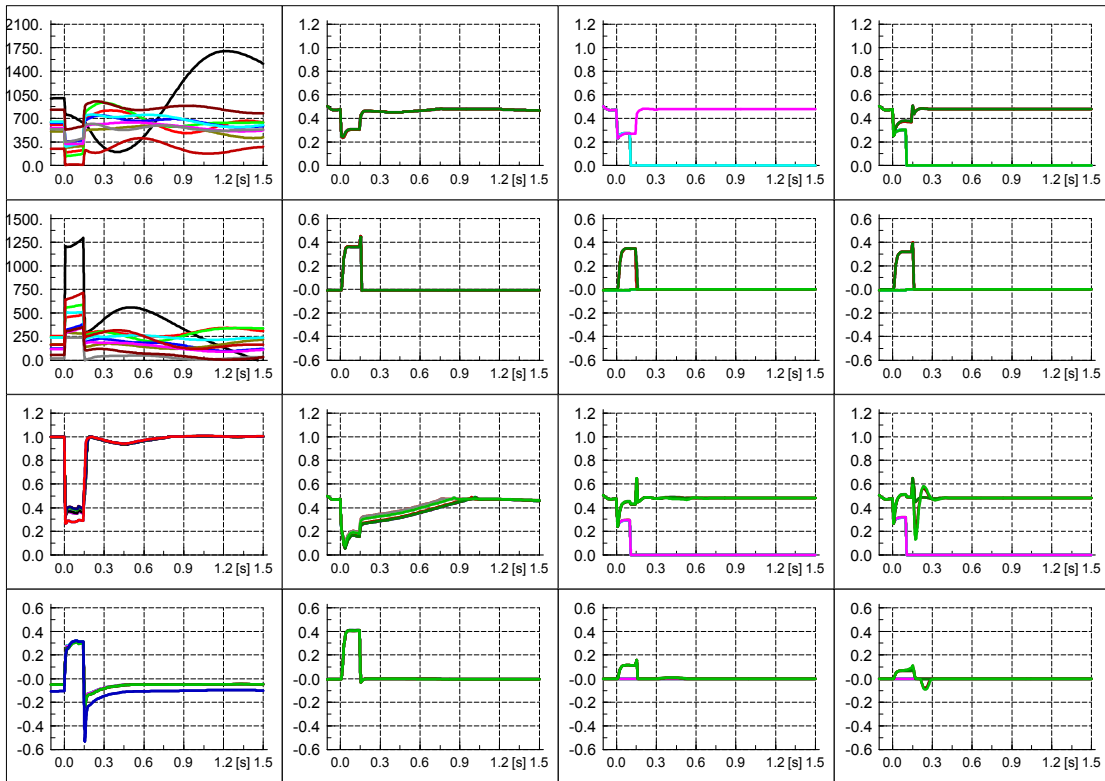
- Voltages



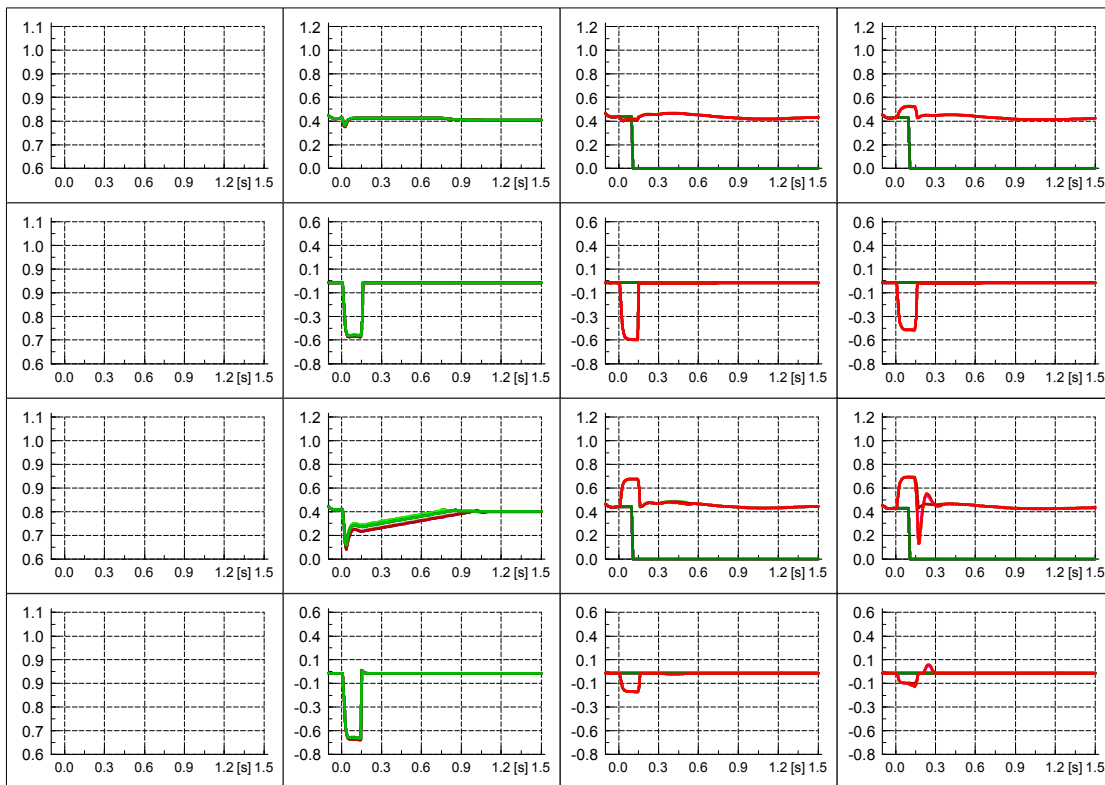
- Power exchange over the transformers



- Power production of DG and SG

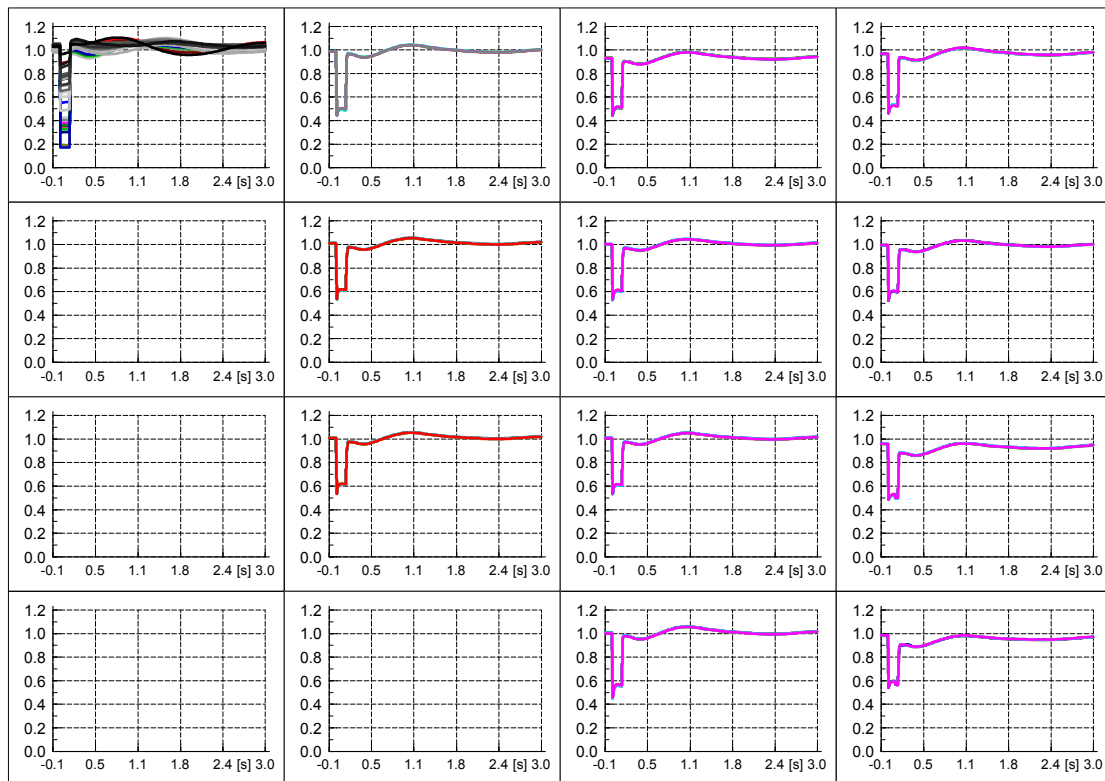


- Direct and quadrature axis currents of PV systems

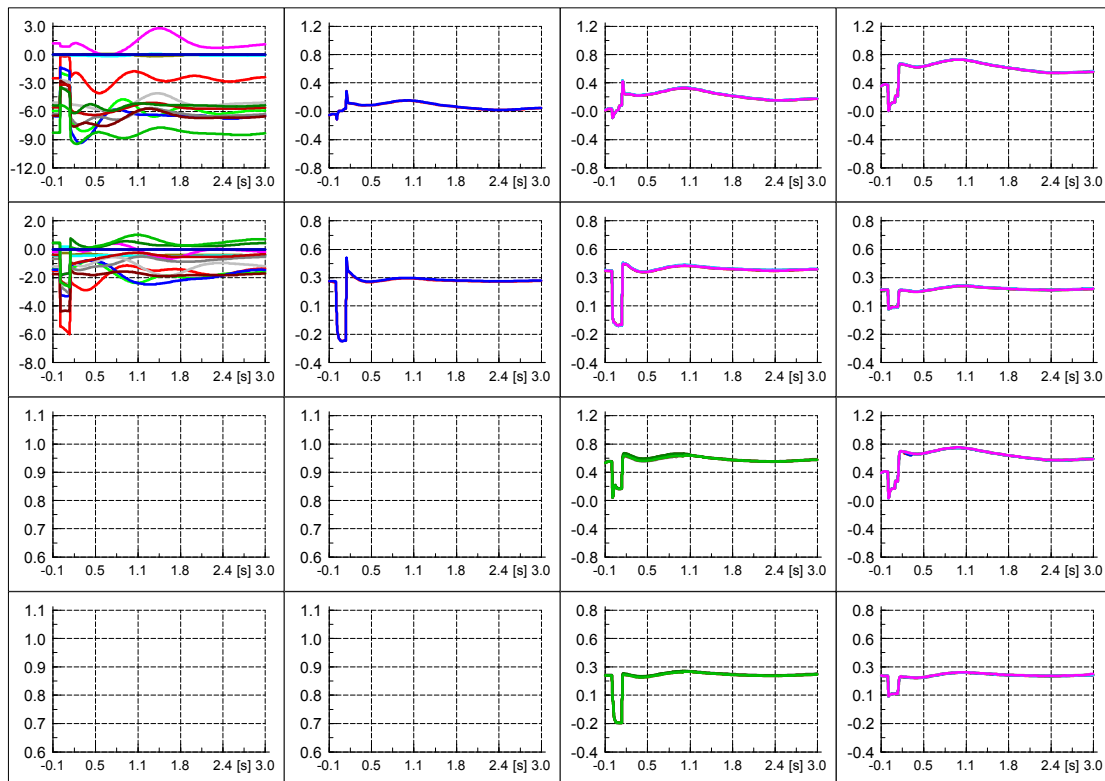


Base case ZPM with delayed APR (3 s period)

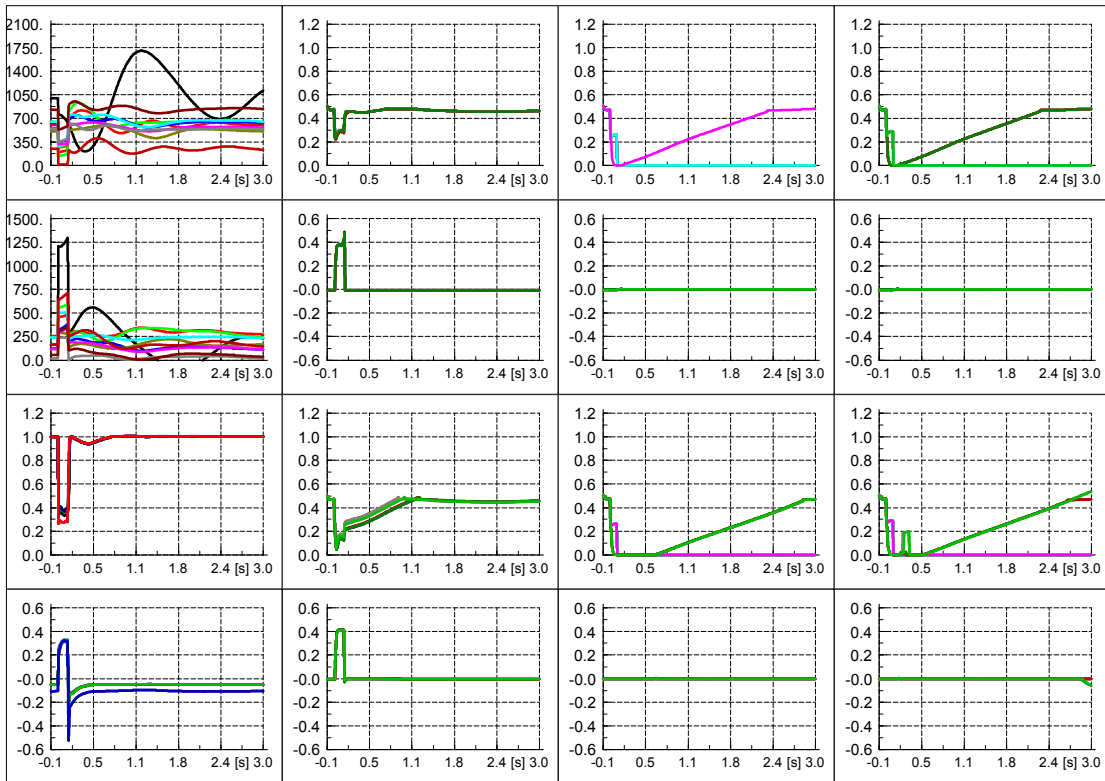
- Voltages



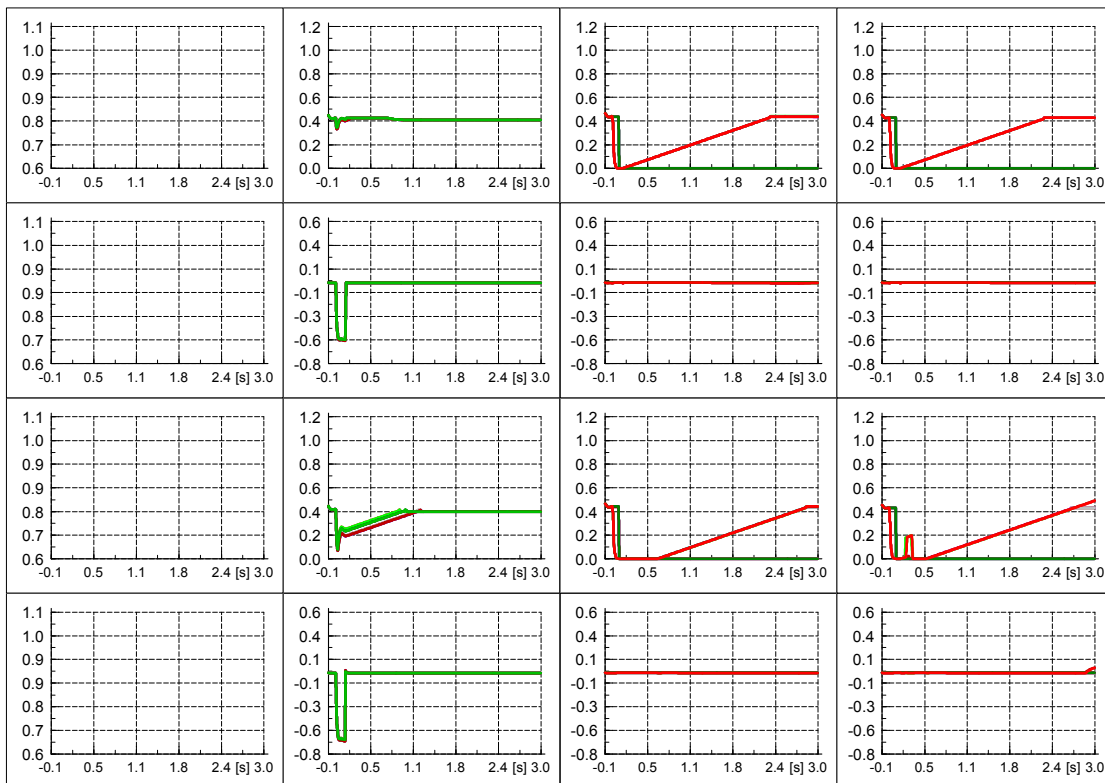
- Power exchange over the transformers



- Power production of DG and SG

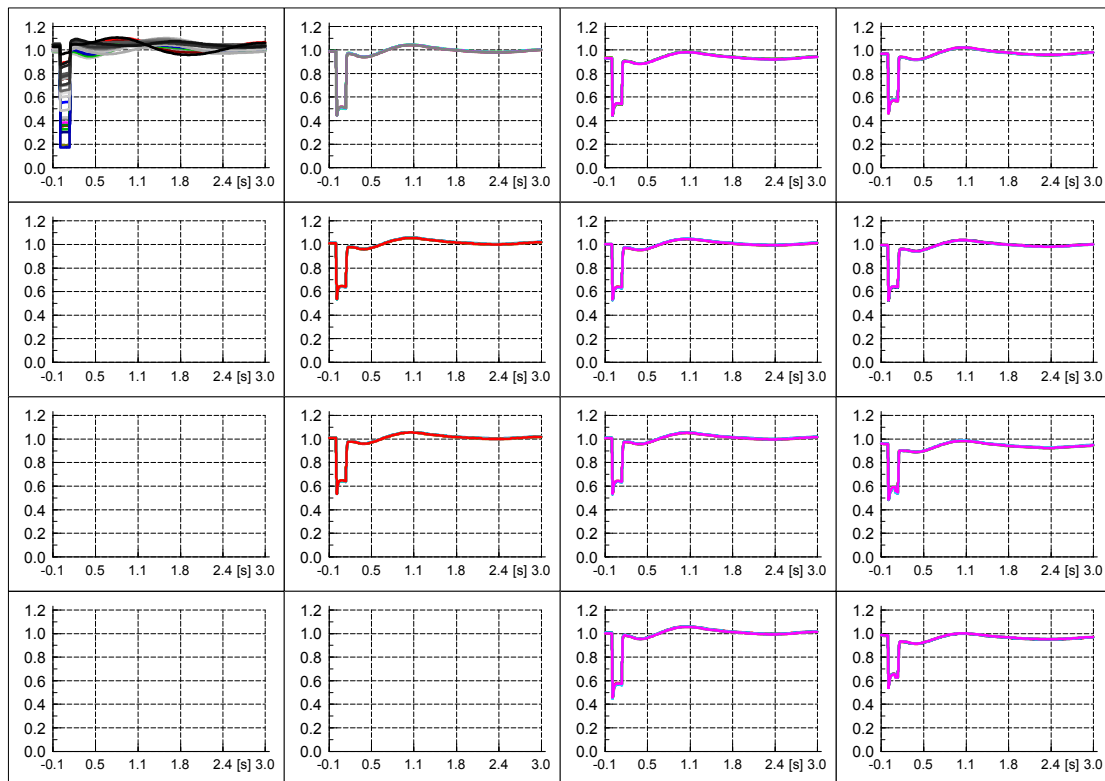


- Direct and quadrature axis currents of PV systems

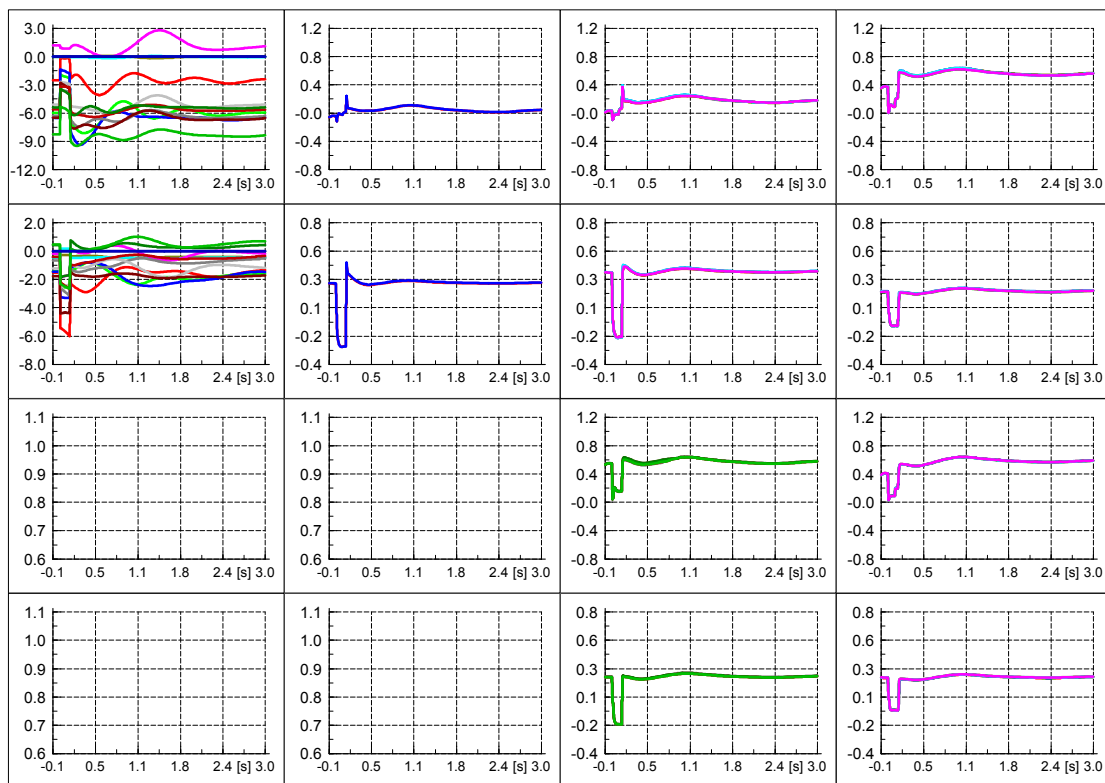


Base case aRCI with delayed APR (3 s period)

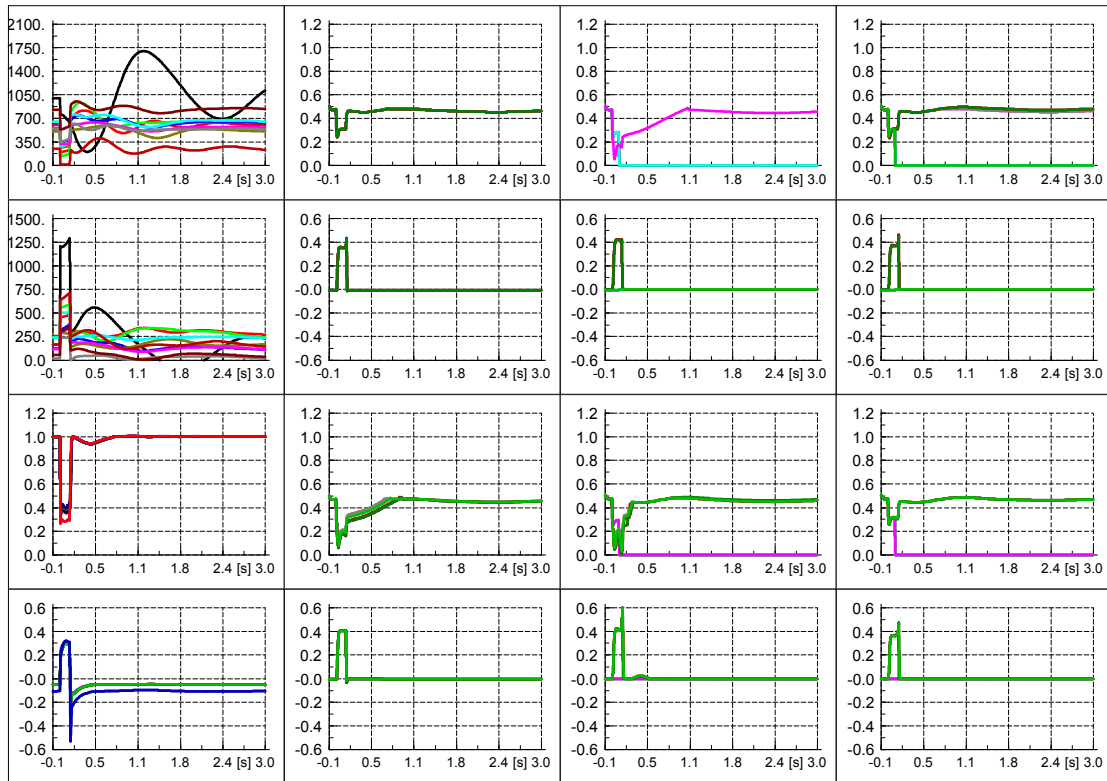
- Voltages



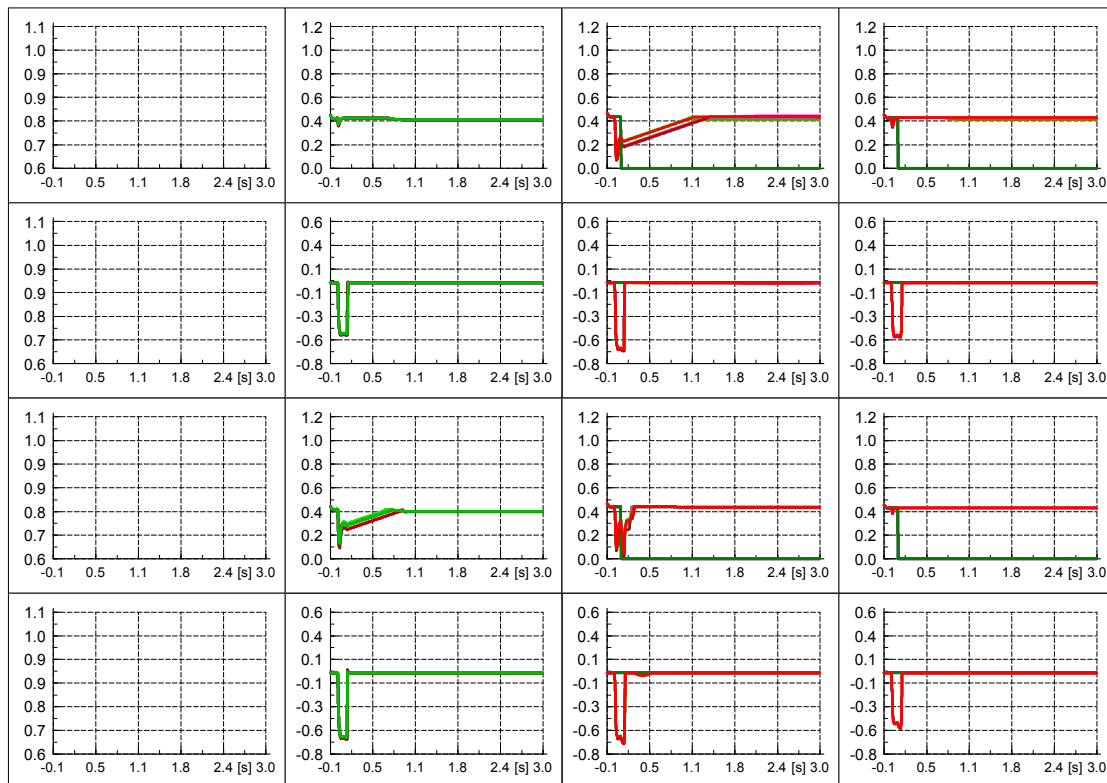
- Power exchange over the transformers



- Power production of DG and SG

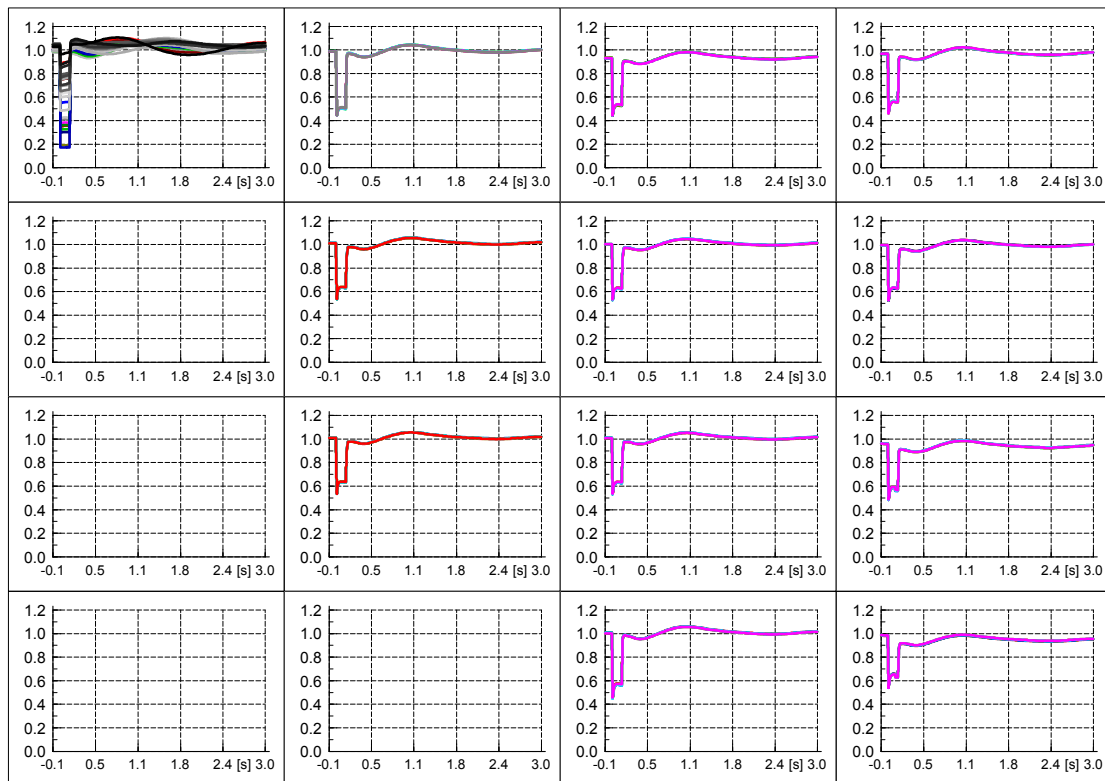


- Direct and quadrature axis currents of PV systems

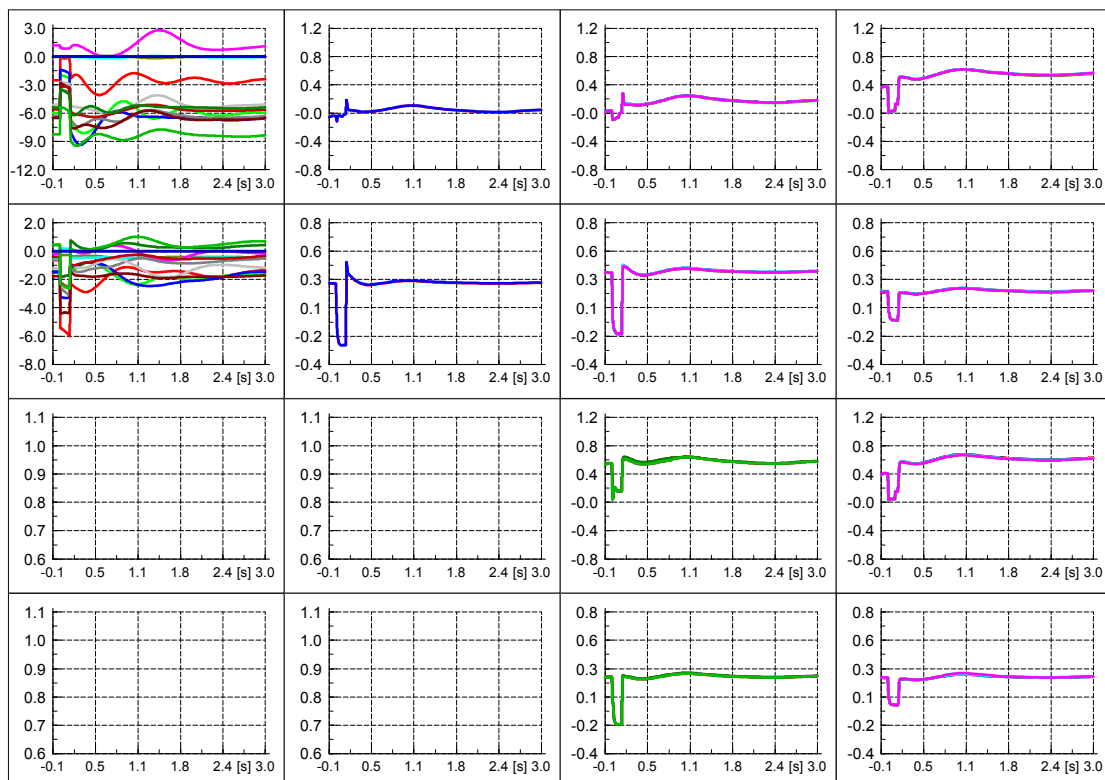


Base case aRACI with delayed APR (3 s period)

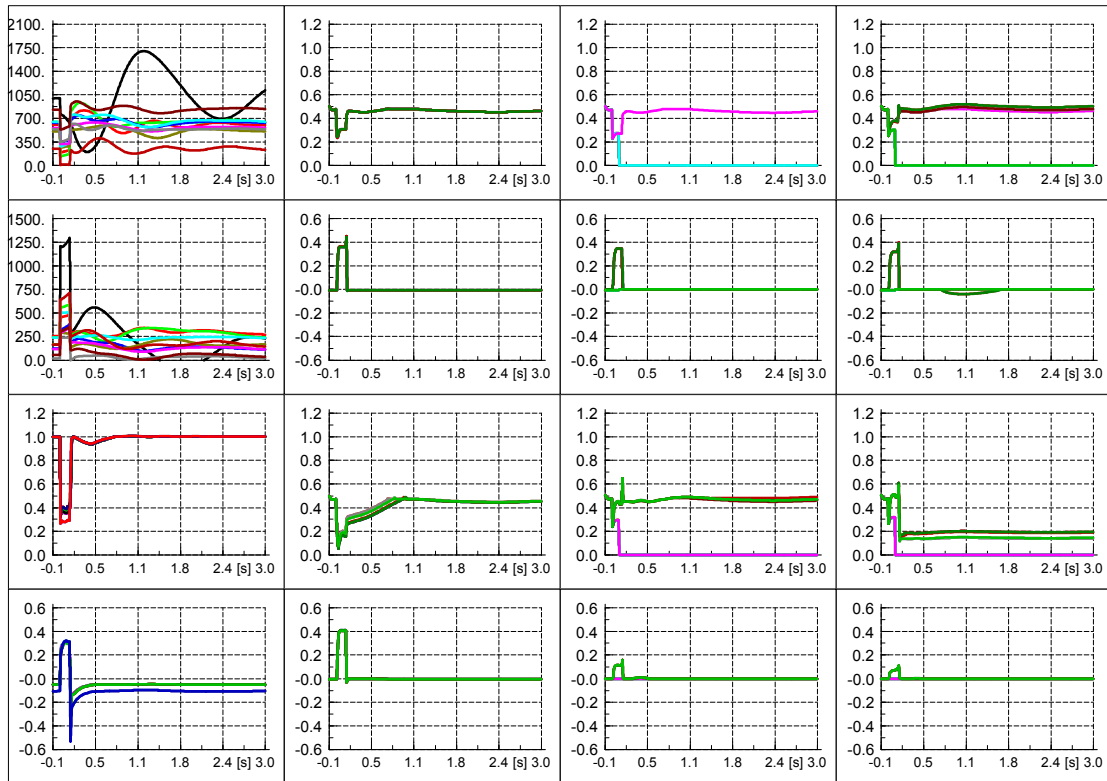
- Voltages



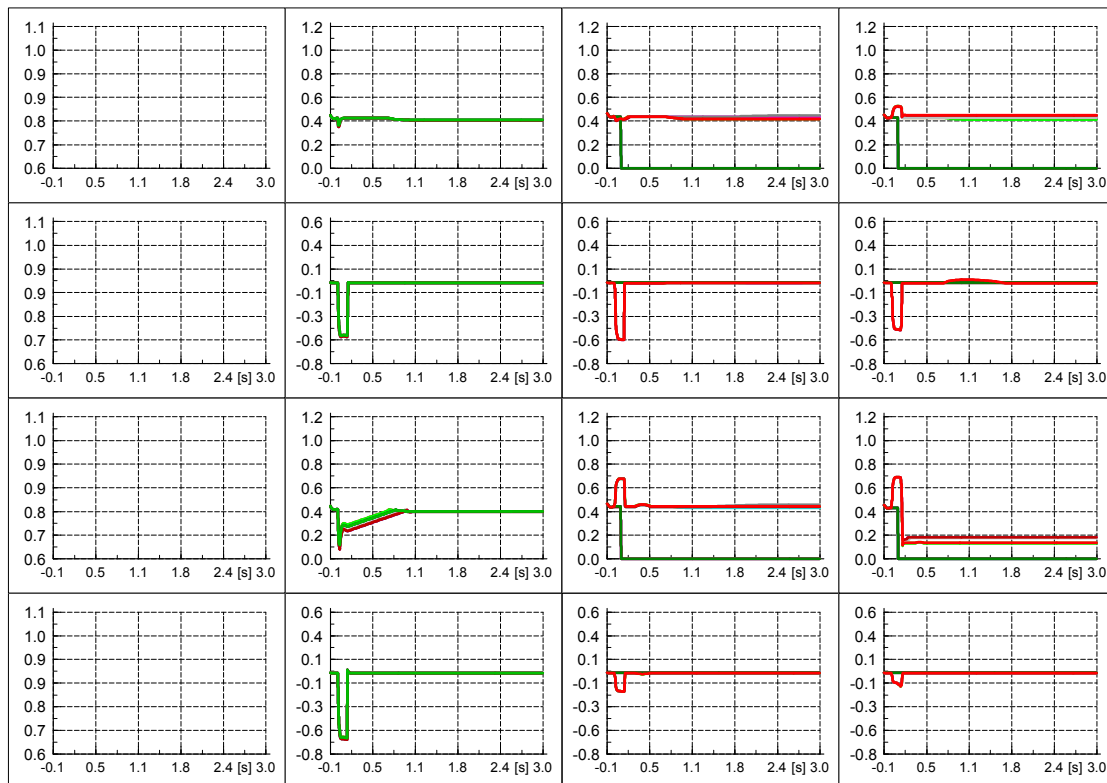
- Power exchange over the transformers



- Power production of DG and SG

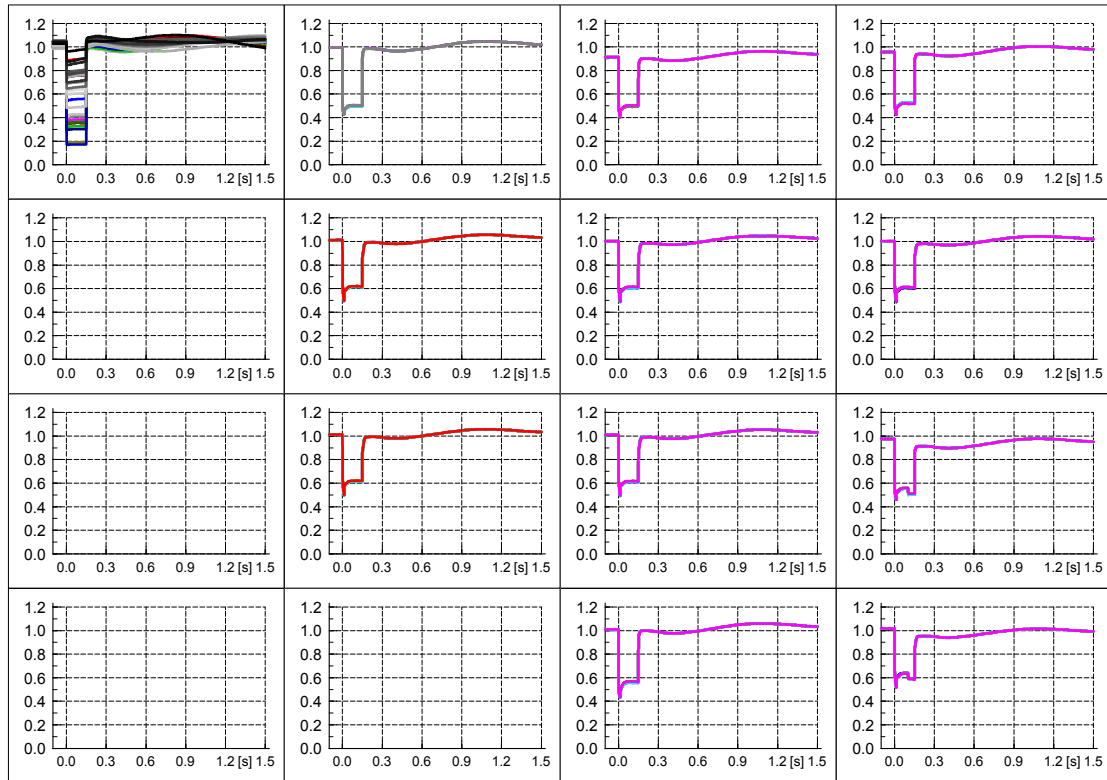


- Direct and quadrature axis currents of PV systems

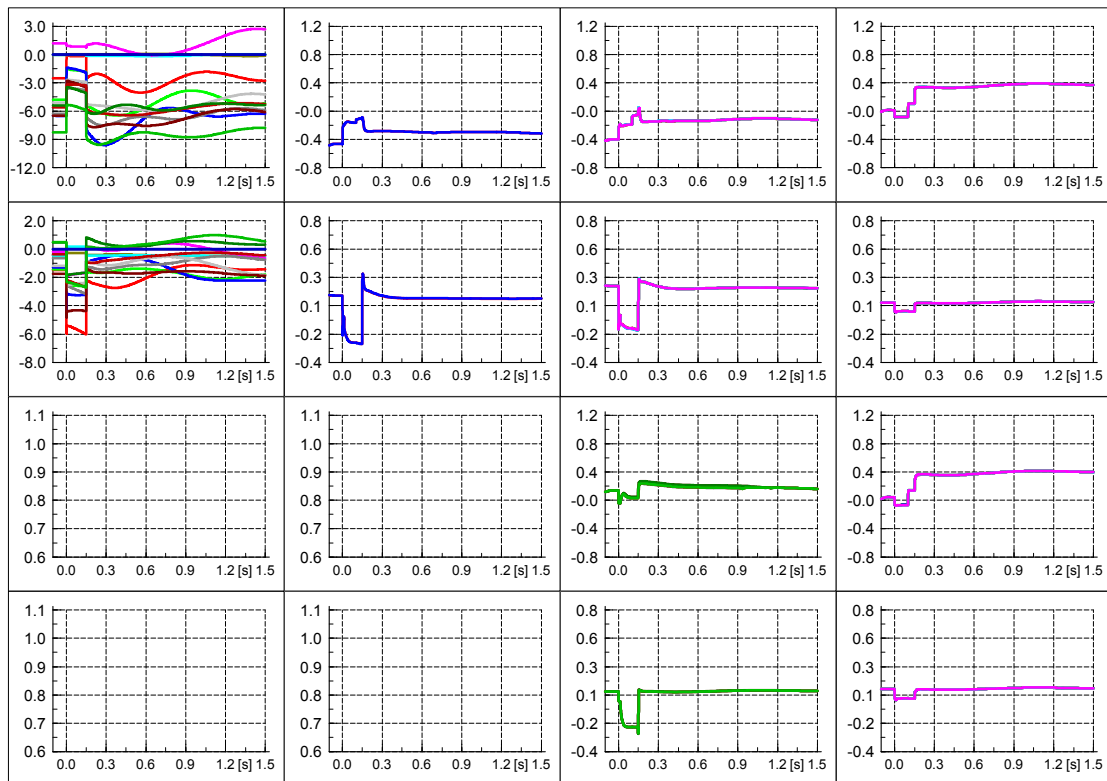


SRPF No-LVRT

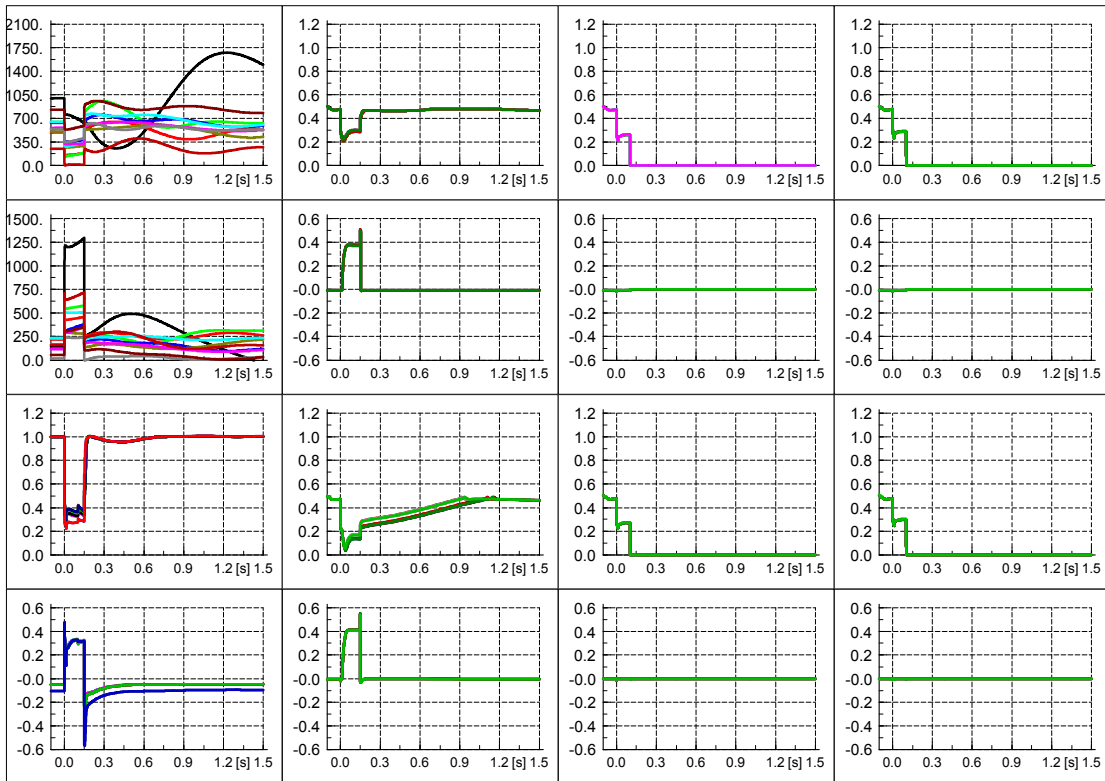
- Voltages



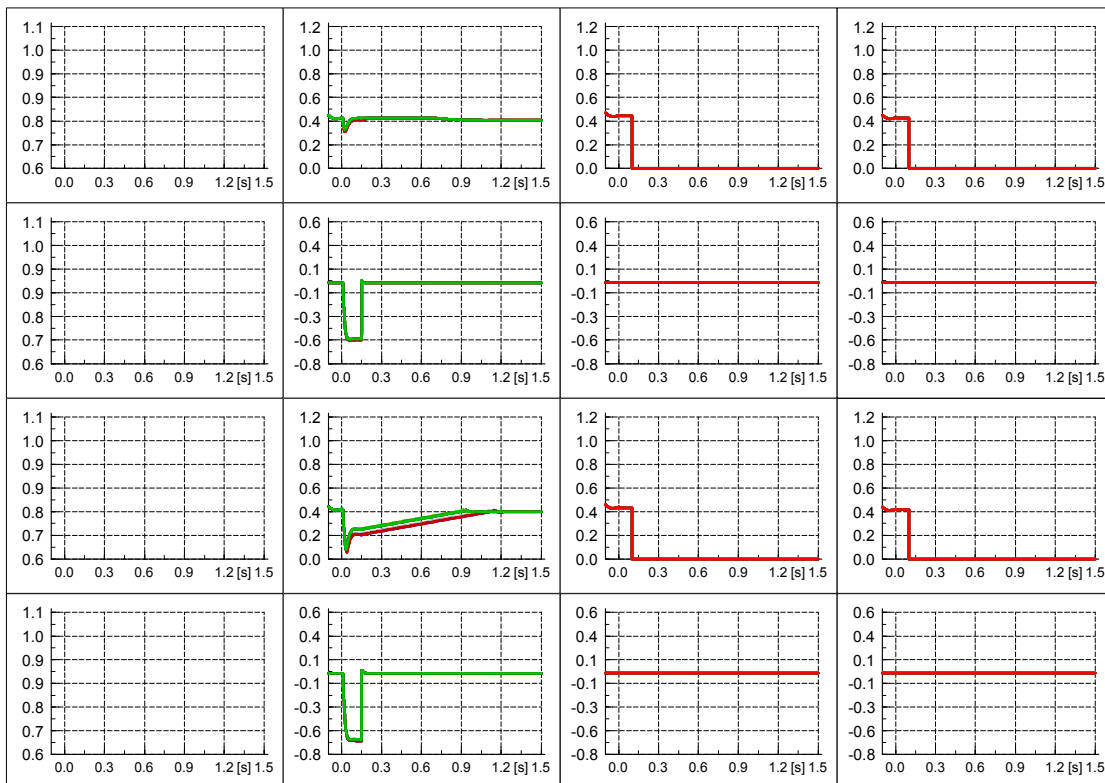
- Power exchange over the transformers



- Power production of DG and SG

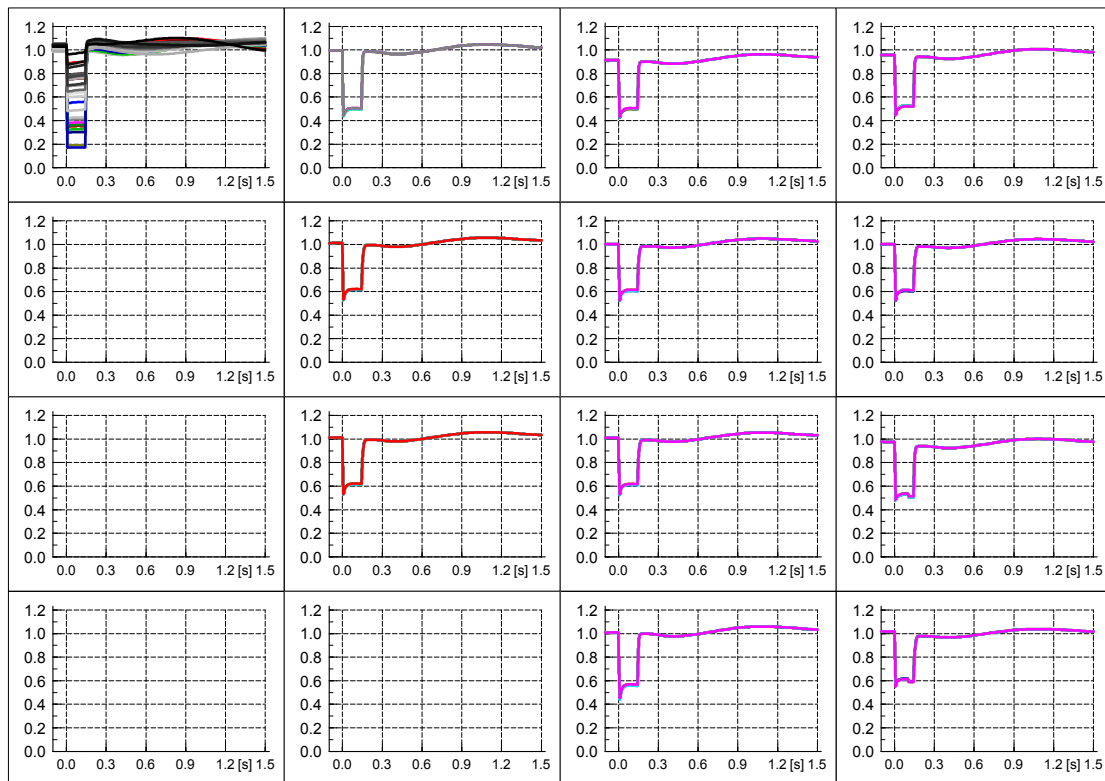


- Direct and quadrature axis currents of PV systems

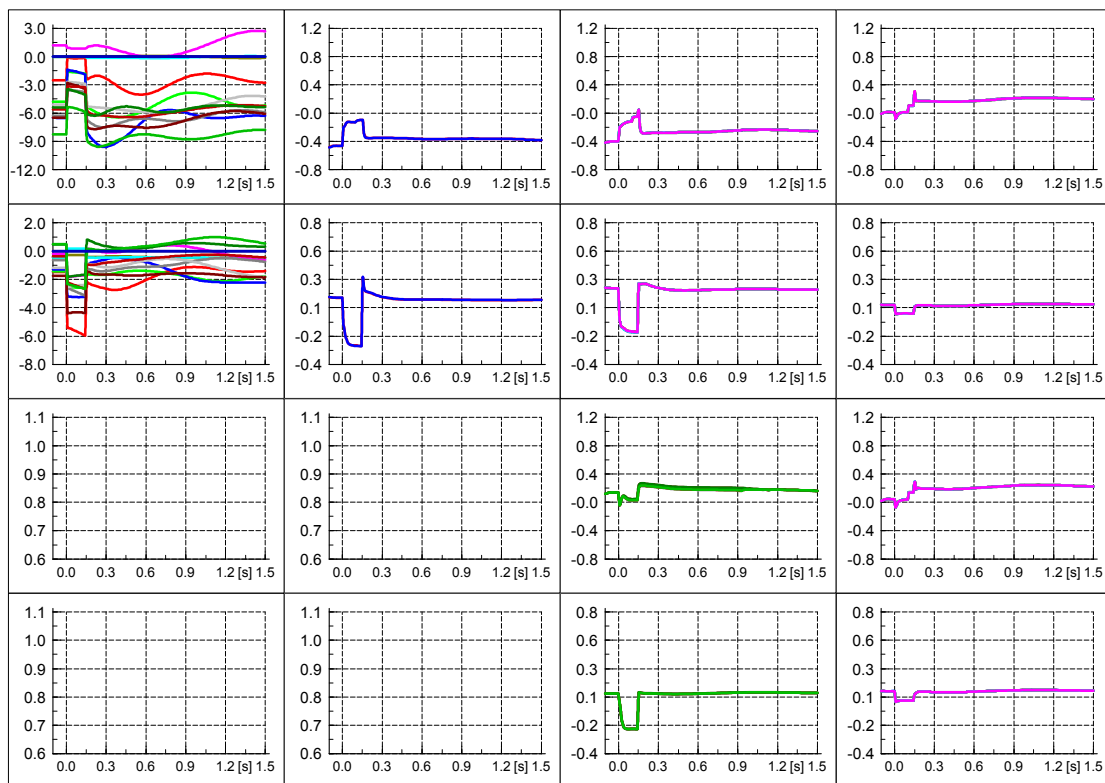


SRPF ZPM

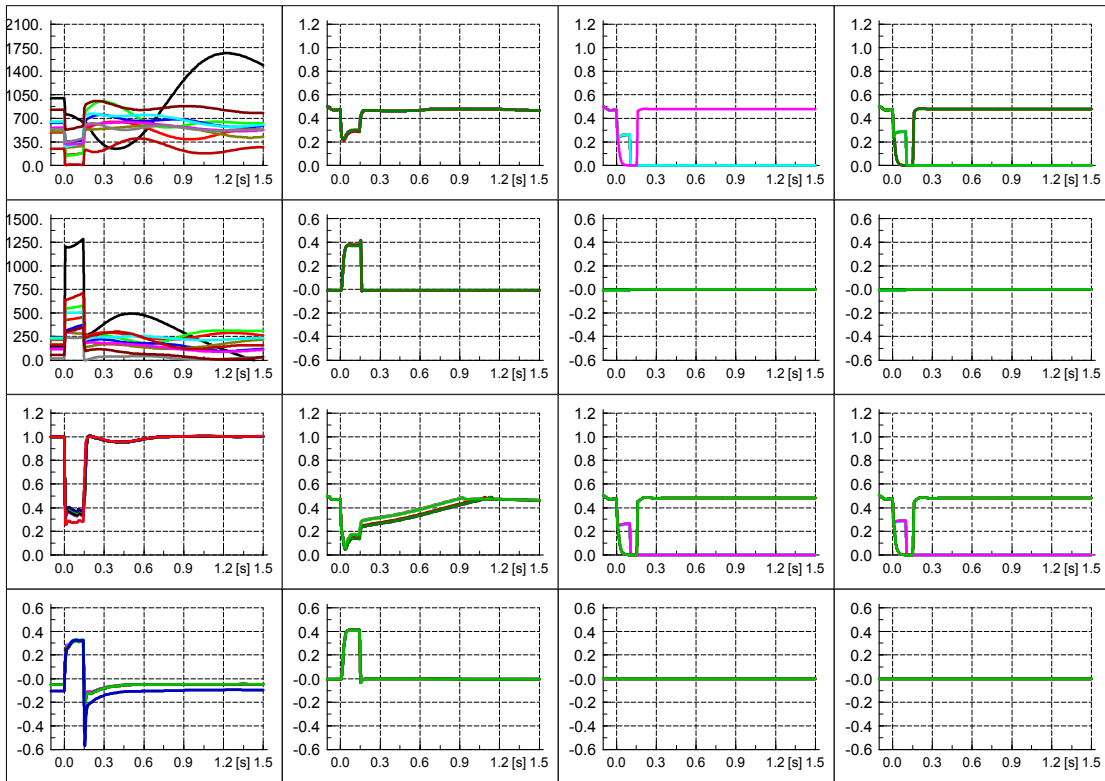
- Voltages



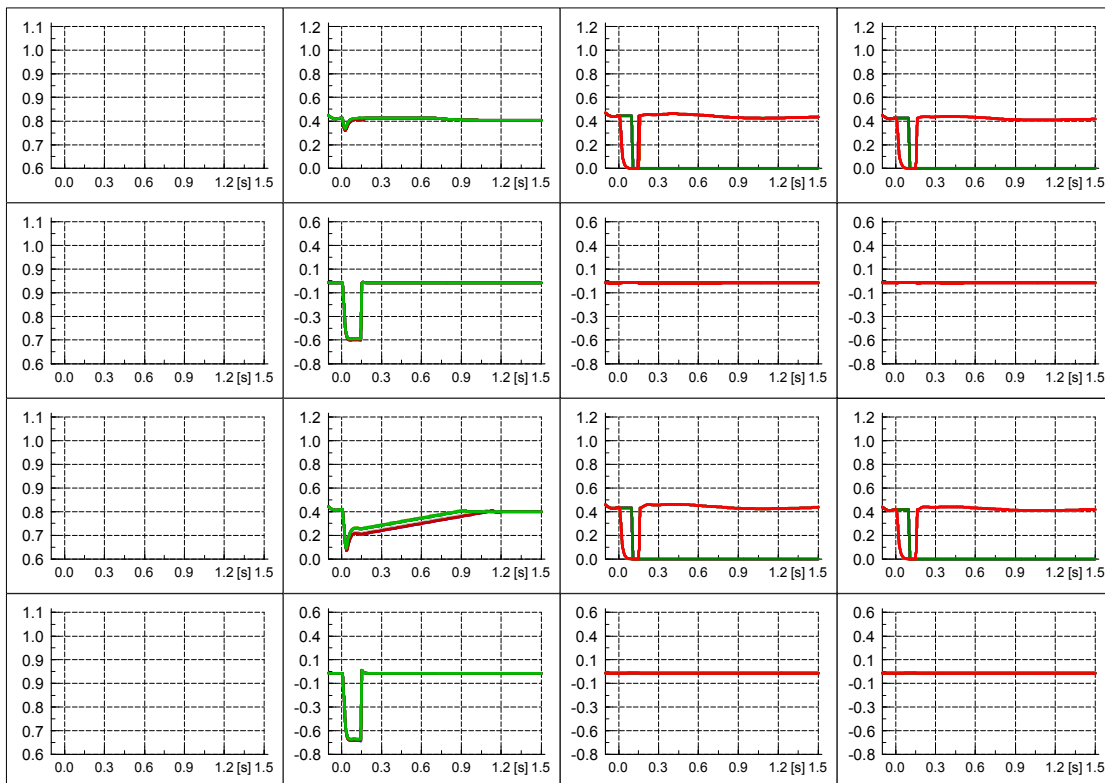
- Power exchange over the transformers



- Power production of DG and SG

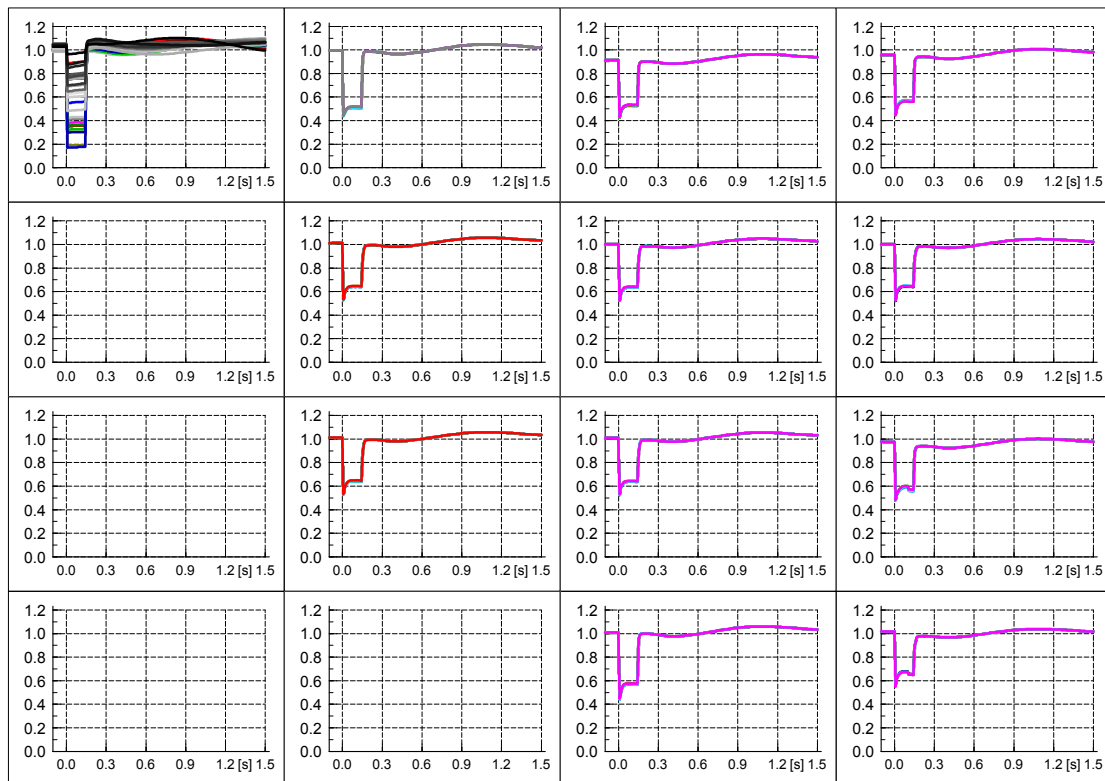


- Direct and quadrature axis currents of PV systems

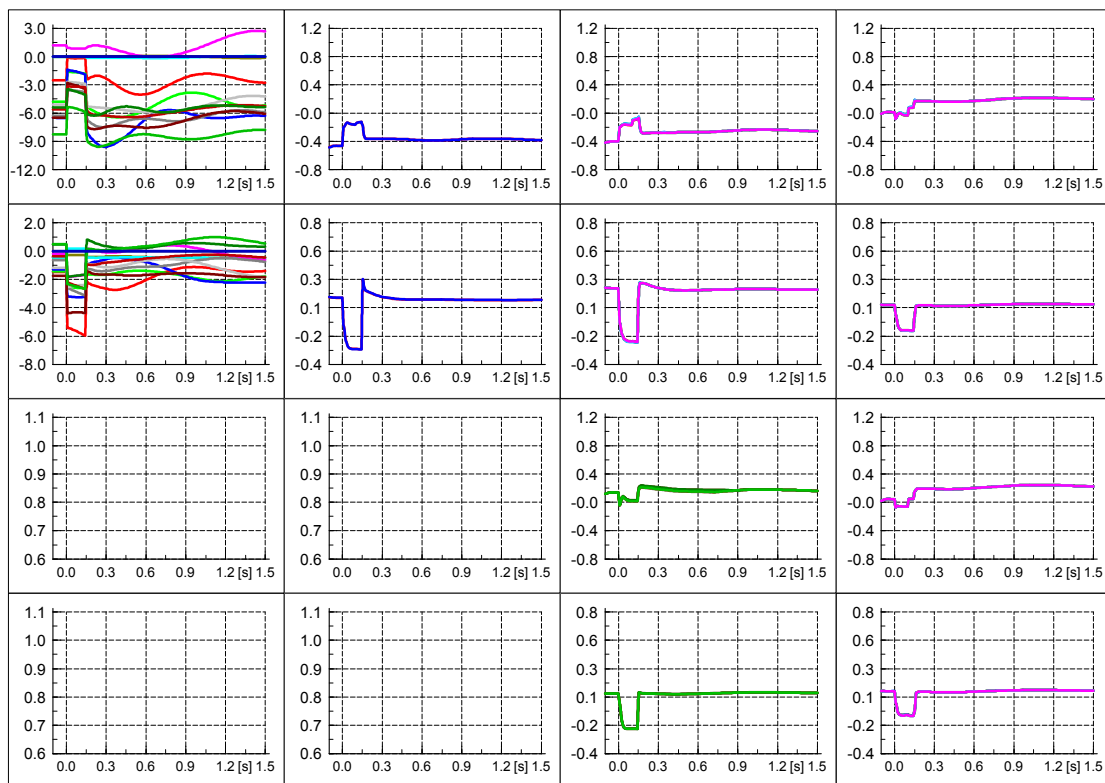


SRPF aRCI

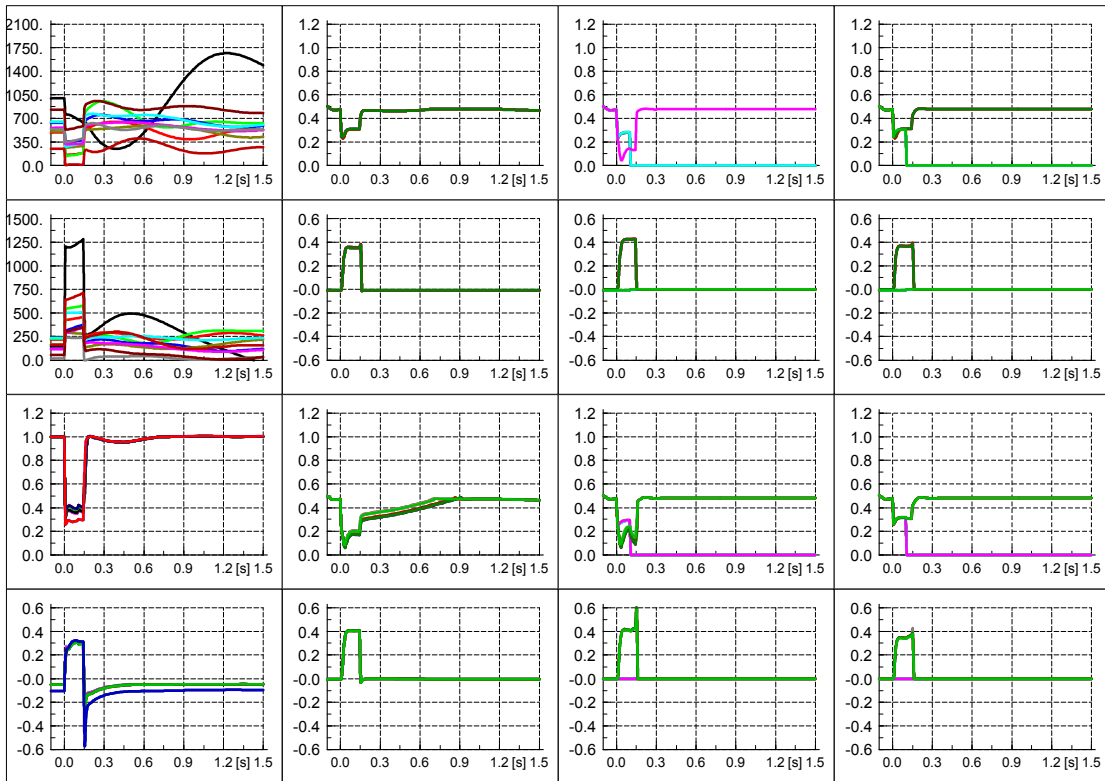
- Voltages



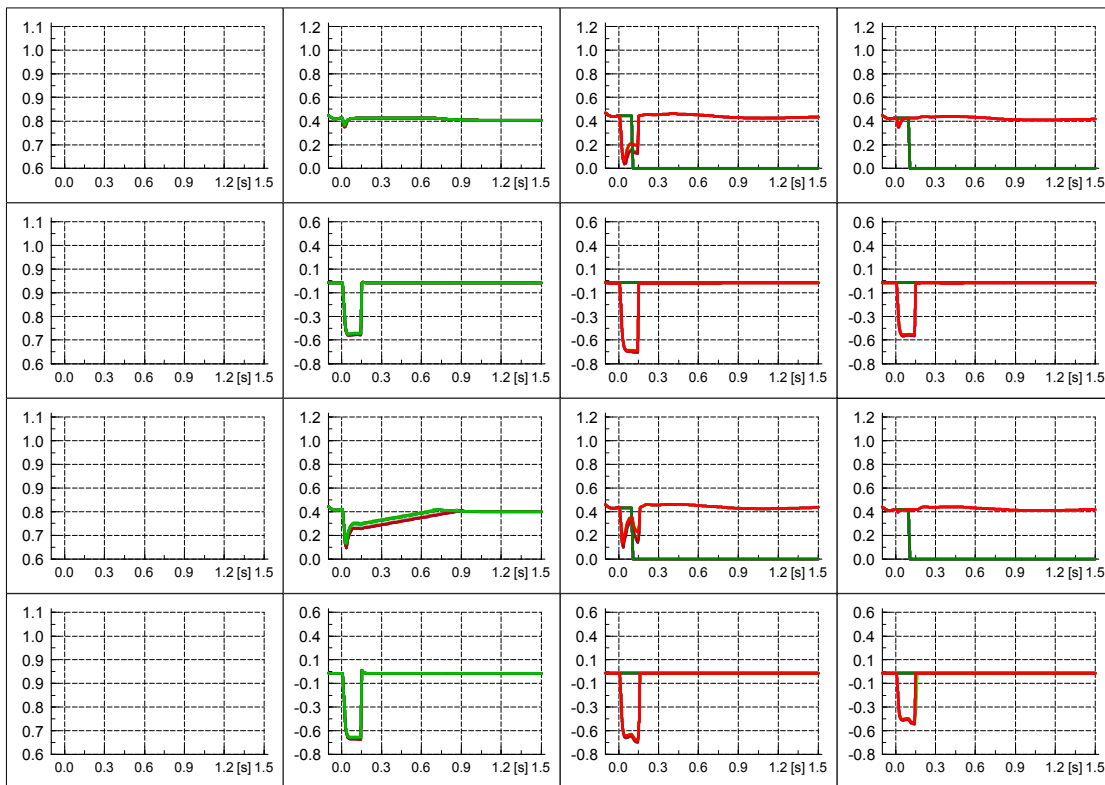
- Power exchange over the transformers



- Power production of DG and SG

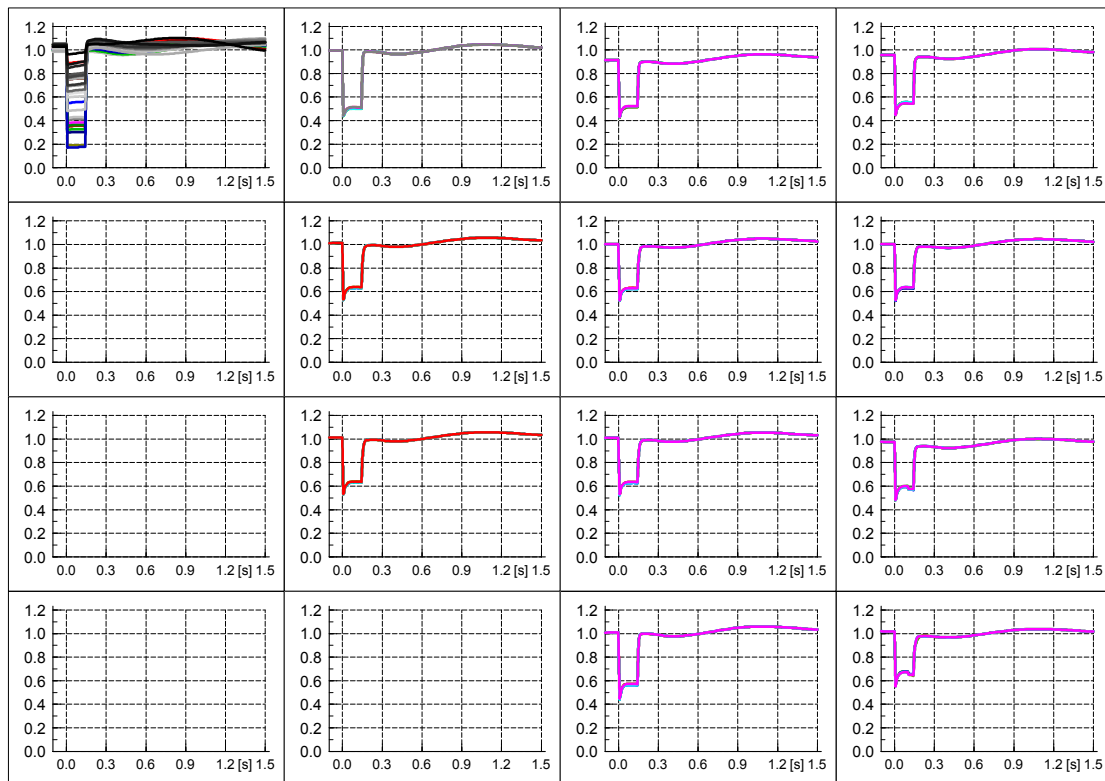


- Direct and quadrature axis currents of PV systems

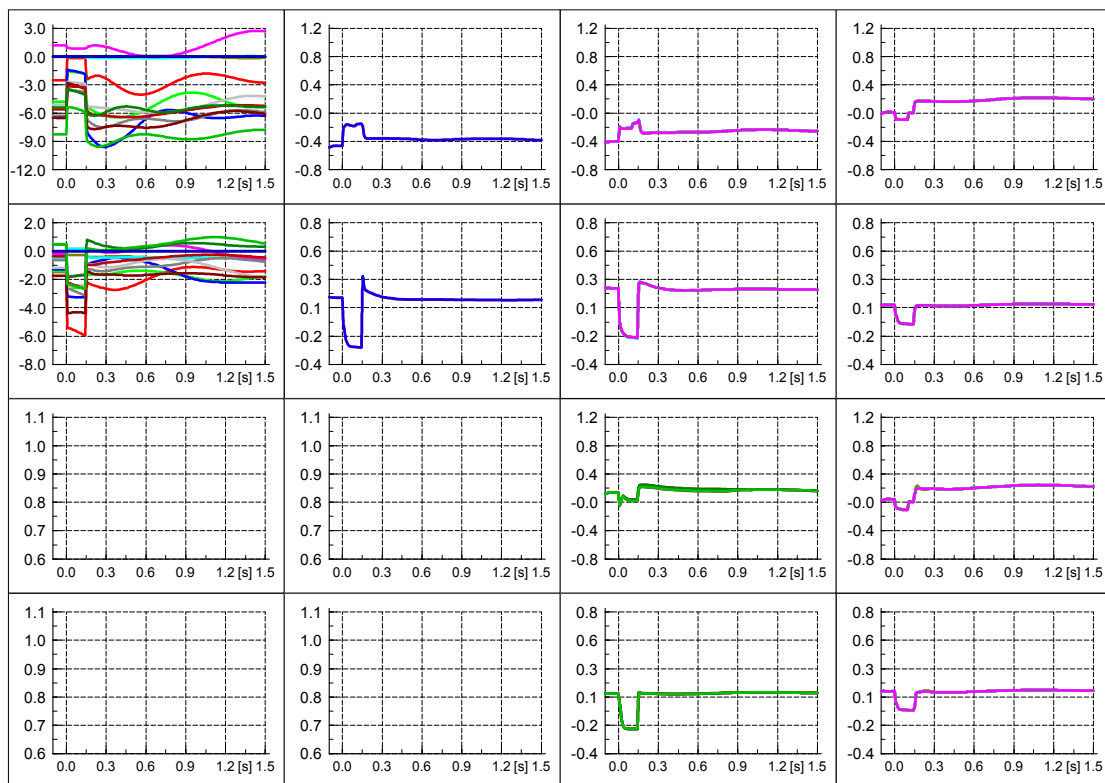


SRPF aRACI

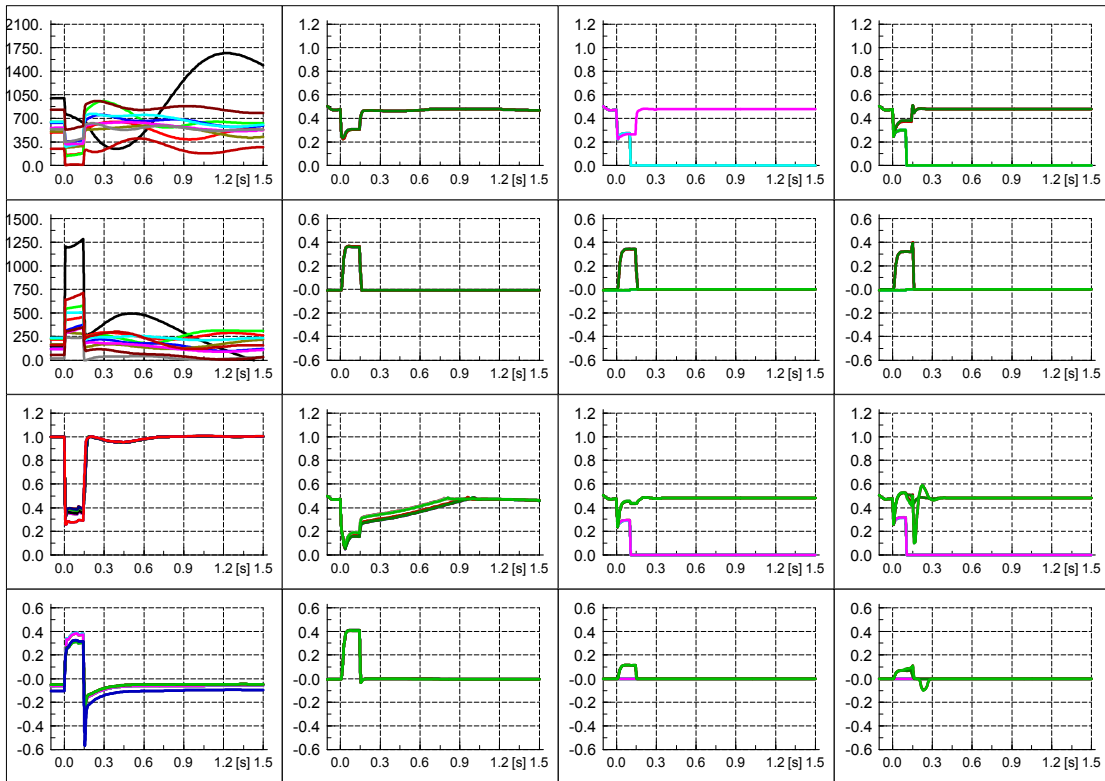
- Voltages



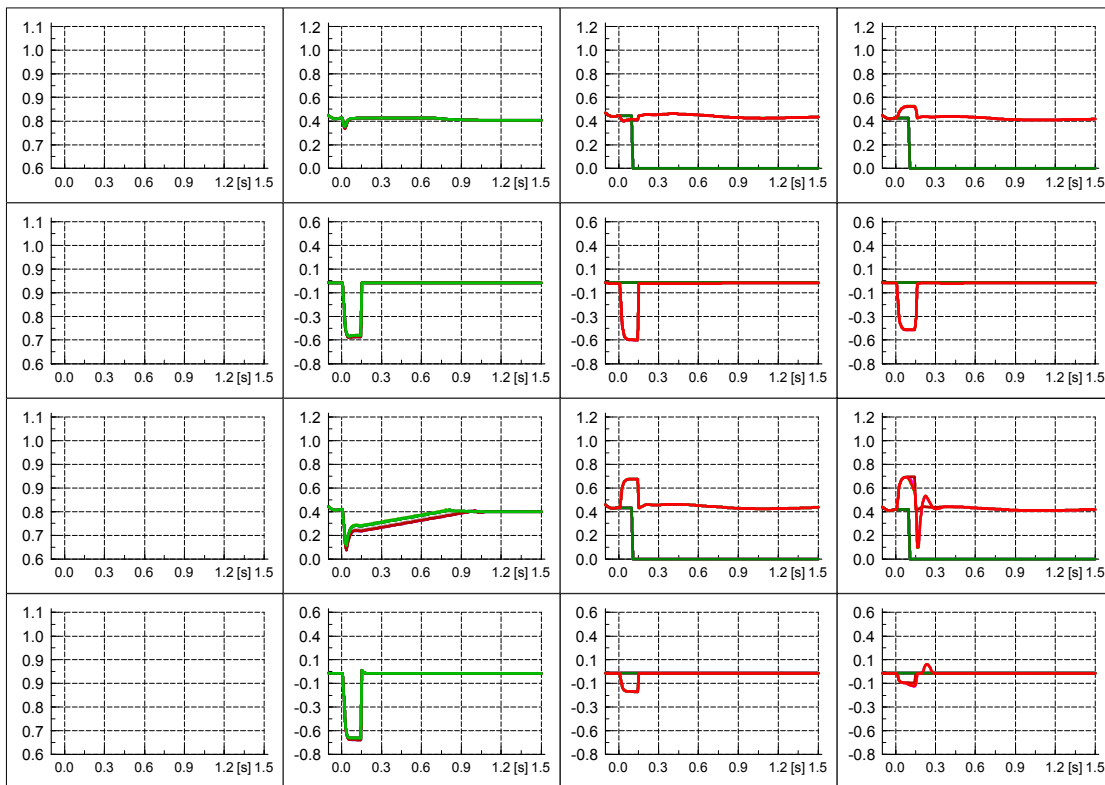
- Power exchange over the transformers



- Power production of DG and SG

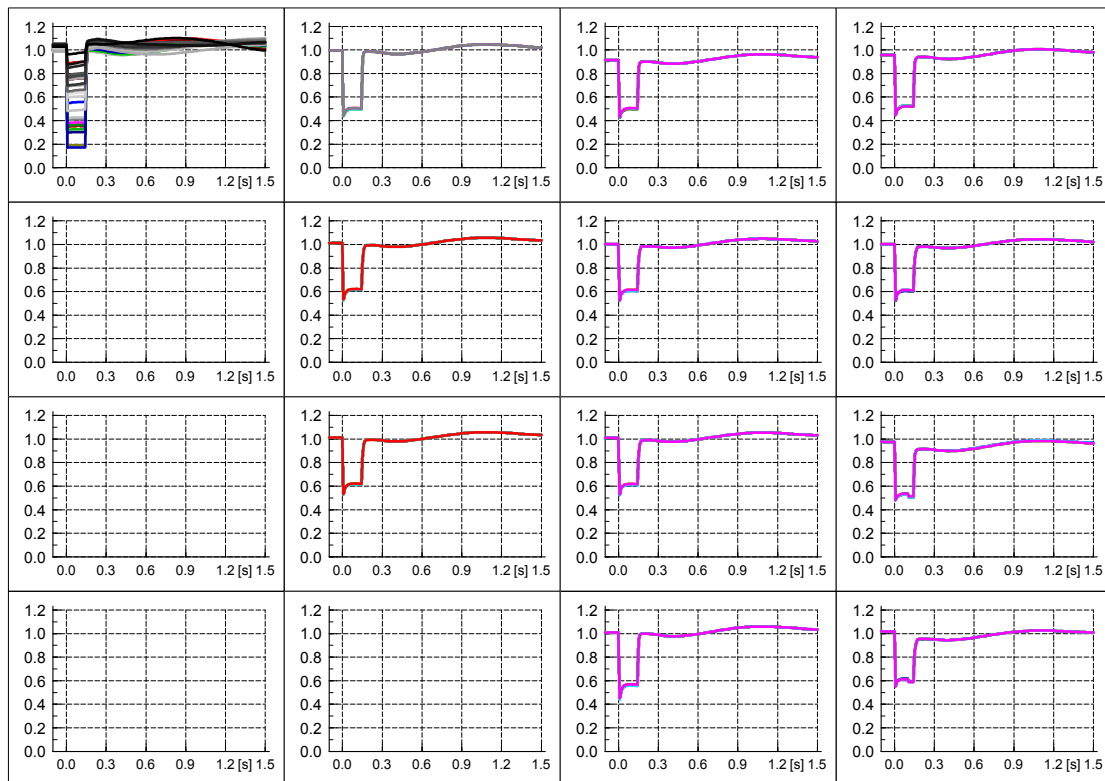


- Direct and quadrature axis currents of PV systems

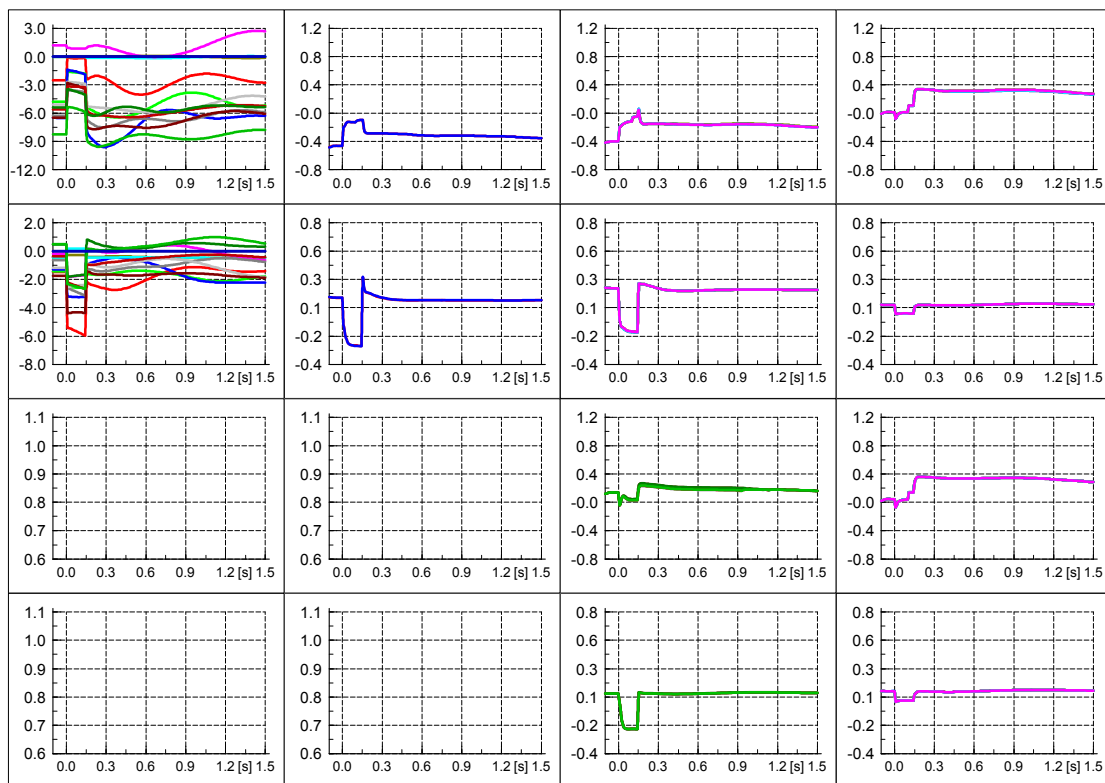


SRPF ZPM with delayed APR (3 s period)

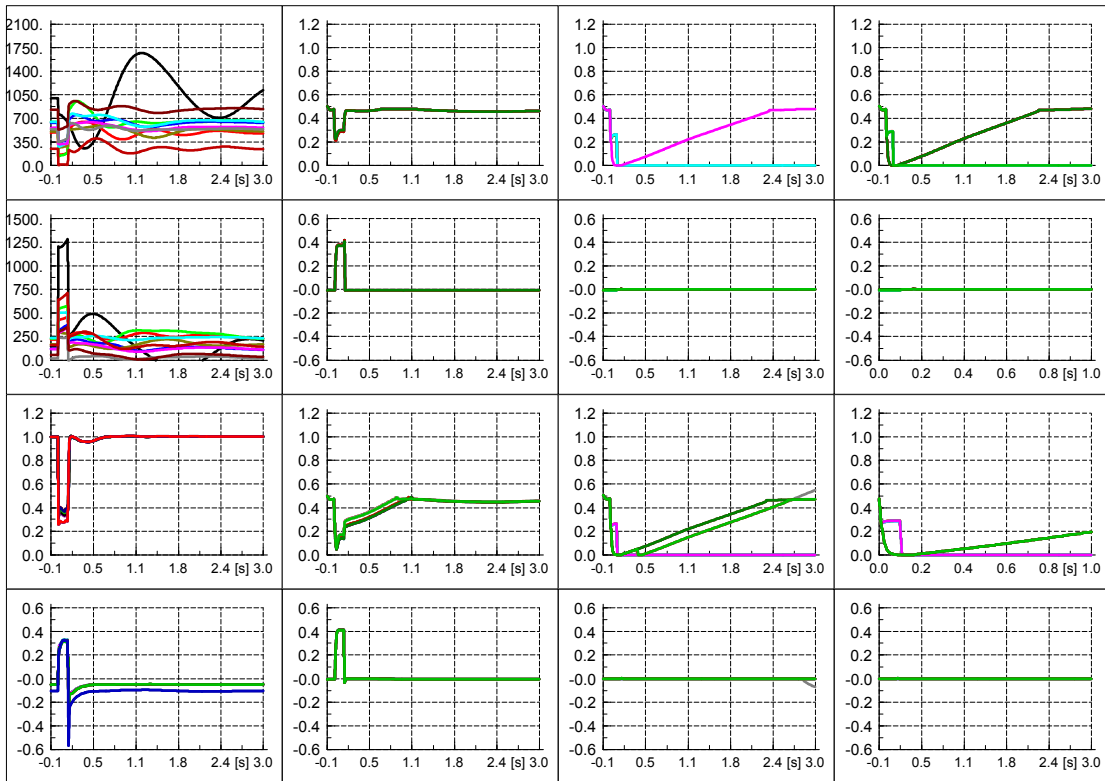
- Voltages



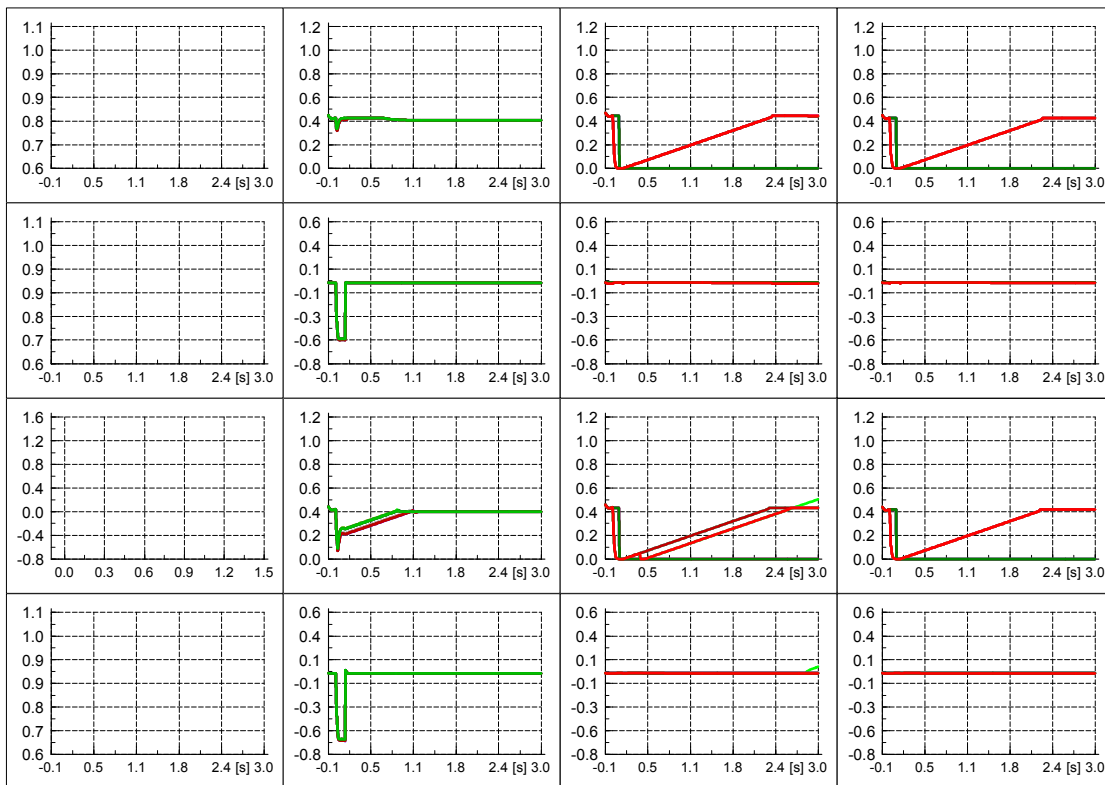
- Power exchange over the transformers



- Power production of DG and SG

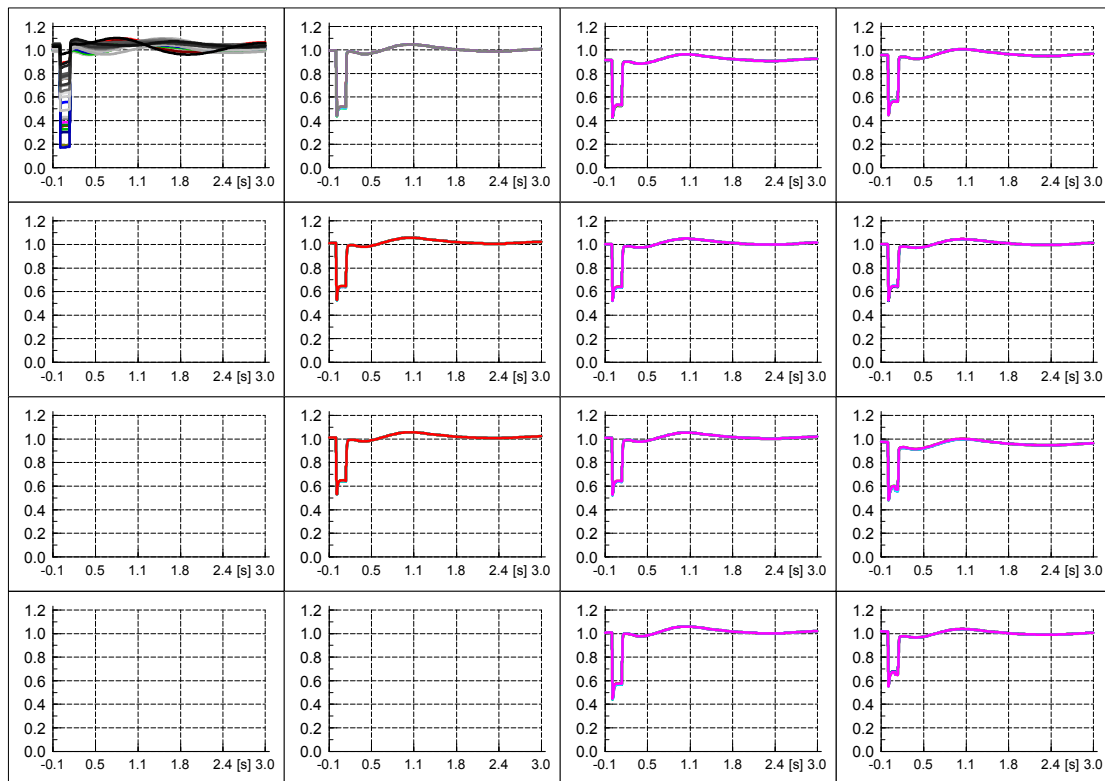


- Direct and quadrature axis currents of PV systems

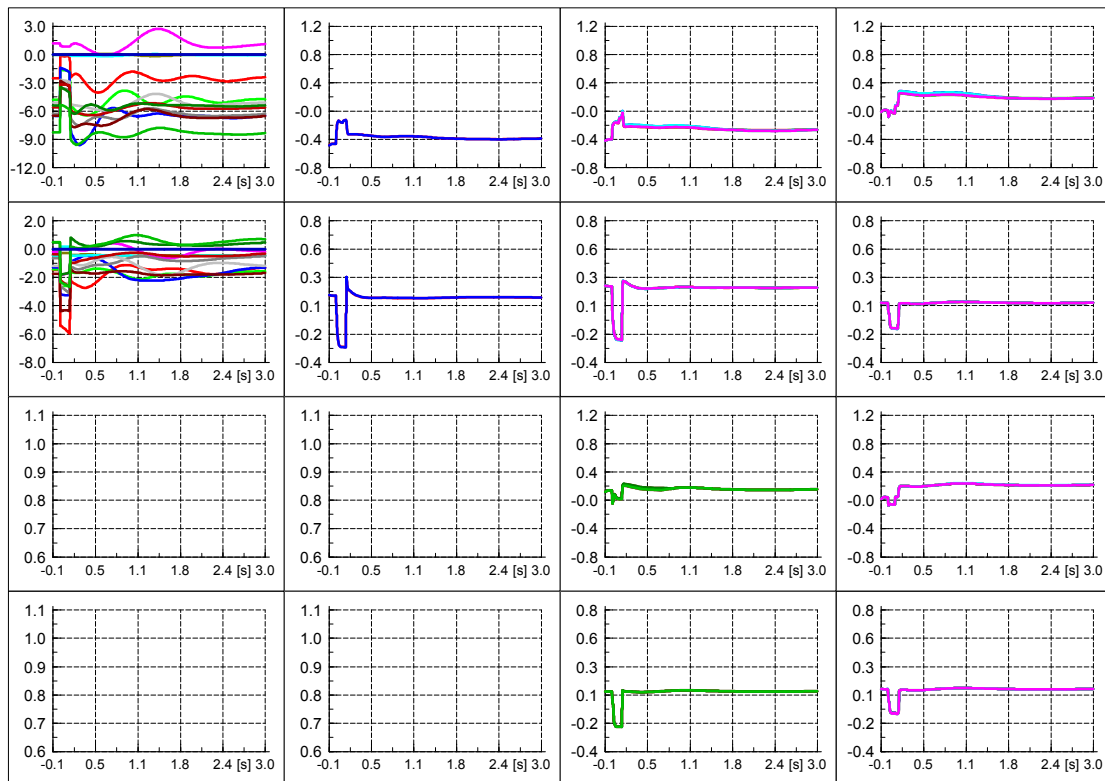


SRPF aRCI with delayed APR (3 s period)

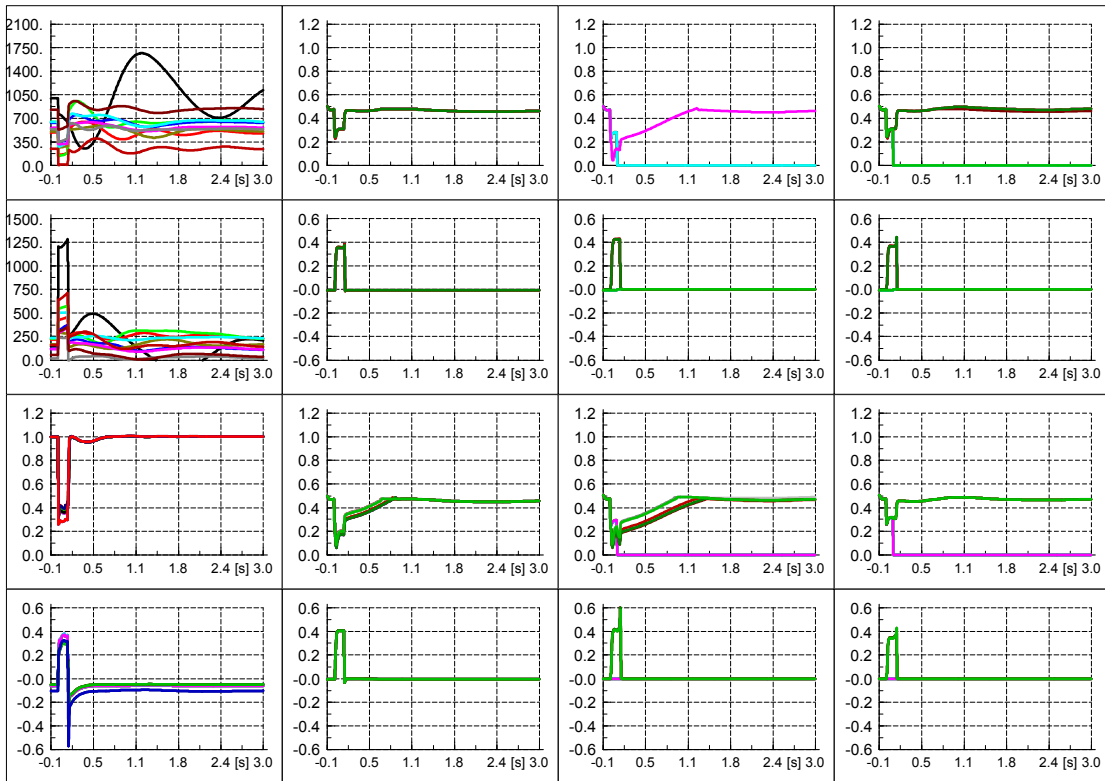
- Voltages



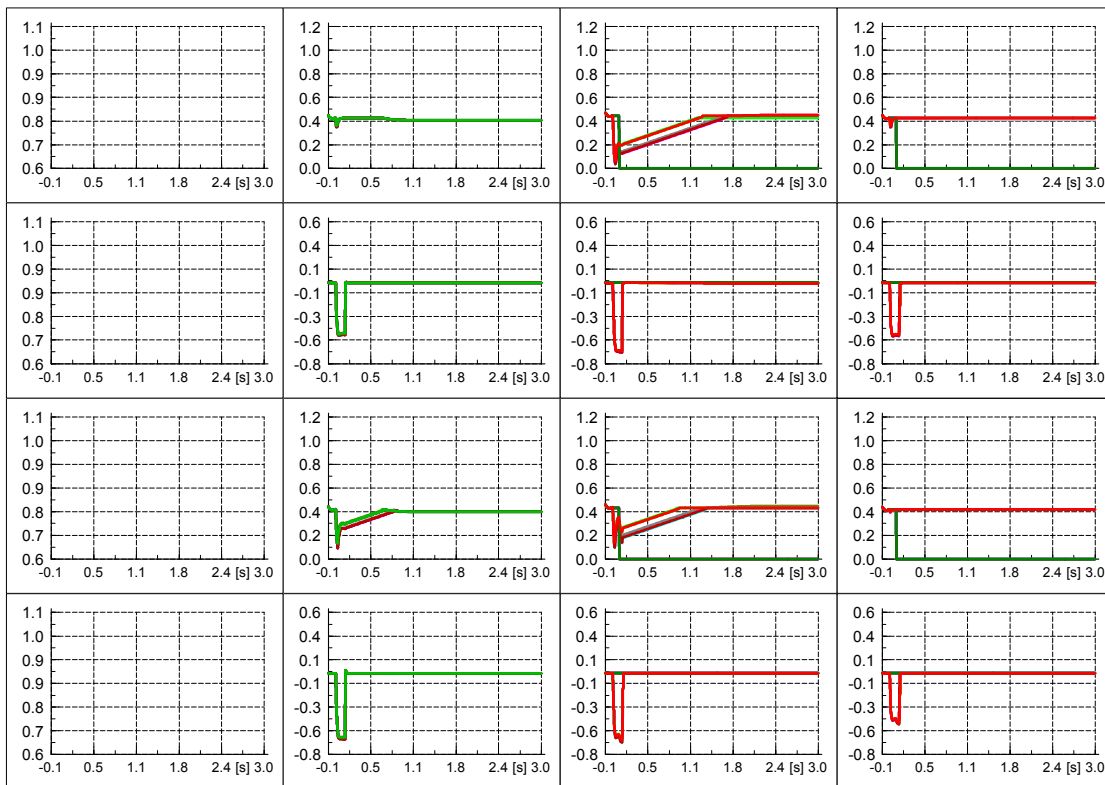
- Power exchange over the transformers



- Power production of DG and SG

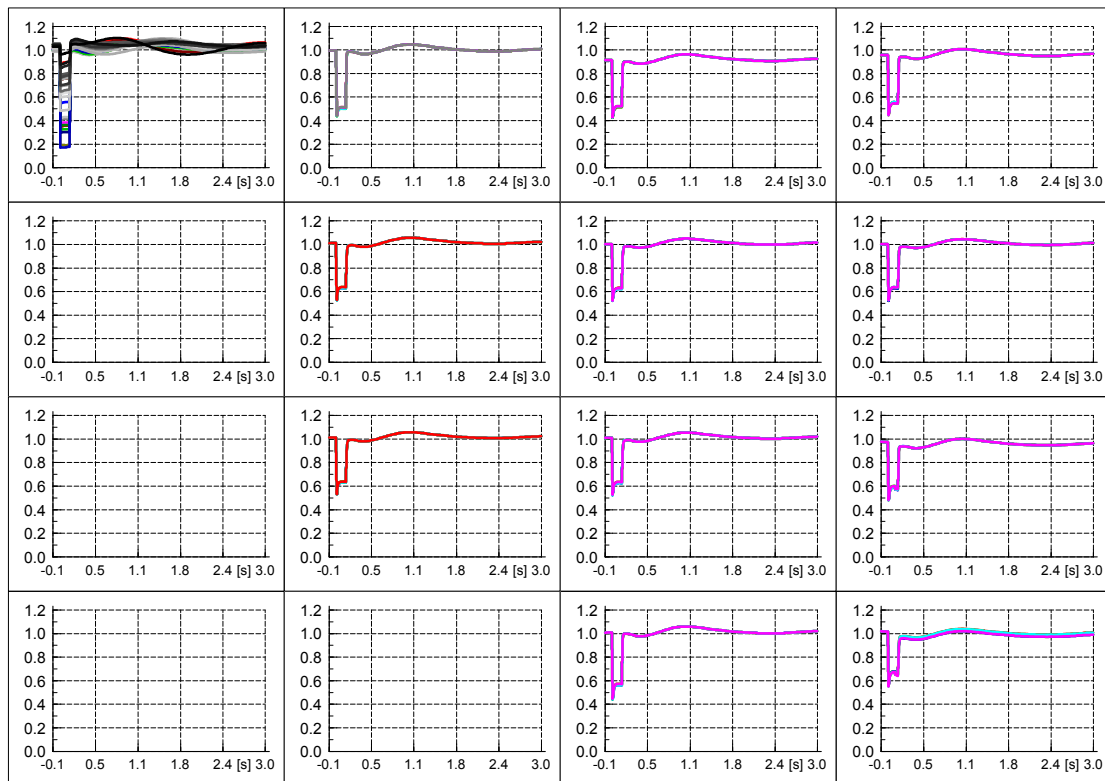


- Direct and quadrature axis currents of PV systems

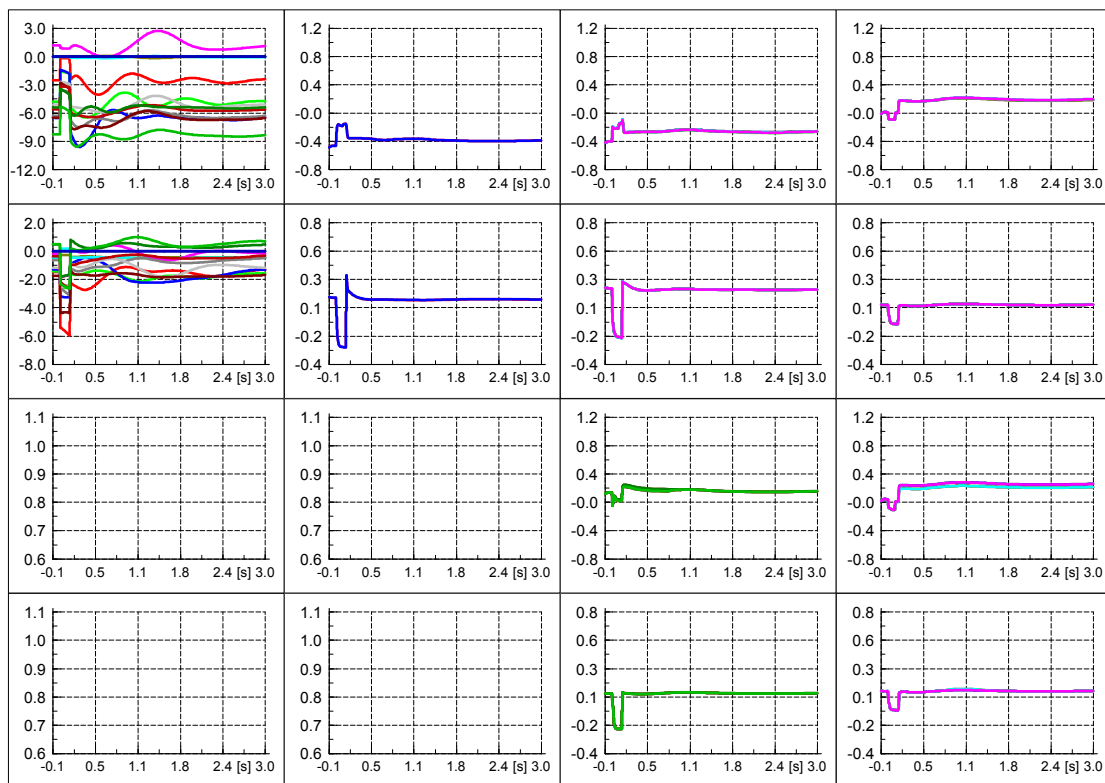


SRPF aRACI with delayed APR (3 s period)

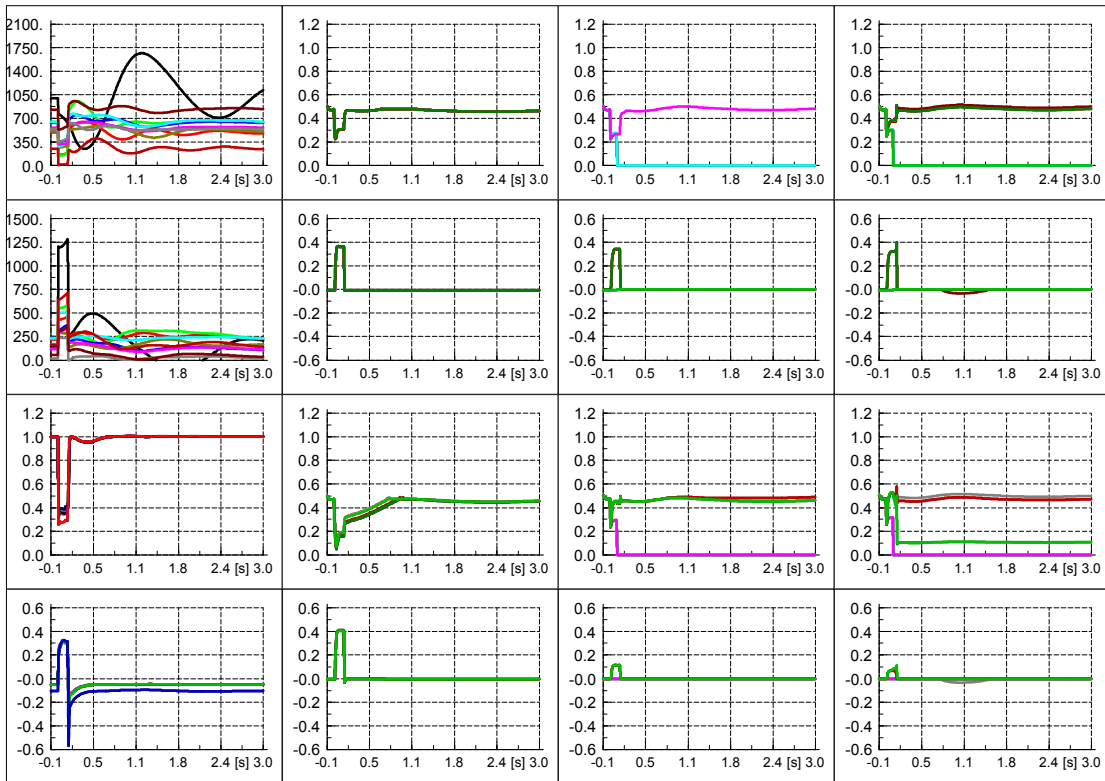
- Voltages



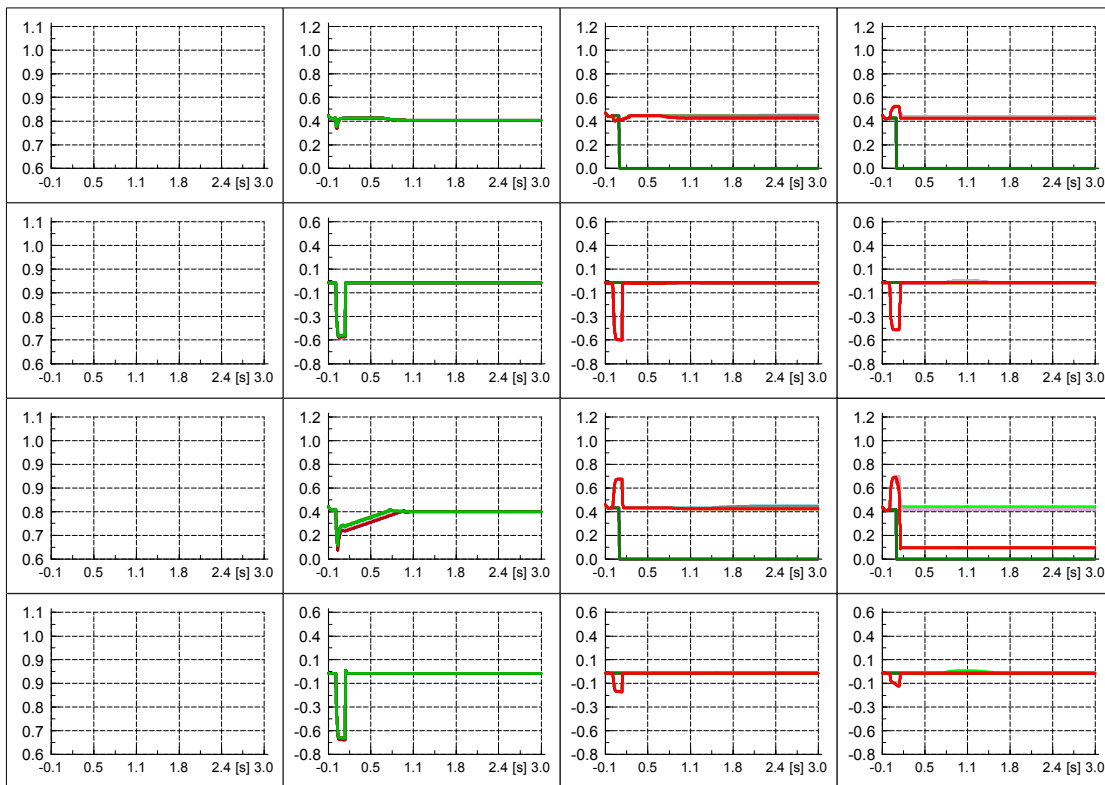
- Power exchange over the transformers



- Power production of DG and SG

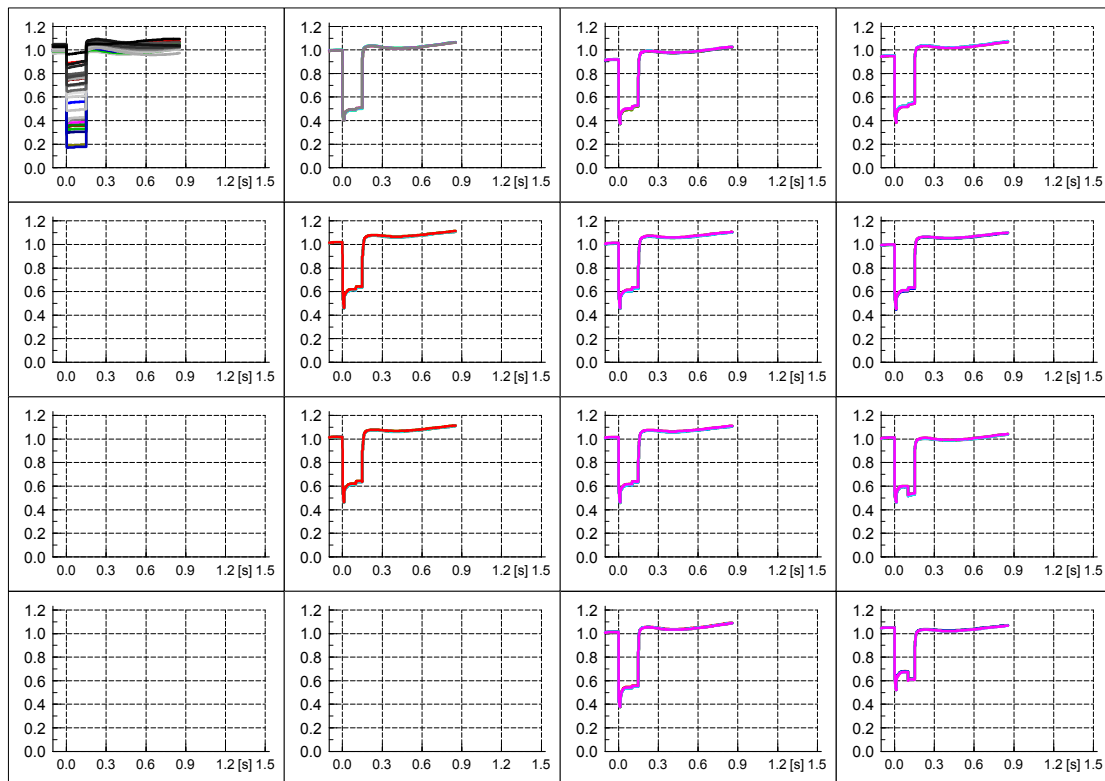


- Direct and quadrature axis currents of PV systems

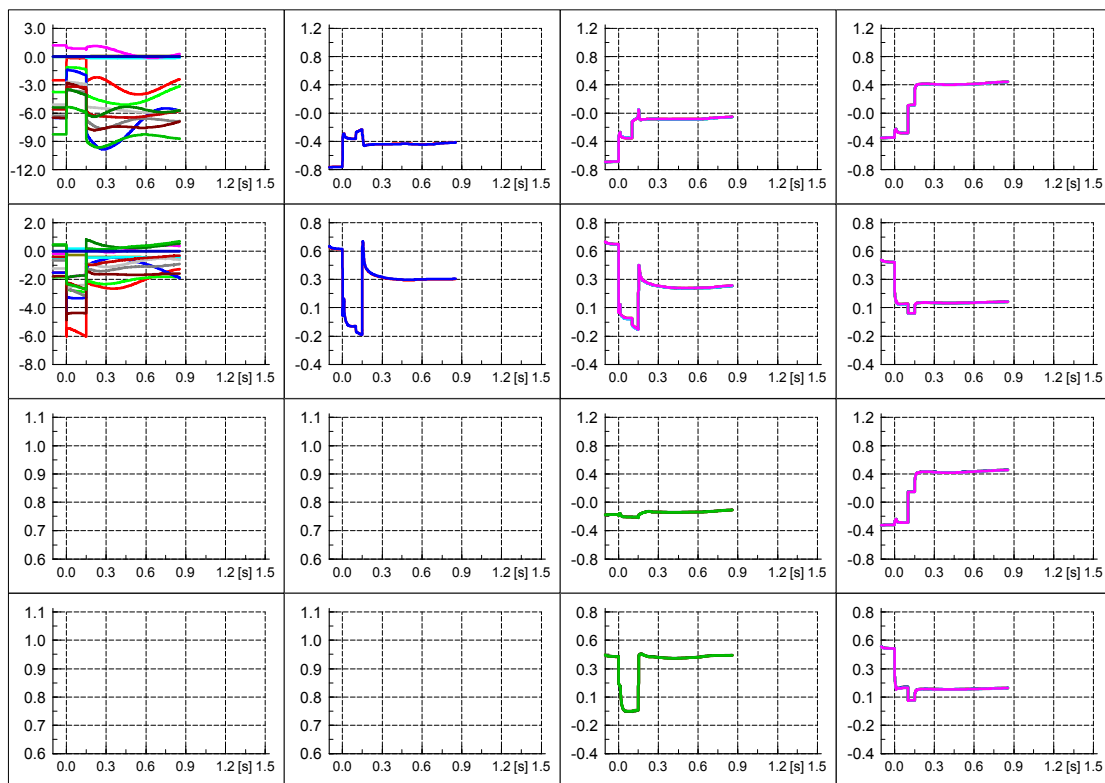


fRPF No-LVRT (no convergence after 0.9 s)

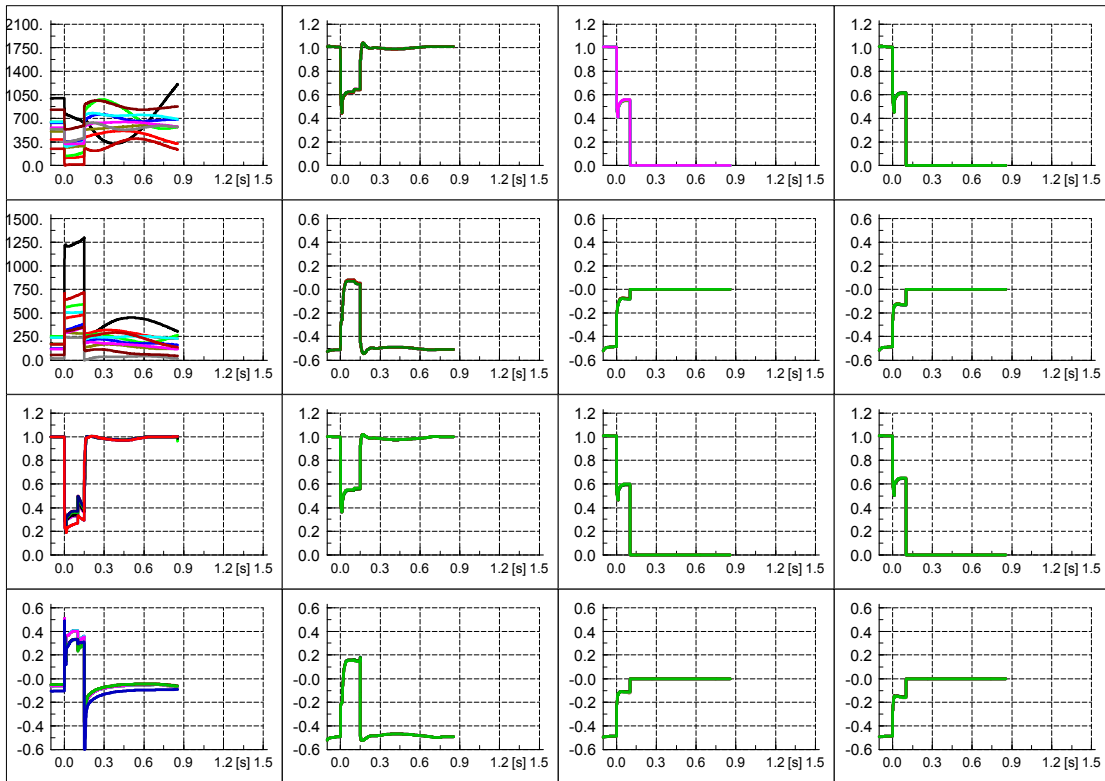
- Voltages



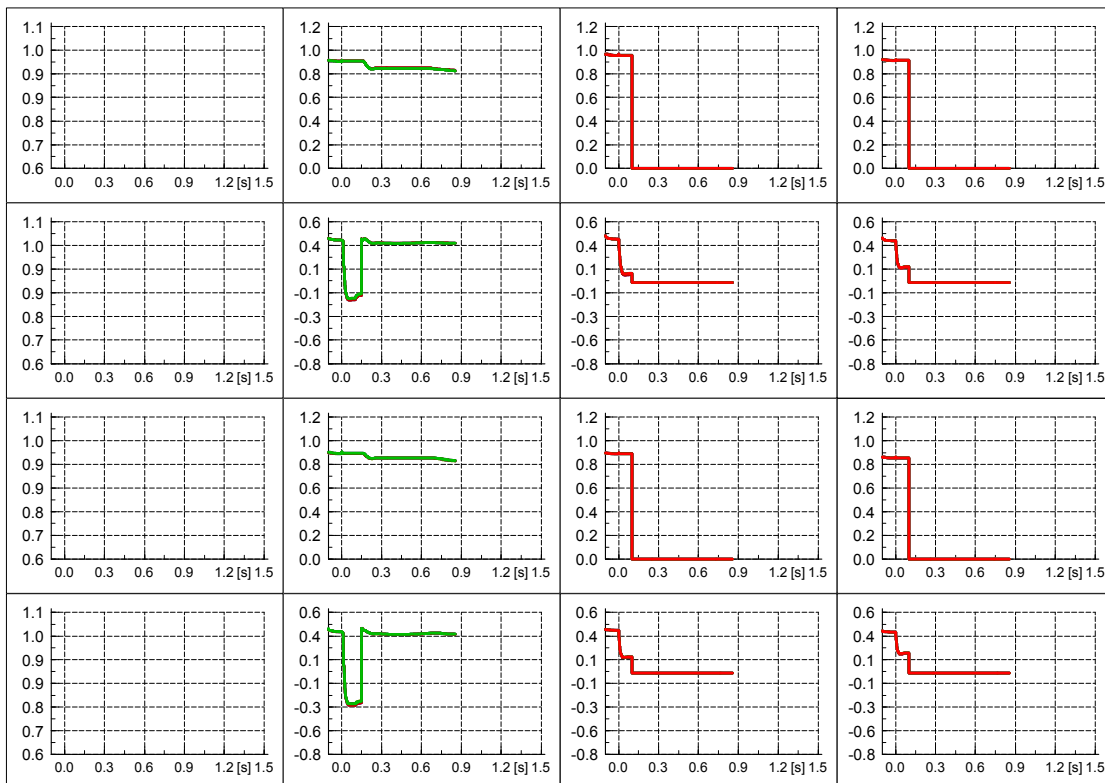
- Power exchange over the transformers



- Power production of DG and SG

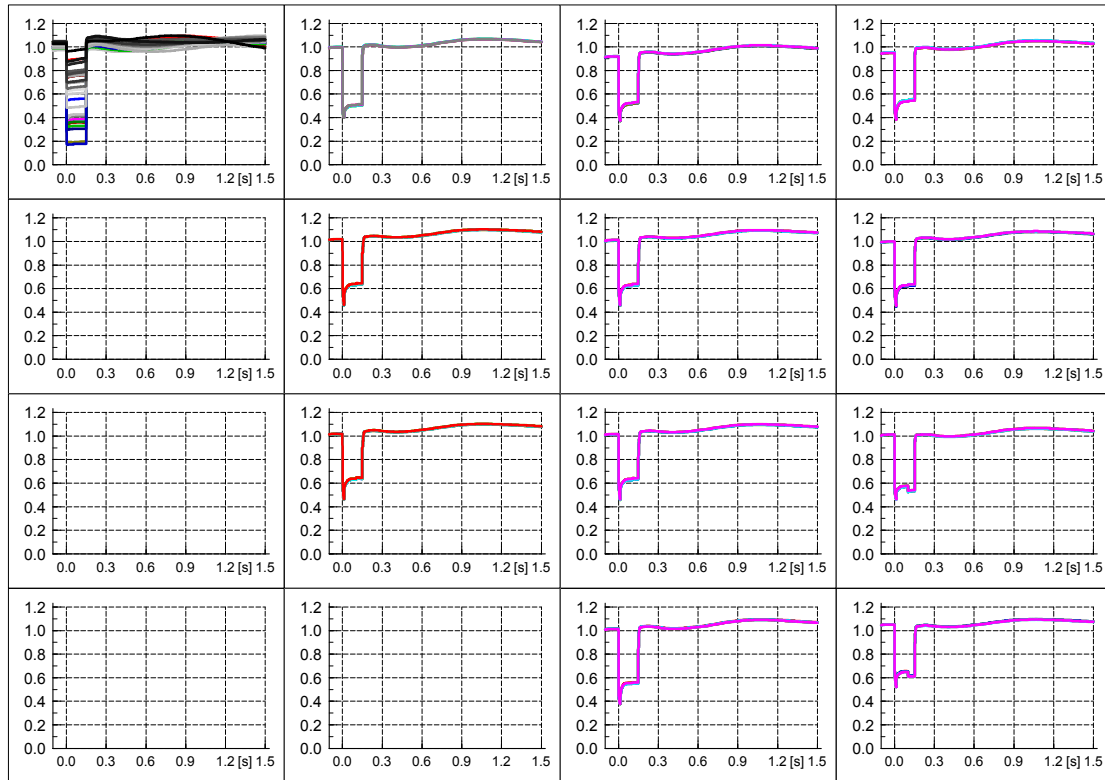


- Direct and quadrature axis currents of PV systems

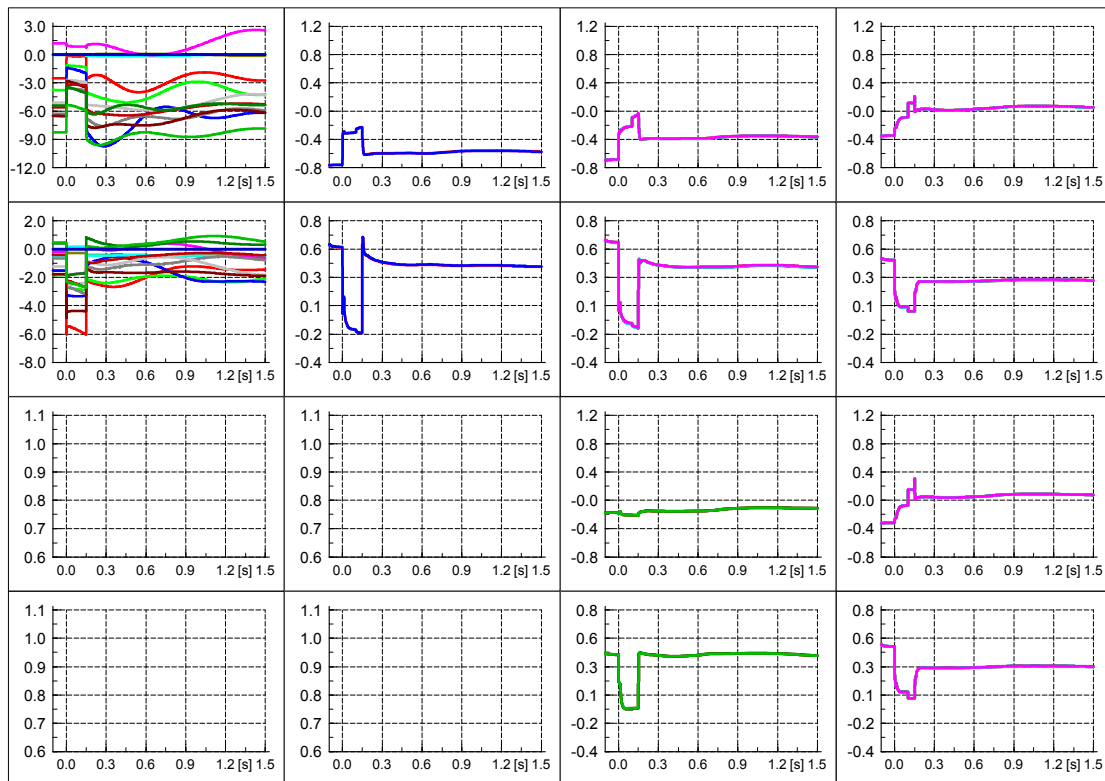


fRPF ZPM

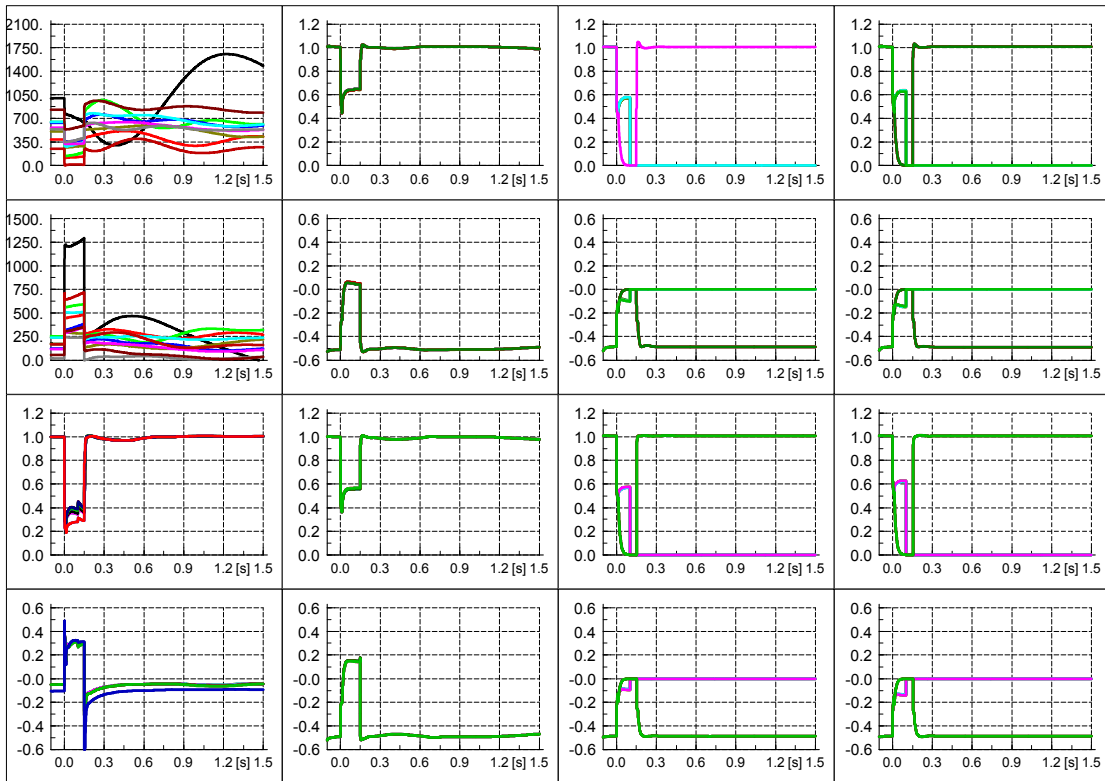
- Voltages



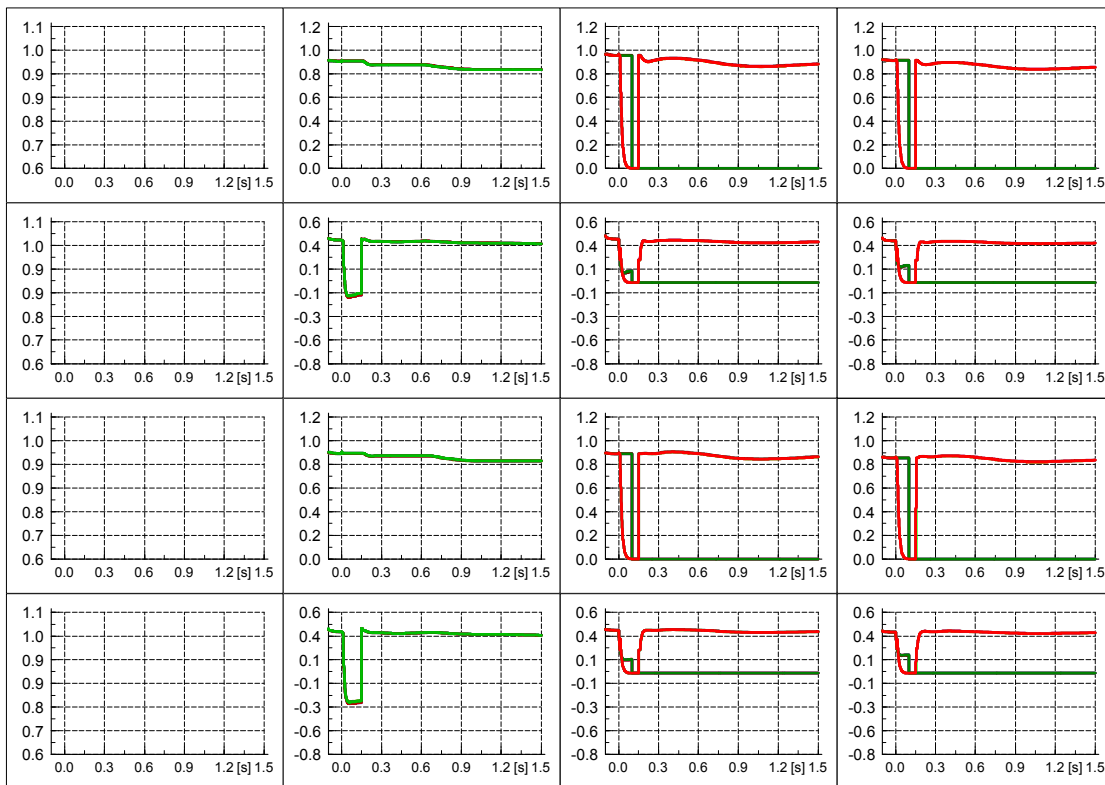
- Power exchange over the transformers



- Power production of DG and SG

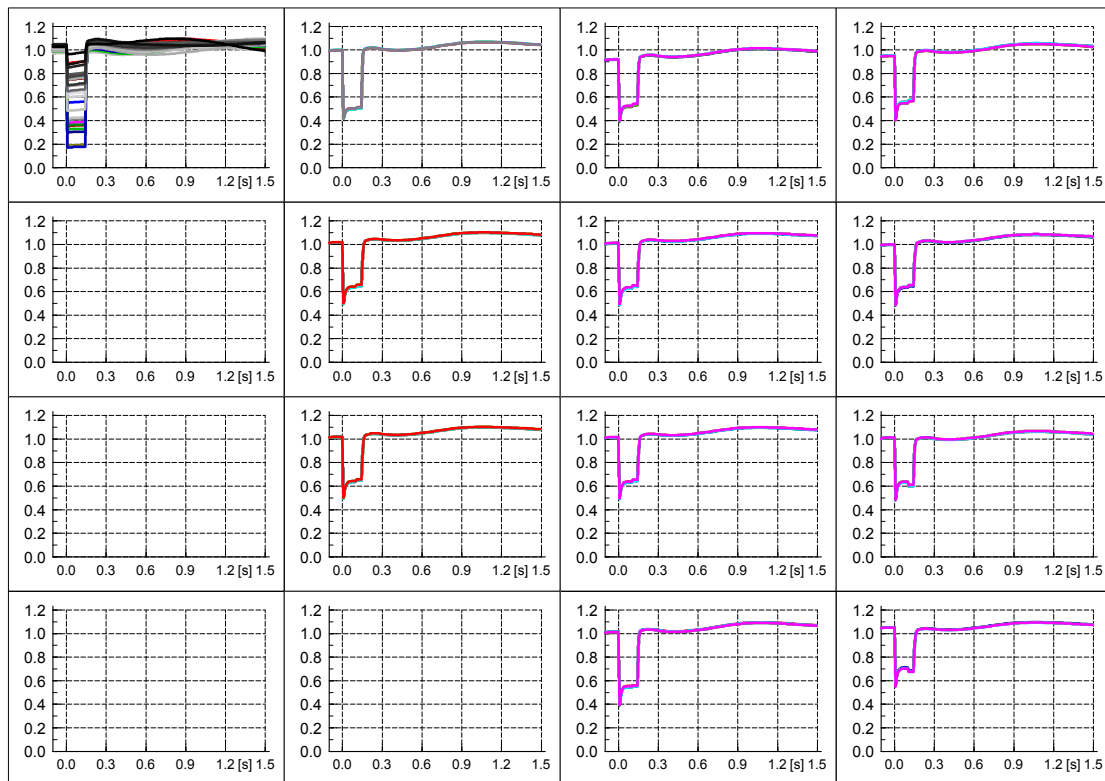


- Direct and quadrature axis currents of PV systems

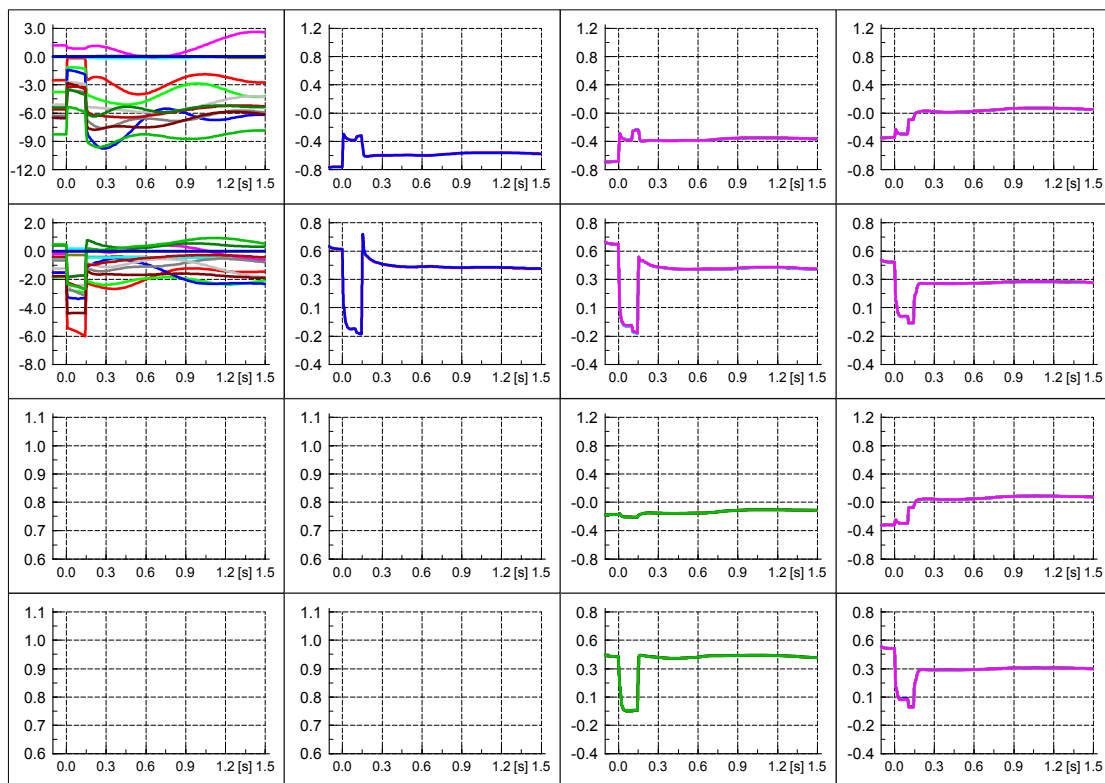


fRPF aRCI

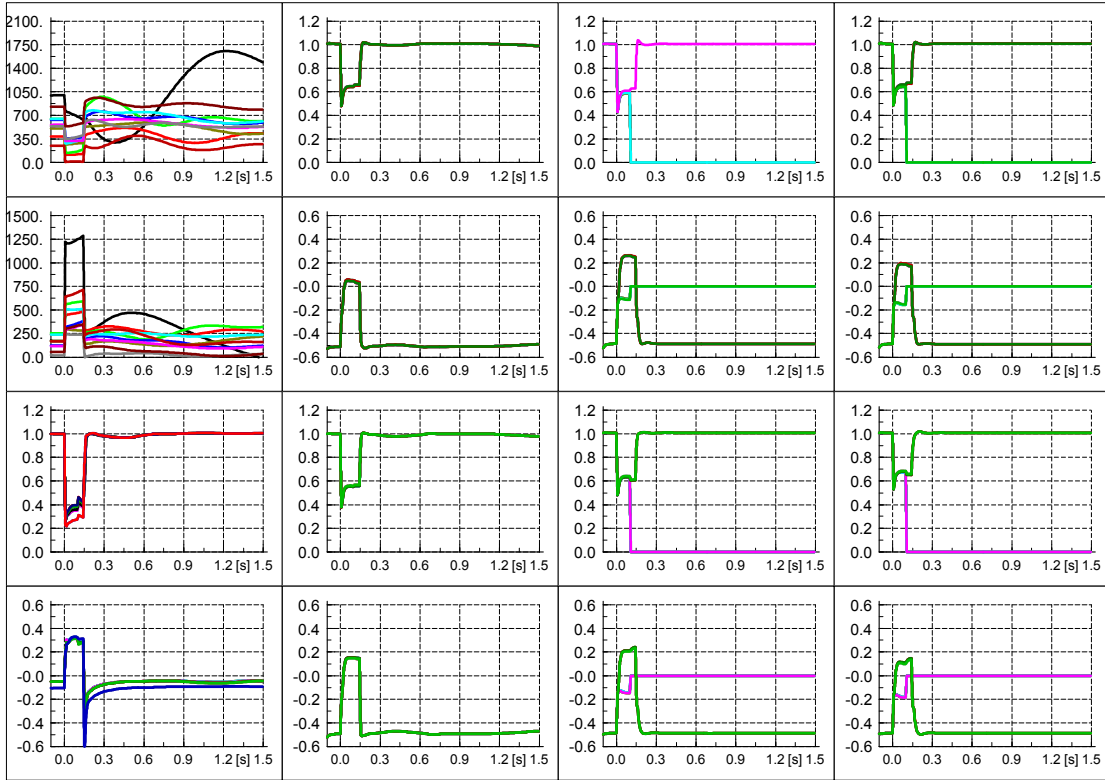
- Voltages



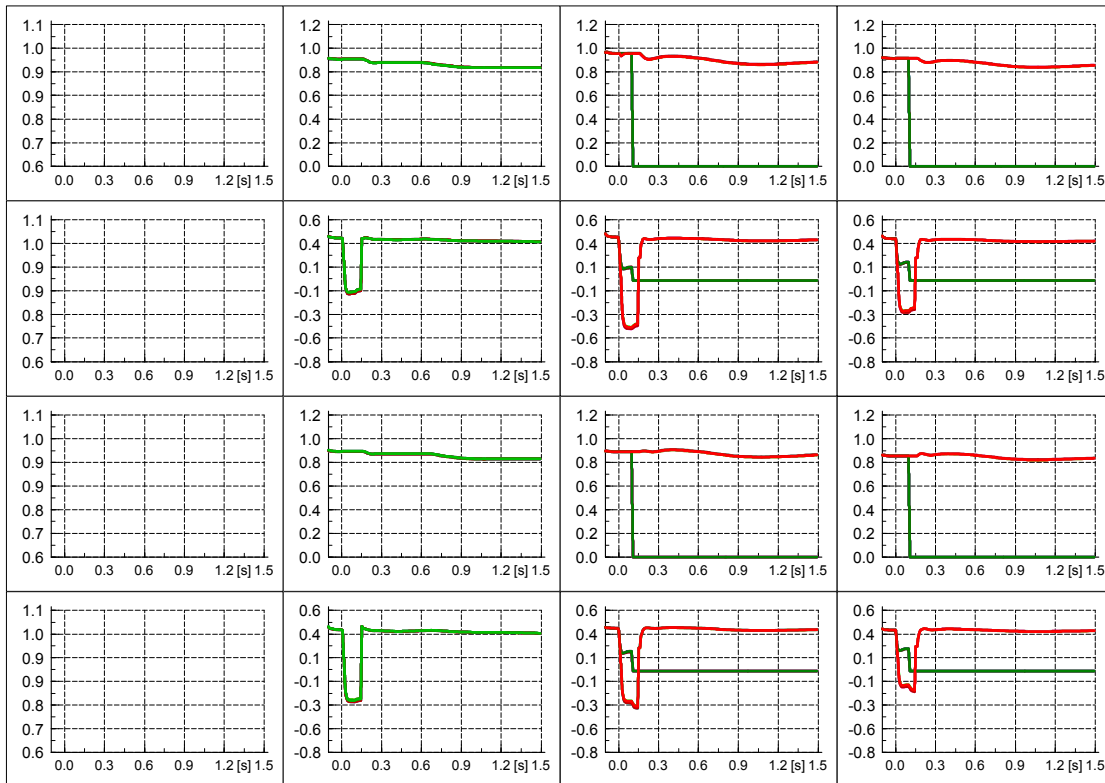
- Power exchange over the transformers



- Power production of DG and SG

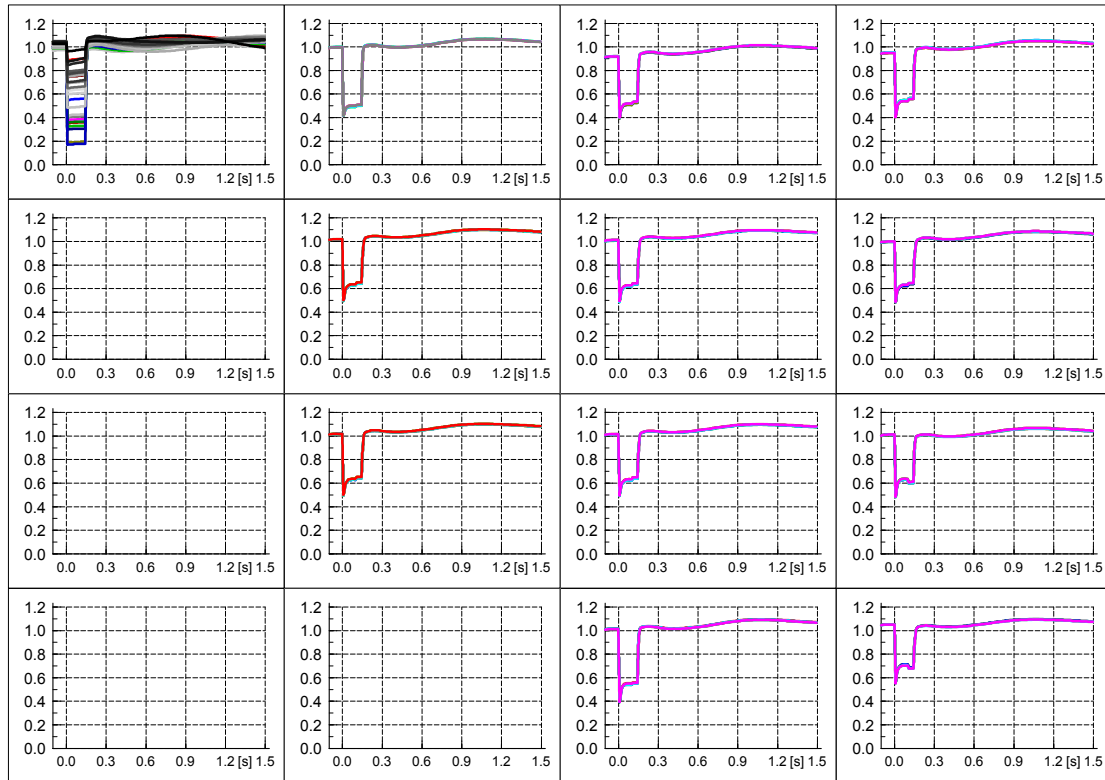


- Direct and quadrature axis currents of PV systems

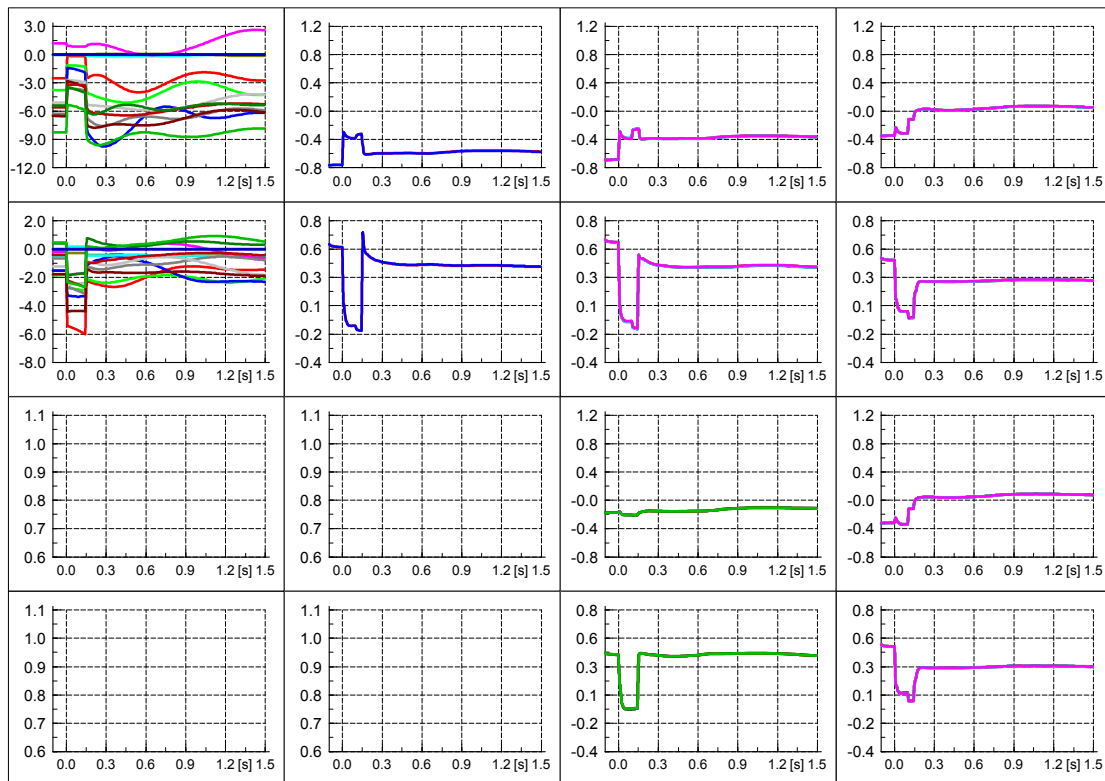


fRPF aRACI

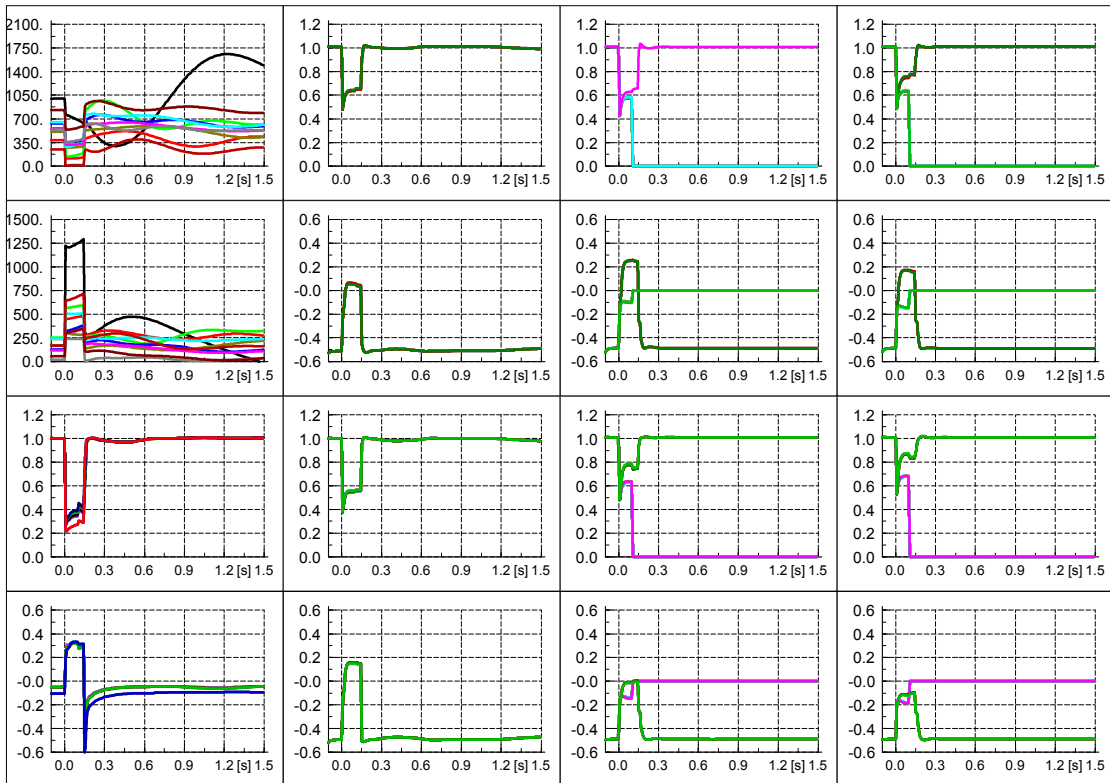
- Voltages



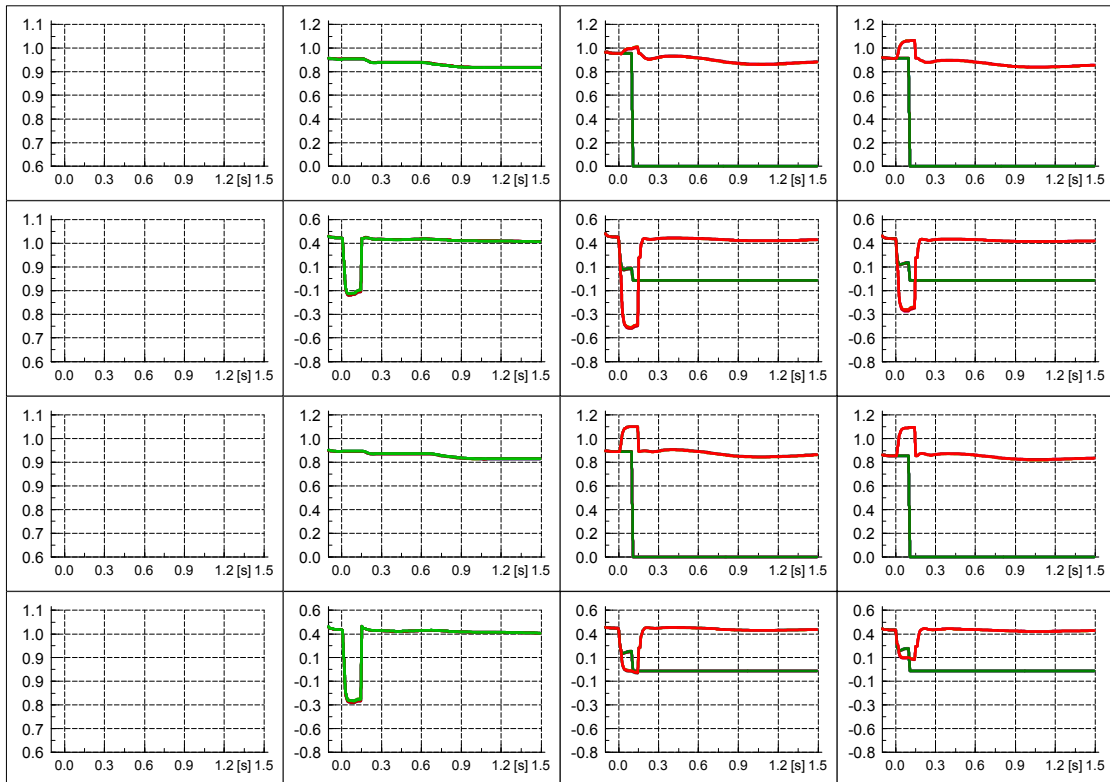
- Power exchange over the transformers



- Power production of DG and SG

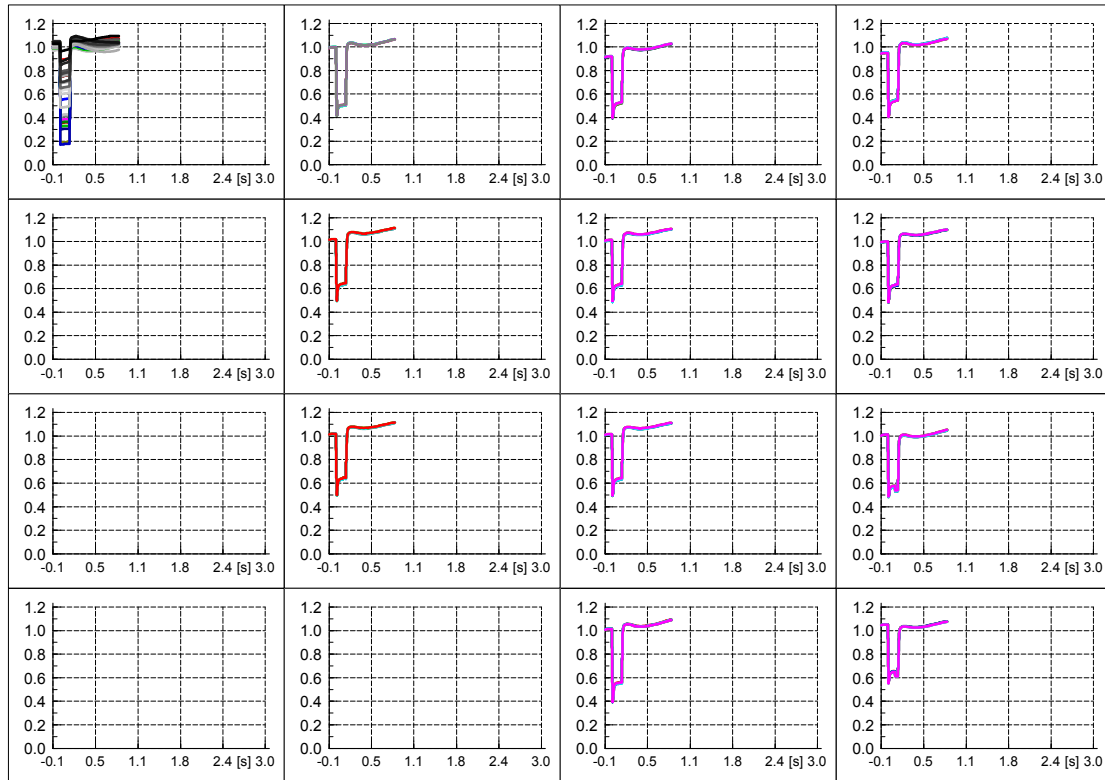


- Direct and quadrature axis currents of PV systems

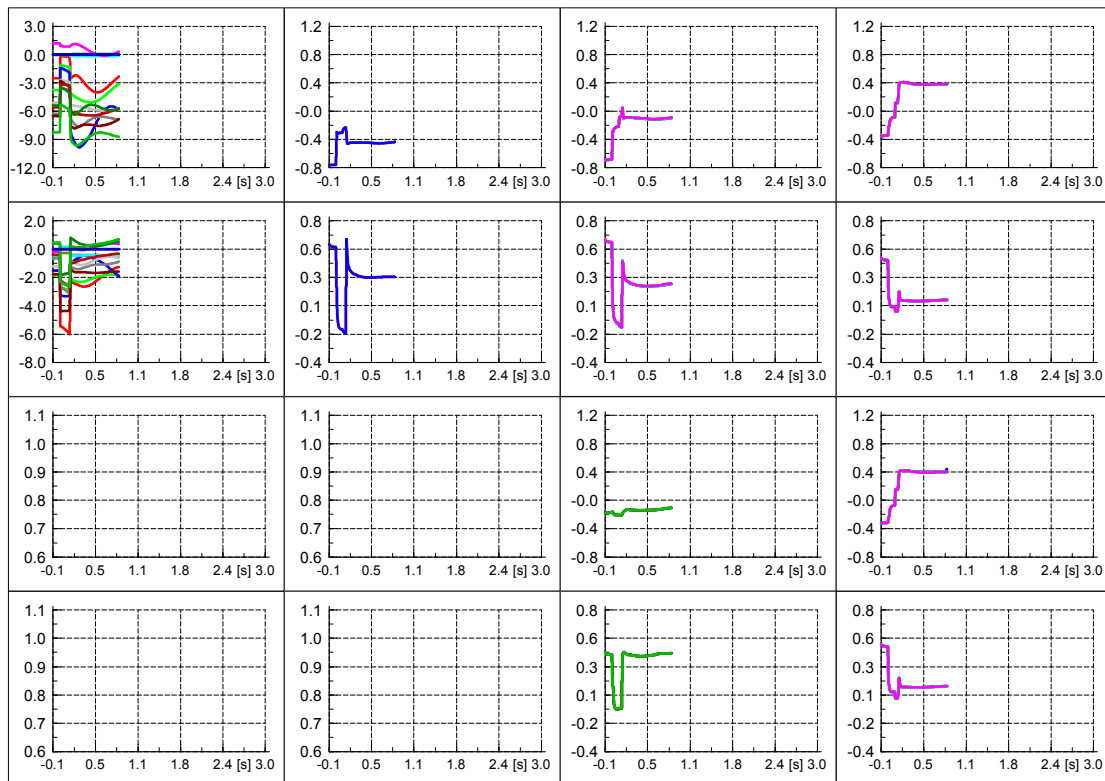


frPF ZPM with delayed APR (3 s period, no convergence after 0.9 s)

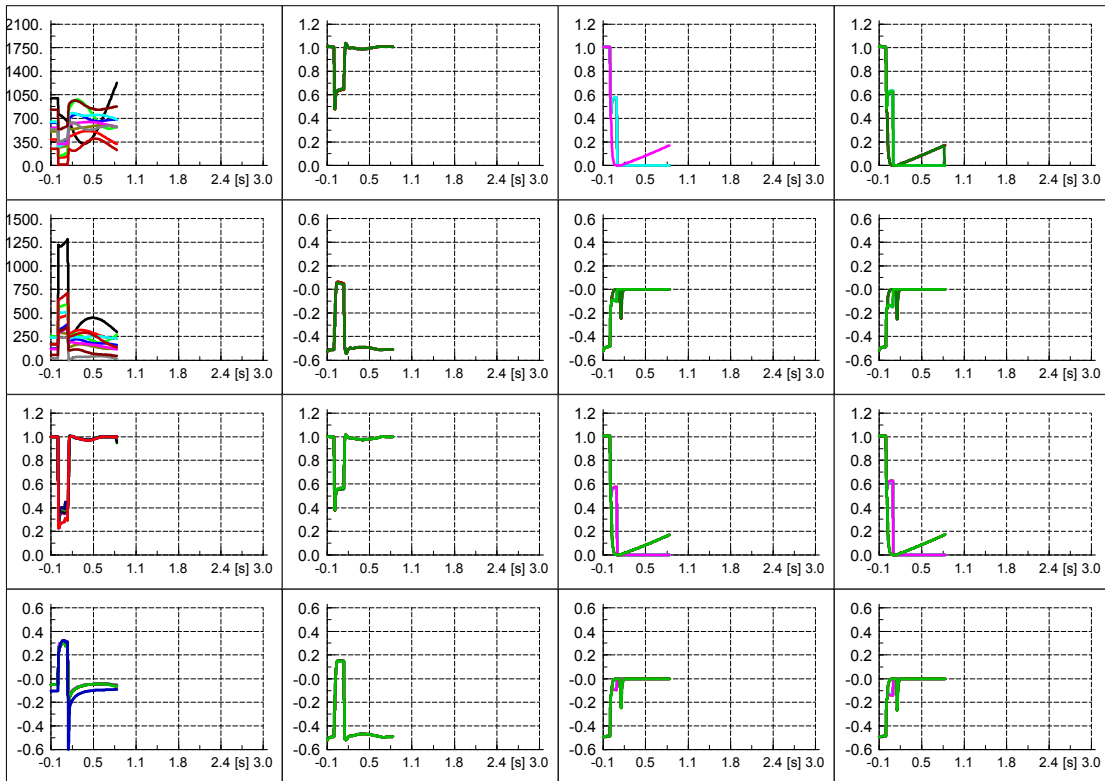
- Voltages



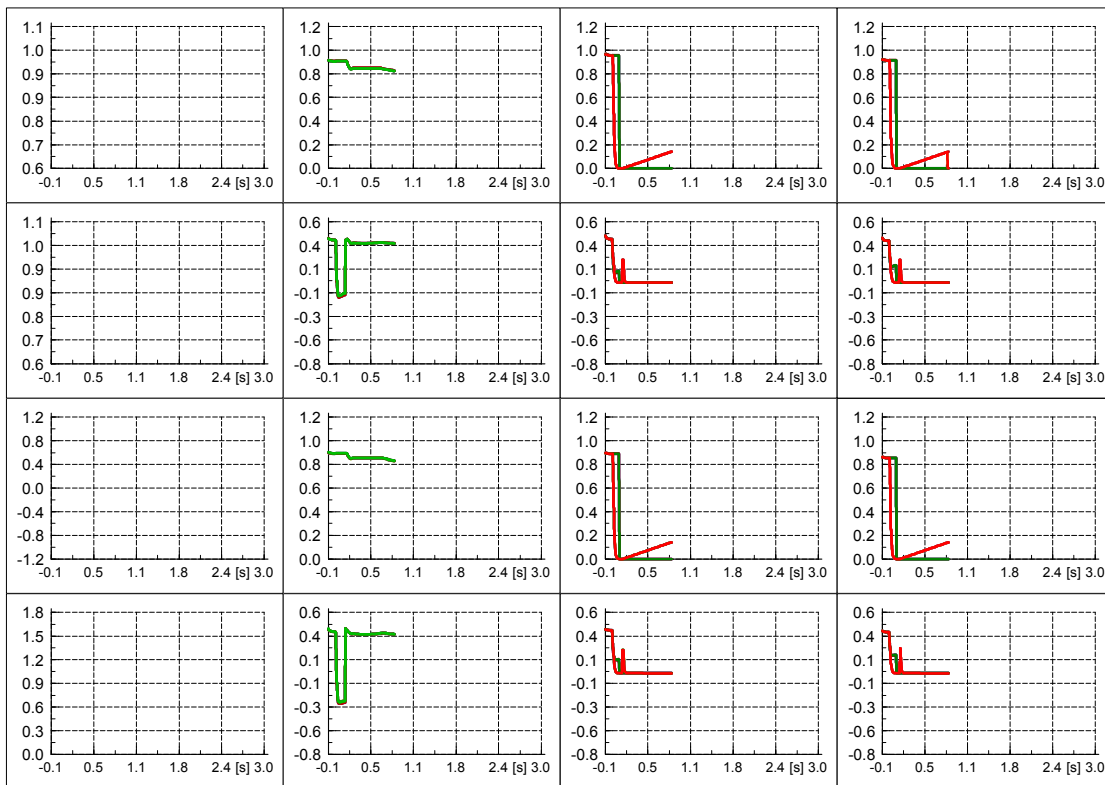
- Power exchange over the transformers



- Power production of DG and SG

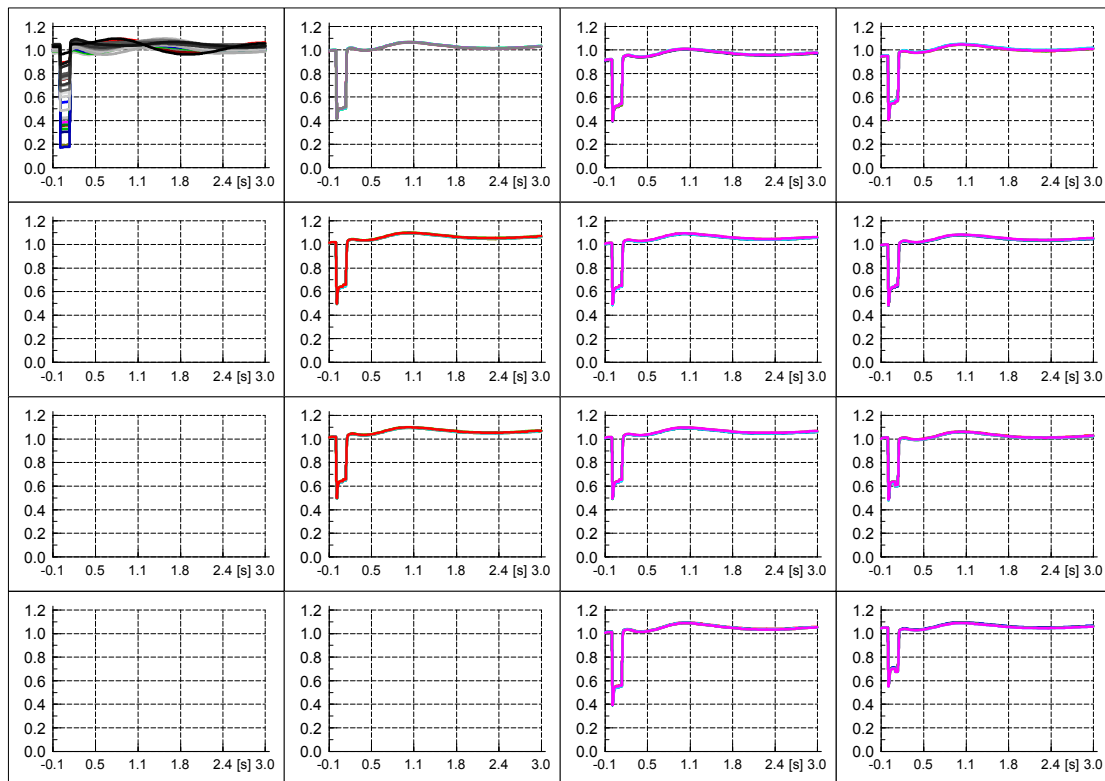


- Direct and quadrature axis currents of PV systems

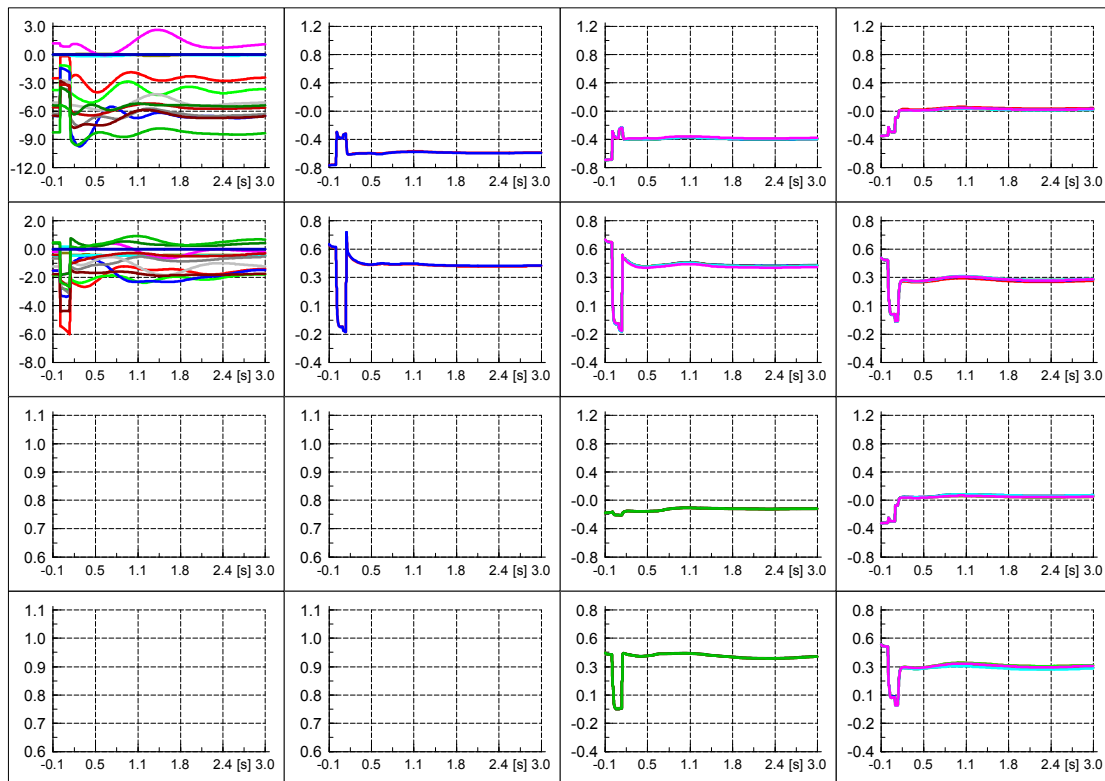


fRPF aRCI with delayed APR (3 s period)

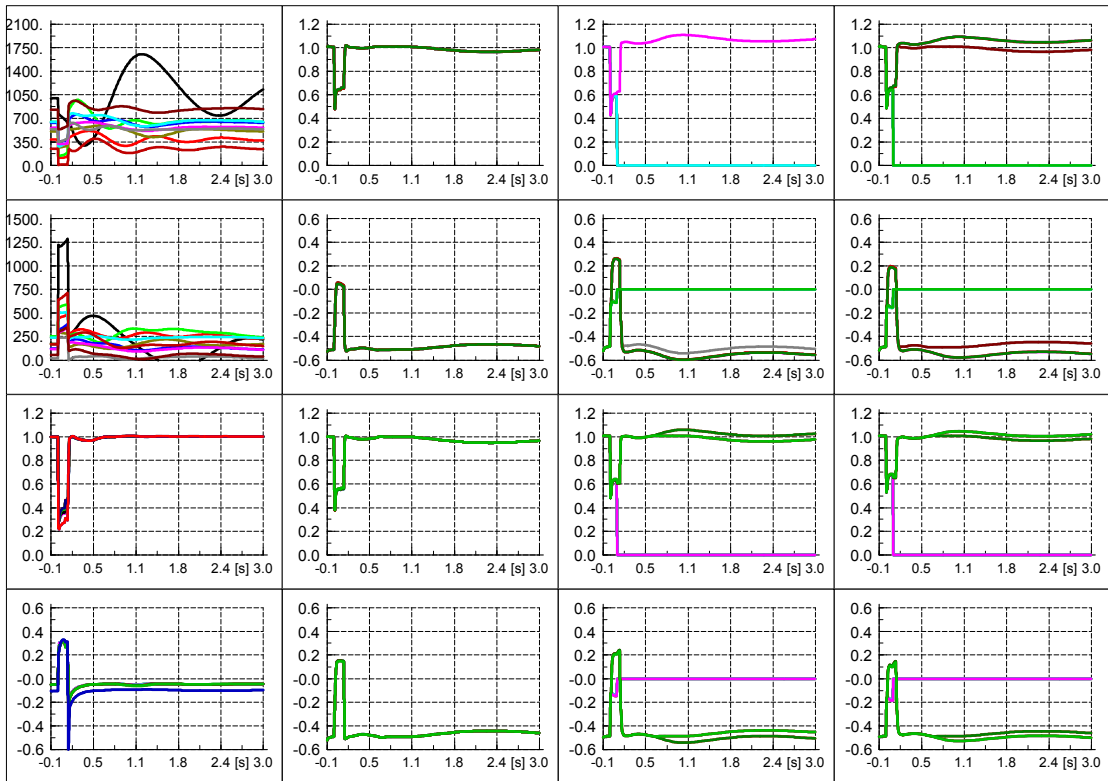
- Voltages



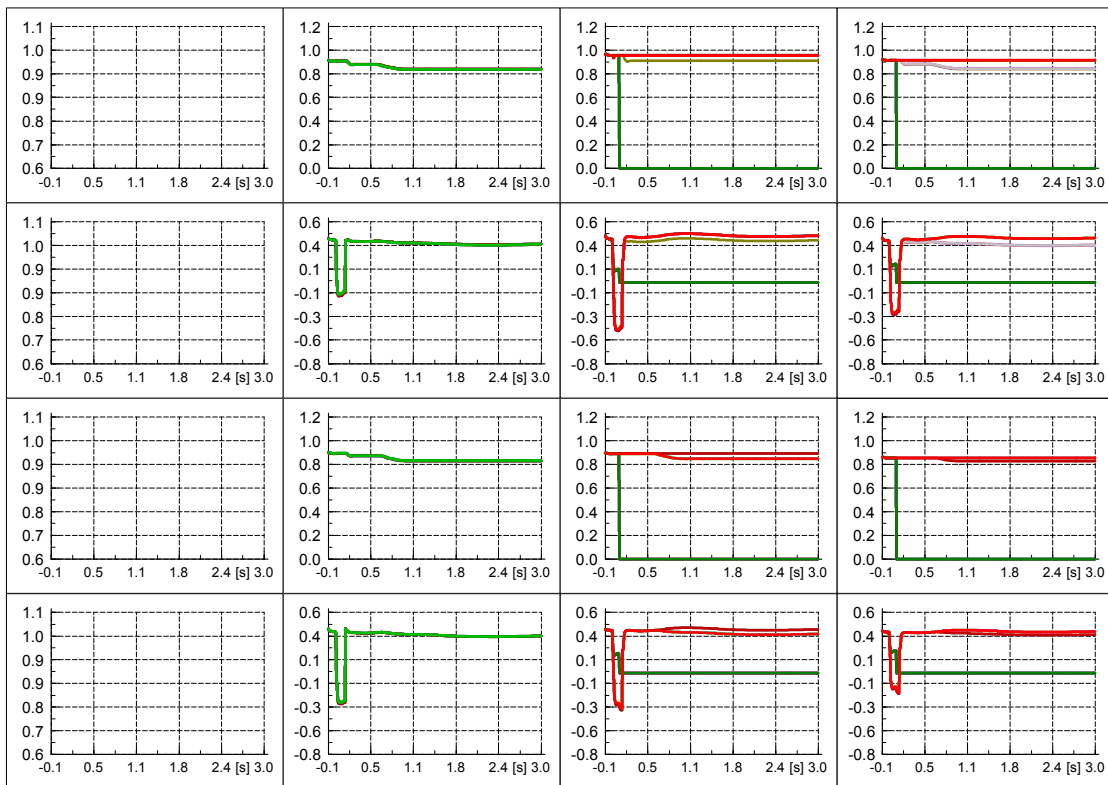
- Power exchange over the transformers



- Power production of DG and SG

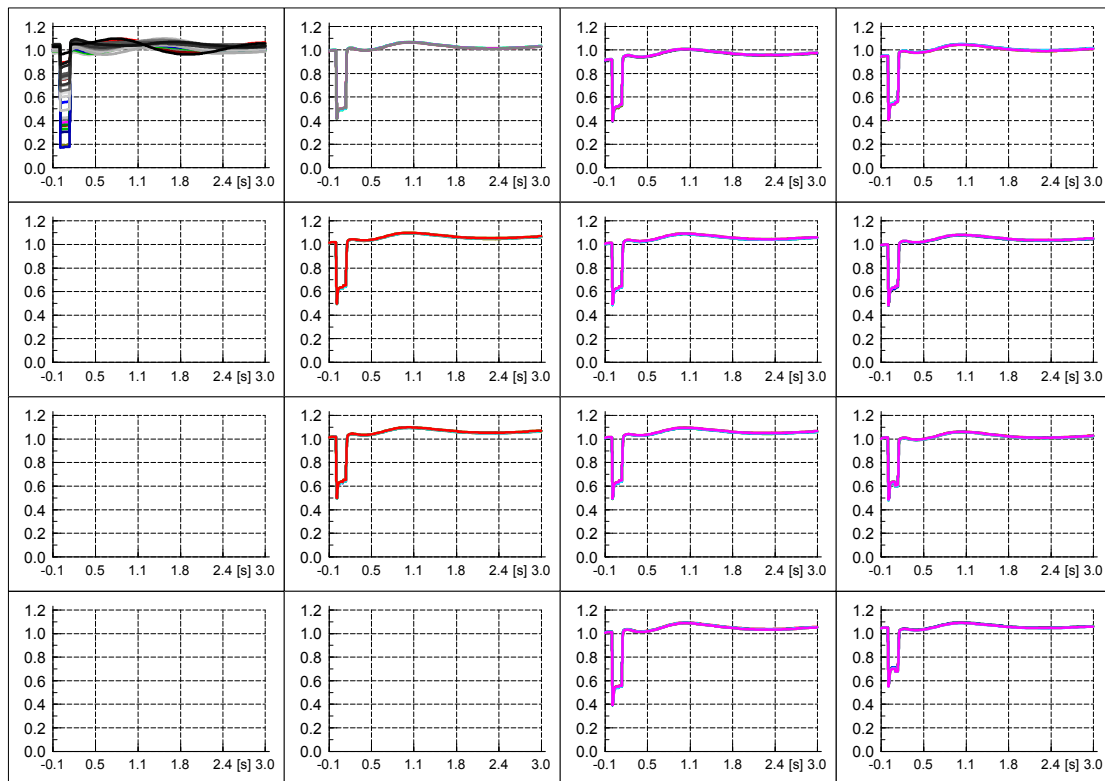


- Direct and quadrature axis currents of PV systems

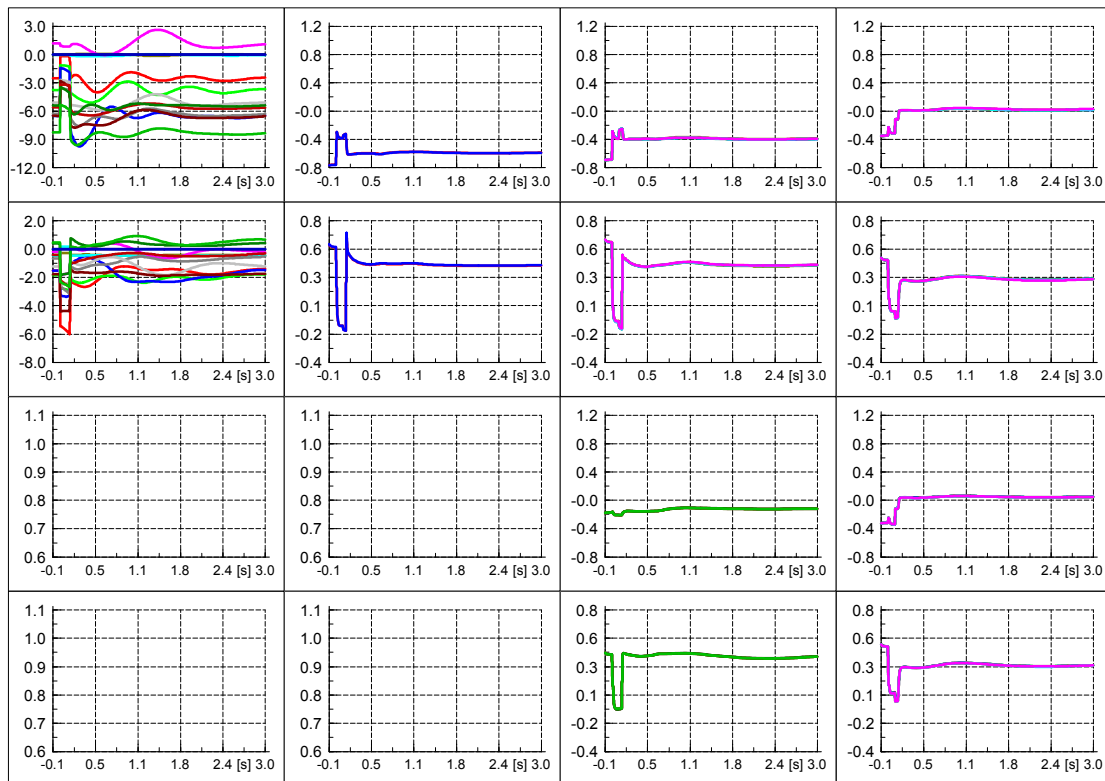


frPF aRACI with delayed APR (3 s period)

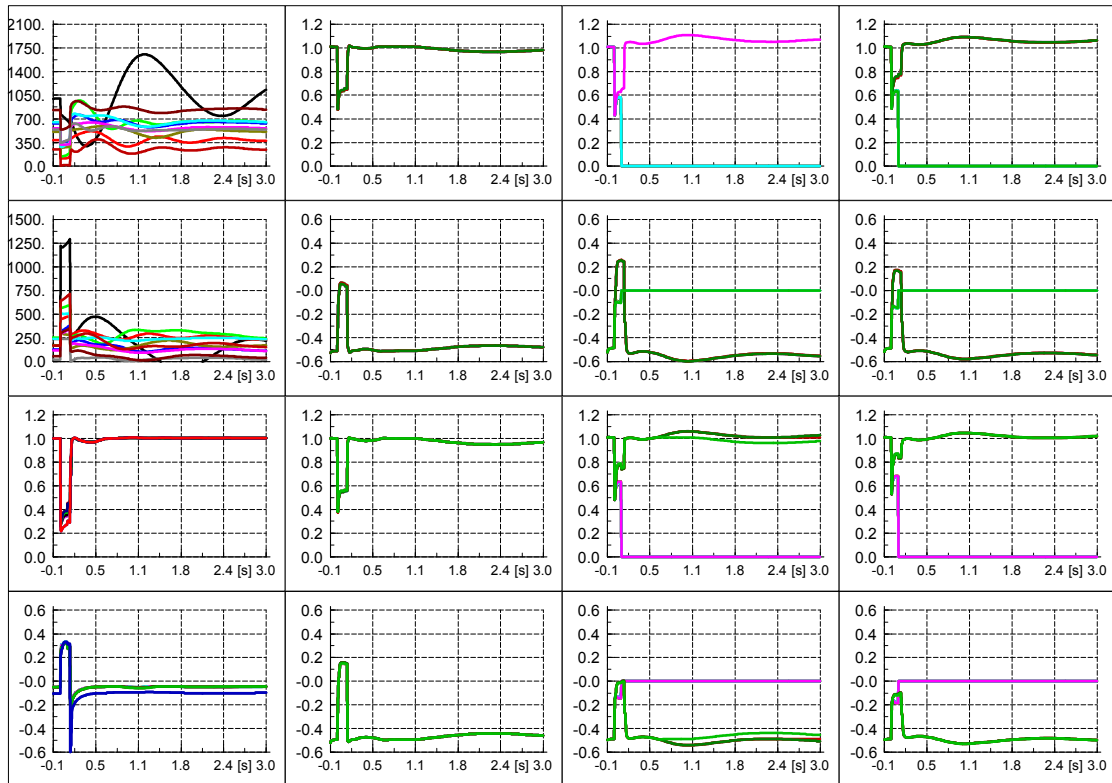
- Voltages



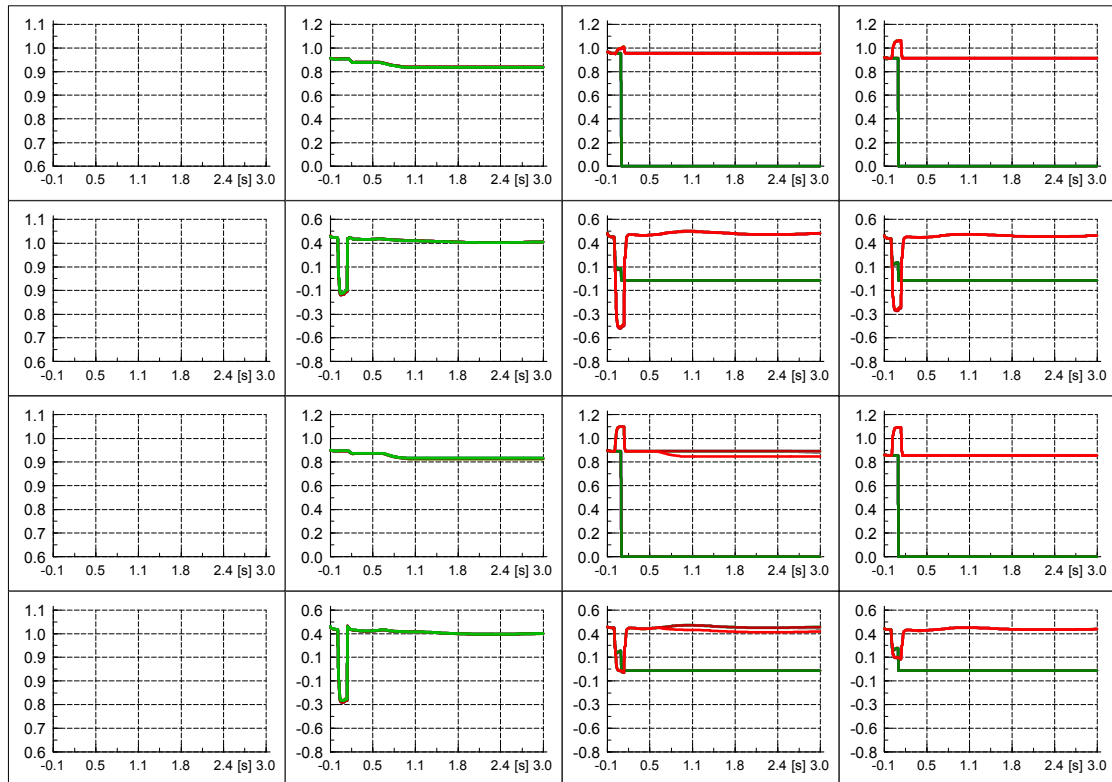
- Power exchange over the transformers



- Power production of DG and SG



- Direct and quadrature axis currents of PV systems



Appendix G PowerFactory Lessons Learned

Scaling the PV Template

- Through DSL Parameters to create templates of different rating
 1. Changes in Network Parameters
 - **PWM Converter**
 - Basic Data/ Rated Power
Multiply the 0.0112 of the 10 kW by the times of scaling
 - Load Flow/ Reactive Power set point
Use the reactive power capability limit (negative) with a capability limit of 0.4324107 p.u.
 - Load Flow/ Reactive Power set point
Use the desired value
 - **Current source**
 - Nominal Current
Divide active power set point by the product of the dc voltage with the maximum module current and the number of parallel modules.
 - **Upgrade lines and transformers accordingly inside the template**
 - **PQ measurement block inside Composite model**
 - Rating according to user
1 MVA for 10 kW and proportionally
 2. Changes in DSL parameters inside the DSL Models
 - **DSL PV module**
 - Scale number of parallel modules n_p to match $P_{PV,base}$
 - Base current $P_{PV,base}$

$$I_{PV,base} = I_{CS,base} = n_p \cdot I_{PV,panel}$$

with $P_{PV,base}$: Base current of PV system

$I_{CS,base}$: Base current of DC current source

$I_{PV,panel}$: Current of one PV panel (determined by other PV module parameters)

- Through parallel machines to upscale the instance of the template

1. Changes in Network Parameters

- **PWM Converter-Lines-Transformers**

- Parallel Machines/Parallel Lines/Parallel Transformers

All this elements inside the template take the multiplier in the corresponding field.

- **Current source-Capacitor**

- Nominal Current/Capacitance

Multiply by the number of parallel machines.

- **PQ measurement block inside Composite model**

- Rating according to user

Multiply the rating by number of parallel machines.

Data management

- It is highly recommended to use a consistent naming convention for all relevant elements right from the beginning of the project setup.
- The following naming convention seems to be ideal:

#eHV-node_#HV-node_#MV-node_#LV-node_#Type_#DATE/#MODE_#COUNT
where

- #eHV-node_#HV-node_#MV-node_#LV-node_ indicates to which node in which (distribution) system the element is connected to (non-applicable voltage levels will be replaced by two underscores (instead of 2-digit number)); this is of special importance if all voltage levels are modelled; example eHV-08_HV-02_MV-01_LV-R01_TERM_01 means
 - LV terminal 01 of
 - LV network connected to MV terminal 01 of
 - MV network connected to HV terminal 02 of
 - HV network connected to eHV terminal 08 of
 - the transmission system
- For edge elements both connection points are included in the name. Example with a MV line: eHV-08_HV-02_MV-01-02_LINE
 - This means the line is connected between MV nodes 01 and 02
- Since transformers connect two different voltage levels, they have the connection points including voltage level in their name, example: eHV-08_HV-02_MV-02_T01-LV-01_T01_TRF
 - This means the transformer is connected between the (first) Terminal at node 02 in the MV system and the (first) Terminal at node 01 in the corresponding LV system
- #Type = PVPPM / WPPM (WPPM_DFIG / WPPM_FC) / SGCHP / SGCONV / STATLD (static load) / DYNLD (dynamic load) / LINE / TERM / SWITCH / TRF
- #DATE = OLD / NEW / specific-year (if desired)
- #MODE = PF100 / PF095 / PFPOW / LVRT / aRCI (for old generators, this indicates their settings (PF100/095/POW gives the power factor settings – constant or based on the active power)
- #COUNT = 2-digit number for duplicates

Steady state Short-circuit calculations

- Short-circuit duration (break time) seems not to make any difference in results.
- S/C calculation fails to provide SHC impedances (X, R, Z) at FCWTG terminals.
- S/C calculation results into higher Sk'' values at all terminals if FCWTG is put out of operation.
- Complete method
 - superpositions the pre-fault values but is not a standardised method.
 - Does not calculate i_k
- Network impedance angle is called phiz

Particularities of Static generator (ElmGenstat)

- The sign convention for P and Q of a static generator is unintuitive.
- VDE-AR-N 4105 uses the passive (consumer oriented) sign convention ($P < 0$ for generation) as follows:

Effect	Sign of Q ($P < 0$)	Sign of Iq ($I_d < 0$)	Operation	Reactive power exchange with grid
Voltage decreases	$Q > 0$ (pos.)	$I_q < 0$ (neg.)	Under-excited	Inductive
Voltage increase	$Q < 0$ (neg.)	$I_q > 0$ (pos.)	Over-excited	capacitive

Table G.1: Passive sign convention

- ElmGenstat uses the active (generator oriented) sign convention ($P > 0$ for generation) as follows:

Effect	Sign of Q ($P > 0$)	Sign of Iq ($I_d > 0$)	Operation	Reactive power exchange with grid
Voltage decreases	$Q < 0$ (neg.)	$I_q > 0$ (pos.)	./.	capacitive
Voltage increase	$Q > 0$ (pos.)	$I_q < 0$ (neg.)	./.	Inductive

Table G.2: Active sign convention

Substation particularities

- The substation has a second voltage setting next to the one on the basic data tab. The additional voltage setting is named 'Nominal Voltage' (U_{nom}) and can be found by right-clicking the substation in the data manager (by going into the grid) and then 'Edit'. The nominal voltage can be changed by clicking the 'Set Nominal Voltage' button. N.B. If a transformer is connected to the substation this is the voltage that the transformer sees.

Project collaboration

- The following function can be used to copy all external references of a project into it. Please be aware that this functionality is still under test so there is a possibility of unexpected results. Therefore, remember to export the project first as a backup.
 1. Deactivate the project.
 2. Focus on the project by making sure it is selected in the left hand pane of the datamanager.
 3. press the input window icon on the data manager and type the following into the command line which appears: `_test/cpex` (from "copy external references")
 4. Run the command that appears. Note, that the underscore is important

You should find a reference folder is included in the project which contains all the external references and you should find that your project's objects link to the new folder.

Source: DIgSILENT Support answer on August 15, 2013

User friendliness

- Once an element window is open, you can select other elements of the same class and show their parameters in the previously opened windows.

Hotline Q&A

- What is the relevance of "Level" in DSL models?

The level of the model representation is only important when using or changing old models. For new created models the highest level should always be used. For macros, this option does not have any impact, because the level of the highest block is important, i.e. the controller definition. Then as summary the level is related with the version on which the model was created, then when the model is used in newer versions PF recognized and "create" the compatibility; the higher the level, the newer the version with which was created. Our recommendation in this regard is do not change the level setting of a model, more even if the model is taken from other version library or it was a model built by someone else.

- How to change the number of ticks (major/minor) in VisPlots?

There is no official way to change the step size of the axis of a plot. But there is a trick that may be helpful although its results will be applied to the complete virtual instrument panel and not only for one plot.

- First you have to create a new style by using the function Style -> create new style in the right mouse button menu.

- The new style could be found in the project folder Settings -> Styles.

- Right click in the plot and select style>>edit style. This will force PowerFactory to create the axis objects that you edit in the data manager in the next step.

- Find the style in the data manager: you should find a folder in the project: Settings -> Styles -> Your style -> VisPlot. The VisPlot folder includes the axis objects.

- If you display the flexible data of the axis by pressing the 'detail mode class select' icon and select axis objects, you should find a variable "Number of Main Ticks". This variable cannot be changed directly because it is greyed out.

- If you open the "Input Window" (icon in the data manager) you could enter the command "xAxis:mTicks=N" (where N is the number of major ticks required).

- Flag "a-stable" always applies on lower-level models inside?

The option A-stable algorithm enabled at advanced options page of Calculation of Initial Conditions menu applies for all models used.

- What does it mean in OPF (optimal power flow) When “the model is unbounded”? (How to find out what to debug?)

This message appears only in the DC OPF if the LP has no unique solution (i.e. infinite valid solutions) and the target function can have unconstrained high values.

This can be the case if you defined not enough limits.

Example: There are two generators, a cheap and an expensive. The OPF should minimize the cost. The LP will increase the cheap and decrease the expensive. If there is no limit for the active power the cheap will go to infinity and the expensive to -infinity. You need more generators and/or load constrains.

- What reasons can there be that a DSL model cannot be edited?

It is quite a general question. If you mean you cannot edit it because it is 'protected', then the reason might be that the DSL model you are trying to modify is the one in the global library, which can only be modified directly by the administrator. In this case you should make a copy of the model in your project library, and then you should be able to make modifications.

- What is a IntVariant element for DPL for? (What is the difference between variants and variations?)

The function IntVariant is used in older versions of the software, where the changes in the system were recorded in a "System Stage", however now the changes are stored in Variations and Operations Scenarios depending of the type of modification.

This change was done in 14.0, so, since you have version 14.1, please ignore the IntVariant methods.